UNIVERSITY OF SOUTHAMPTON

FACULTY OF NATURAL AND ENVIRONMENTAL SCIENCES

School of Chemistry

Novel Antibiotics from DNA Adenine Methyltransferase Inhibitors

by

Jennifer Claire McKelvie

Thesis for the degree of Doctor of Philosophy

October 2011

Abstract

The re-emergence of plague as a world-wide health concern and the potential risk posed by bioterrorism has led to an increased interest in available treatments for the disease. The bacterial DNA adenine-*N*6 methyltransferase, Dam, is involved in the regulation of a range of pathogenic bacteria and has been validated as a target for the development of antimicrobial agents with activity against *Yersinia pestis*, the causative agent of plague. The lack of a functionally similar enzyme in mammals suggests that highly selective Dam inhibitors could be developed. A coupled, real-time break light Dam activity assay has been optimised for HTS, and assays for the validation and characterisation of screening hits have also been developed. Screening of random and *in silico* enriched compound libraries, and the subsequent application of counter-screening and hit confirmation assays, resulted in the identification of a single viable lead, (4-(*N*-(2-hydroxyethyl)sulfamoyl)phenyl) stibonic acid (**13776**).

Screening of compounds analogous to **13776** identified a series of arylstibonic acids with activity against Dam. Kinetic characterisation of the most potent arylstibonic acid, 4-stibonobenzenesulfonic acid (**13746**), revealed a DNA-competitive mode of action, and a K_i of 6.46 ± 0.07 nM. However, selectivity assays have revealed a potentially non-specific mode of action for the stibonic acids, which have shown activity against a range of DNA and protein binding enzymes. *Yersinia* cell culture experiments have shown a single compound, (3-((2-hydroxyethyl)carbamoyl)phenyl)stibonic acid (**13782**), to be capable of penetrating *Yersinia* cells and partially inhibiting methylation, and mRNA profiling experiments have shown **13782** to induce a statistically significant change in several genes involved in the pathogenicity of *Y. pestis*. Attempts at resynthesising **13782** have proved challenging, with only a fraction of the activity of the original sample reproduced. HPLC analysis of the original and resynthesised samples has shown the former to comprise two components, with only one present in both samples.

The *in vitro* evaluation of a series of bisubstrate analogues designed to mimic both the methyl donor *S*-adenosylmethionine (AdoMet), and the methylation target (adenine) has shown that substitution of the AdoMet sulfur for nitrogen results in a significant but not total loss of activity. Furthermore, the addition of a bicyclic heteroaromatic adenine analogue mimic to this scaffold led to an increase in potency and selectivity for Dam over the human cytosine methyltransferase DNMT1 but a reduction in selectivity for Dam over the restriction enzyme *Dpn*I. These results suggest that a selective and potent Dam inhibitor can be obtained by carefully modifying both components of the bisubstrate analogue inhibitor.

Contents

List of Figures

List of Tables

List of Equations

Declaration of Authorship

I, Jennifer Claire McKelvie

declare that the thesis entitled

Novel Antibiotics from DNA Adenine Methyltransferase Inhibitors

and the work presented in the thesis are both my own, and have been generated by me as the result of my own original research. I confirm that:

- this work was done wholly or mainly while in candidature for a research degree at this University;
- where any part of this thesis has previously been submitted for a degree or any other qualification at this University or any other institution, this has been clearly stated;
- where I have consulted the published work of others, this is always clearly attributed;
- where I have quoted from the work of others, the source is always given. With the exception of such quotations, this thesis is entirely my own work;
- I have acknowledged all main sources of help;
- where the thesis is based on work done by myself jointly with others, I have made clear exactly what was done by others and what I have contributed myself;
- parts of this work have been published as: Hobley, G., McKelvie, J. C., Harmer, J. E., Howe, J. Oyston, P. C. F. and Roach, P. L. (2012) Development of rationally designed DNA N6 adenine methyltransferase inhibitors, *Bioorg Med Chem Lett 22*, 3079-3082.

Signed: J C McKelvie

Date: 14th May 2012

Acknowledgements

First and foremost I would like to thank my supervisor Dr Peter Roach and members of the Roach group past and present; specifically Dr Robert Wood, Jenny Harmer, Dr Martin Challand, Dr Gerald Hobley, Dr Graham Broder, Dr Sam Birtwell and Dr Michael Maynard-Smith, for their advice and support during the completion of this thesis. I am also extremely grateful to Professor Petra Oyston, Dr Kaye Barnes, Dr Mark Richards and Dr Tim Milne of the Defence Science and Technology Laboratory (dstl) for their hard work and helpful advice. Finally I would like to thank my colleagues at the School of Chemistry, University of Southampton and my friends and family for their support.

Abbreviations

ADMET	absorption, distribution, metabolism, excretion and toxicology
AdoHcy	*S*-adenosylhomocysteine
AdoMet	*S*-adenosylmethionine
AIDS	acquired immune deficiency syndrome
BSA	bovine serum albumin
CcrM	cell-cycle regulated methyltransferase
CNS	central nervous system
COMT	catechol-*O*-methyltransferase
CV	coefficient of variation
Dam	DNA adenine-*N*6 methyltransferase
dAMP	2'-deoxyadenosine-5'-monophosphate
dmAMP	2'-deoxy-*N*6-methyladenosine-5'-monophosphate
DMHA	*N*,*N*-dimethylhexylamine
DMSO	dimethylsulfoxide
DNA	2'-deoxyribonucleic acid
dNMP	2'-deoxyribonucleotide monophosphate
DTT	dithiothreitol
ELISA	enzyme-linked immunosorbent assay
FBS	fragment-based screening
FID	fluorescent intercalator displacement
FIPAs	fluorescence polarisation immunoassays
FP	fluorescence polarisation
GAMT	guanidinoacetate methyltransferase
GNMT	glycine *N*-methyltransferase
HGT	horizontal gene transfer
HIV	human immunodeficiency virus
HMT	histone methyltransferase
HNMT	histamine *N*-methyltransferase
HPLC	high-pressure liquid chromatography
HTS	high-throughput screening
IC_{50}	half maximal inhibitory concentration
ITC	isothermal titration calorimetry
k_{cat}	catalytic enzyme rate
K_D	dissociation constant
K_i	inhibition dissociation constant
K_M	Michaelis-Menten constant

MDR..... multidrug resistant
mRNA..... messenger RNA
MRSA..... methicillin-resistant *Staphylococci aureus*
NCI/DTP..... National Cancer Institute's Developmental Therapeutics Program
ODN..... oligonucleotide
ORF..... open reading frame
PEMT..... phosphatidylethanolamine *N*-methyltransferase
PMSF..... phenylmethylsulfonyl fluoride
PNMT..... phenylethanolamine *N*-methyltransferase
PRMT..... protein arginine methyltransferase
R^2 ..... coefficient of determination
RM..... restriction-modification
rRNA..... ribosomal RNA
SAR..... structure activity relationship
SDS-PAGE..... sodium dodecyl sulfate polyacrylamide gel electrophoresis
siRNA..... small interfering RNA
snRNA..... small nuclear RNA
STAT..... signal transducer and activator of transcription
TLC..... thin layer chromatography
T_m..... melting temperature
TRD..... target recognition domain
tRNA..... transfer RNA
V_{max}..... maximum enzyme velocity
WHO..... World Health Organisation
XDR..... extensively drug-resistant
Ybt..... Yersiniabactin
Yop..... *Yersinia* outer protein
2AP..... 2-aminopurine

1 Introduction

1.1 Antibiotics and the emergence of resistant bacteria

1.1.1 Discovery and development of antibiotics

The term antibiotic was first used by the biochemist Selman Waksman in the 1940s to describe a compound that antagonises the growth of a microbe (*1*). Although originally used to describe antibacterial agents of natural origin, the term is now frequently used to describe any compound that inhibits (bacteriostatic) or kills (bactericidal) microbes by specific interaction with bacterial targets (*2*).

The discovery of the antibacterial agent penicillin (**Figure 1.1**), isolated from *Penicillium* mould by Alexander Fleming in the early 20th century is often considered as the dawn of the modern age of antibiotics (*3, 4*). However the first commercially available antibiotic was the synthetic drug prontosil, developed at Bayer by Gerhard Domagk and co-workers (*5*). The active component of prontosil was later identified by Daniel Bovet at the Pasteur Institute as sulfanilamide, a metabolite of prontosil formed *in vivo* and the parent compound of the sulfa drugs (**Figure 1.1**) (*6*). The first naturally derived antibiotic, tyrothricin (a mixture of tyrocidine and gramicidin), was isolated from the soil bacterium *Bacillus brevis* in 1939 by Rene Dubos (*7*).

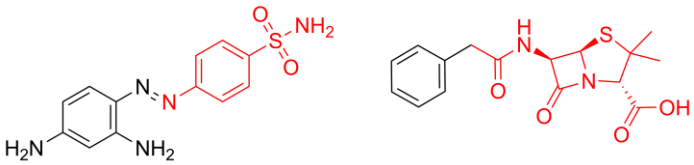

Prontosil Penicillin G

Figure 1.1 Structures of the early antibiotics prontosil and penicillin
The prontosil metabolite and active component sulfanilamide, and the core penicillin structure (in this case for benzylpenicillin) are highlighted in red.

Continuing the work of Fleming, in the early 1940s Florey and Chain developed a method for producing and purifying penicillin, with the purified antibiotic showing a broad-spectrum of activity and low levels of toxicity in humans (*6, 8*). The isolation and development of a large number of antibiotics quickly followed, with a substantial proportion of new antibiotic classes introduced between 1930 and 1968 (**Figure 1.2**). Since this time only two new classes of antibiotic have been introduced, the oxazolidinones (linezolid, Pfizer) and the lipopeptides (daptomycin, Cubist) although other new antibiotics have been introduced within existing classes (*9-11*).

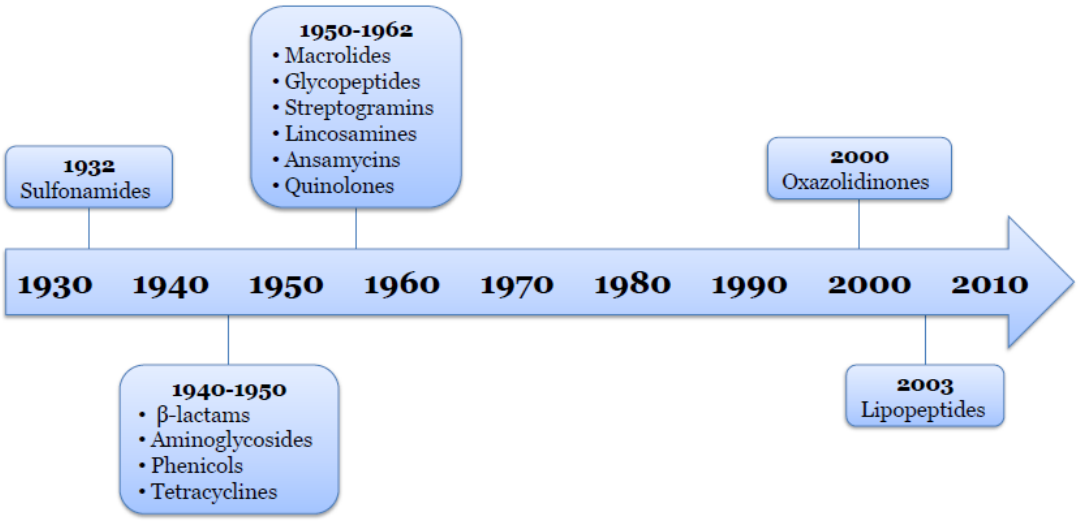

Figure 1.2 A timeline of antibiotic drug discovery
Adapted from references (*12*, *13*).

1.1.2 Antibiotic resistance

The rapid increase in antibiotic use during the past century has been accompanied by the concurrent emergence of resistance to these drugs amongst bacterial populations. The first reports of sulfonamide resistance appeared in the late 1930s, shortly after the introduction of prontosil (*14*). In the case of penicillin, a bacterial penicillinase was identified prior to the introduction of penicillin onto the market, with resistance in hospitals reported shortly after its introduction (*2, 15*). A similar course of events has been observed for subsequent antibiotics with resistance emerging soon after their introduction into the clinic (**Table 1.1**).

Bacteria targeted by the first commercially available antibiotics were initially resistant to single antibiotics, for example penicillin-resistant *Staphylococci aureus* (*16*). Over time the continued selection pressure applied by different drugs has resulted in the emergence of multidrug resistant (MDR) bacteria with multiple resistance mechanisms. Examples of MDR bacteria include methicillin-resistant *S. aureus* (MRSA), which also displays an increased level of virulence over methicillin-sensitive strains, and extensively drug-resistant (XDR) *Mycobacterium tuberculosis*, which can require the use of 6-7 different drugs during treatment (*17, 18*).

Table 1.1 Mode of action and resistance mechanisms of commonly used antibiotics

Antibiotic Class[#]	**Original Example**	**Target**	**Mode(s) of Resistance**
Sulfonamide	Prontosil (Sulfanilamide)	C_1 Metabolism	Efflux; Altered target
β-Lactam	Penicillin	Peptidoglycan biosynthesis	Hydrolysis; efflux; altered target
Aminoglycoside	Streptomycin	Translation	Phosphorylation; acetylation; nucleotidylation; efflux; altered target
Phenicol	Chloramphenicol	Translation	Acetylation; efflux; altered target
Tetracycline	Chlortetracycline	Translation	Monooxygenation; efflux; altered target
Macrolide	Erythromycin	Translation	Hydrolysis; glycosylation; phosphorylation; efflux; altered target
Glycopeptide	Vancomycin	Peptidoglycan biosynthesis	Reprogramming of peptidoglycan biosynthesis
Streptogramin (types A and B)	Virginiamycin	Translation	C-O lyase (type B); acetylation (type A); efflux; altered target
Lincosamide	Lincomycin	Translation	Nucleotidylation; efflux; altered target
Ansamycin	Rifamycin	Transcription	ADP-ribosylation; efflux; altered target
Quinolone	Nalidixic acid	DNA replication	Acetylation; efflux; altered target
Oxazolidone	Linezolid	Translation	Efflux; altered target
Lipopeptide	Daptomycin	Cell membrane	Altered target

Adapted from references (*13, 19*).

[#] In order of discovery.

Antibiotic resistance has evolved naturally in some bacteria, and occurs via intrinsic mechanisms encoded by genes located on the host chromosome. Other mechanisms of resistance are acquired through mutation or horizontal gene transfer (HGT). Mutation rates among bacterial populations are typically low, helping them to preserve their genomes, however under stress, such as in the presence of an antibiotic, the number of hypermutators increases, enhancing the probability of acquiring resistance. The transfer of genetic material encoding resistance occurs via bacteriophage infection (transduction), conjugation of plasmids or transposons, and transformation of naked DNA (**Figure 1.3**) (*17, 20*).

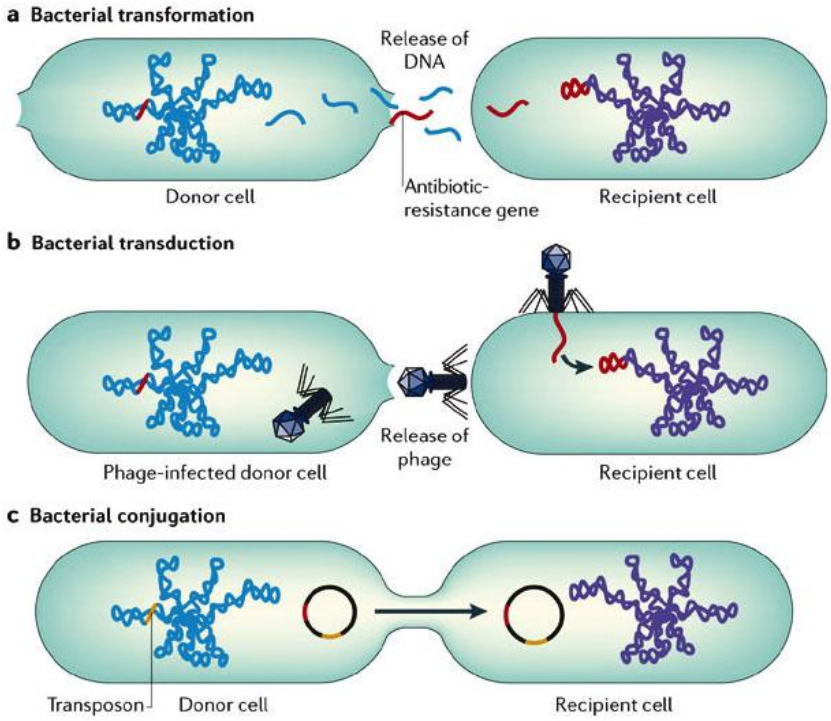

Figure 1.3 Acquisition of antibiotic resistance
Copyright Nature Reviews Microbiology by Nature Publishing Group.
Reproduced with permission from reference (*21*).

Resistance mechanisms include the alteration of molecular targets (often by mutation), efflux, and the chemical inactivation of antibiotics, with many resistant bacteria employing a combination of these methods (*19*). Alteration of molecular targets can occur at the drug binding site, directly affecting binding affinity, or by the reprogramming of molecular pathways to bypass the affected process. Efflux pumps work by removing drug molecules from the cell at a faster rate than they can enter, keeping the intrabacterial concentration low and relatively ineffectual. Direct inactivation of antibiotics occurs either by their degradation, for example by hydrolysis, or through chemical modifications, such as acetylation or phosphorylation.

Both methods drastically alter drug structure, leading to decreased binding affinity (*22*).

Antibiotics have revolutionised modern medicine, providing not only a treatment route for bacterial infections but enabling medical procedures to be carried out with minimal risk of infection (*19*). However, with ever increasing numbers of MDR bacterial species, methods for tackling the problem of resistance must be identified. Approaches to solving this problem include the reduction of inappropriate antibiotic use, the isolation of patients colonized with potentially dangerous resistant bacteria, combination therapy, the development of further analogues of current antibiotic classes, and the development of novel antibiotics (*14*).

1.1.3 Antibiotic resistance in Yersinia pestis

The pathogen of specific interest for this project is the bacterium *Yersinia pestis*, the causative agent of plague. *Y. pestis* is a gram-negative bacterium dependent on a host-species for survival, alternating between flea vectors and mammalian (primarily rat) hosts. In humans, the majority of naturally occurring plague cases are caused by the bite of a flea carried by an infected host (typically a wild rodent) resulting in the onset of bubonic plague symptoms within 2 to 6 days. Septicemic and pneumonic plague can occur as either a secondary infection to bubonic plague, or in a minority of cases, as the primary infection. Whilst 40-60% of untreated bubonic plague cases are fatal, the septicemic and pneumonic forms of the disease have a near 100% fatality rate if left untreated (*23*).

Several major plague pandemics have occurred throughout human history, claiming millions of lives. During the 15-year period from 1989 to 2003 an average 2,554 cases of plague were reported annually to the World Health Organisation (WHO), with an average 7% of these cases resulting in fatalities. Whilst improvements in sanitation and treatment routes make the outbreak of future pandemics unlikely, an increase in the number of cases reported to the WHO since the early 1990s and the re-emergence of plague in India (1994 and 2002), Indonesia (1997), and Algeria (2003) after a 30-50 year period has led to plague being characterised as a re-emerging disease (*24, 25*).

The outbreak of plague following the release of a biological weapon has also been identified as a plausible threat. Both United States and Soviet Union biological weapons programs are reported to have developed techniques to aerosolize plague, the dissemination of which would cause primary pneumonic plague, resulting in a high number of fatalities (*26*).

Treatment of plague is achieved by the rapid administration of antibiotics, typically streptomycin, tetracycline and chloramphenicol. The successful use of gentamicin, trimethoprim-sulfamethoxazole, doxycycline and amoxicillin has also been reported (*23, 26, 27*). Although antibiotic resistance in *Y. pestis* is rare, in recent years two separate cases have been identified, both occurring in Madagascar in 1995 (*28, 29*). One of the isolated strains exhibited MDR, with resistance to 8 different antibiotics, including all of the drugs currently recommended for the treatment of plague.

A single, conjugative plasmid (pIP1202) was found to encode all of the resistance genes. Experimental evidence has suggested the source of this plasmid to be HGT in the gut of the flea vector, where dense bacterial aggregates are formed, producing a favourable environment for the transfer of genetic material (**Figure 1.4**). The natural

development of two separate antibiotic resistant strains of *Y. pestis* implies that such an event is not an isolated occurrence, making the continued emergence of *Y. pestis* strains with antibiotic resistance highly likely (*30, 31*).

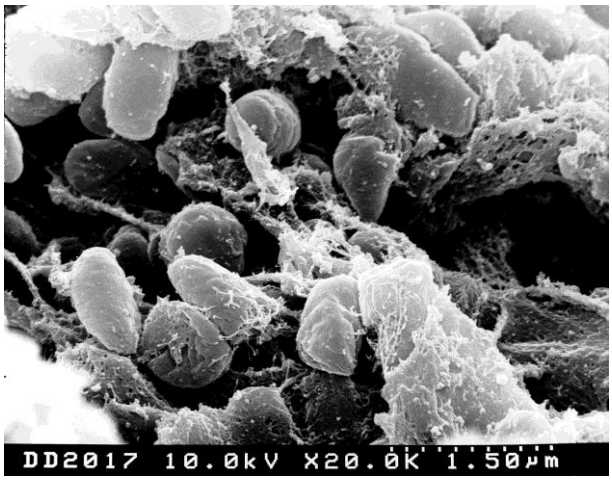

Figure 1.4 Scanning electron micrograph depicting a mass of *Yersinia pestis* bacteria in the foregut of the flea vector
Source – Rocky Mountain Laboratories, NIAID, NIH.

The global re-emergence of plague, potential threat from biological weapons, and the isolation of antibiotic resistant *Y. pestis* strains have led to a renewed interest in the development of improved treatment methods. Such methods include immunotherapy, immunomodulatory therapy, phage therapy, bacteriocin therapy, symptomatic treatment, and the inhibition of virulence factors. Therapeutic agents targeting virulence factors would be expected to interfere with infection rather than viability and are therefore unlikely to be affected by current resistance mechanisms, making them an attractive prospect for the development of novel antimicrobials (*32*).

All *Yersinia* spp. contain a plasmid which encodes the Yop (*Yersinia* outer protein) virulon. This system is comprised of the type III secretion system apparatus (the Ysc), the translocation apparatus, a set of intracellular effector proteins, and a control system. On contact with eukaryotic cells the Yops are secreted and the translocation apparatus delivers the effector proteins into the cell, inducing apoptosis (**Figure 1.5**). The Yop virulon is considered to be the main pathogenicity factor of *Yersinia* spp., with the ability to disarm host-immune response making it essential for virulence (*32, 33*). Inhibitors targeting specific proteins within the Yop virulon have been developed and some have shown attenuation in eukaryotic models (*32, 34-37*).

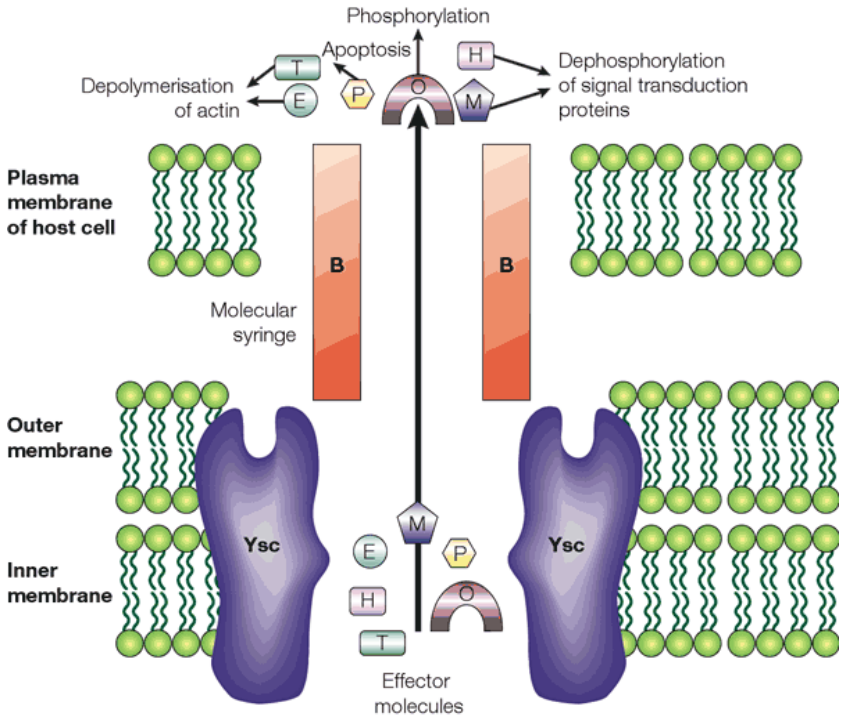

Figure 1.5 *Yersinia* type III secretion system (Ysc)
YopB labelled B, effector proteins Yops E, H, M, O, P and T labelled E, H, M, O, P and T.
Copyright Nature Reviews Genetics by Nature Publishing Group.
Reproduced with permission from reference (*38*).

An alternative approach has been suggested involving the inhibition of the DNA adenine-*N*6 methyltransferase (Dam) which is involved in the regulation of virulence proteins, including Yops (*39*). A *Y. pestis dam* mutant has shown a 2000-fold attenuation in mouse models (*40*), and the inoculation of mice with a *Yersinia pseudotuberculosis dam* mutant led to their subsequent protection from plague infection (*41*). The potential for hypermutation due to the disruption of the mismatch repair mechanism in *dam* mutants mean it is unlikely they can be used as effective vaccines. However, Dam inhibitors may represent a valid target for the development of novel antimicrobials effective against plague (*42*).

1.2 Methyltransferases

1.2.1 Overview

Dam is a member of the *S*-adenosylmethionine-dependant methyltransferases (AdoMet-dependant methyltransferases), a family of enzymes responsible for the transfer of a methyl group from the methyl donor AdoMet to a wide range of biological substrates. Methylation is known to occur at sulfur, carbon, nitrogen and oxygen atoms on small molecules, such as metabolites, and on biological macromolecules (*43, 44*).

One of the most widely studied small molecule methyltransferases is the catechol-*O*-methyltransferase (COMT), which catalyses the transfer of a methyl group to catecholamines and other catechols in the presence of magnesium ions. COMT catalysed methylation of these substrates leads to their inactivation, and can play a role in Parkinson's disease, with COMT inhibitors being used in the treatment of Parkinson's as an adjunct to L-DOPA therapy (*45, 46*). Other examples of small molecule methyltransferases include: glycine *N*-methyltransferase (GNMT), which methylates glycine to form sarcosine, and has been implicated in the regulation of AdoMet (*47, 48*); histamine *N*-methyltransferase (HNMT), which forms the first step in the metabolism of histamine, and has been linked with allergic/inflammatory disease (*49*); phenylethanolamine *N*-methyltransferase (PNMT), which catalyses the formation of epinephrine (adrenaline) from norepinephrine (noradrenaline) and is implicated in a wide range of central nervous system (CNS) related conditions (*50*); and guanidinoacetate methyltransferase (GAMT), which catalyses the final step in creatine biosynthesis, and has been linked to speech delay, learning disorders, autism, epilepsy, hyperactivity and movement disorders (*51*).

Fewer examples of lipid methyltransferases are known, with perhaps the most significant example being the phospholipid methyltransferase phosphatidylethanolamine *N*-methyltransferase (PEMT) which methylates phosphatidylethanolamine (PE) to form the membrane protein phosphatidylcholine (PC). PEMT is found primarily in the liver where it is responsible for the formation of ~30% of hepatic PC, with the remainder coming from the CDP-choline pathway, which relies on dietary choline (*52*).

The protein methyltransferases form a much larger group of enzymes, with methylation known to occur at arginine, lysine, histidine, proline and carboxyl groups (*53*). Methyltransferases which methylate arginine are known as protein arginine methyltransferases (PRMTs) and can be broadly divided into three types: type I, which form ω-monomethyl- and asymmetric dimethyl- arginine; type II, which form ω-

monomethyl- and symmetric dimethyl- arginine; and type III, which form δ-monomethylarginine (**Figure 1.6**) (*54*). PRMTs are known to methylate a growing number of proteins, including histones, fibrillarin and STATs (signal transducer and activator of transcription), and have been implicated in numerous biological processes, including signal transduction, cellular proliferation and transcriptional processing (*55*).

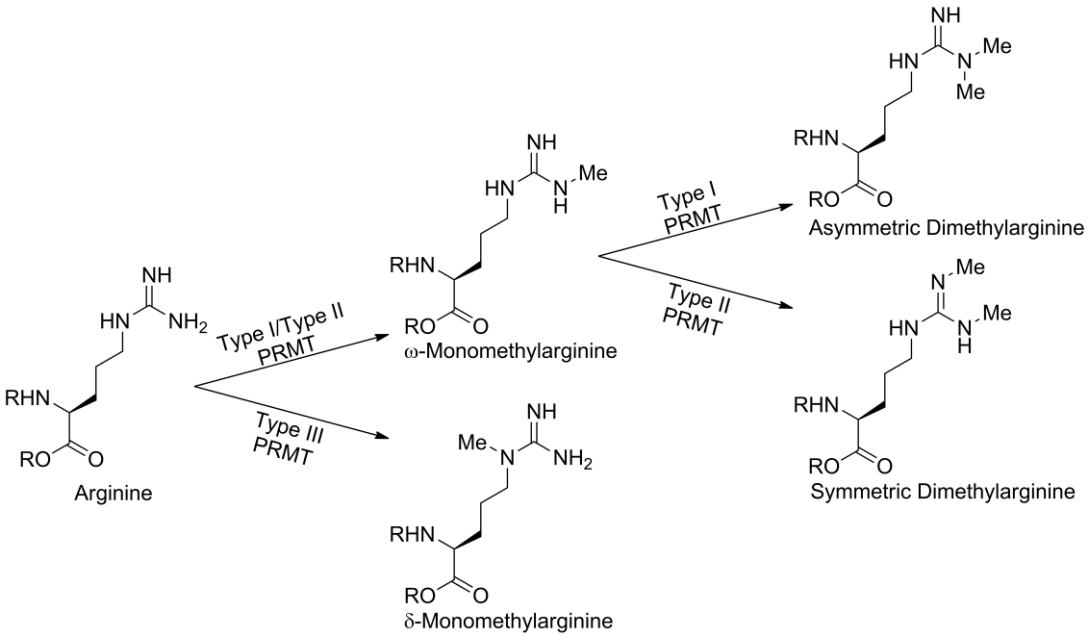

Figure 1.6 Protein arginine methylation by types I, II and III PRMTs

Another family of methyltransferases methylate lysine residues, within which the medically important family of histone methyltransferases (HMTs) have been particularly well studied. The vast majority of histone lysine methylation is carried out by the SET-domain family of proteins, targeting the ε-amino centre and resulting in the formation of mono-, di-, and tri-methylated lysine residues (*56*). Both lysine and arginine HMTs are involved in numerous cellular processes, including heterochromatin formation, X-chromosome inactivation and transcription regulation and as such are associated with numerous human developmental disorders and diseases (*57*).

Nucleic acid methyltransferases include both RNA and DNA methyltransferases, the latter of which will be discussed in detail in the following Section (1.2.2). The methylation of RNA occurs at a vast array of positions in transfer RNA (tRNA), ribosomal RNA (rRNA), small nuclear RNA (snRNA) and messenger RNA (mRNA) (*58*). Biological functions of RNA methylation include the maintenance of RNA structures (specifically tRNA), the control of decoding specificity during translation and antibiotic resistance (*44, 59, 60*).

1.2.2 DNA methyltransferases

DNA methylation is catalysed by the DNA methyltransferases and occurs at the *N*6 position of adenine and the *N*4 or *C*5 position of cytosine (**Figure 1.7**). Whilst all three types of methylation are observed in prokaryotes, to date only cytosine-*C*5 methylation has been identified in higher eukaryotes, although *N*6-methyladenine has been identified in several lower eukaryotes (*61-63*).

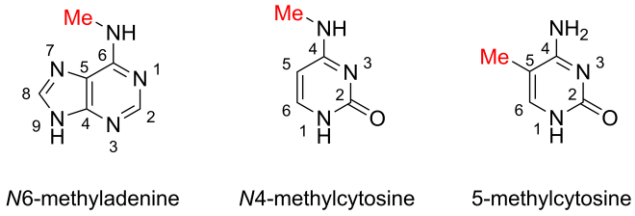

Figure 1.7 Structures of the methylated bases

The DNA methyltransferases of eukaryotes are involved in epigenetic processes such as the control of gene transcription, maintaining genome stability and integrity, genomic imprinting, and X-chromosome inactivation (44, 64). In mammals cytosine-*C*5 methylation occurs primarily at CG-rich regions known as CpG islands, and is carried out by a group of enzymes called the DNMTs. The DNMTs include the maintenance methyltransferase DNMT1, the de novo methyltransferases DNMT3A and DNMT3B, and the activator DNMT3L (65). The enzyme DNMT2 has also been classed as a mammalian DNA methyltransferase due to sequence similarities with other DNMTs, however the DNA methyltransferase activity of this enzyme is poor, and the discovery of its ability to act as an RNA methyltransferase has led to the suggestion that DNMT2 may share an evolutionary origin with the DNMT1 and DNMT3 family (66). The hypo- and hyper-methylation of CpG islands has been linked to many human diseases, including cancer, and is a validated target for the development of drugs targeting leukaemia (*64, 67, 68*).

In prokaryotes, DNA methyltransferases have a range of biological roles: as part of restriction-modification (RM) systems they are responsible for the protection of cells from invading foreign DNA, enabling the distinction of self and non-self DNA through the methylation of specific recognition sites, blocking cleavage by cognate restriction enzymes; DNA methyltransferases which are not part of an RM system, such as the adenine-*N*6 methyltransferases Dam and CcrM (cell-cycle regulated methyltransferase), play a role in DNA repair, the control of gene expression, phase variation, bacterial virulence, and cell cycle regulation; and in phage, methyltransferases can be used to improve survival of DNA in host-cells by mimicking the methyltransferases of host RM systems (*44, 61*).

Both prokaryotic and eukaryotic DNA methyltransferases have a two-domain structure consisting of a catalytic domain, which contains up to ten characteristic amino acid motifs and encompasses both the AdoMet binding site and the methyl transfer active site, and a smaller target recognition domain (TRD). DNA binding occurs at the cleft between the two domains, with sequence-specific DNA recognition controlled by the variable TRD (*44, 61*). The catalytic domains of all DNA methyltransferases share a structural core common to the vast majority of AdoMet-dependant methyltransferases (*43, 69*). This core consists of alternating β-sheets and α-helices which form a seven-stranded β-sheet, with each β-sheet flanked by one or two α-helices (**Figure 1.8**) (*44, 61*). The mammalian DNMT1 and DNMT3 family of enzymes also possess an *N*-terminal regulatory domain, which in DNMT1 is thought to be required for the formation of the correct tertiary protein structure (*70*).

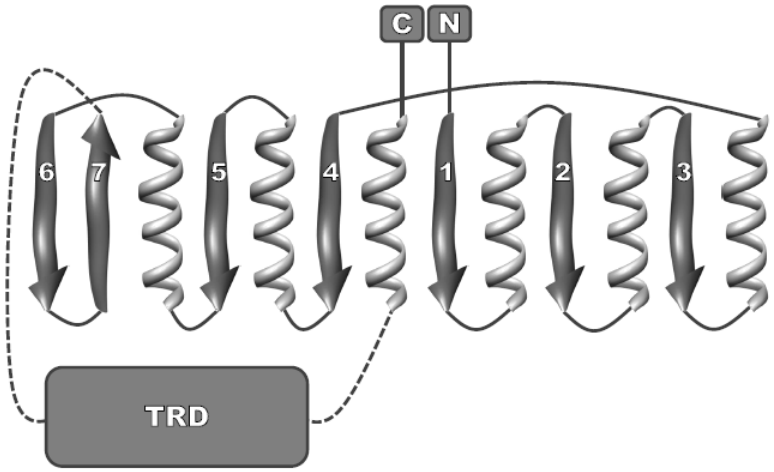

Figure 1.8 Conserved central structure of the DNA methyltransferases
Adapted from reference (*61*).

DNA methyltransferases have been observed to show both distributive and processive modes of methylation, with a distributive mechanism generally identified for DNA methyltransferases involved in an RM system, and a processive mechanism generally observed for solitary DNA methyltransferases (71). In both cases DNA binding is thought to follow a multi-step process in which the enzyme binds non-specifically, diffusing linearly along the DNA until the target site is reached, with specific binding facilitated by the interaction between the TRD and the DNA recognition site (61). Once a specific interaction is formed the target nucleotide is rotated out of the double helix, and positioned into the catalytic domain active site pocket in a process known as base flipping (69, 72). In the case of cytosine-*C*5 methylation addition of a cysteine residue to the 6 position leads to the formation of a nucleophilic enamine which reacts with

the AdoMet (**Figure 1.9**). In the case of adenine-*N*6 and cytosine-*N*4 methylation, the reaction follows a simple direct S_N2 type mechanism (61, 73, 74).

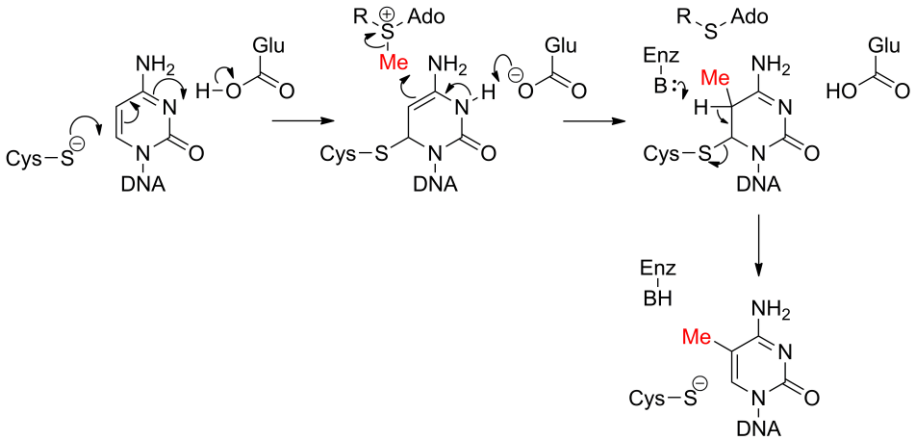

Figure 1.9 Methylation mechanisms for cytosine-*C*5 methylation
Adapted from reference (*61*).

1.2.3 DNA adenine-N6 methyltransferase

The solitary prokaryotic DNA methyltransferase Dam catalyses the methylation of adenine at the *N*6 position in the recognition sequence GATC. Dam is found in a range of gram-negative proteobacteria such as *Escherichia coli*, *Vibrio cholerae*, *Yersinia* spp. and *Salmonella* spp.; it is also present in a number of bacteriophages such as HP1, P1, T1 and T4 phage (*75*). Adenine-*N*6 methylation decreases the thermodynamic stability of DNA and alters the curvature of the DNA backbone (**Figure 1.10**), acting as an epigenetic signal by influencing protein:DNA binding interactions (*76*). As such Dam has been implicated in critical cellular processes including the initiation of chromosome replication, mismatch repair, the regulation of gene expression, and pathogenicity (*42, 75, 76*).

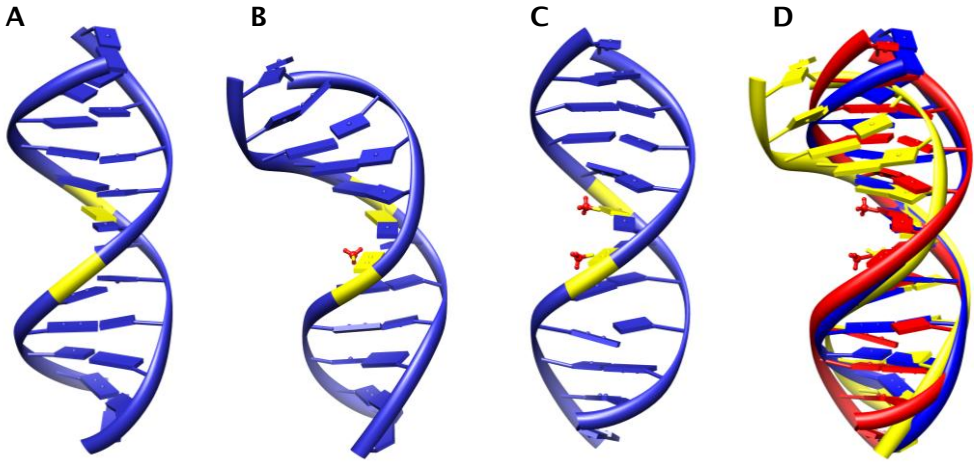

Figure 1.10 Effect of methylation of DNA backbone curvature
(A-C): DNA duplex containing un- (A), hemi- (B) and fully (C) methylated GATC site, with DNA shown in blue, A of GATC site in yellow and transferred methyl group in red.
(D): Overlay of DNA duplexes containing un- (blue), hemi- (yellow) and fully (red) methylated GATC site.
Image created using pdb files 1OPQ (A), 1OQ2 (B) and 2KAL (C) with the program UCSF Chimera (*77*).

Chromosome replication: Dam methylation occurs at the majority of hemimethylated GATC sites, where, shortly after DNA replication, the nascent daughter strand is unmethylated and the parent strand methylated. At the origin of DNA replication (*oriC*) a high density of GATC sites facilitates the binding of the protein SeqA, which preferentially binds to two or more hemimethylated GATC sites. Sequestration of the GATC sites at *OriC* by SeqA persists for approximately one-third of the cell cycle, preventing re-initiation of chromosome replication from occurring more than once per cell cycle by delaying methylation and subsequent DnaA binding at *OriC (78)*.

Mismatch repair: When a base mismatch is formed during DNA replication in *E. coli* it is recognised by the protein MutS, which binds DNA at the mismatch site. MutS then recruits the activator MutL and, in the presence of ATP, forms a ternary complex with MutH. Upon complex formation MutH is able to cleave the unmethylated daughter strand at a hemimethylated GATC site adjacent to the mismatch, providing an initiation site for excision of the DNA containing the mismatch (*79*). Dam methylation acts as a signal, directing post-replication mismatch-repair to the nascent, unmethylated DNA strand. The absence or over-production of Dam results in increased mutation rates, with MutH unable to distinguish between the parent and daughter strands, leading to both being cleaved, sometimes simultaneously (*80*).

Regulation of gene expression: The blocking of methylation by the binding of regulatory proteins at or adjacent to GATC sites leads to the formation of heritable DNA methylation patterns. In cases where the methylation state of GATC sites affects the binding of regulatory proteins, gene expression can be influenced. An example of how DNA methylation patterns influence gene expression is provided by the regulation of phase variation in the pyelonephritis-associated pili (Pap) of uropathogenic *E. coli*. Pap phase variation is controlled through the methylation of two GATC sites, one proximal to the *pap* promoter ($GATC^{prox}$) and one located upstream of $GATC^{prox}$ ($GATC^{dist}$). In the off-phase, the leucine-responsive protein (Lrp) binds at sites overlapping $GATC^{prox}$, blocking methylation and allowing the unblocked $GATC^{dist}$ site to become fully methylated. Switching to the on-phase occurs following replication, upon translocation of Lrp to binding sites overlapping $GATC^{dist}$ in the presence of PapI and hemimethylated $GATC^{dist}$; methylation of $GATC^{prox}$ then occurs preventing further Lrp binding at this site (**Figure 1.11**) (*81, 82*).

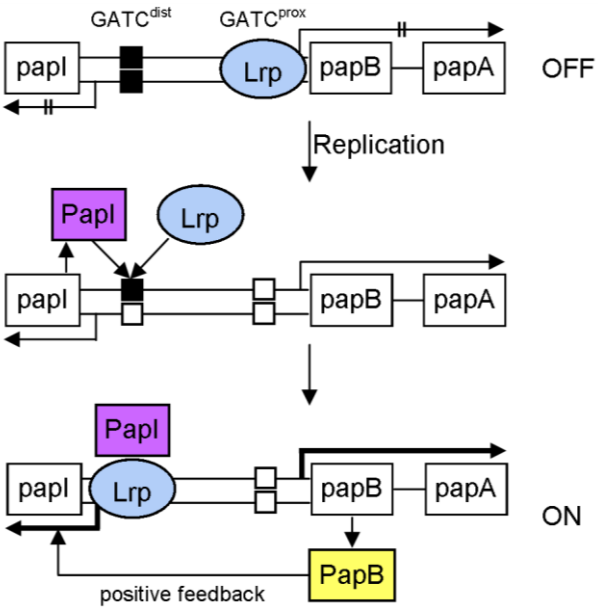

Figure 1.11 Regulation of Pap phase variation
Where two black squares represent a fully methylated GATC site, one black and one white square represents a hemimethylated GATC site, and two white squares represent an unmethylated GATC site.
Adapted from reference (*81*)

Pathogenicity: The effect of Dam methylation on bacterial pathogenesis has been documented in a range of pathogens. In *dam* mutant strains of *Salmonella enterica* (*83-85*), *Haemophilus influenzae* (*86*), *Y. pseudotuberculosis* strain IP32953 (*41*) and *Y. pestis* (*40*) attenuation has been observed in animal models. Where Dam is essential for viability, Dam over-producing (Dam^{OP}) strains have been used as a tool to study the effects of alterations in Dam levels within the cell, with Dam^{OP} strains of *Y. pseudotuberculosis* strain YPIII (*87*), *V. cholerae* (*87*), *Pasteurella multocida* (*88*) and *Aeromonas hydrophila* (*89*) also showing attenuation in animal models. The disruption of mismatch repair and the expression of virulence genes caused by changes in cellular Dam concentrations have been shown to produce a range of affects. Examples include the increased bile sensitivity and envelope instability of *S. enterica dam* mutants and the deregulation of Yop secretion in *Y. pseudotuberculosis* Dam^{OP} strains (*39, 42, 75*).

1.2.4 Structural and kinetic characterisation of DNA adenine-N6 methyltransferase

The structures of T4 and *E. coli* Dam have been solved in binary complexes with the methyl donor product *S*-adenosylhomocysteine (AdoHcy) or the AdoMet analogue sinefungin, and in tertiary complexes with either AdoHcy or sinefungin and DNA. Both *E. coli* and T4 Dam share the same two-domain structure as all DNA methyltransferases with the TRD of each comprising of a five-helix bundle and a β-hairpin loop which is conserved across the GATC-specific DNA methyltransferases (*90-93*). Whilst the sequence similarity between the two enzymes is only 25%, the active site is more highly conserved, with both enzymes containing the DPPY variant of the (D/N/S)PP(Y/F) active site motif (**Figure 1.12**), which is characteristic of the adenine-*N*6 methyltransferases (*94*). There is also sequence conservation between T4 and *E. coli* Dam and the Dams of other microorganisms, most notably between *E. coli* Dam and the Dams of pathogenic bacteria where there is a high level of sequence conservation (**Figure 1.12**).

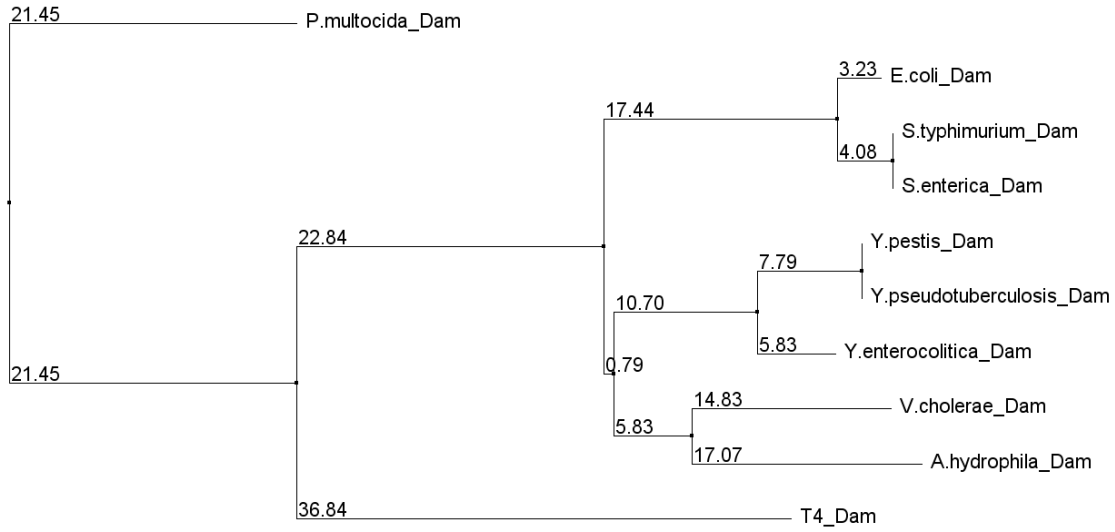

Figure 1.12 Neighbour joining tree for *E. coli*, T4 and some pathogenic Dams. Calculated by percentage identity using the program Jalview (*95, 96*).

For both *E. coli* and T4 bacteriophage Dam DNA binding has been shown to be regulated by the β-hairpin loop, and to a lesser extent the *N*-terminal loop. Transition from non-specific to specific DNA binding interactions are facilitated by binding interactions between the GATC recognition sequence and the specific residues within these loops. Specific binding re-orientates the protein on the DNA, allowing the adenine base to be flipped out of the double helix and into the active site for methylation to occur (**Figure 1.13**). The double helix is stabilised during base flipping

through protein:DNA stacking and hydrogen-bonding interactions (*91, 92*). Studies using the stacking-interaction dependent, fluorescent base analogue, 2-aminopurine (2AP), have shown base-flipping to comprise of two steps, flipping of the target out of the double helix, followed by binding of the flipped base into the active site. Interestingly the second step is not observed when AdoHcy is employed as a substrate, suggesting that different binding modes are employed for substrate and product (*91, 97, 98*).

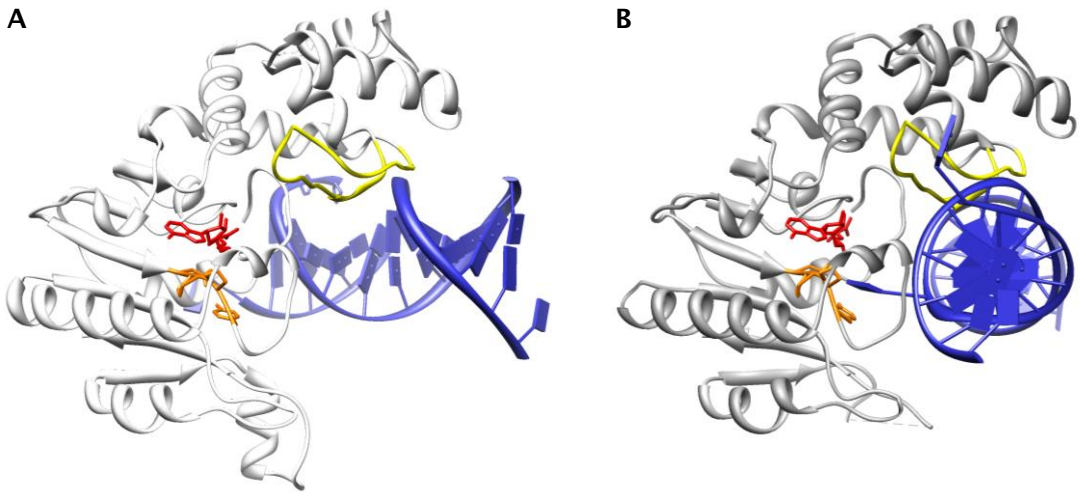

Figure 1.13 Non-specific and specific DNA binding interactions of T4 Dam
Non-specific T4 Dam:DNA:AdoHcy complex (A) and specific T4 Dam:DNA:Sinefungin complex (B). Protein shown in grey, DNA in blue, AdoHcy or sinefungin in red, β-hairpin loop in yellow and DPPY active site motif in orange.
Image created using pdb files 1YF3 molecule A (A) and 1YFL molecule E (B) with the program UCSF Chimera (*77*).

A combination of hydrogen bonding and stacking interactions mediated by the amino acids of the DPPY motif help to stabilise the flipped conformation and facilitate methyl transfer (*91, 98*). Dam catalysed methylation has been shown to occur in a processive manner (*99-101*), with subsequent methylations taking place prior to DNA release. *E. coli* Dam processivity has been shown to occur via intersite (methylation of multiple GATC sites on the same strand of DNA) and intrasite (methylation of both adenines in a fully unmethylated GATC site) mechanisms, with intersite processivity regulated by the DNA sequences flanking the recognition site (*102-104*).

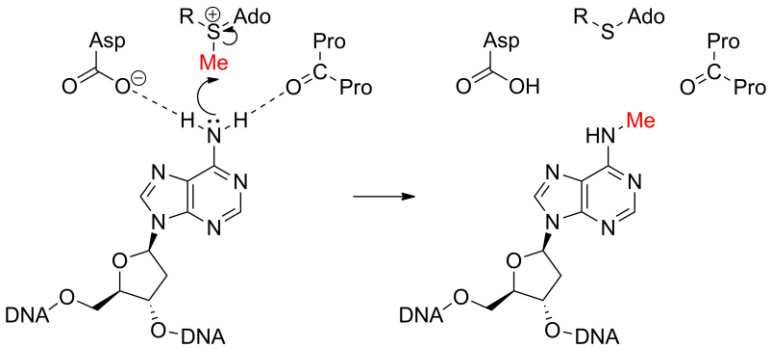

Figure 1.14 The role of residues in the DPPY motif in methyl transfer
The carbonyl of proline and the carboxylate of asparagine form hydrogen bonds to the *N*6 amine, with aspartic acid proposed to function as a base, removing a proton in concert with the methyl transfer step.
Adapted from reference (*61*).

The most detailed kinetic studies of the methylation reaction have used the *E. coli* and T4 Dam enzymes, as reported by the groups of Hattman, Reich and Jeltsch. An ordered bi-bi reaction mechanism in which AdoMet binds prior to the formation of a specific complex with DNA at the GATC recognition site has been proposed for both enzymes (*99, 101, 105*). The rate limiting step in this process has been identified as the release of methylated DNA, again for both T4 and *E. coli* Dam (*104-106*). Monomeric and dimeric forms of the enzyme have been observed, however T4 and *E. coli* Dam have each been shown to form functional dimers only under single turnover conditions (*103, 107*). Kinetic parameters have been determined using short synthetic DNA substrates and are tabulated below (**Table 1.2**).

Table 1.2 Kinetic parameters for *E. coli* and T4 Dam

Protein	Substrate	Methylation state*	K_M^{DNA} nM	K_M^{AdoMet} μM	k_{cat} min^{-1}	Source
E. coli Dam	21-mer duplex	UM	81 ± 4	-	0.91 ± 0.03	(*104*)
	20-mer duplex	UM	17.4 ± 3.0	5.6 ± 1.1	0.93 ± 0.06	(*105*)
	20-mer hairpin	UM	28.6 ± 0.16	6.4 ± 1.2	1.19 ± 0.33	(*105*)
T4 Dam	24-mer duplex	UM	7.7	0.33	0.84	(*108*)
	20-mer duplex	UM	6.3 ± 1.5	0.49	0.9 ± 0.06	(*109*)
		HM	6.0 ± 1.3	-	0.6 ± 0.006	(*109*)

* UM – Unmethylated GATC site, HM – hemimethylated GATC site.

The Michaelis-Menten constants (K_Ms) vary between T4 and *E. coli* Dam, with the latter showing weaker affinities for both DNA and AdoMet. Some variation in K_M^{DNA} is observed for *E. coli* Dam over different experiments, however the minimal difference in values obtained with an oligonucleotide duplex and hairpin suggest that both substrates are suitable for measuring the kinetic parameters of Dam. Constants for T4 Dam were determined for both an unmethylated and hemimethylated version of the same duplex, with similar K_M^{DNA} and k_{cat} values obtained in both cases, demonstrating the lack of preference shown by T4 Dam for hemimethylated over unmethylated sites. A lack of preference for DNA methylation state has also been observed for *E. coli* Dam, which methylates unmethylated and hemimethylated duplex DNA with the same efficiency *in vitro* (*110*).

1.2.5 Methyltransferase inhibitors

The wide range of biological functions carried out by methyltransferases makes them attractive targets for drug development, with methyltransferase inhibitors currently being used in the treatment of cancer (*111*) and Parkinson's disease (*112*) amongst others. As a common reaction product for all AdoMet catalysed methyltransfer reactions, AdoHcy (**Figure 1.15**) has been widely investigated as a methyltransferase inhibitor. Whilst AdoHcy is a potent inhibitor of many different methyltransferases the use of the compound as a drug has been ruled out due to its poor selectivity, lack of cellular uptake, and rapid metabolism by AdoHcy hydrolase within cells (*113*).

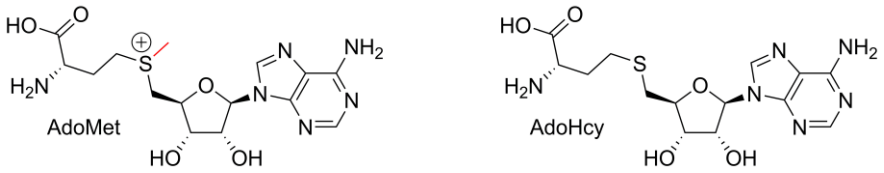

Figure 1.15 Structures of the methyl donor AdoMet and methyl donor product AdoHcy

In order to overcome these issues AdoHcy and AdoMet analogues have been synthesised, with modifications made to the sugar, amino acid and adenosine moieties (*114-121*). In addition to synthetic AdoHcy analogues a natural product analogue, sinefungin, isolated from *Streptomyces griseolus* at Lilly (*122*), was found to have activity against a wide range of methyltransferases (*123-127*). Unfortunately, the severe nephrotoxicity provoked by sinefungin in higher mammals makes it unfeasible as a drug candidate (*128*). More recent efforts with analogues have attempted to address selectivity issues by comparing the effects of inhibitors on multiple methyltransferases (*129-131*), however such studies often compare only closely related enzymes, with broader selectivity concerns overlooked.

The bisubstrate nature of methyltransferases makes them ideal candidates for multisubstrate analogue inhibitor design, a process in which two or more enzyme substrates are combined to develop more potent and selective inhibitors (*132, 133*). A major caveat of AdoHcy analogue inhibitors is the lack of specificity inherent in compounds based on a product common to all AdoMet-dependent methyltransferases. By combining the structural features of AdoHcy and the individual methylation target, specificity can likely be improved due to the synergistic effect on active site recognition. In addition, potency is also likely to improve due to an increase in binding affinity. A multisubstrate analogue inhibitor design approach has been applied to a range of methyltransferases including HMTs (*134*), PRMTs (*135*), COMTs (*136-140*), mycolic acid methyltransferases (*141*), and bacterial DNA methyltransferases (*142*).

Several inhibitors have also been designed based on the structure of the methyl target alone. Perhaps the best examples of such compounds are the cytidine analogue inhibitors of cytosine-*C*5 methyltransferase, such as 5-azacytidine (azacitidine), 5-aza-2'-deoxycytidine (decitabine), β-D-arabinofuranosyl-5-azacytosine (fazarabine), and dihydro-5-azacytidine (DHAC) (*143, 144*). These compounds are incorporated into DNA and inhibit cytosine-*C*5 methyltransferases by forming a covalent adduct and preventing further methylation. Other examples of molecules that modify methyltransferase activity include antisense oligonucleotides, which are short synthetic nucleic acids designed to bind to specific mRNA sequences and block translation, leading to the downregulation of methyltransferase expression (*144, 145*), and the polyamines spermidine and putrescine, which have been shown to inhibit bacterial cytosine-*C*5 methyltransferases (*146*).

The importance of Dam to the virulence of pathogenic bacteria and the lack of a functionally similar enzyme in mammals has made it a target for the development of novel antibacterial agents (*84, 105*). To this end several different strategies have been employed in the development of Dam inhibitors (**Figure 1.16**). In 2005 Benkovic *et al.* published a paper describing the identification of a series of bisubstrate borinic ester inhibitors of the bacterial adenine-*N*6 methyltransferase CcrM which also showed activity against Dam (*147, 148*). Subsequently Mashhoon *et al*. published the results of a 50,000 compound high-throughput screen, identifying 57 small molecule Dam inhibitors with IC_{50} (50% inhibitory concentration) values of 25 μM or less. Of these 57 compounds, 55 were found to be selective for Dam over DNMT1 and 38 were found to be selective for Dam over CcrM (*149*). Finally, Naumann *et al.* used a genetic selection method combined with split intein-mediated ligation of peptides and proteins (SICLOPPS) technology to identify 3 cyclic peptide Dam inhibitors with IC_{50} values ranging from 50 to 144 μM, each of which showed selectivity for Dam over the bacterial cytosine-*C*5 methyltransferase M.HhaI (*150*).

In silico methods have also been utilised for the identification of Dam inhibitors, with Cheng and co-workers identifying several small molecule inhibitors (**Figure 1.16**) from the National Cancer Institute's Developmental Therapeutics Program (NCI/DTP) library (*151*). Compounds were identified based on three-dimensional docking interactions with the active sites of both *E. coli* and T4 Dam, and validated as inhibitors using both biochemical and whole-cell assays.

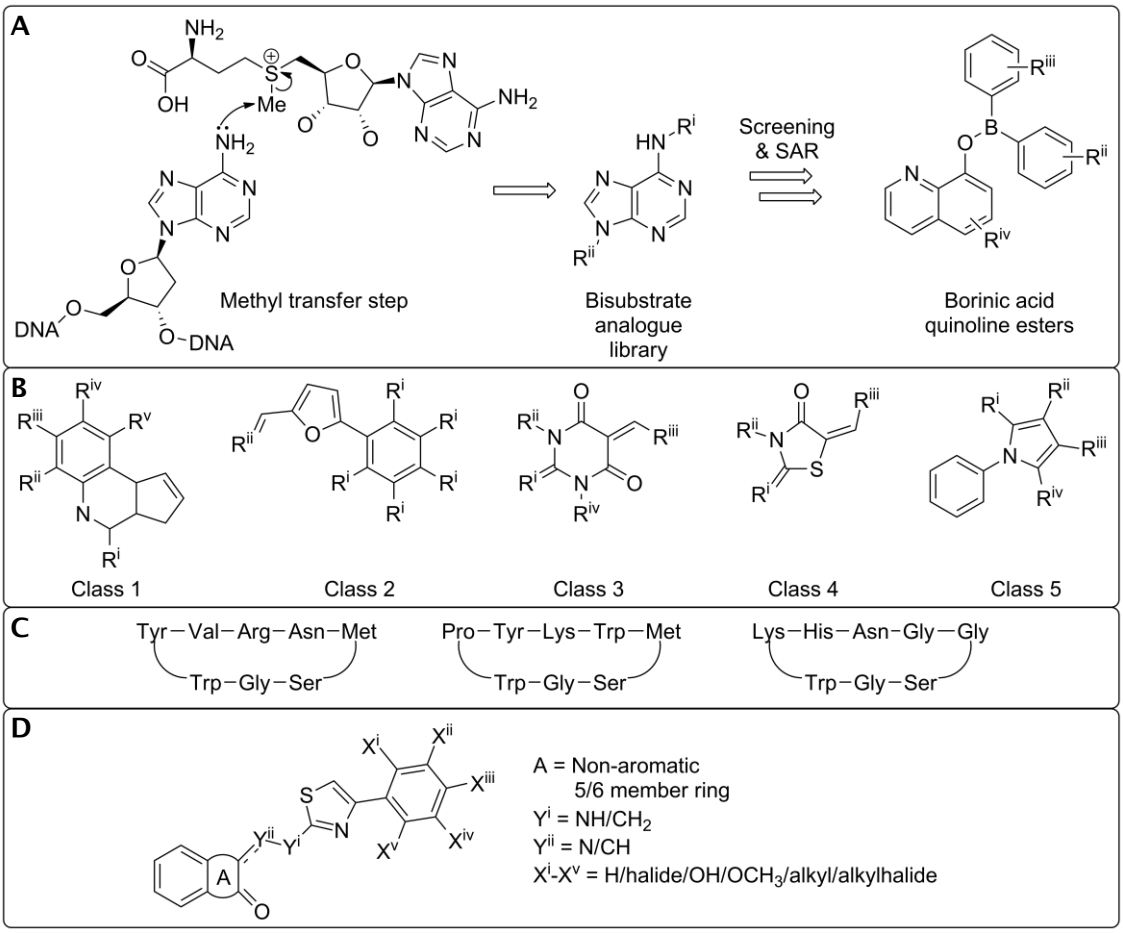

Figure 1.16 Dam inhibitors

Bisubstrate borinic esters (A), five classes of inhibitor identified from a high-throughput screen (B), cyclic peptides (C), single class of inhibitor identified from an *in silico* screen (D).

Adapted from references (*147, 149-151*).

1.2.6 Methyltransferase assays

The high level of interest in methyltransferases as potential therapeutic targets has led to a range of activity assays for the detection and characterisation of these enzymes being developed. Early methyltransferase assays monitored the incorporation of radiolabelled methyl groups from ^{3}H or ^{14}C labelled AdoMet into methylated products. The separation of unreacted labelled substrate from labelled product was then achieved through filter binding (*152*), chromatography (*153, 154*), gel electrophoresis (*155*), immobilisation of labelled product (e.g. through biotin/avidin interactions) (*156-158*), or coupling to cellulose (*159*). Whilst such assays can be highly sensitive and are still widely used, they are time-consuming and often involve the undesirable use of radioactive material, making them less than ideal for high-throughput applications.

The difficulties inherent in radiolabelling assays have led to the development of a number of alternative methyltransferase assays. A series of 'universal' assays with potential for use against all methyltransferases have been developed in which the universal methyl donor product, AdoHcy, is modified to yield a detectable product (**Figure 1.17**). Enzymes which catalyse the degradation of AdoHcy and its breakdown products, such as AdoHcy hydrolase, AdoHcy nucleosidase, adenine deaminase and adenosine deaminase, are used alone or in conjunction with derivatising agents to produce compounds which are detectable by absorbance or fluorescence spectroscopy (*160-163*).

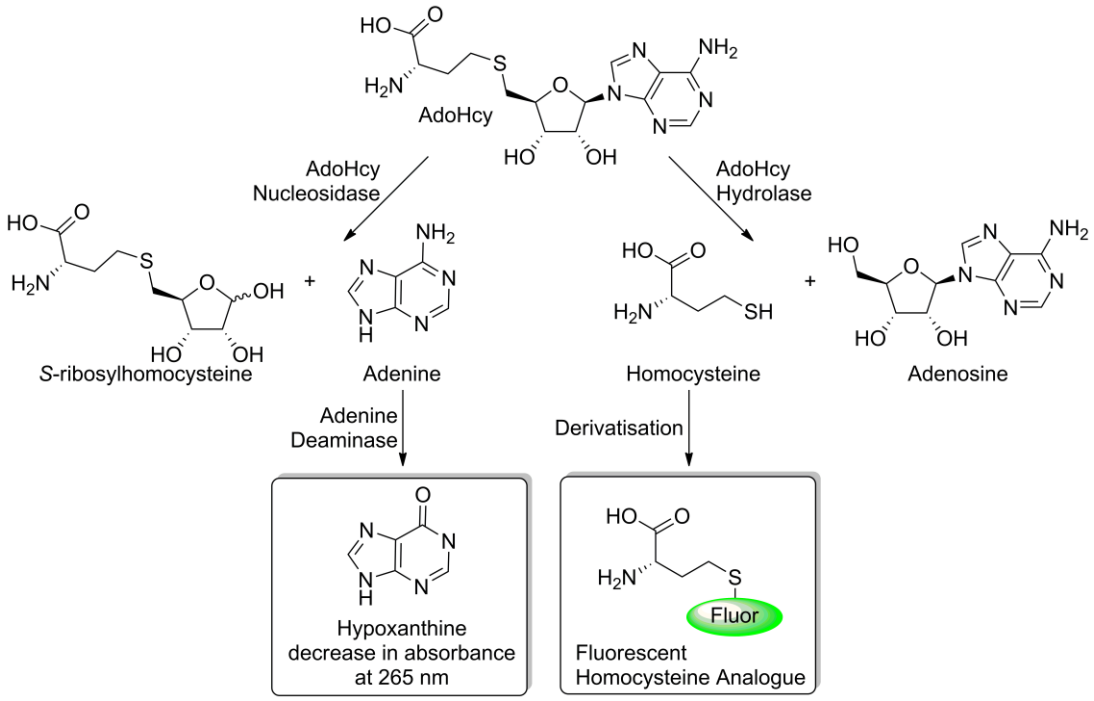

Figure 1.17 Universal AdoHcy-specific methyltransferase assays
Adapted from references (*160-163*).

Although the removal of AdoHcy is advantageous, preventing potential product inhibition, the adverse affect of coupling enzymes on potential inhibitors (especially those based on AdoHcy) mean that these assays are not suitable for the characterisation of some classes of methyltransferase inhibitors. Another common issue arising from the use of these assays is the possible interference of protein and substrates on the spectroscopic signal.

Other 'universal' methyltransferase assays include the detection of methylated product by mass spectrometry (*164*), and competitive fluorescence polarisation immunoassays (FIPAs), in which a fluorescent tracer (a fluorescein-AdoHcy conjugate) competes with AdoHcy for binding of an AdoHcy antibody leading to a decrease in fluorescence polarisation signal as the reaction progresses (*165*). Detection by mass spectrometry is highly accurate but not compatible with high-throughput applications, whereas FIPAs are conducive to high-throughput applications but can show high levels of background interference.

Assay technologies specific to the DNA methyltransferases often rely on the ability of methylation-sensitive restriction enzymes to cleave methylated DNA sequences. Examples include: DNA-modified gold nanoparticle assays in which methylation and subsequent cleavage induces DNA duplex dehybridisation, allowing the nanoparticles to aggregate, causing a red-to-blue colour change (*166*); a methylation-responsive DNAzyme strategy in which methylation and subsequent cleavage activates a horseradish peroxidise mimicking DNAzyme, which can then catalyse the H_2O_2 induced oxidation of 2,2'-azino-bis(3-ethylbenzothiazoline)-6-sulfonate disodium salt ($ABTS^{2-}$) to a coloured radical (*167*); and an enzyme-linked immunosorbent (ELISA) based assay in which methylation leads to the inhibition of restriction enzyme catalysed cleavage, protecting a duplex labelled on either end with biotin (used to immobilise one strand to a streptavidin coated plate) and digoxigenin which is recognised by Anti-Dig-Alkaline phosphatase and detected by bound *p*-nitrophenyl phosphate (pNPP) (*168*).

Another DNA methyltransferase specific assay methodology utilises small hairpin oligonucleotide probes known as 'molecular break lights' (*169*) in the detection of DNA methylation. In the hairpin form a quencher and fluorophore on either end of the oligonucleotide are held in close proximity, leading to fluorescence quenching. Cleavage of the probe leads to the separation of fluorophore and quencher and a subsequent increase in fluorescence (**Figure 1.18**). Methylation of a DNA recognition site within the probe can either protect from or promote restriction enzyme catalysed cleavage. This methodology has been applied by Mashhoon *et al.*, who employed a protection-based assay for the end-point monitoring of Dam activity, utilising the

methylation-sensitive restriction enzyme *Dpn*II (*149*), and Li *et al.*, who developed a real-time Dam activity assay which monitored the increase in fluorescence observed upon methylation promoted *Dpn*I cleavage of an unmethylated break light probe (*170*).

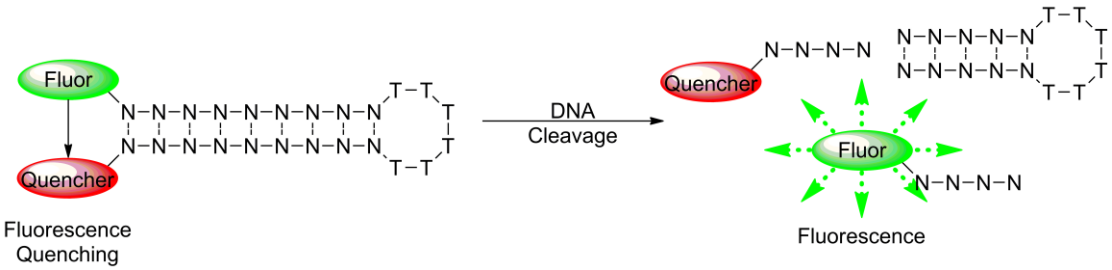

Figure 1.18 Molecular break light principle
Adapted from reference (*169*).

Although the method proposed by Li *et al.* enables real-time monitoring of Dam methylation *in vitro* it does not allow for the determination of kinetic parameters, as the unmethylated oligonucleotide substrate employed requires two methylations, inducing a lag phase and preventing the easy determination of initial rate. To address this problem Wood *et al.* employed a similar method using a hemimethylated oligonucleotide substrate which circumvented the issues experienced by Li *et al.* and allowed them to kinetically characterise *Y. pestis* Dam (*171*). Wood *et al.* successfully applied the same approach to the development of a cytosine-*C*5 methyltransferase assay (*172*), demonstrating the broad applicability of this approach as a method for assessing the activity of DNA methyltransferases, provided a methylation sensitive restriction enzyme is available.

1.3 Drug discovery

The drug discovery process (**Figure 1.19**) is a complex multistep process that can take years of research effort and millions of pounds of investment. In addition, the process of developing a safe and profitable drug is fraught with problems that frequently result in the failure of the programme (*173, 174*). The first key stage in the process is the identification and validation of a druggable target. In the most widely adopted approach assay techniques are then developed and used to screen compound libraries for 'hits' with activity against the target of interest. Hit validation is then followed by hit-to-lead optimisation where potency, selectivity and physiochemical properties of the original hit compound are optimised. Compound absorption, distribution, metabolism, excretion and toxicology (ADMET) are then assessed, with successful candidates progressing to clinical trials and, in a small minority of cases, to market (*175*).

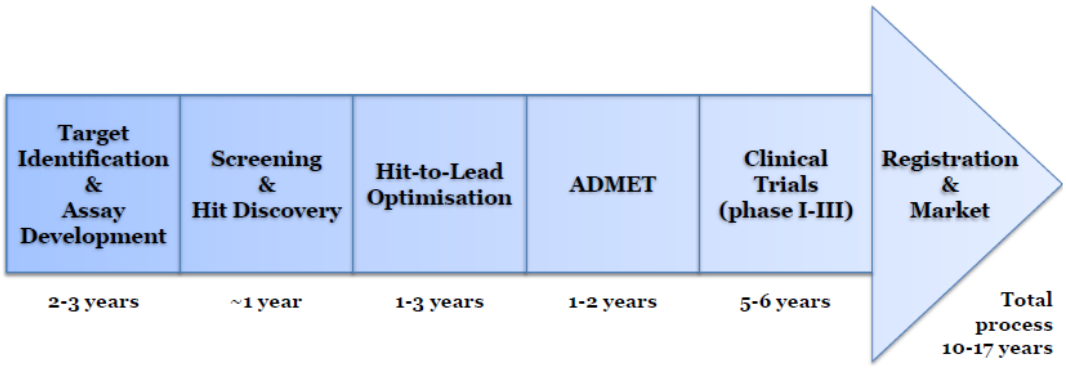

Figure 1.19 The *de novo* drug discovery process
Adapted from reference (*176*).

In 2006 the number of drug targets was estimated at 324, with only 6% of novel therapeutics targeting previously undrugged domains (*177*). Established targets include kinases, proteases, phosphatases, oxidoreductases, phosphodiesterases, transferases, G-protein coupled receptors, nuclear hormone receptors and some ion channels and signalling pathways (*178*). Examples of methods involved in the identification and validation of novel targets include: microarray analysis, bioinformatics, deletion mutants, gene silencing via antisense oligonucleotides and small interfering RNAs (siRNAs), activation and repression of genes with zinc finger proteins, haplotype analysis, and random chemical mutagenesis (*179, 180*).

Once a target has been identified and validated, assay techniques must be developed to assess the effect of potential therapeutics. High-throughput assays are often based on fluorescent or colorimetric techniques as they are fast, highly sensitive and easy to miniaturise for use in a high-throughput format (*181*). Alternative techniques such as

X-ray crystallography (*182*), NMR (*183*), mass spectrometry (*184*), microcalorimetry (*185*) and biosensors (*186*) are generally used in a lower throughput format and, although often obtaining more detailed information, can induce artefacts due to labelling, immobilisation of target or ligand, and acquisition of measurements in gas or solid phase (*187*). The majority of assays are carried out *in vitro* using solution- or cell- based methods (*188*), and validated using a range of techniques which assess accuracy, detection limit, and reproducibility, amongst others (*189*).

Initial hit discovery is usually accomplished via high-throughput screening (HTS), fragment-based screening (FBS), *in silico* screening, or a combination of all three (*190*). *In silico* screening can be used in its own right or to enrich HTS and FBS libraries through 'cherry-picking' structurally diverse compounds to cover the broadest possible range of chemical space, pharmacophore-based screening to identify ligand-like molecules, and docking compounds into the active site of a target to identify the most likely binders (*191, 192*). HTS campaigns tend to employ large compound libraries selected randomly or through *in silico* techniques as described above. However the high rate of false positives and negatives observed in HTS due to non-specific binding, poor solubility, aggregation, reactive functionalities, assay signal interference and experimental error have provided the drive to develop alternative methodologies (*193*).

FBS libraries contain small, structurally diverse 'fragments' which are screened at high concentration to identify low-affinity binders which can be linked together to produce potent leads. The use of far fewer compounds means libraries can be easily pre-filtered to remove compounds with characteristics leading to artefacts in HTS, and that low throughput techniques, such as X-ray crystallography, can be used to identify binding sites and inform lead development (*194, 195*). Alternatively, structural knowledge of the target, privileged scaffolds or scaffold-hopping can be used in the rational design of small focussed libraries with improved chances of success (*196-198*).

Validation of hits identified during screening involves counter-screening to eliminate false positives, such as 'promiscuous binders' (*199*) or compounds interfering with the assay signal, and confirmation of activity via a secondary assay. Depending on resources hit compounds are then re-synthesised and re-tested to ensure that activity is not a result of impurities present in the original sample. Hit-to-lead optimisation involves the determination of hit potency, selectivity, mode of action and ADMET properties, followed by analogue screening to improve these parameters and obtain structure activity relationship (SAR) data. Once a lead compound has been identified, cell based and *in vivo* studies are required to assess pharmacokinetic properties and the potential for progression into clinical trials (*200*).

1.4 Aims of the project

The re-emergent status of plague, the isolation of MDR strains of *Y. pestis* and the risk posed by bioterrorism have led to an increased interest in available treatments for the disease (*24, 26, 28*). The bacterial methyltransferase Dam, which is involved in the regulation of virulence in a range of pathogenic bacteria, has been identified as a potential target for the development of antimicrobial agents (*42, 201*). Dam knockout strains of *Y. pestis* have shown a greater than 2000-fold level of attenuation in mouse models, validating Dam as a target for drug discovery (*40*). In addition, the lack of a functionally similar enzyme in mammals implies that highly selective Dam inhibitors could be developed, reducing the risk of unwanted side-effects (*105*).

A molecular break light Dam activity assay has previously been used in an HTS campaign (*149*), and a real-time version of this assay, suitable for the determination of kinetic parameters, has been developed by the Roach group in a 96 well plate format (*171*). Validation of this assay for HTS has shown it to be highly robust and reproducible, with a Z'-value (*202*) of 0.71 ± 0.07 obtained over three separate 96 well plates. Dam inhibitors have previously been identified using *in silico* docking (*151*), HTS (*149*), genetic selection (*150*), and rational design (*147*) techniques, and libraries employed have included large random libraries of small molecules, potential cancer therapeutics and cyclic peptides, and small focussed libraries of bisubstrate mimics. Our approach involved the application of a combination of these screening techniques and library types to assess their effectiveness and achieve optimal results. In addition counter-screens, validation and specificity assays, potency and mode of binding determination, and *in cell* and toxicity assays, were applied to establish the potential of screening hits as therapeutics.

The objective of the project was to identify compounds that efficiently and selectively inhibit Dam and to assess their potential as antimicrobial compounds. This approach required the optimisation of the real-time molecular break light Dam activity assay to high-throughput screening conditions, and its subsequent use in the screening of both random and focused libraries. Further characterisation of screening hits was achieved through the development and application of assay methodologies for the validation and characterisation of identified hits.

2 Primary Assay Development

2.1 Introduction

2.1.1 Enzyme assays

Enzyme activity can be measured by monitoring the consumption of substrate, or the accumulation of product over time, in an *in vivo* or *in vitro* format. Measurements can be either continuous, monitoring real-time turnover of substrate to product, or discontinuous, determining only the end-point concentrations of reactants and/or products. Whilst continuous assays are more informative, discontinuous assays tend to be favoured for high-throughput applications, due to the ease with which they can be adapted to this format. Ideally enzymatic reactions should be monitored directly; however this requires products or substrates to be spectroscopically active. Where this is not the case, coupled assays, in which a secondary enzyme or derivatising agent is used to convert reactants or products into a readily detectable form, are often applied (*203*).

Typical assay formats include absorbance, luminescence and fluorescence spectroscopy, isothermal titration calorimetry (ITC), radioactivity, and chromatography (*187*). The specific assay methodology selected is dependent on a number of variables, in particular: the cost and availability of reagents, specialist equipment and consumables; the speed of processing; and the level of sensitivity required. Once a format has been selected initial assay parameters, such as measurement detection limits, buffer conditions, temperature, substrate concentrations, coupling enzyme/derivatising agent concentration, target enzyme concentration, and reagent stability are optimised to ensure accurate and reliable assay performance is achieved (*204, 205*).

Assessment of enzyme activity is typically carried out under initial velocity conditions, where less than 10% of the substrate has been depleted, helping to ensure that the reaction proceeds linearly with respect to enzyme concentration and allowing Michaelis-Menten kinetics to be applied (*203, 205*). Where enzyme inhibition is reversible, inhibitors are typically classed as competitive, uncompetitive or noncompetitive with respect to individual substrates (**Figure 2.1**) (*206*). In the case of competitive inhibition, uncompetitive inhibition, and noncompetitive inhibition where $\alpha \neq 1$, the concentration of substrate directly affects the observed inhibition constant (K_i), with higher substrate concentrations favouring uncompetitive inhibitors and lower substrate concentrations favouring competitive inhibitors. Identification of all inhibitor

modalities is therefore best achieved by holding substrate concentrations at or close to K_M (*203, 204*).

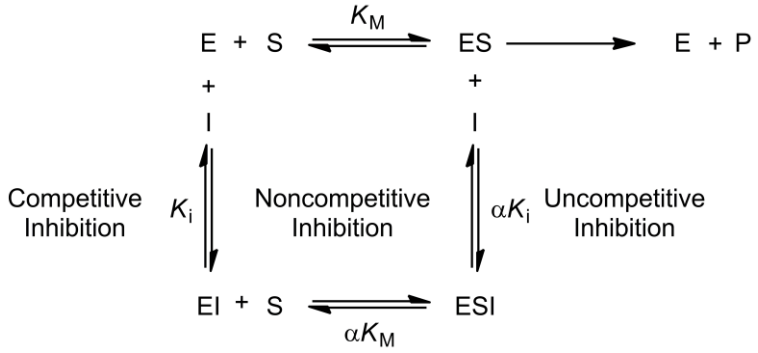

Figure 2.1 Reversible enzyme inhibition in a single substrate system
Where E = enzyme, S = substrate, I = inhibitor, P = product, K_M = the Michaelis-Menten constant, K_i = the dissociation constant for the equilibrium between free and bound enzyme and inhibitor and α = a constant describing the degree to which inhibitor binding affects the affinity of the enzyme for substrate. For competitive inhibition α tends towards ∞, for noncompetitive inhibition $0 < \alpha < \infty$ and for uncompetitive inhibition α tends towards 0.

After initial optimisation, assays are validated to determine their quality and consistency (*189, 205*). Specifically: the effective assay range can be established by determining the linearity of reaction rate with respect to target enzyme concentration; the stability of the target enzyme during the life-time of the assay can be determined by evaluating reaction progress curves at different target enzyme concentrations; and the reproducibility and quality of the assay can be assessed by determining the coefficient of variation (CV, **Equation 2.1**) and effective screening window (Z'-value (*202*), **Equation 2.2** and **Figure 2.3**) over multiple measurements.

$$CV = \frac{\sigma}{\mu} \times 100$$

Equation 2.1 Coefficient of variation
Where μ = average and σ = standard deviation.

$$Z' = 1 - \left(\frac{3\sigma_{(+)} + 3\sigma_{(-)}}{\left| \mu_{(+)} + \mu_{(-)} \right|} \right)$$

Equation 2.2 The Z'-value

Where $\sigma_{(+)}$ = standard deviation of the positive controls, $\sigma_{(-)}$ = standard deviation of the negative controls, $\mu_{(+)}$ = average of the positive controls and $\mu_{(-)}$ = average of the negative controls.

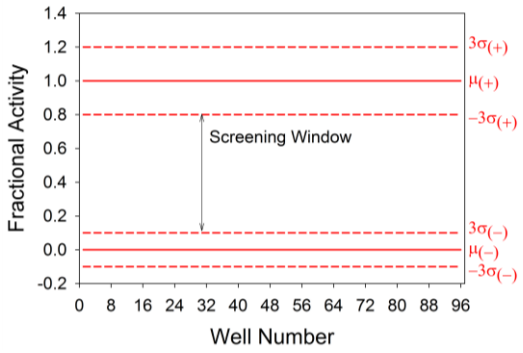

Figure 2.2 The screening window

Parameters as for **Equation 2.2**.

Z'-values of 0.5 and above represent an acceptable screening window and values of 0.7 and above an excellent screening window.

If an assay is to be adapted for high-throughput application, further optimisation and validation is required. Specifically: solvents and reagents used must be compatible with HTS consumables such as microplates and pipette tips; the assay format must be amenable to miniaturisation for use in low volume microplates; equipment used should minimise plate variations such as edge effects and the appropriate controls should be employed to ensure minimal impact on results; and the compound library solvent (typically dimethyl sulfoxide (DMSO)) must be tested for its affect on target enzyme activity and an appropriate concentration of this solvent used for HTS (*205*). Validation is then repeated, with CV and Z'-value determinations used to assess the reproducibility and quality of the assay under HTS conditions.

2.1.2 The real-time break light DNA adenine-N6 methyltransferase activity assay

In the real-time break light Dam activity assay a hemimethylated break light oligonucleotide probe is fully methylated by Dam and subsequently cleaved by the methylation specific restriction enzyme *Dpn*I, producing a fluorescence signal (**Figure 2.3**) (*171*). Including an excess of *Dpn*I in the reaction ensures that restriction is not rate limiting, the fluorescence increase therefore becomes directly proportional to the rate of Dam catalysed methylation and can be used to continuously determine initial rates in real-time.

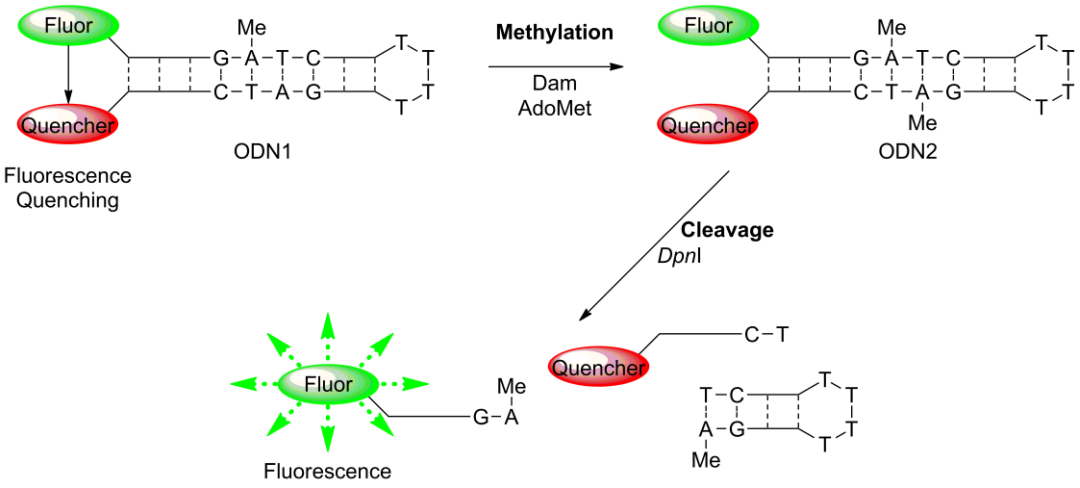

Figure 2.3 Real-time break light Dam activity assay

A hemimethylated break light oligonucleotide substrate (ODN1) containing a GATC methylation site is fully methylated by Dam to form ODN2, which is a substrate for the restriction enzyme *Dpn*I. Cleavage by *Dpn*I results in the separation of fluorophore (fluorescein) and quencher (dabcyl) and a subsequent proportional increase in fluorescence.

Similar assays have been developed using *Dpn*I, or the related methylation sensitive restriction enzyme *Dpn*II, to cleave either fully or unmethylated molecular break light probes (*149, 170*). Neither of these assays allows for continuous real-time monitoring of DNA methylation, with the *Dpn*II assay relying on end-point measurements, and the alternative *Dpn*I assay utilising an unmethylated probe requiring two methylation steps which cannot be easily differentiated. The real-time break light Dam activity assay overcomes these limitations by using a hemimethylated oligonucleotide substrate and an excess of *Dpn*I to enable real-time, continuous monitoring of Dam catalysed methylation.

All three assays require the addition of a secondary enzyme in order to obtain an observable change in fluorescence upon methylation, and as such are classified as

coupled enzyme assays. Problems frequently encountered in coupled assay systems include an observed lag phase in the time course of product formation where the target enzyme is not completely rate limiting, and the identification of false positives with activity against the coupling enzyme in HTS (*203, 204*).

For the primary enzyme to be rate limiting, and to minimise the effect of coupled enzyme inhibition, it is common for the secondary enzyme to be added in excess. This in itself can induce further problems, as increasing coupling enzyme concentration can lead to increased non-specific background activity. When optimising such assays it is therefore necessary to carefully balance assay conditions to ensure the greatest possible signal:noise ratio is achieved. Furthermore, it is essential that the appropriate controls are employed, enabling activity data to be corrected for the effects of background noise (*207*).

The following chapter describes the initial optimisation of the real-time break light Dam activity assay and subsequent optimisation of this assay for use in HTS.

2.2 Protein expression and purification

The aim of this project was to identify inhibitors of *Y. pestis* Dam, which has been validated as a target for the treatment of plague (*40*). Previous attempts at identifying Dam inhibitors have employed the *E. coli* Dam enzyme (*147, 149-151*), which is available commercially (New England Biolabs, UK) and has been expressed and purified by various groups (*99, 105, 208*). Both wild-type and *N*-terminal six-histidine tagged *E. coli* Dam have been kinetically characterised, with minimal difference observed between the two (*105*). It therefore seems probable that the Six-histidine tag has close to no effect on the kinetics of Dam, and as the tagged *Y. pestis* enzyme can be purified much more readily it was used throughout this project.

Although *Y. pestis* Dam shares a considerable sequence similarity (70.5% identity over 271 amino acids) with *E. coli* Dam (**Figure 2.4**) it is preferable to use the target enzyme for the identification of inhibitors, consequently *N*-terminal six-histidine tagged *Y. pestis* Dam has been expressed, purified and kinetically characterised previously in the research group (*171*).

```
Y.pestis_Dam    1 MKKNRAFLKWAGGKYPLVDDIRRHLPAGDCLIEPFVGAGSVFLNTEFESY 50
E.coli_Dam      1 MKKNRAFLKWAGGKYPLLDDIKRHLPKGECLVEPFVGAGSVFLNTDFSRY 50

Y.pestis_Dam   51 ILADINNDLINLYNIVKLRTDDFVRDARVLFTGDFNHSELFYQLRQEFNA 100
E.coli_Dam     51 ILADINSDLISLYNIVKMRTDEYVQAARELFVPETNCAEVYYQFREEFNK 100

Y.pestis_Dam  101 STDAYRRALLFLYLNRHCYNGLCRYNLSGEFNVPFGRYKKPYFPEAELYW 150
E.coli_Dam    101 SQDPFRRAVLFLYLNRYGYNGLCRYNLRGEFNVPFGRYKKPYFPEAELYH 150

Y.pestis_Dam  151 FAEKSQNAVFVCEHYQETLLKAVQGAVVYCDPPYAPLSATANFTAYHTNN 200
E.coli_Dam    151 FAEKAQNAFFYCESYADSMARADDASVVYCDPPYAPLSATANFTAYHTNS 200

Y.pestis_Dam  201 FGIADQQNLARLAYQLSTESKVPVLISNHDTELTRNWYHQAASLHVVTAR 250
E.coli_Dam    201 FTLEQQAHLAEIAEGL-VERHIPVLISNHDTMLTREWY-QRAKLHVVKVR 248

Y.pestis_Dam  251 RTISRNILGRSKVNELLALYS                              271
E.coli_Dam    249 RSISSNGGTRKKVDELLALYK                              269
```

Figure 2.4 Pairwise alignment of *Y. pestis* and *E. coli* Dam
Calculated by percentage identity using the program Jalview (*95, 96*). 100% identity shown in blue.

The coupling enzyme, *Dpn*I, from *Streptococcus pneumoniae* (previously *Diplococcus pneumoniae*) has been expressed and purified in *E. coli* (*209*) and is also available commercially (New England Biolabs, UK). Even though potentially suitable Dam (*E. coli*) and *Dpn*I enzymes were available commercially, both *Y. pestis* Dam and *Dpn*I were purified in the research group to afford tighter control over purity and minimise costs.

2.2.1 Expression and purification of DpnI

An expression system for *Dpn*I was previously prepared by M.D. Maynard-Smith (*210*). Briefly, *N*-terminal six-histidine tagged *Dpn*I expression vector **pMMS/4958/59**, under the control of the arabinose-inducible pBAD expression system, was prepared and transformed into *E. coli* GM43. The optimal growth conditions for protein expression were then determined by small scale expression study.

2.2.1.1 Large scale growth and purification

A large scale growth of *E. coli* GM48 harbouring the *Dpn*I expression vector, **pMMS/4958/59**, under optimised conditions yielded 5.2 g of cell paste per litre of culture. After cell lysis by sonication purification of the cleared lysate by nickel affinity column chromatography was monitored by Bradford Assay (*211*) and fractions with a protein concentration of greater than 0.75 mg ml^{-1} were pooled and dialysed. The purification yielded 9.8 mg of purified *Dpn*I from 7 g of cell paste (1.4 mg g^{-1}); however SDS-PAGE analysis of the individual and pooled fractions (**Figure 2.5**) showed the sample to be contaminated by two lower molecular weight proteins.

The molecular weight of *Dpn*I (~30 kDa) is approximately equal to the sum of the molecular weights of the contaminants (~12 and 17 kDa), suggesting that *Dpn*I had undergone proteolytic cleavage during expression and purification (**Figure 2.5**). To circumvent this process, growth time was reduced and protease inhibitor tablets and phenylmethylsulfonyl fluoride (PMSF (*212*)) were added to the cell lysis buffer and purification column wash buffers.

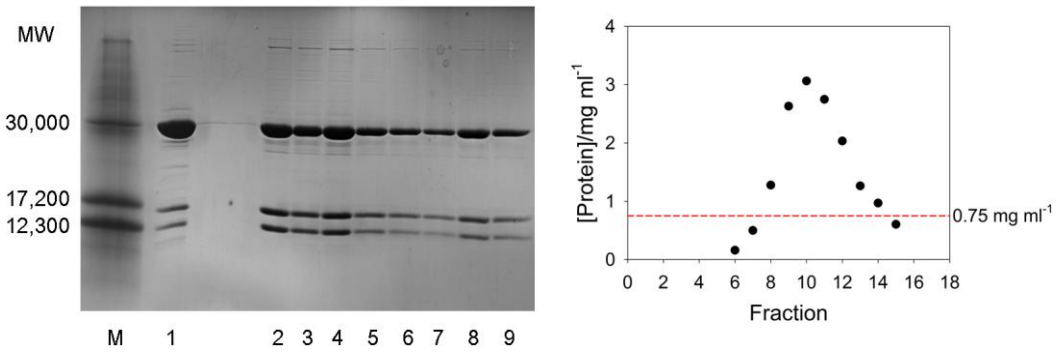

Figure 2.5 *Dpn*I purification

SDS-PAGE gel (left) and graph of protein concentration versus fraction number (right) of initial *Dpn*I purification.

(M): marker, (1): *Dpn*I standard[1], (2): pooled fractions 8-14, (3-9): fractions 8-14.

[1] *Dpn*I expressed and purified by M. D. Maynard-Smith.

A second large scale growth of *E. coli* GM48 harbouring the *Dpn*I expression vector, **pMMS/4958/59**, was carried out, with the time between induction and cell harvest reduced from 4 to 3 hours. A yield of 4.7 g of cell paste per litre of culture was obtained from the second growth, comparable to the yield obtained from the first growth (**Table 2.1**). The cleared lysate was purified by nickel affinity column chromatography, using cell lysis and wash buffers supplemented with protease inhibitor tablets and PMSF. The protein concentration was monitored by Bradford Assay (*211*) and fractions with a protein concentration of greater than 0.25 mg ml^{-1} were analysed by SDS-PAGE, pooled and dialysed. The purification yielded a total of 27 mg of protein from 10 g of cell paste (2.7 mg g^{-1}), with SDS-PAGE analysis (**Figure 2.6**) showing a reduction in the proteolysis of *Dpn*I compared with the initial purification.

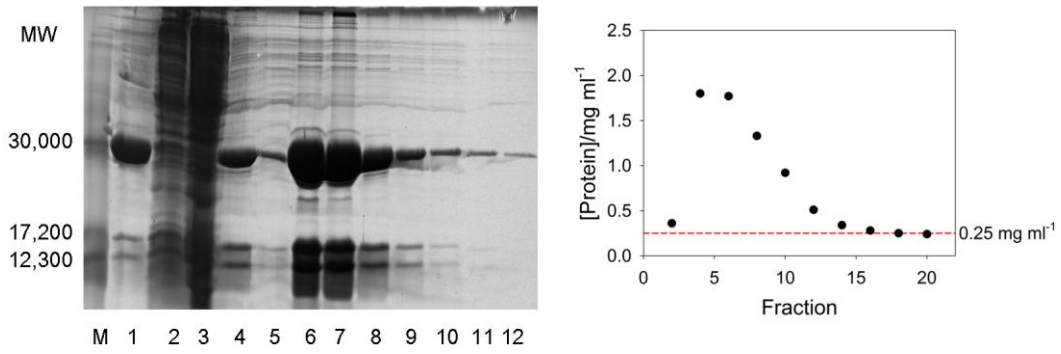

Figure 2.6 *Dpn*I purification II

SDS-PAGE gel (left) and graph of protein concentration versus fraction number (right) of *Dpn*I purification II.

(M): marker, (1): *Dpn*I standard[1], (2): supernatant, (3): flow-through, (4): pooled fractions 2-16, (5-12): fractions 2-16.

Table 2.1 Protein yields from *Dpn*I purifications

Growth time hrs	Source	[Protein] mg ml^{-1}	Volume ml	Total Protein mg
4	Lysate (from 7 g of cell paste)	22	30	660
	Purified protein	0.96	10	9.6
3	Lysate (from 10 g of cell paste)	26	30	780
	Purified protein	1.4	20	27

Data given to 2 significant figures

The specific (cleavage of a fully methylated oligonucleotide substrate) and non-specific (cleavage of a hemimethylated oligonucleotide substrate) activities of *Dpn*I from both purifications (*Dpn*I^{A} and *Dpn*I^{B}) and a *Dpn*I standard[2] (*Dpn*I^{std}) were assessed by real-time break light *Dpn*I activity assay (**Table 2.2**). Both *Dpn*I^{A} and *Dpn*I^{B} were found to have similar specific and non-specific activities, whilst the specific and non-specific activities of *Dpn*I^{std} were considerably higher, possibly due to small differences in purification method. Although little difference in specific:non-specific activity ratio was observed for the freshly prepared samples, *Dpn*I^{B} was shown by SDS-PAGE to be of higher purity than *Dpn*I^{A}, having undergone less proteolytic cleavage. *Dpn*I^{B} (referred to from this point forward as *Dpn*I) was therefore used in all subsequent activity assays.

Table 2.2 Activity of purified *Dpn*I samples

Sample	Specific Activity*† pmol s^{-1} μg^{-1}	Non-specific Activity#† pmol s^{-1} μg^{-1}	Ratio Specific:Non-specific Activity‡
*Dpn*I^{A}	6.77 ± 0.47	1.03 ± 0.07	6.6
*Dpn*I^{B}	4.58 ± 0.09	0.650 ± 0.024	7.0
*Dpn*I^{std}	24.0 ± 1.0	2.19 ± 0.03	11

* Fully methylated substrate, 0.08 nM *Dpn*I.

\# Hemimethylated substrate, 0.8 nM *Dpn*I.

† Average of triplicate measurements ± standard deviation.

‡ Given to 2 significant figures.

Assay conditions: 0.08 nM or 0.8 nM *Dpn*I, 300 nM fully methylated (ODN2) or hemimethylated (ODN1) oligonucleotide, 25 µM AdoMet, 20 mM Tris, 50 mM KOAc, 10 mM $Mg(OAc)_2$, 20 mM NaCl, 0.1 mg ml^{-1} BSA, 1 mM DTT, pH 7.9. Total assay volume 100 µl, in 96 well plate, gain 100, temperature 30 ˚C.

[2] *Dpn*I expressed and purified by M.D. Maynard-Smith *(210)*.

2.2.2 Expression and purification of Y. pestis Dam

2.2.2.1 Selection of an expression system

The overexpression of Dam has been shown to affect the virulence of a number of different pathogens (*87-89*) and may prove toxic to host cells. To minimise the effects of high Dam concentrations on host cells, *dam* mutant strains (lacking the chromosomal copy of *dam*) of *E. coli* were selected for the overexpression of *Y. pestis* Dam. *N*-terminal six-histidine tagged *Y. pestis* Dam was expressed from the **pBAD/HisA** derivative **pRJW/4213/07**, originally prepared by Dr R.J. Wood (*171*). The plasmid was transformed into the *E. coli dam* knockout strains GM2929 and ER2925. Negative controls of **pBAD/HisA** transformed into both *E. coli* strains were also prepared.

To confirm that no Dam was being expressed prior to induction of the arabinose-regulated pBAD expression system plasmids were isolated from cultures of transformed *E. coli* and digested with the restriction enzymes *Nco*I, *Dpn*I and *Mbo*I to confirm their mwthylation state. The results were analysed by 1% agarose gel electrophoresis (**Figure 2.7**).

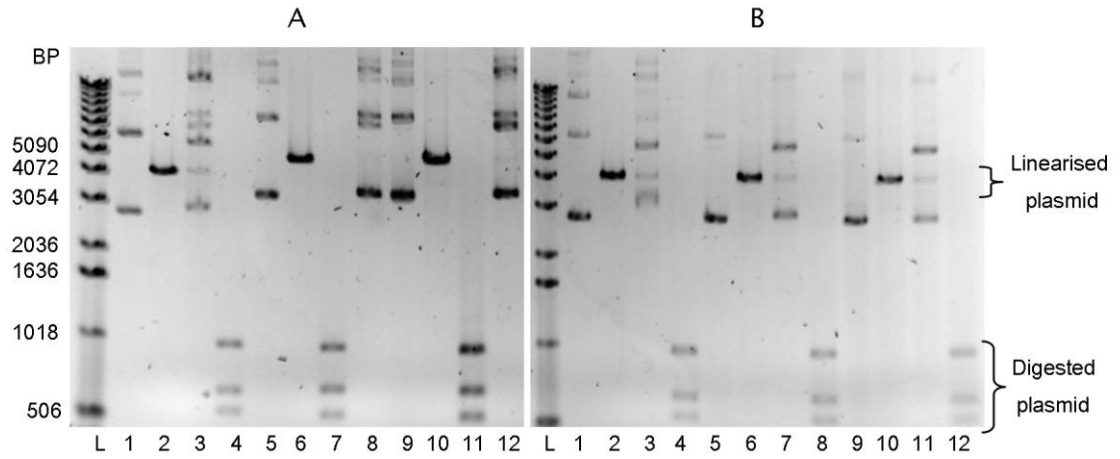

Figure 2.7 pRJW4213/07 and pBAD/HisA analytical digests
1% agarose gel electrophoresis of plasmids isolated from GM2929 (A) and ER2925 (B) *E. coli* and digested with *Nco*I, *Dpn*I or *Mbo*I.
(L): Ladder, (1-4): **pBad/HisA**, (5-12): **pRJW4213/07**, (1, 5 and 9): unlinearised plasmid, (2, 6 and 10): *Nco*I digested plasmid, (3, 7 and 11): *Dpn*I digested plasmid, (4, 8 and 12): *Mbo*I digested plasmid.

The control samples showed no *Dpn*I digestion, confirming that no Dam methylation occurs in either *E. coli* GM2929 or ER2925 in the absence of the *Y. pestis* Dam expression plasmid **pRJW/4213/07**. Samples of **pRJW/4213/07** isolated from *E. coli* GM2929 were digested by *Mbo*I, but not *Dpn*I, indicative of an unmethylated plasmid.

However samples of **pRJW/4213/07** isolated from *E. coli* ER2925 were digested by *Dpn*I, but not *Mbo*I, indicating that the plasmid was fully methylated. This result suggests that in *E. coli* ER2925, *Y. pestis* Dam was expressed prior to the induction of the arabinose-regulated pBAD expression system. Both ER2925 and GM2929 were derived from the same original strain (GM2163) and differ only slightly in genotype[3]. It is therefore surprising that uninduced expression was only observed for ER2925. To investigate the effects of uninduced expression on the final yield of *Y. pestis* Dam from an induced system, both transformed strains were carried forward for large scale growth and purification.

2.2.2.2 Large scale growth and purification

Small scale expression studies of *E. coli* strains ER2925 and GM2929 harbouring the *Y. pestis* Dam expression vector **pRJW/4213/07**, showed very low levels of *Y. pestis* Dam expression and could not be used to determine optimal growth conditions prior to large scale expression. The optical density at 600 nm (OD_{600}) was therefore used to determine when a stationary phase in *E.* coli growth had been reached, at which point cells were harvested (**Figure 2.8**). GM2929 cells were harvested at 290 minutes, yielding 5.14 g of cell paste per litre of culture, and ER2925 cells were harvested at 320 minutes, yielding 7.84 g of cell paste per litre of culture.

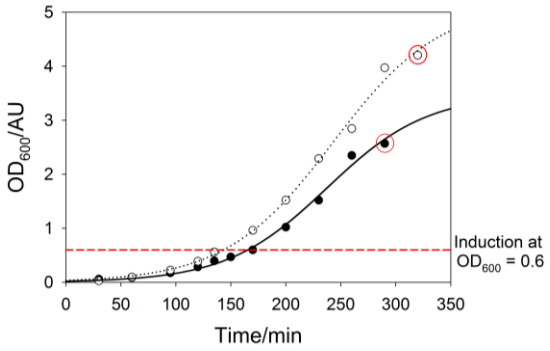

Figure 2.8 Growth curves for *E. coli* GM2929 and ER2925 harbouring **pRJW/4213/07** Data were fitted to a sigmoidal curve of the form f = a/(1+exp(-(x-x0)/b)). GM2929 growth (filled circles, solid line), ER2925 growth (open circles, dotted line), induction at OD_{600} = 0.6 (dashed red line), cells harvested at circled data point.

Cells were lysed by sonication and the protein purified from the cleared lysate by nickel affinity column chromatography and the protein content of eluted fractions determined by Bradford Assay (*211*). Fractions with a protein concentration of at least

[3] ER2925 carries the *endA1* mutation which abolishes the activity of nonspecific endonuclease I, whereas GM2929 carries the *recF143* mutation, making it deficient for plasmid recombination.

0.15 mg ml^{-1} were analysed by SDS-PAGE (**Figure 2.9**), pooled, dialysed into storage buffer and stored at -80 ˚C until required. The yields of purified protein obtained from each expression strain are tabulated overleaf (**Table 2.3**).

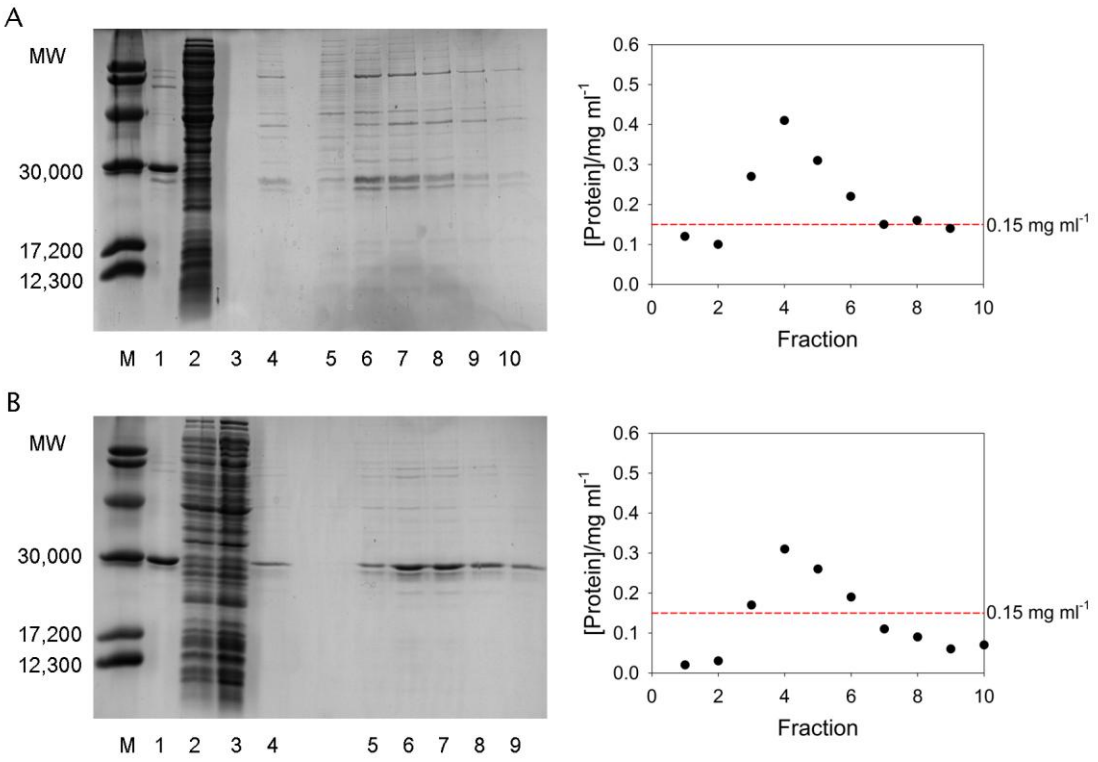

Figure 2.9 *Y. pestis* Dam purification

SDS-PAGE gels (left) and graphs of protein concentration versus fraction number (right) for GM2929 (A) and ER2925 (B) purifications.

(M): marker, (1): *Y. pestis* Dam standard[4], (2): supernatant, (3): flow-through, (4A): pooled GM2929 fractions 3-8, (4B): pooled ER2925 fractions 3-6, (5-10A): fractions 3-8, (5-9B): fractions 3-6.

Table 2.3 Protein yields from *Y. pestis* Dam purifications

Expression Strain	Source	[Protein] mg ml^{-1}	Volume ml	Total Protein mg
E. coli GM2929	Lysate (from 10 g of cell paste)	25	30	750
	Purified protein	0.27	10	2.7
E. coli ER2925	Lysate (from 10 g of cell paste)	20	30	600
	Purified protein	0.15	6.5	0.98

Data given to 2 significant figures

[4] *Y. pestis* Dam expressed and purified by M. D. Maynard-Smith.

A higher yield of protein was obtained from the GM2929 expression and purification, however the protein isolated from ER2925 cells was shown to be of higher purity. The activity of the *Y. pestis* Dam protein obtained from both purifications (Dam^{GM2929} and Dam^{ER2925}) was assessed alongside a *Y. pestis* Dam reference sample[4] (Dam^{std}). A short lag phase was observed in the assay time courses, most likely due to the addition of an insufficient concentration of the coupled enzyme, *Dpn*I. As this issue would be resolved during assay optimisation the lag phase was discounted and activity determined from the data obtained immediately after it. Total and non-specific (as determined for negative controls lacking *Dpn*I) activities for each protein sample are tabulated below (**Table 2.4**).

Table 2.4 Activity of purified *Y. pestis* Dam samples

Sample	Total Activity* pmol s^{-1} μg^{-1}	Non-specific Activity# pmol s^{-1} μg^{-1}	Ratio Total:Non-specific Activity†
Dam^{GM2929}	0.0216 ± 0.0028	0.0171	1.3
Dam^{ER2925}	0.0729 ± 0.0036	0.0128	5.7
Dam^{std}	0.189 ± 0.033	ND	-

* Average of triplicate measurements ± standard deviation.

Single measurement.

† Given to 2 significant figures.

ND – not detectable.

Assay conditions: 2 nM Dam, 0.8 nM *Dpn*I, 30 nM hemimethylated oligonucleotide (ODN1), 25 µM AdoMet, 20 mM Tris, 50 mM KOAc, 10 mM $Mg(OAc)_2$, 20 mM NaCl, 0.1 mg ml^{-1} BSA, 1 mM DTT, pH 7.9. Total assay volume 100 µl, in 96 well plate, gain 130, temperature 30 °C.

The similar total and non-specific activities observed for Dam^{GM2929} imply that minimal active *Y. pestis* Dam was purified from the GM2929 expression system. The higher total:non-specific activity ratio observed for Dam^{ER2925} compared to Dam^{GM2929} suggests that *Y. pestis* Dam of higher activity and specificity was obtained from the ER2925 expression system, however a significant level of non-specific activity was also observed for this sample. *Y. pestis* Dam isolated from ER2925 cells was therefore carried forward for further optimisation.

2.2.2.3 Improving Y. pestis Dam specific activity

A second purification was investigated to improve the specific activity of Dam^{ER2925}. The detergent Triton X-100 was added to cell lysis and column wash buffers, in order to disrupt protein:protein interactions and increase the proportion of impurities removed prior to elution. Fractions with a protein concentration of at least 0.08 mg ml^{-1} were analysed by SDS-PAGE (**Figure 2.10**), pooled fractions were then dialysed and stored at -80 ˚C until required. The second ER2925 purification yielded 0.72 mg of protein from 8.5 g of cell paste (0.084 mg g^{-1}), comparable with the yield of 0.098 mg g^{-1} obtained for the initial purification.

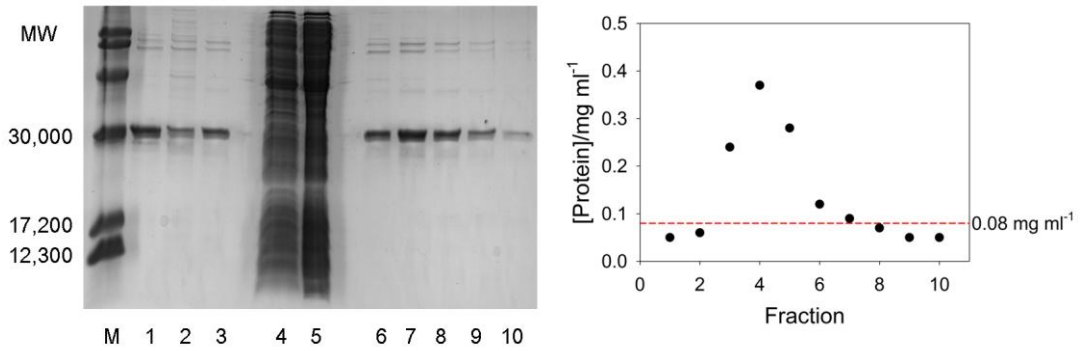

Figure 2.10 ER2925 *Y. pestis* Dam purification II

SDS-PAGE gel (left) and graph of protein concentration versus fraction number (right) of ER2925 purification II.

(M): marker, (1): *Y. pestis* Dam^{std}, (2): Dam^{ER2925}, (3): pooled fractions 3-7, (4): supernatant, (5): flow-through, (6-10): fractions 3-7.

Comparison of *Y. pestis* Dam from the first and second purification (Dam^{ER2925} and Dam$^{ER2925/2}$) by SDS-PAGE showed Dam$^{ER2925/2}$ to contain fewer contaminating proteins. No non-specific activity was detected for Dam$^{ER2925/2}$ (under assay conditions as for **Table 2.4**) and the total activity of Dam$^{ER2925/2}$ was found to be 0.0942 ± 0.0118 pmol s^{-1} µg^{-1}, compared with 0.0729 ± 0.0036 pmol s^{-1} µg^{-1} for the initial purification. The addition of detergent to cell lysis and column wash buffers during purification therefore significantly improved the ratio of total:non-specific activity whilst not significantly decreasing purification yield. Dam$^{ER2925/2}$ (referred to from this point forward as *Y. pestis* Dam) was therefore used in all subsequent activity assays.

2.3 Optimisation

Specific assay parameters to be optimised included: buffer conditions, substrate concentrations, enzyme concentrations, temperature, enzyme stability, assay volume, and the effect of compound library solvent on enzyme activity. Conditions were carefully balanced to obtain the optimal screening window by maximising the specific activities of the target and coupling enzyme, whilst minimising non-specific activity. Validation of conditions included assessment of signal:noise ratios (**Equation 2.3**), size of screening window (Z-value, **Equation 2.2**), and reproducibility (CV, **Equation 2.1**).

$$\text{Signal:Noise Ratio} = \frac{v_T - v_{BG}}{v_{BG}}$$

Equation 2.3 Signal:noise ratio
Where v_T = initial rate of full assay and v_{BG} = initial rate of negative controls.

As parameters must be varied separately in order to ascertain their individual affects on assay quality, optimisation can be a complex process. It is therefore helpful to have an initial set of conditions from which to start, with parameters optimised one-by-one until the final assay conditions are determined. **Table 2.5**, below, lists initial conditions for the real-time break light Dam activity assay, as employed previously for the kinetic characterisation of *Y. pestis* Dam (*171*).

Table 2.5 Initial conditions for real-time break light Dam activity assay

Parameter	Initial Conditions
Buffer	NEBuffer 4: [20 mM Tris-acetate, 50 mM potassium acetate, 10 mM magnesium acetate, 1 mM dithiothreitol, 0.1 mg ml^{-1} bovine serum albumin, pH 7.9]
Substrate concentrations	K_M^{AdoMet} = 11.3 ± 0.63 µM K_M^{DNA} = 3.43 ± 1.68 nM
Enzyme concentrations	*Y. pestis* Dam = 2 nM *Dpn*I = 3 U (~0.8 nM)
Volume	100 µl (96 well plate)
Temperature	30 ˚C

2.3.1 Buffer conditions

Assay buffers generally contain a buffering agent, mono- and di- valent cations, and a range of additives. Previously the general buffer NEBuffer 4 (New England Biolabs, UK, **Table 2.4**) was used in the real-time break light Dam activity assay, demonstrating the effectiveness of a Tris-based buffer system. To assess the effects of other components on overall assay quality a buffer comprising of Tris-HCl at pH 7.9, the reducing agent dithiothreitol (DTT), and the non-specific blocking agent bovine serum albumin (BSA), was employed, whilst mono- and di-valent salt concentrations were varied independently.

2.3.1.1 Sodium chloride concentration

High concentrations of sodium ions (above 50 mM) have been shown to increase the specificity of *Dpn*I for the fully methylated product of Dam methylation, over the hemimethylated substrate (*213*). Whilst concentrations below 100 mM have been shown to have minimal effect on Dam activity (*208*).

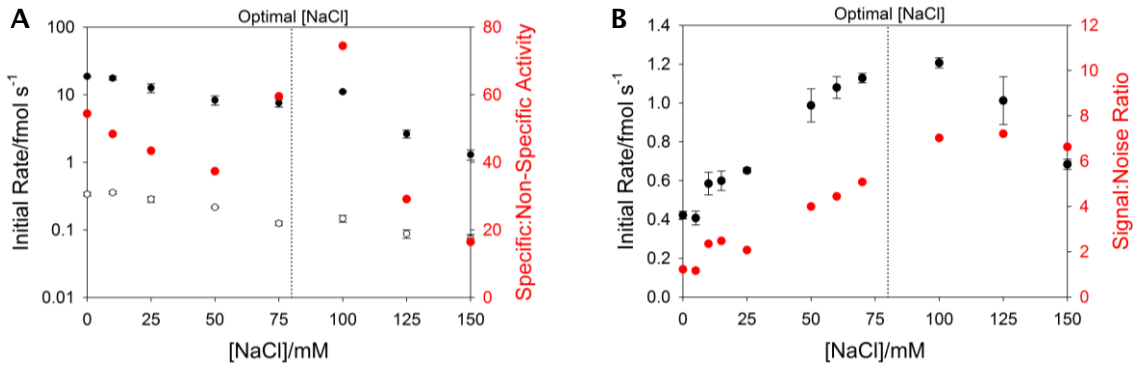

Figure 2.11 Sodium chloride concentration optimisation

A: Specific initial rate of cleavage of fully methylated product (filled circles) and non-specific initial rate of cleavage of hemimethylated substrate (open circles) by *Dpn*I, and ratio of specific:non-specific activity (red circles).

Assay conditions: 0.8 nM *Dpn*I, 30 nM fully methylated (ODN2) or hemimethylated (ODN1) oligonucleotide, 25 µM AdoMet, 0-150 mM NaCl, 20 mM Tris, 10 mM $MgCl_2$, 0.1 mg ml^{-1} BSA, 1 mM DTT, pH 7.9. Total assay volume 100 µl, in 96 well plate, gain 130, temperature 30 ˚C.

B: Background subtracted initial rate of methylation by *Y. pestis* Dam (black) and signal:noise ratio (red).

Assay conditions: 2 or 0 nM *Y. pestis* Dam, 0.8 nM *Dpn*I, 30 nM hemimethylated oligonucleotide (ODN1), 25 µM AdoMet, 0-150 mM NaCl, 20 mM Tris, 10 mM $MgCl_2$, 0.1 mg ml^{-1} BSA, 1 mM DTT, pH 7.9. Total assay volume 100 µl, in 96 well plate, gain 130, temperature 30 ˚C.

The effect of varying sodium chloride concentration on *Y. pestis* Dam and *Dpn*I activity was assessed (**Figure 2.11**) and both specific and non-specific *Dpn*I activity were found to be reduced by the addition of sodium chloride (**Figure 2.11A**). In the full assay (**Figure 2.11B**) concentrations of up to 100 mM sodium chloride appeared to improve both specific activity and signal:noise ratio. The maximum initial activity and signal:noise ratio were observed between 75 and 125 mM sodium chloride, with a more rapid reduction in activity observed after 100 mM than before. To preserve enzyme activity and maximise signal:noise ratio, a sodium chloride concentration of 80 mM was selected, at which small variations in concentration would have minimal effect on activity.

2.3.1.2 Magnesium chloride concentration

As a type II restriction enzyme *Dpn*I requires divalent metal ions, most commonly magnesium ions, to catalyse the cleavage of DNA (*214*). The effect of magnesium ions on Dam activity has not been reported.

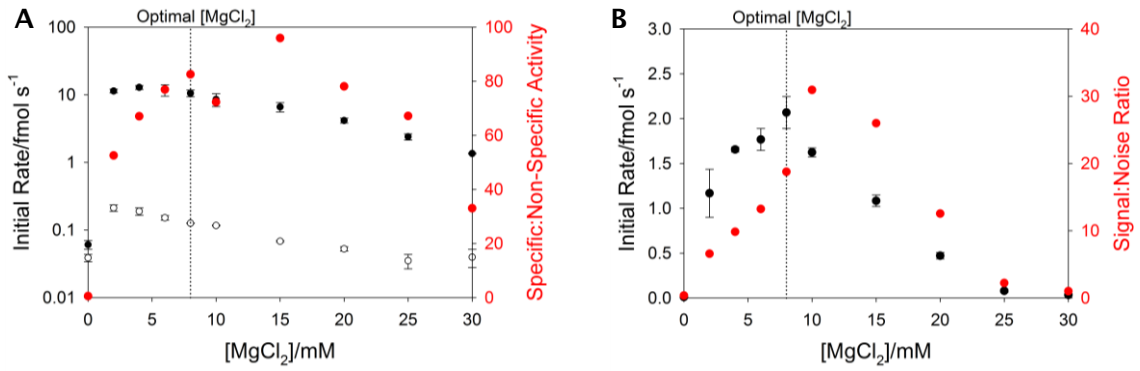

Figure 2.12 Magnesium chloride concentration optimisation

A: Specific initial rate of cleavage of fully methylated product (filled circles) and non-specific initial rate of cleavage of hemimethylated substrate (open circles) by *Dpn*I, and ratio of specific:non-specific activity (red circles).

Assay conditions: 0.8 nM *Dpn*I, 30 nM fully methylated (ODN2) or hemimethylated (ODN1) oligonucleotide, 25 µM AdoMet, 0-30 mM $MgCl_2$, 20 mM Tris, 80 mM NaCl, 0.1 mg ml^{-1} BSA, 1 mM DTT, pH 7.9. Total assay volume 100 µl, in 96 well plate, gain 130, temperature 30 ˚C.

B: Background subtracted initial rate of methylation by *Y. pestis* Dam (black) and signal:noise ratio (red).

Assay conditions: 2 or 0 nM *Y. pestis* Dam, 0.8 nM *Dpn*I, 30 nM hemimethylated oligonucleotide (ODN1), 25 µM AdoMet, 0-30 mM $MgCl_2$, 20 mM Tris, 80 mM NaCl, 0.1 mg ml^{-1} BSA, 1 mM DTT, pH 7.9. Total assay volume 100 µl, in 96 well plate, gain 130, temperature 30 ˚C.

Y. pestis Dam and *Dpn*I activity assays carried out at a range of magnesium chloride concentrations (**Figure 2.12**) showed *Dpn*I activity to be dependent on a low concentration (~2-6 mM) of magnesium chloride, with concentrations up to 15 mM increasing the ratio of specific:non-specific cleavage. In the full assay maximum signal was obtained between 6 and 10 mM magnesium chloride, whilst the optimum signal:noise ratio was achieved between 8 and 15 mM. A final assay concentration of 8 mM magnesium chloride was therefore selected to ensure optimal enzyme activity whilst maintaining a good signal:noise ratio.

2.3.1.3 Additives

Dam activity assays were routinely supplemented with two additives: BSA was added to reduce non-specific binding interactions, and DTT was added to ensure thiols remained reduced (*215*). Additionally, glycerol is often added to buffers to help stabilise proteins in solution (*216, 217*); however glycerol is also known to affect the specificity of restriction enzymes, with high concentrations inducing non-specific or 'star' activity (*218*). To achieve the stabilisation effect of glycerol whilst minimising the risk of 'star' activity, a small quantity of glycerol (5%) was also added to the real-time break light Dam activity assay buffer.

2.3.2 Assay temperature

The temperature at which an assay is incubated affects enzyme and substrate stability, as well as reaction rates. The achievement of the maximum initial rate may require the application of incubation temperatures at which the enzyme(s) and/or substrate(s) are unstable, making the assessment of initial rate data potentially difficult. To determine the optimum assay temperature for the real-time break light Dam activity assay a series of assays were carried out at a range of temperatures (**Figure 2.13**).

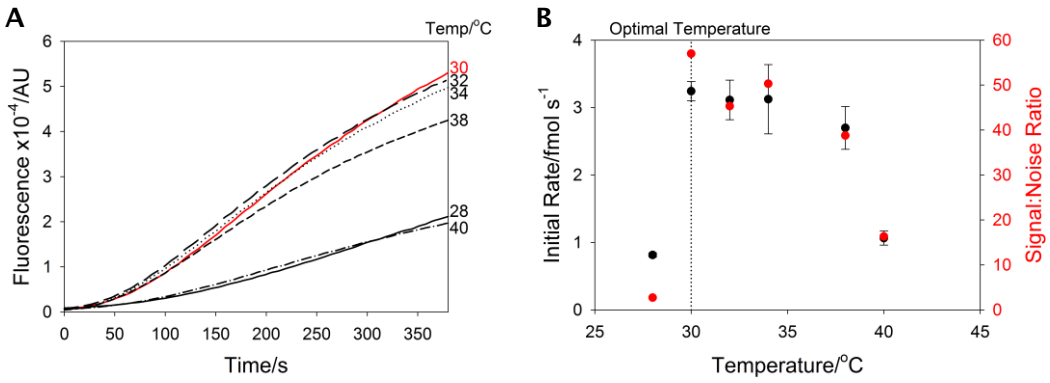

Figure 2.13 Temperature optimisation

A: Activity assay time course

B: Background subtracted initial rate of methylation by *Y. pestis* Dam (black) and signal:noise ratio (red).

Assay conditions: 1 or 0 nM *Y. pestis* Dam, 0.8 nM *Dpn*I, 10 nM hemimethylated oligonucleotide (ODN1), 25 µM AdoMet, 20 mM Tris, 80 mM NaCl, 8 mM $MgCl_2$, 1 mM DTT, 0.1 mg ml^{-1} BSA, 5% glycerol, pH 7.9. Total assay volume 100 µl, in 96 well plate, gain 130.

Temperature (˚C): 28 (black solid line), 30 (red solid line), 32 (black long dash line), 34 (black dotted line), 38 (black short dash line), or 40 (black dash and dotted line).

An increase in initial activity and signal:noise ratio was observed between 28 and 30 ˚C, and a decrease was observed between 30 and 40 ˚C (**Figure 2.13B**). The time courses show the fluorescence reached after 380 seconds to be greatest for the assay carried out at 30 ˚C, with assays carried out at 32 ˚C and above showing a loss of enzyme activity over time (**Figure 2.13A**). To maintain enzyme activity whilst maximising initial rate an assay temperature of 30 ˚C was selected, which correlates well with the optimal temperature for the growth of *Y. pestis* bacteria (30 ˚C (*23*)).

2.3.3 Enzyme concentration and stability

2.3.3.1 Coupling enzyme concentration

In general, an insufficient quantity of coupling enzyme will lead to an increasingly significant lag phase during a coupled assay (*219*). This was observed for the *Dpn*I coupled Dam activity assay (Sections 2.2.1, 2.2.2 and 2.3.2). Lag phases generally make the determination of initial rate data more challenging, and in some cases, where the lag phase exceeds the initial rate phase, impossible.

Evaluation of the effect of coupled enzyme concentration on overall rate (**Figure 2.14A**) shows that at 2 nM *Dpn*I initial rate reaches 99.8% of the maximum (as determined by fitting the data to an exponential rise to a maximum). Furthermore, 50% inhibition of *Dpn*I at this concentration (equivalent to 1 nM) would lead to only a minimal drop in initial rate, with 95.8% of the maximum rate still reached. Increasing *Dpn*I concentration leads to a decrease in signal:noise ratio (**Figure 2.14B**), due to an increase in non-specific cleavage of the hemimethylated substrate oligonucleotide. There is therefore a delicate balance to be struck between adding too much *Dpn*I (resulting in excessive non-specific cleavage) and too little (resulting in a significant lag phase). The selected compromise concentration (2 nM) was selected to minimise the effects of non-specific cleavage on signal:noise ratio.

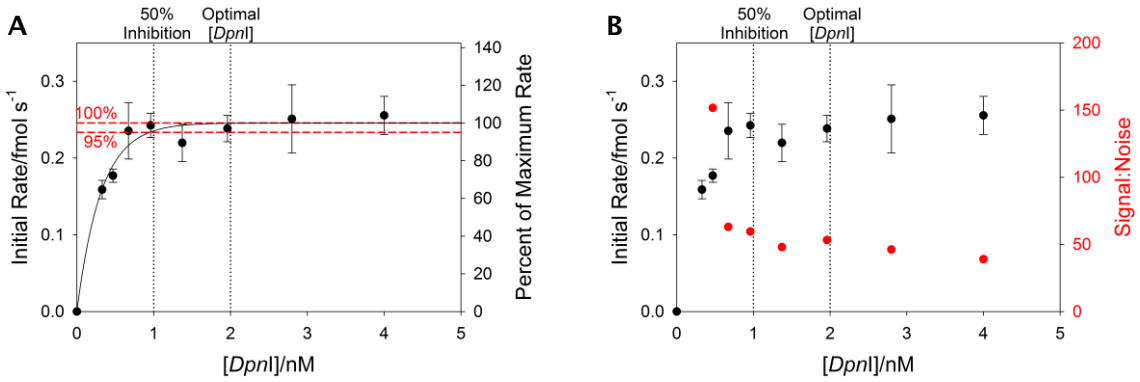

Figure 2.14 *Dpn*I concentration optimisation

A: Background subtracted initial rate of methylation by *Y. pestis* Dam. Data fitted to an exponential rise to a maximum of the form f=a*(1-exp(-b*x)).

B: Background subtracted initial rate of methylation by *Y. pestis* Dam (black) and signal:noise ratio (red).

Assay conditions: 1 nM *Y. pestis* Dam, 0-4 nM *Dpn*I, 10 nM hemimethylated oligonucleotide (ODN1), 25 or 0 µM AdoMet, 20 mM Tris, 80 mM NaCl, 8 mM $MgCl_2$, 1 mM DTT, 0.1 mg ml^{-1} BSA, 5% glycerol, pH 7.9. Total assay volume 20 µl, in 384 well plate, gain 170, temperature 30 ˚C.

2.3.3.2 Primary enzyme concentration

The classical kinetic model for enzyme catalysis requires that the enzyme is present at very low concentrations relative to the substrate. Addition of insufficient substrate or excess enzyme can lead to significant deviation from this condition, substantially complicating the kinetic analysis. By monitoring the effect of increasing *Y. pestis* Dam concentration on initial rate the effective range of the real-time break light Dam activity assay was established (**Figure 2.15**).

Initial rate was plotted against *Y. pestis* Dam concentration (**Figure 2.15**) and a line of best fit was plotted through data points correlating to 0.25 nM *Y. pestis* Dam and above. A negative y-axis intercept was observed, indicating a lower *Y. pestis* Dam concentration limit at the x-axis intercept (~0.276 nM). At higher concentrations of *Y. pestis* Dam a linear plot was observed, suggesting an upper concentration limit of greater than 4 nM. The non-linear reduction in rate observed for lower *Y. pestis* Dam concentrations could be caused by a number of factors, including the signal detection limit being reached, and the loss of a small amount of enzyme through non-specific binding or denaturation.

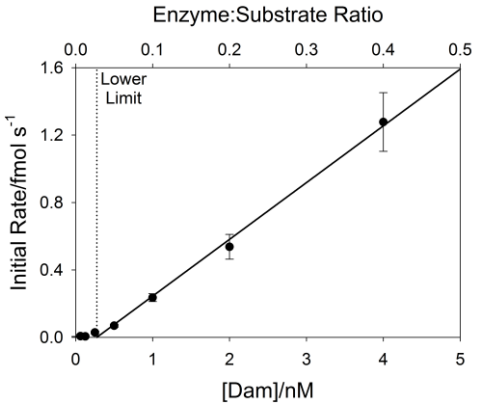

Figure 2.15 Effective assay range

Background subtracted initial rate of methylation by *Y. pestis* Dam. Data fitted to a linear equation of the form $f=y_0+a*x$.

Assay conditions: 0-4 nM *Y. pestis* Dam, 2 nM *Dpn*I, 10 nM hemimethylated oligonucleotide (ODN1), 25 or 0 µM AdoMet, 5% DMSO, 20 mM Tris, 80 mM NaCl, 8 mM $MgCl_2$, 1 mM DTT, 0.1 mg ml^{-1} BSA, 5% glycerol, pH 7.9. Total assay volume 20 µl, in 384 well plate, gain 170, temperature 30 ˚C.

Whilst *Y. pestis* Dam concentrations of up to 4 nM were accommodated under the conditions of this experiment (**Figure 2.15** legend) it is common practise to use a minimum of a 10-fold excess of substrate(s) to enzyme (*205, 219*). In this case 10 nM DNA and 25 µM AdoMet were used, suggesting an optimum *Y. pestis* Dam

concentration of 1 nM, which falls within the effective assay range as shown in **Figure 2.15**. A *Y. pestis* Dam concentration of at most one-tenth the lowest substrate concentration was therefore selected for all subsequent assays.

2.3.3.3 Stability

Temperature optimisation assays (Section 2.3.2, **Figure 2.13A**) showed a temperature dependant loss of enzyme activity over time. As *Y. pestis* has a lower optimal growth temperature than *S. pneumoniae* (30 versus 37 ˚C (*23, 220*)) and the suggested reaction temperature for commercially available *Dpn*I is 37 ˚C, it was hypothesised that the loss in activity observed was due to the inactivation of *Y. pestis* Dam. To test this theory *Y. pestis* Dam was incubated with and without substrates and the effect on initial rate assessed over a range of time points.

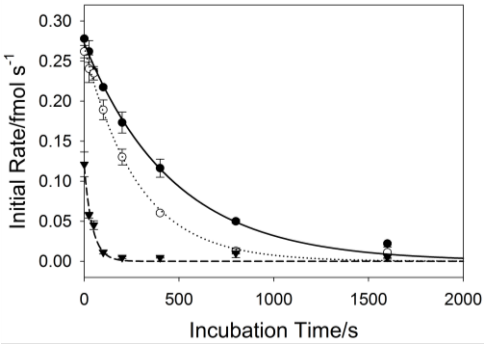

Figure 2.16 Inactivation of *Y. pestis* Dam
Initial rate of methylation by *Y. pestis* Dam incubated with DNA (filled circles), AdoMet (open circles) or no substrates (filled triangles) at 30 ˚C for 0-1600 s prior to assay initiation. Data fitted to an exponential decay curve of the form f = a*exp(-b*x).
Assay conditions: 1 nM *Y. pestis* Dam, 2 nM *Dpn*I, 10 nM hemimethylated oligonucleotide (ODN1), 25 or 0 µM AdoMet, 5% DMSO, 20 mM Tris, 80 mM NaCl, 8 mM $MgCl_2$, 1 mM DTT, 0.1 mg ml^{-1} BSA, 5% glycerol, pH 7.9. Total assay volume 20 µl, in 384 well plate, gain 170, temperature 30 ˚C.

A plot of initial rate against incubation time (**Figure 2.16**) showed inactivation of *Y. pestis* Dam to occur at 30 ˚C. The rate of *Y. pestis* Dam decay, determined by fitting data to an exponential decay curve, was found to be slowest for samples incubated in the presence of DNA (b = 0.0021 ± 0.0001 s^{-1}), and fastest for samples incubated with no substrate (b = 0.0231 ± 0.0030 s^{-1}). The inactivation of *Y. pestis* Dam has previously been reported by Wood *et al.* (*171*), however inactivation has not been reported for other Dam proteins.

Whilst the preparation of *Y. pestis* Dam samples for addition to assays in the presence of DNA should help to reduce the effects of inactivation, these findings demonstrate that rapid collection of early data points is required for the determination of accurate initial rates.

2.3.4 Effect of compound library solvent

The high solubility of a wide range of chemical functionalities in DMSO has made it the solvent of choice for the majority of compound libraries. Although tolerance of low concentrations of DMSO by enzymes is generally good, this is not always the case, and as such the effect of DMSO on enzyme activity should be assessed (*204*). The DMSO tolerance of the real-time break light Dam activity assay system was determined by monitoring the effect of increasing concentrations of DMSO on initial rate (**Figure 2.17**).

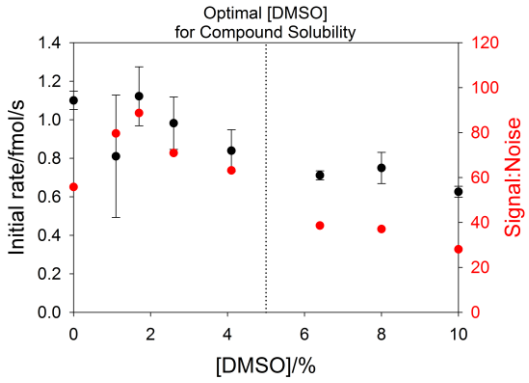

Figure 2.17 DMSO titration

Background subtracted initial rate of methylation by *Y. pestis* Dam (black) and signal:noise ratio (red).

Assay conditions: 1 nM *Y. pestis* Dam, 2 nM *Dpn*I, 10 nM hemimethylated oligonucleotide (ODN1), 25 or 0 µM AdoMet, 0-10% DMSO, 20 mM Tris, 80 mM NaCl, 8 mM $MgCl_2$, 1 mM DTT, 0.1 mg ml^{-1} BSA, 5% glycerol, pH 7.9. Total assay volume 20 µl, in 384 well plate, gain 170, temperature 30 ˚C.

Addition of 10% DMSO led to a significant loss of both activity and signal:noise ratio, raising two possibilities, the first, that DMSO has a greater effect on the activity of Dam than *Dpn*I, and the second, that DMSO has an effect on the specificity of *Dpn*I. Although high concentrations of DMSO are clearly detrimental to assay quality, lower concentrations induce smaller reductions in activity and signal:noise ratios, with 5% DMSO maintaining both assay quality and compound solubility.

2.3.5 Assay volume

The large number of compounds available for HTS campaigns has led to the miniaturisation of assay technologies, with many companies now choosing to screen in 384, 1536 and even 3456 well plates. Although the reduction of assay volume appears to be an attractive concept due to the potential for decreased reagent cost and increased throughput, the set-up cost, and potential effect of low assay volumes on reagent absorption and stability, has led to many companies choosing to remain with the 384 well format, as these plates can accommodate assay volumes as low as 10-20 µl whilst using well spacing compliant with liquid handling technology designed for 96 well plates (*178*).

To assess the effect of reducing assay volume from 100 µl (in 96 well plates) to 20 µl (in 384 well plates) CV (**Equation 2.1**) and Z'-values (**Equation 2.2**) were calculated from a series of positive (full) and negative (lacking AdoMet) control assays in each plate format (**Table 2.6**, experiment 1). Assays from the 96 well plate showed a good level of reproducibility (CV = 10.6 and 18.5%), and a good screening window (Z' = 0.65). Assays from the 384 well plate however showed poor reproducibility (CV = 28.7 and 54.3), with no screening window observed (Z' = 0).

Table 2.6 CV and Z'-value for 96 and 384 well plates

Plate	Experiment	Positive Control*	CV	Negative Control*	CV	Z'-value
96 well	1[#]	0.588 ± 0.062	10.6	0.021 ± 0.004	18.5	0.65
384 well	1[†]	0.116 ± 0.033	28.7	0.006 ± 0.003	54.3	0.00
	2[‡]	0.227 ± 0.021	9.05	0.003 ± 0.001	33.1	0.71

* Average of the positive or negative (lacking AdoMet) control assays ± standard deviation, given to 3 decimal places.

[#] 72 assays total, 36 positive, 36 negative (lacking AdoMet).

[†] 80 assays total, 40 positive, 40 negative (lacking AdoMet).

[‡] 96 assays total, 48 positive, 48 negative (lacking AdoMet).

CV and Z'-value calculated using **Equation 2.1** and **Equation 2.2** respectively.

Assay conditions as **Figure 2.18**. Total assay volume 100 µl and gain 120 for 96 well plate. Total assay volume 20 µl and gain 170 for 384 well plate.

Analysis of initial rate data from the 1[st] 384 well plate experiment (**Figure 2.18A** and **B**) showed rates to decrease across the plate, a trend which correlates with the order in which assays were initiated by the addition of *Y. pestis* Dam and *Dpn*I. Previous experiments (Sections 2.3.2 and 2.3.3) have shown *Y. pestis* Dam to become

inactivated over time at 30 ˚C, therefore the temperature at which enzymes were incubated during plate addition was reduced from 25 to 4 ˚C and the experiment repeated (**Figure 2.18C** and **D**, and **Table 2.6** experiment 2). Initial rate plots showed no decrease in enzyme activity across the plate and calculated values for CV and Z'-value showed the assay to be highly reproducible, with an excellent screening window. These experiments validate the transfer of the real-time Dam activity assay from 96 to 384 well plate formats, with a slight modification of the assay initiation step to reduce *Y. pestis* Dam inactivation.

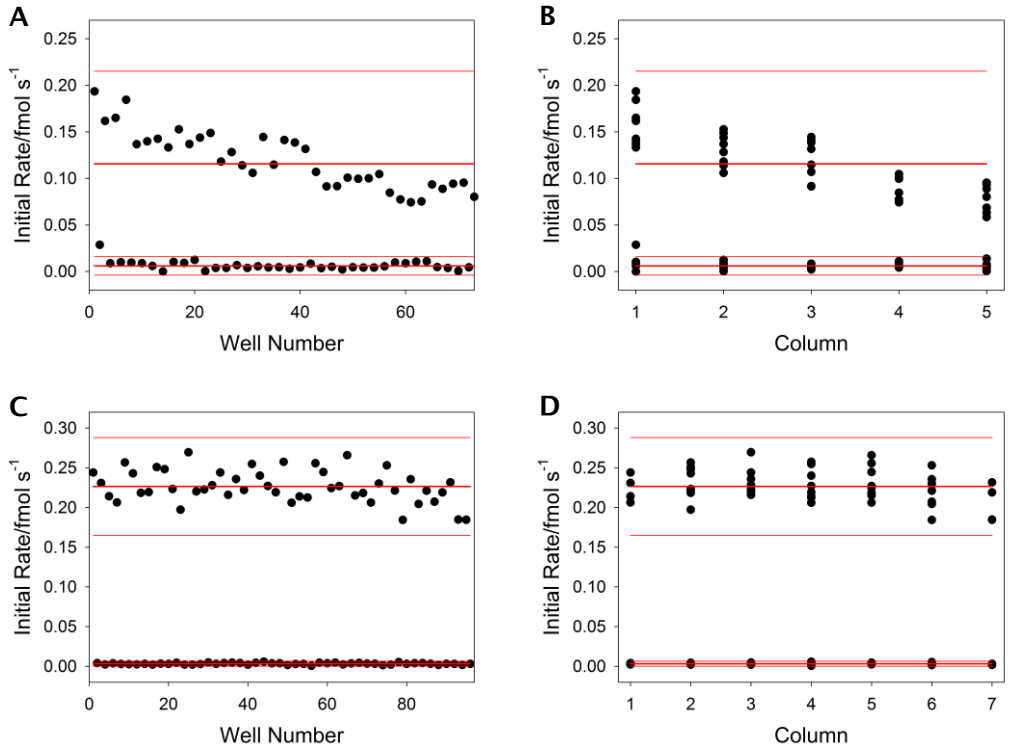

Figure 2.18 Variation in assay signal across a 384 well plate

A: Experiment 1 – initial rate versus well number (top to bottom, left to right of plate).

B: Experiment 1 – initial rate versus column number.

C: Experiment 2 – initial rate versus well number (top to bottom, left to right of plate).

D: Experiment 2 – initial rate versus column number.

Positive and negative control averages and ± 3 standard deviations shown as red lines. Assay conditions: 1 nM *Y. pestis* Dam, 2 nM *Dpn*I, 10 nM hemimethylated oligonucleotide (ODN1), 25 or 0 µM AdoMet, 5% DMSO, 20 mM Tris, 80 mM NaCl, 8 mM $MgCl_2$, 1 mM DTT, 0.1 mg ml^{-1} BSA, 5% glycerol, pH 7.9. Total assay volume 20 µl, in 384 well plate, gain 170, 30 ˚C. Enzyme stock maintatined at ambient temperature (~25 ˚C) for experiment 1, and at 4 ˚C for experiment 2.

2.3.6 Substrate concentrations

The optimisation of assay conditions for the non-biased identification of competitive, uncompetitive, and noncompetitive reversible inhibitors requires the determination of substrate K_M values, as discussed in Section 2. For a single substrate system (**Equation 2.4A**) this process is relatively simple, requiring the evaluation of initial rate at a range of substrate concentrations. The kinetic constants K_M and V_{max} can then be determined by directly fitting a plot of initial rate against substrate concentration to the Michaelis-Menten equation (**Equation 2.4B**), or by fitting a double reciprocal plot of initial rate against substrate concentration to a rearranged form of the Michaelis-Menten equation known as the Lineweaver-Burk equation (**Equation 2.4C**).

A: $E + S \underset{k_{off}}{\overset{k_{on}}{\rightleftharpoons}} ES \xrightarrow{k_{cat}} E + P$

B: $$\nu = \frac{V_{max}[S]}{[S] + K_M}$$

C: $$\frac{1}{\nu} = \frac{K_M}{V_{max}} \times \frac{1}{[S]} + \frac{1}{V_{max}}$$

Equation 2.4 Single substrate enzymatic reaction mechanism (A), the Michaelis-Menten equation (B), and the Lineweaver-Burk equation (C)
Where E = enzyme, S = substrate, P = product, k_{on} = rate of substrate binding, k_{off} = rate of substrate dissociation, k_{cat} = rate of product formation, ν = initial rate, V_{max} = maximum rate, [S] = concentration of substrate, K_M = substrate concentration at half V_{max} (the Michaelis-Menten constant).
For derivation of A-C see Appendix Section 0.

Methods for the determination of kinetic constants for bi-substrate enzyme systems can be challenging (*219*), however pseudo-first order kinetics can be achieved by the addition of a large excess of the second substrate. It is then possible to assess K_M using the methods described in the previous paragraph. Although this method represents a good approximation to K_M care should be taken to ensure that the second substrate is present at saturating concentrations, and that results are not affected by substrate inhibition.

2.3.6.1 AdoMet

To determine K_M^{AdoMet} a series of assays were prepared containing an excess of DNA (relative to K_M^{DNA} as calculated previously, **Table 2.5**, (*171*)) and a range of AdoMet concentrations. A plot of initial rate against substrate concentration was fitted to a hyperbola of the form f=a*x/(b+x), and V_{max} (a) and K_M (b) were determined as 0.091 ± 0.004 fmol s^{-1} and 16.4 ± 2.29 µM respectively (**Figure 2.19**). K_M^{AdoMet} is slightly higher than the value of 11.3 ± 0.63 µM determined previously for *Y. pestis* Dam (*171*), possibly due to variations in assay conditions between the two experiments. Lower values for K_M^{AdoMet} have also been reported for *E. coli* and T4 Dam (approximately 6 and 0.4 µM respectively (*104, 105, 108, 109*)).

The calculated k_{cat} for *Y. pestis* Dam determined from this experiment is 0.273 ± 0.012 min^{-1}, which is again high in comparison with reported values of k_{cat} for the *E. coli* and T4 enzymes (0.6-1.2 min^{-1}) (*104, 105, 108, 109*). Whilst these results may represent a true difference in the kinetics of *Y. pestis*, T4 and *E. coli* Dam it is perhaps more likely that the difference observed is due to variations in experimental method, specifically the type of assay used (fluorescence-based for *Y. pestis* Dam versus radiation-based for T4 and *E. coli* Dam).

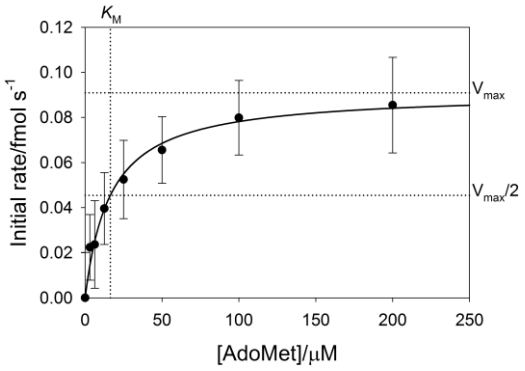

Figure 2.19 Graphical determination of *Y. pestis* Dam K_M^{AdoMet}
Initial rate versus concentration of AdoMet. Data fitted to **Equation 2.4B**.
Assay conditions: 1 nM *Y. pestis* Dam, 2 nM *Dpn*I, 30 nM hemimethylated oligonucleotide (ODN1), 0-200 µM AdoMet, 5% DMSO, 20 mM Tris, 80 mM NaCl, 8 mM $MgCl_2$, 1 mM DTT, 0.1 mg ml^{-1} BSA, 5% glycerol, pH 7.9. Total assay volume 20 µl, in 384 well plate, gain 170, 30 ˚C.

2.3.6.2 DNA

A similar process was used to determine K_M^{DNA}, with a series of assays prepared containing a range of hemimethylated oligonucleotide concentrations and an excess of AdoMet. A plot of initial rate against substrate concentration showed an apparent inhibitory effect at higher concentrations of DNA, a further series of experiments were therefore prepared containing both higher and lower fixed concentrations of AdoMet (**Figure 2.20**). A reduction in the concentration of AdoMet led to a decrease in maximum rate, whilst having no effect on the apparent inhibition, whereas an increase in the concentration of AdoMet had little effect on either maximum rate or inhibition.

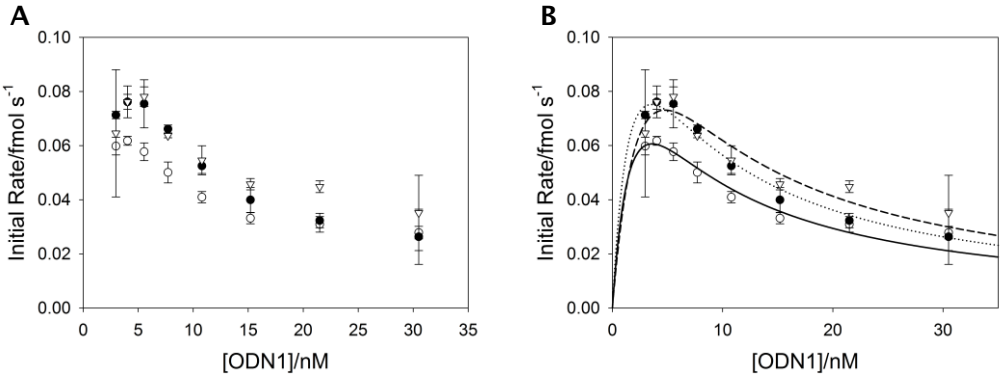

Figure 2.20 Graphical determination of *Y. pestis* Dam K_M^{DNA}
A: Background subtracted initial rate versus concentration of ODN1 at 25 (open circles), 50 (filled circles) and 100 (open triangles) µM AdoMet.
B: Data from (A) fitted globally to **Equation 2.5**, with K_i fixed.
Assay conditions: 0.3 nM *Y. pestis* Dam, 2 nM *Dpn*I, 3-30.5 nM hemimethylated oligonucleotide (ODN1), 0, 25, 50 or 100 µM AdoMet, 5% DMSO, 20 mM Tris, 80 mM NaCl, 8 mM $MgCl_2$, 1 mM DTT, 0.1 mg ml^{-1} BSA, 5% glycerol, pH 7.9. Total assay volume 20 µl, in 384 well plate, gain 170, 30 ˚C.

$$v = \frac{V_{max}[S]}{K_M\left(1+\frac{[S]}{K_{is}}\right)+[S]}$$

Equation 2.5 Competitive substrate inhibition
Where v = initial rate, V_{max} = maximum rate, [S] = concentration of substrate, K_M = the Michaelis-Menten constant and K_{is} = the substrate inhibition dissociation constant.
For derivation see Appendix Section 0.

It is unusual to observe substrate inhibition at concentrations close to K_M, as in this case, suggesting that the effect observed may be more complicated. However, in the interest of obtaining estimates for kinetic parameters, data were fitted to an equation describing competitive substrate inhibition (**Equation 2.5**). As concentration of AdoMet

was shown to have little or no effect on apparent substrate inhibition, each data set were fitted globally to the substrate inhibition equation with the value of K_i fixed, allowing for a more accurate approximation of K_M and V_{max}. The values and associated coefficients of determination (R^2) obtained are listed in **Table 2.7** below.

Table 2.7 Kinetic parameters derived from the graphical determination of K_M^{DNA}

[AdoMet] μM	V_{max} fmol s^{-1}	k_{cat} min^{-1}	K_M nM	R^2
25	0.140 ± 0.042	1.40 ± 0.42	2.35 ± 1.65	0.944
50	0.172 ± 0.051	1.72 ± 0.51	2.28 ± 1.57	0.979
100	0.200 ± 0.061	2.00 ± 0.61	4.15 ± 2.24	0.894
AVERAGE	**0.171 ± 0.051**	**1.71 ± 0.51**	**2.93 ± 1.88**	**0.939 ± 0.043**

Where errors shown are the standard error of fit or an average of the standard error of fit. K_{is} = 5.49 ± 2.20 for all experiments.

The values of K_M^{DNA}, k_{cat} and V_{max} obtained for each concentration of AdoMet were averaged, giving V_{max} as 0.171 ± 0.051 fmol s^{-1}, k_{cat} as 1.71 ± 0.51 min^{-1} and K_M^{DNA} as 2.93 ± 2.20 nM. At 100 μM AdoMet k_{cat} is comparable to that determined in the K_M^{AdoMet} experiment, as would be expected, and K_M^{DNA} is within error of that determined previously for *Y. pestis* Dam (3.43 ± 1.68 nM (*171*)). Reported values of K_M^{DNA} for both *E. coli* and T4 Dam are higher (18-81 and 6-8 μM respectively (*104, 105, 108, 109*)), however this may again be due to differences in experimental method, as discussed previously.

Inhibition by AdoMet has been ruled out, and the inhibition of Dam by concentrations of hemimethylated oligonucleotide substrate only slightly higher than the apparent K_M^{DNA} is unlikely. The most probable explanation for the observed effects therefore lies within the coupled nature of the assay, and more specifically with the coupling enzyme *Dpn*I. Kinetic characterisation of *Dpn*I has shown the enzyme to display Michaelis-Menten kinetics with respect to the fully methylated oligonucleotide, with K_M^{DNA} determined as 14.1 ± 2.3 nM (**Figure 2.21A**). However for the hemimethylated oligonucleotide sigmoidal kinetics, indicative of cooperative binding, were observed, with a Hill parameter of 2.26 ± 0.09 suggesting positive cooperative binding (**Figure 2.21B**). The apparent substrate inhibition observed in the full assay and the kinetics of *Dpn*I with respect to the fully and hemimethylated DNA substrates will be discussed further in Chapter 3, Section 3.5.3.

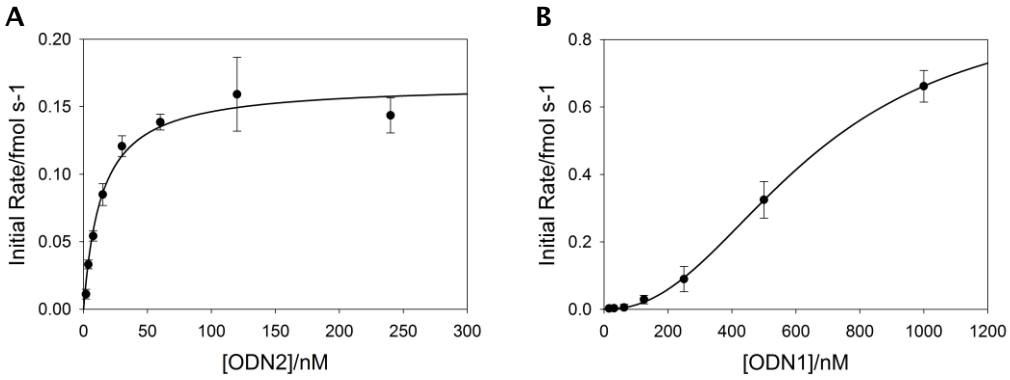

Figure 2.21 Graphical determination of *Dpn*I K_M^{DNA}

A: Background subtracted initial rate versus concentration of fully methylated oligonucleotide ODN2. Data fitted to a hyperbola of the form f=a*x/(b+x), where a = V_{max} and b = K_M.

B: Background subtracted initial rate versus concentration of hemimethylated oligonucleotide ODN1. Data fitted to a sigmoidal Hill equation of the form f=a*x^b/(c^b+x^b), where a = V_{max}, b = the Hill parameter and c = K_M.

Assay conditions: 0 (background), 2 nM (A) or 12.5 pM (B) *Dpn*I, 0-250 nM fully methylated oligonucleotide (ODN2) or 0-1000 nM hemimethylated oligonucleotide (ODN1), 5% DMSO, 20 mM Tris, 80 mM NaCl, 8 mM $MgCl_2$, 1 mM DTT, 0.1 mg ml^{-1} BSA, 5% glycerol, pH 7.9. Total assay volume 20 µl, in 384 well plate, gain 140 (A) or 150 (B), 30 ˚C.

Whilst the apparent substrate inhibition effect observed at higher concentrations of DNA may affect the kinetic constants obtained for *Y. pestis* Dam with respect to DNA concentration, the assay can still be applied to the identification of inhibitors of all modalities, providing DNA concentration (and consequently substrate inhibition) is kept to a minimum. In addition, kinetic characterisation of inhibitors can also be achieved, although K_i values determined with respect to varying DNA concentration may be affected and should be carefully assessed.

2.3.6.3 Optimisation of substrate concentrations for HTS

Ideally substrate concentrations for HTS should be held at K_M for the target enzyme. However this can seriously impair the observed screening window, reducing the overall quality of the assay. To ensure a suitable screening window whilst keeping substrate concentrations close to K_M, AdoMet concentration was held constant and the effect of increasing DNA concentration on Z'-value monitored.

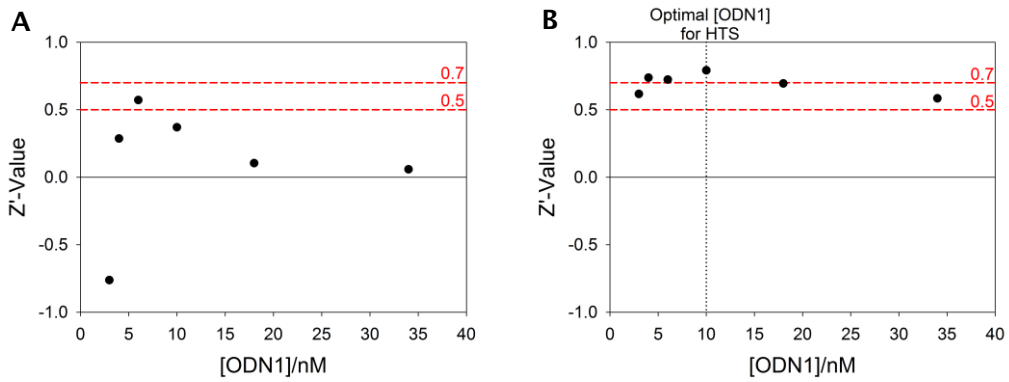

Figure 2.22 Optimisation of substrate concentrations for HTS

A: Z'-value for 12.5 µM AdoMet and varying DNA.

B: Z'-value for 25 µM AdoMet and varying DNA.

Z'-value calculated using **Equation 2.2**, from 8 positive and 8 negative (lacking Dam) assays. Z' = 0.5 (good) and 0.7 (excellent) shown as dashed red lines.

Assay conditions: 1 nM *Y. pestis* Dam, 0.8 nM *Dpn*I, 3-34 nM hemimethylated oligonucleotide (ODN1), 0 (A and B), 12.5 (A) or 25 (B) µM AdoMet, 20 mM Tris, 80 mM NaCl, 8 mM $MgCl_2$, 1 mM DTT, 0.1 mg ml^{-1} BSA, 5% glycerol, pH 7.9. Total assay volume 100 µl, in 96 well plate, gain 130, 30 ˚C.

At concentrations of AdoMet slightly lower than K_M the screening window was generally poor (**Figure 2.22A**), however increasing the concentration of AdoMet to slightly higher than K_M increased the Z'-value to at least 0.5, with the optimum at 10 nM DNA (**Figure 2.22B**). Under the optimum conditions (25 µM AdoMet, 10 nM DNA) the screening window was maximised and substrates were present in at least a 10-fold excess over the target enzyme.

2.3.7 Assay optimisation for the kinetic characterisation of Dam inhibitors

2.3.7.1 Half maximal inhibitory concentration

The half maximal inhibitory concentration, known as the IC_{50}, relates to the concentration of an inhibitor which elicits a 50% reduction in the activity of a target enzyme *in vitro*. IC_{50} values can be determined by fitting a plot of fractional activity against inhibitor concentration to a logistic sigmoid (**Equation 2.6A** and **B**).

A: $$\text{Fractional Activity} = \frac{v_i}{v_0}$$

B: $$\text{Fractional Activity} = FA_{min} + \frac{FA_{max} - FA_{min}}{1 + \left(\frac{[I]}{IC_{50}}\right)^h}$$

Equation 2.6 Fractional activity (A) and determination of IC_{50} (B)

Where v_i = inhibited rate, v_0 = uninhibited rate, FA_{min} = minimum fractional activity, FA_{max} = maximum fractional activity, IC_{50} = concentration of inhibitor at a fractional activity of 0.5, [I] = inhibitor concentration and h = the Hill coefficient.

For derivation of B see Appendix Section 0.

Unlike the inhibition constant K_i, IC_{50} values are dependent on both the mode of inhibition and substrate concentration. This relationship is described by the Cheng-Prusoff equations (**Equation 2.7**), which express the relationship between IC_{50} and K_i for competitive, noncompetitive and uncompetitive reversible inhibition (*221*). Application of the Cheng-Prusoff equations for the determination of K_i from IC_{50} requires prior knowledge of inhibitor modality. Where substrate concentrations are held at K_M, the Cheng-Prusoff equations can be simplified to give $IC_{50} = 2K_i$, $IC_{50} = 2\alpha K_i/(\alpha+1)$, and $IC_{50} = 2\alpha K_i$ for competitive, noncompetitive and uncompetitive reversible inhibition respectively. By preparing IC_{50} experiments with substrate concentrations held equal to K_M it is therefore possible to make an approximation to K_i of $IC_{50}/2$. Inhibitor IC_{50} values determined for different targets can then be compared to determine selectivity in addition to assessing potency.

A: $$IC_{50} = K_i\left(1 + \frac{[S]}{K_M}\right)$$

B: $$IC_{50} = \frac{[S] + K_M}{\frac{K_M}{K_i} + \frac{[S]}{\alpha K_i}}$$

C: $IC_{50} = \alpha K_i \left(1 + \frac{K_M}{[S]}\right)$

Equation 2.7 The Cheng-Prusoff equations

For competitive (A), noncompetitive (B) and uncompetitive (C) reversible inhibition (*221*).

Where IC_{50} = half maximal inhibitory constant, K_i = the inhibitory dissociation constant, K_M = the Michaelis-Menten constant, α = constant describing the degree to which inhibitor binding affects the affinity of the enzyme for substrate, S = substrate concentration.

For derivation of A-C see Appendix Section 0.

Validation with AdoHcy

Validation of the real-time break light Dam activity assay for the determination of IC_{50} values was achieved by preparing a dose-response curve for the known Dam inhibitor AdoHcy, under conditions where substrate concentrations were equal to K_M (**Figure 2.23**). Values obtained for IC_{50}^{AdoHcy} from two separate experiments (each with triplicate data points) were 8.5 ± 2.1 and 15.3 ± 8.1 µM respectively. These values compare well with a previously determined value for K_i^{AdoHcy}, with an average of the two (11.9 ± 4.2 µM) being within error double K_i^{AdoHcy} for *Y. pestis* Dam (6.93 ± 2.01 µM) as determined by Wood *et al.* (*171*).

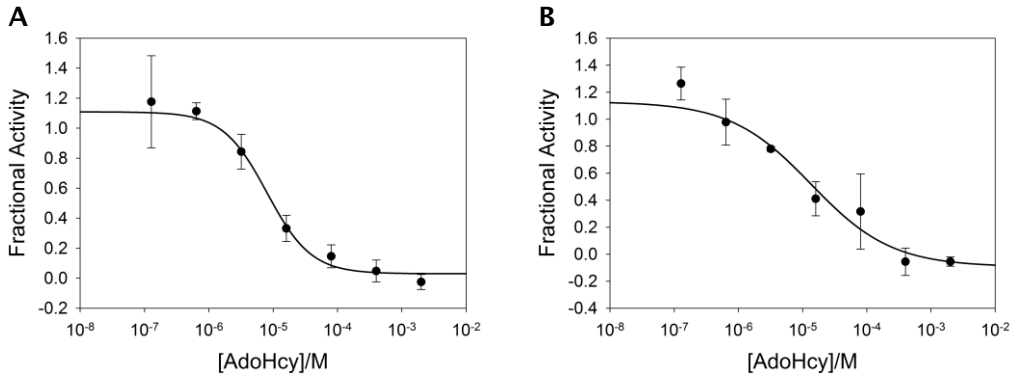

Figure 2.23 IC_{50}^{AdoHcy} determination

Fractional activity, calculated using **Equation 2.6A** versus concentration of AdoHcy for experiment 1 (A) and 2 (B). Data fitted to **Equation 2.6B**.

Assay conditions: 0.3 nM *Y. pestis* Dam, 2 nM *Dpn*I, 3.5 nM hemimethylated oligonucleotide (ODN1), 0 or 16 µM AdoMet, 0-1000 µM AdoHcy, 5% DMSO, 20 mM Tris, 80 mM NaCl, 8 mM $MgCl_2$, 1 mM DTT, 0.1 mg ml^{-1} BSA, 5% glycerol, pH 7.9. Total assay volume 20 µl, in 384 well plate, gain 190, 30 ˚C.

2.3.7.2 Inhibition constant

The inhibition constant (K_i) is the dissociation constant for the binding of a reversible inhibitor to an enzyme. To determine K_i, plots of 1/rate against 1/substrate concentration at various concentrations of inhibitor are fitted to the Lineweaver-Burk equation (**Equation 2.8A**). Re-plots of gradient (K_M^{app}/V_{max}^{app}) and y-axis intercept ($1/V_{max}^{app}$) against inhibitor concentration are then used to determine K_i and αK_i respectively from the negative of the re-plot x-axis intercepts (**Equation 2.8B** and **C**).

A:
$$\frac{1}{v} = \frac{K_M^{app}}{V_{max}^{app}} \times \frac{1}{[S]} + \frac{1}{V_{max}^{app}}$$

$$K_M^{app} = \frac{K_M\left(1+\frac{[I]}{K_i}\right)}{\left(1+\frac{[I]}{\alpha K_i}\right)}$$

$$V_{max}^{app} = \frac{V_{max}}{\left(1+\frac{[I]}{\alpha K_i}\right)}$$

B:
$$\frac{K_M^{app}}{V_{max}^{app}} = \frac{K_M}{V_{max}K_i} \times [I] + \frac{K_M}{V_{max}}$$

C:
$$\frac{1}{V_{max}^{app}} = \frac{1}{V_{max}\alpha K_i} \times [I] + \frac{1}{V_{max}}$$

Equation 2.8 The Lineweaver-Burk equation for reversible inhibition (A) and re-plots of gradient (B) and y-axis intercept (C) against inhibitor concentration

Where v = initial rate, K_M^{app} = apparent substrate concentration at half V_{max} (the Michaelis-Menten constant), V_{max}^{app} = apparent maximum rate, [S] = concentration of substrate, S = substrate, I = inhibitor, K_M = the Michaelis-Menten constant, V_{max} = maximum rate, K_i = the inhibition dissociation constant.

For derivation of A-C see Appendix Section 0.

For inhibitors displaying a competitive mode of inhibition, αK_i will be much greater than K_i, with Lineweaver-Burk y-axis intercepts being approximately equal for different concentrations of inhibitor. Inhibitors displaying an uncompetitive mode of inhibition will have Lineweaver-Burk gradients of approximately equal value for different inhibitor concentrations due to K_i being much greater than αK_i. For noncompetitive inhibitors both y-axis intercepts and gradients will vary with inhibitor concentration giving values for both αK_i and K_i. A schematic representation of how mode of inhibition affects Lineweaver-Burk plots is shown in **Figure 2.24**.

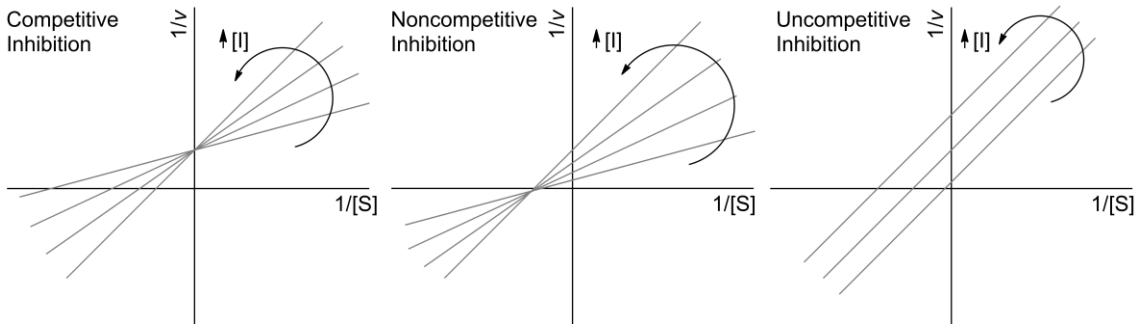

Figure 2.24 Effect of inhibition mode on Lineweaver-Burk plots
For competitive inhibitors (left) plots of $1/v$ against 1/[S] for increasing inhibitor concentrations intersect on the y-axis. For noncompetitive inhibitors where $\alpha = 1$ (centre) plots intersect on the x-axis, where $\alpha \neq 1$ plots intersect to the left of the y-axis. For uncompetitive inhibitors (right) plots do not intersect.

For inhibitors of bi-substrate enzymes such as Dam, a pseudo-first order approximation can again be made by having a fixed excess of one substrate, whilst varying the concentration of the second. This method has previously been used to determine K_i^{AdoHcy} with the real-time break light Dam activity assay, giving a competitive mode of inhibition with respect to AdoMet and a K_i^{AdoHcy} of 6.93 ± 2.01 μM (*171*). The observed competitive mode of inhibition of AdoMet by AdoHcy is as expected, validating this method as a means of establishing inhibitory mode for AdoMet competitive inhibitors. However, as mentioned previously care will have to be taken when assessing mode of inhibition and K_i with respect to DNA concentration, due to the effect of apparent substrate inhibition at concentrations of DNA above K_M.

2.4 Summary

The expression and purification of active recombinant *Y. pestis* Dam and *Dpn*I for use in the real-time break light activity assay has been achieved through the optimisation of expression systems, growth conditions, and purification buffers. Initial optimisation experiments have found the optimum buffer system for the maximisation of *Y. pestis* Dam activity and the minimisation of non-specific activity, to consist of 20 mM Tris (pH 7.9), 80 mM NaCl, 8 mM $MgCl_2$, 1 mM DTT, 0.1 mg ml^{-1} BSA and 5% glycerol, and validation of the assay under HTS conditions has shown the addition of up to 5% DMSO to be well tolerated. Experiments to determine the optimum assay temperature found the maximum initial rate to be achieved and maintained at 30 °C, with a loss in the activity of *Y. pestis* Dam over time observed at higher temperatures. This loss in activity was minimised by incubating the stock solution of *Y. pestis* Dam in the presence of DNA at 4 °C prior to assay initiation.

To ensure that Dam catalysed methylation is the rate limiting step, and eliminate any lag phase, the coupling enzyme concentration was optimised, with 99.8% of the maximum initial rate achieved upon addition of 2 nM *Dpn*I to activity assays. Furthermore, the inhibition of up to 50% of the coupling enzyme led to a decrease in initial rate of only 4%, minimising the observable effect of any *Dpn*I inhibition on the overall assay. The optimal concentration of the primary enzyme was determined by assessing the effective assay range, with a *Y. pestis* Dam concentration of 10% of the minimum DNA concentration found to fall within the upper (>40% of the DNA concentration added) and lower (<3% of the DNA concentration added) assay limits.

The optimal substrate concentrations for the identification and characterisation of inhibitors were established by determining K_M values for each substrate, with K_M^{AdoMet} found to be 16.4 ± 2.29 μM, and K_M^{DNA} found to be 2.93 ± 2.20 nM. Whilst simple Michaelis-Menten kinetics were observed for experiments in which AdoMet concentration was varied, experiments in which DNA concentration was varied showed an apparent substrate inhibition effect. This effect has been identified as an artefact of the coupled enzyme assay system, and will be discussed further in Chapter 3, Section 3.5.3. Since the coupled enzyme *Dpn*I, and not *Y. pestis* Dam, is inhibited the effect of inhibitors on the primary enzyme can still be readily assessed with the real-time break light Dam activity assay. However experiments in which DNA concentration is varied should be carefully interpreted as the true concentration of DNA available for reaction may be limited by the apparent substrate inhibition observed.

Validation of HTS conditions for the identification of inhibitors was achieved by assessing CV and Z-values for assays prepared in both 96 and 384 well microplates, with substrate concentrations varied around K_M. The reduction of total assay volume from 100 µl (96 well) to 20 µl (384 well) was found to severely reduce CV and Z-value when *Y. pestis* Dam was not incubated at 4 ˚C prior to assay initiation, however when *Y. pestis* Dam was cooled prior to assay initiation a good level of reproducibility (CV) and excellent screening window (Z-value) were observed. Although an unbiased HTS assay should be carried out at substrate concentrations equal to K_M to allow for all inhibitor modalities to be identified, in the case of the real-time Dam activity assay a poor screening window was achieved under such conditions. Substrate concentrations were therefore increased until an appropriate screening window was achieved, with the optimum concentrations identified as 25 µM AdoMet and 10 nM DNA.

Finally, validation of IC_{50} and K_i assay conditions for the characterisation of inhibitors was achieved by assessing a known Dam inhibitor, the methyl donor product AdoHcy. Use of the real-time break light Dam activity assay for the determination of K_i^{AdoHcy} was previously achieved by Wood *et al.* (*171*) who identified a competitive mode of inhibition for AdoHcy with respect to AdoMet and a K_i^{AdoHcy} of 6.93 ± 2.01 µM. The validation of the assay for the determination of IC_{50} values was achieved by calculating IC_{50}^{AdoHcy} from two separate experiments, each consisting of triplicate data points. The average IC_{50}^{AdoHcy} was determined as 11.9 ± 4.2 µM, approximately double the reported K_i^{AdoHcy} for *Y. pestis* Dam, as would be expected for a competitive inhibitor, thus validating the measurement.

3 Secondary Assay Development

3.1 Introduction

In HTS, primary assays are used to screen compound libraries, establish initial hits, and in some cases, to kinetically characterise compounds. Secondary assays are required for the validation of primary screening results, and the assessment of lead potency and selectivity. The hit validation process includes hit confirmation in which the reproducibility and purity of an inhibitor are assessed and hit verification in which false positives are identified (*204*).

Hit verification can be achieved through counter-screening and/or the application of an alternative assay format, with both methods designed to validate hits through the identification and elimination of false positives. Whilst hit confirmation generally involves the re-testing of identified hits sourced from both original and fresh stocks, and the assessment of compound purity via chromatographic techniques such as high-pressure liquid chromatography (HPLC) or thin layer chromatography (TLC) (*204*).

The following chapter describes the development activity and binding assays in a number of formats. These assays have been used to validate *in vitro* and in cell activity and to provide detailed kinetic and thermodynamic data for validated hits.

3.2 Counter-screening

3.2.1 DpnI activity assay

A limitation of the coupled enzyme assay format is that inhibition of the coupling enzyme could lead to the identification of false positives. Due to careful optimisation of the real-time break light Dam activity assay, the coupled enzyme *Dpn*I can be inhibited by up to 50% with minimal effect on the overall assay (Chapter 2, Section 2.3.3.1). However, potent inhibitors may inhibit *Dpn*I by greater than 50%, causing a significant decrease in the overall observed assay rate and the identification of false positives. To identify and eliminate such compounds a *Dpn*I activity assay was developed, in which a fully methylated break light probe (ODN2) is cleaved by *Dpn*I, leading to an increase in fluorescence (**Figure 3.1**).

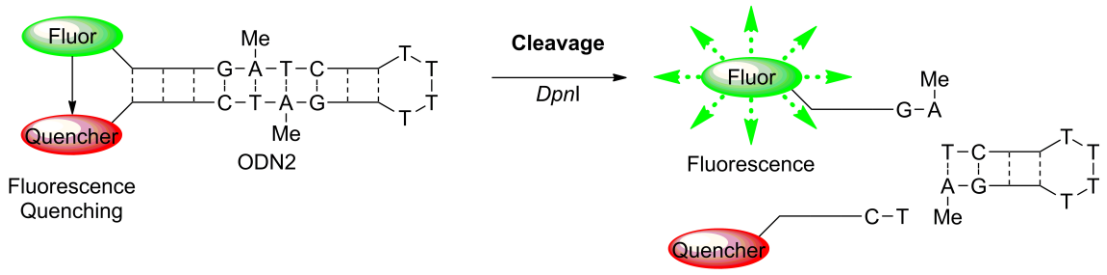

Figure 3.1 Real-time break light *Dpn*I activity assay
A fully methylated break light oligonucleotide substrate (ODN2) containing a GATC recognition site is cleaved by the restriction enzyme *Dpn*I, resulting in the separation of fluorophore (fluorescein) and quencher (dabcyl) and a subsequent proportional increase in fluorescence.

For the results of the *Dpn*I counter-screen to be directly comparable with the HTS results, conditions were kept constant, with the exception of the enzyme concentration. This was optimised to ensure the assay was carried out within the valid detection range. A plot of initial rate against *Dpn*I concentration showed the upper assay limit to be at approximately 25 pM *Dpn*I, with concentrations greater than this showing saturation (**Figure 3.2**). To ensure the accurate determination of initial rate a *Dpn*I concentration of 12.5 pM was selected for the *Dpn*I counter-screen.

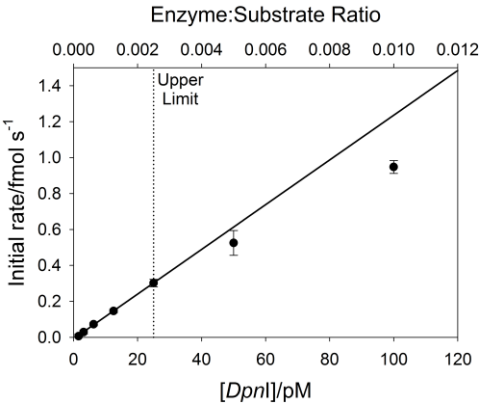

Figure 3.2 *Dpn*I counter-screen effective assay range

Background subtracted initial rate of cleavage by *Dpn*I. Data points from 0-12.5 pM *Dpn*I fitted to a linear equation of the form $f=y_0+a*x$.

Assay conditions: 0-100 pM *Dpn*I, 10 nM fullymethylated oligonucleotide (ODN2), 5% DMSO, 20 mM Tris, 80 mM NaCl, 8 mM $MgCl_2$, 1 mM DTT, 0.1 mg ml^{-1} BSA, 5% glycerol, pH 7.9. Total assay volume 20 µl, in 384 well plate, gain 170, temperature 30 ˚C.

3.2.2 Fluorescent intercalator displacement assay

Another potential source of false positives is through assay signal interference, which can occur directly, or via the modification of assay components. Measuring the fluorescence and absorbance properties of compounds can determine if their spectra overlap with the wavelength used for the assay signal, however compounds affecting assay components can be more difficult to detect. The real-time break light Dam activity assay utilises a hairpin oligonucleotide probe for the detection of methylation; in this type of assay compounds which intercalate DNA may prevent either methylation or cleavage occurring by inducing a conformational change in the oligonucleotide probe. Although DNA intercalators have been successfully employed in the treatment of cancer (*222*), the Dam recognition sequence is unlikely to provide a unique enough intercalation site to eliminate the potential mutagenic effect of such compounds.

The identification of DNA intercalation can be achieved through the application of a fluorescent intercalator displacement (FID) assay. Originally developed as a method for establishing DNA binding selectivity and affinity (*223, 224*), FID assays utilise the fluorescence decrease associated with the displacement of a fluorescent intercalator, such as thiazole orange (*225*), from DNA to establish the DNA binding properties of a secondary compound. Adaptation of this assay for the identification of DNA intercalators was previously reported by Mashhoon *et al.* who used the relative fluorescence decrease upon displacement of thiazole orange by a compound as a measure of DNA intercalation (*149*). We have employed a similar method to assess the ability of HTS hits to displace thiazole orange from an unlabelled oligonucleotide substrate (**Figure 3.3**), with compounds showing significant displacement of thiazole orange being discarded from further investigation.

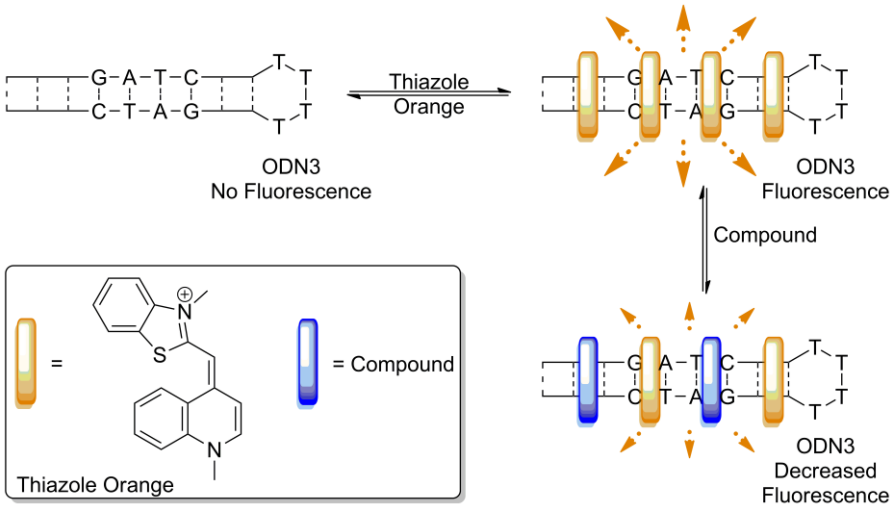

Figure 3.3 Fluorescent intercalator displacement assay
Intercalation by thiazole orange of an unmethylated oligonucleotide substrate (ODN3) containing a GATC recognition site produces a fluorescence signal, which is decreased when thiazole orange is displaced by a DNA intercalating test compound.

3.3 Gel-based Dam methylation assay

It is common for HTS hits to be validated using a secondary assay to confirm inhibition of activity in more than one assay format. This increases confidence in the ability of a ligand to inhibit the target and reduces the possibility of false positives being identified by eliminating artefacts associated with a single assay format. The real-time break light Dam activity assay is a coupled, fluorescence-based assay which utilises a short, hairpin, oligonucleotide probe as a substrate. To maximise its value an alternative assay format should therefore employ a non-fluorescence-based detection method, a different/no coupling enzyme, and a different oligonucleotide substrate.

Whilst the adaptation of the primary assay to a high-throughput format is essential for HTS, a secondary assay need not be readily adaptable as the number of compounds to be screened is generally greatly reduced. A low-throughput gel-based methylation assay was therefore appropriate for hit confirmation. The gel-based assay is a protection-based, stopped assay, in which Dam methylation protects a plasmid substrate from cleavage by the methylation-sensitive restriction enzyme *Bcl*I, with results visualised by agarose gel electrophoresis (**Figure 3.4**). False positives which inhibit the coupling enzyme *Dpn*I, or interfere with either the assay signal or oligonucleotide substrate would not be expected to affect the secondary assay in the same way and would therefore not be confirmed as hits.

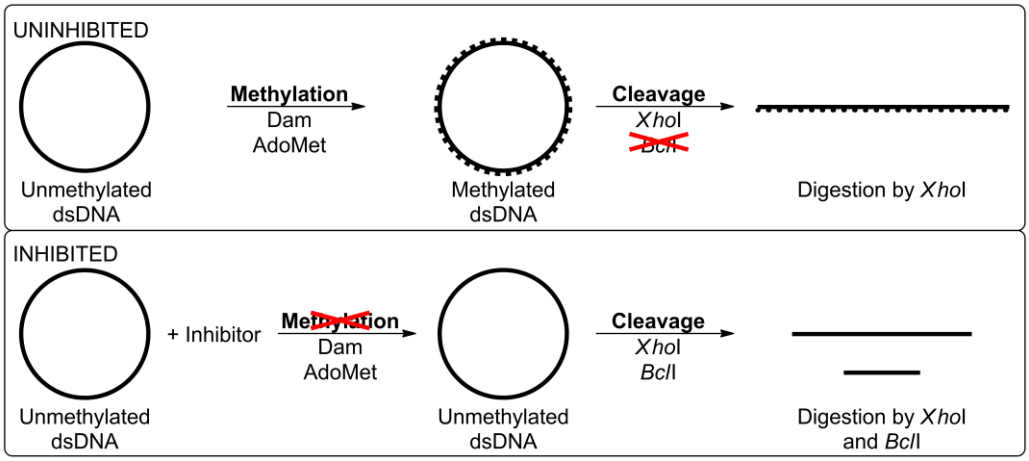

Figure 3.4 Gel-based Dam methylation assay
Methylation of a plasmid substrate by Dam protects it from *Bcl*I cleavage. In the presence of an inhibitor, methylation is prevented allowing *Bcl*I cleavage to occur. Results are visualised by agarose gel electrophoresis, with a single band representing an unmethylated plasmid, three bands representing a partially methylated plasmid, and two bands representing an unmethylated plasmid.

3.3.1 Optimisation

The commercially available restriction enzymes *Bcl*I and *Xho*I show optimal activity in two out of four supplied buffers, one of which (NEBuffer 3[5]) is comparable to the real-time break light Dam activity assay buffer[6] and was therefore selected for use in the gel-based assay. For ease of quantification a plasmid containing a single *Xho*I site for linearisation and a non-equidistant single *Bcl*I site for methylation-sensitive restriction was selected (**Figure 3.5**). Unmethylated plasmid was obtained by isolating **pRL821** (*226*) from the *E. coli dam* knockout strain ER2925.

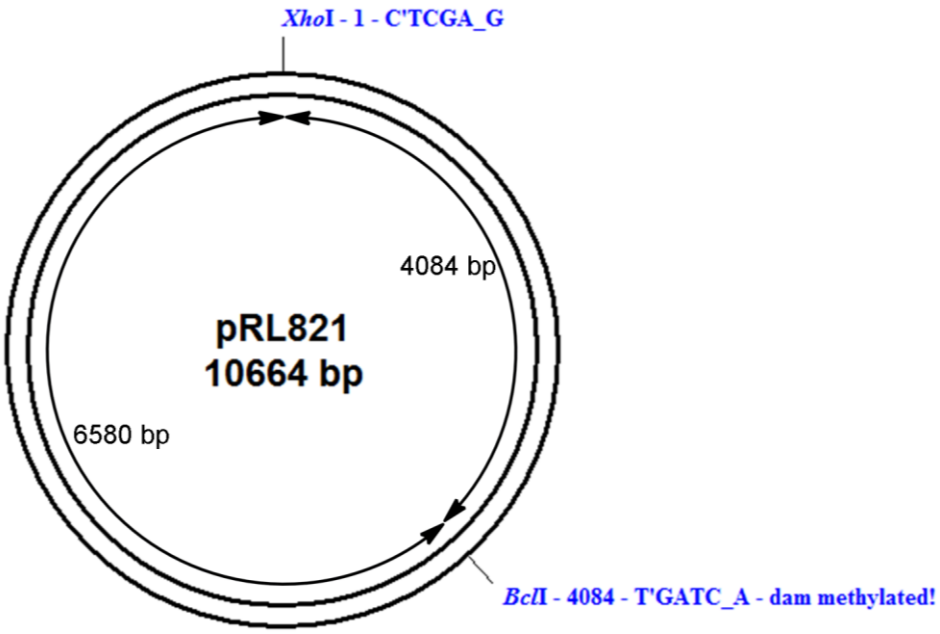

Figure 3.5 Gel-based Dam activity assay plasmid

Plasmid pRL821 was originally constructed by Dr R. Leonardi (*226*) and contains 46 Dam recognition sites (GATC), 1 *Xho*I recognition site (CTCGAG), and 1 *Bcl*I recognition site (TGATCA). Cleavage by *Xho*I and *Bcl*I results in the formation of two fragments of 4084 and 6580 base pairs in length.

3.3.1.1 Enzymes

Dam

Initial experiments with *Y. pestis* Dam showed incomplete digestion of plasmid DNA at various enzyme concentrations. Previous experiments (Chapter 2, Section 2.3.3.3) have shown *Y. pestis* Dam to rapidly lose activity at 30 ˚C, suggesting that it is not ideal for use in extended assays. The closely related *E. coli* Dam has been expressed and purified by J.E Harmer, and may represent a more stable alternative due to the higher

[5] NEBuffer3: [50 mM Tris-HCl, 100 mM NaCl, 10 mM $MgCl_2$, 1 mM DTT, pH 7.9].

[6] Real-time break light Dam activity assay buffer: [20 mM Tris, 80 mM NaCl, 8 mM $MgCl_2$, 1 mM DTT, 0.1 mg ml^{-1} BSA, 5% glycerol, pH 7.9].

optimal growth temperature of the *E. coli* bacterium (37 ˚C (*220*), compared with 30 ˚C for *Y. pestis* (*23*)). To test this theory the activity of *E. coli* Dam was assessed after incubation at 30 ˚C with or without substrates using the real-time break light Dam activity assay (see Appendix Section 9.5 for optimisation of the real-time break light Dam activity assay for *E. coli* Dam), and compared to a previous experiment which measured the activity of *Y. pestis* Dam (Section 2.3.3.3, **Figure 3.6**).

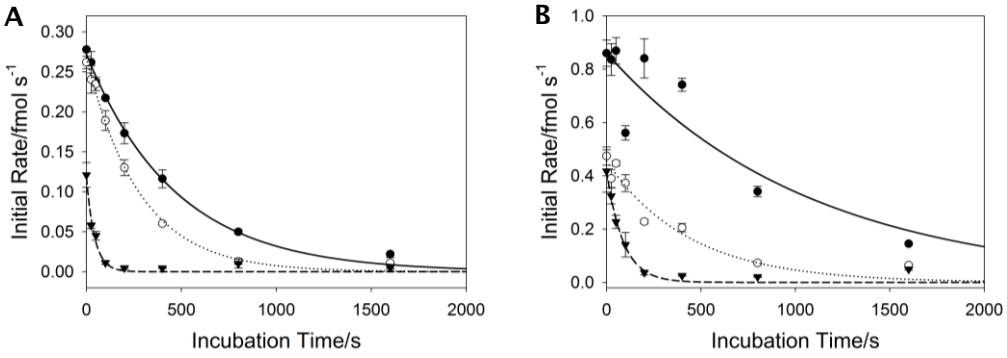

Figure 3.6 Comparison of the inactivation of *Y. pestis* (A) and *E. coli* (B) Dam
Initial rate of methylation by *Y. pestis* Dam (A) or *E. coli* Dam (B) incubated with DNA (filled circles), AdoMet (open circles), or no substrates (filled triangles) at 30 ˚C for 0-1600 s prior to determination of initial rate. Data fitted to an exponential decay curve of the form f = a*exp(-b*x).
Assay conditions: 1 nM *Y. pestis* Dam (A) or *E. coli* Dam (B), 2 (A) or 10 (B) nM *Dpn*I, 10 (A) or 25 (B) nM hemimethylated oligonucleotide (ODN1), 25 (A), 12 (B) or 0 (A and B) µM AdoMet, 5% DMSO, 20 mM Tris, 80 mM NaCl, 8 mM $MgCl_2$, 1 mM DTT, 0.1 mg ml^{-1} BSA, 5% glycerol, pH 7.9. Total assay volume 20 µl, in 384 well plate, gain 170 (A) or 150 (B), temperature 30 ˚C.

Table 3.1 Comparison of the inactivation of *Y. pestis* and *E. coli* Dam at 30 ˚C

Incubated With	**Enzyme**	**Rate of Decay min^{-1}**	**R^2**
DNA	*Y. pestis* Dam	0.128 ± 0.007	0.995
	E. coli Dam	0.059 ± 0.010	0.817
AdoMet	*Y. pestis* Dam	0.214 ± 0.012	0.996
	E. coli Dam	0.137 ± 0.010	0.942
No substrates	*Y. pestis* Dam	1.385 ± 0.178	0.974
	E. coli Dam	0.679 ± 0.270	0.978

Assay conditions as for **Figure 3.6**.
Data given to 3 decimal places.

Plots of initial rate against incubation time were fitted to first order exponential decay curves and the rate constant for decay tabulated for each enzyme and incubation condition (**Table 3.1**). *E. coli* Dam was found to be approximately twice as stable as *Y. pestis* Dam at 30 °C with or without substrates present. The *E. coli* enzyme was therefore selected for the gel-based Dam activity assays due to its increased stability. The concentration of *E. coli* Dam to be used in the gel-based assay was optimised by assessing the fraction of plasmid DNA methylated (**Equation 3.1**) at a range of *E. coli* Dam concentrations (**Figure 3.7**).

$$\text{Fraction of methylated DNA} = \frac{I_1}{\text{SUM}(I_{1-3})}$$

Equation 3.1 Fraction of methylated DNA
Where I_1 = the intensity of the 10664 base pair band and $I_{1\text{-}3}$ = the intensities of the 10664, 6580 and 4084 base pair bands.

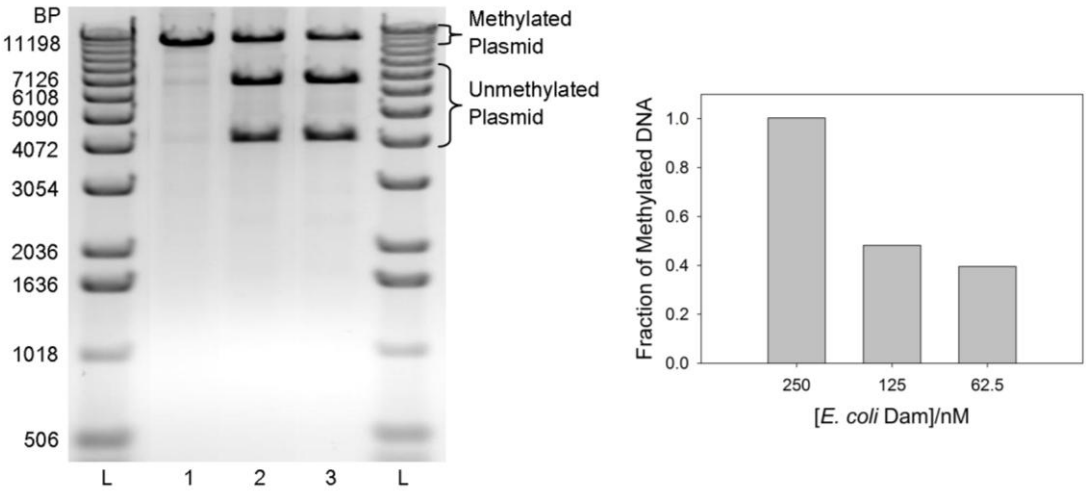

Figure 3.7 Gel-based Dam activity assay *E. coli* Dam concentration optimisation
0.8% agarose gel electrophoresis of *E. coli* Dam concentration optimisation assay (left) and fraction of methylated DNA, quantified from gel band intensity using **Equation 3.1**, for varying *E. coli* Dam concentration (right).
(L): ladder, (1-3): 250-62.5 nM *E. coli* Dam.
Assay conditions: 62.5-250 nM *E. coli* Dam, 6 nM plasmid (**pRL821**), 10 U μl^{-1} *Xho*I, 7.5 U μl^{-1} *Bcl*I, 60 µM AdoMet, 5% DMSO, 50 mM Tris, 100 mM NaCl, 10 mM $MgCl_2$, 1 mM DTT, pH 7.9. Step 1 (methylation) – total assay volume 20 µl, temperature 30 °C, 1 hr; Step 2 (denaturation) – total assay volume 20 µl, temperature 95 °C, 5 min; Step 3 (cleavage) – restriction enzymes *Xho*I and *Bcl*I added, total assay volume 22 µl, temperature 37 °C, 1 hr and 50 °C, 1 hr. Digested plasmid analysed by 0.8% agarose gel electrophoresis, bands quantified using the program ImageJ (*227*).

Complete methylation of 6 nM plasmid (equivalent to ~276 nM GATC sites) required the addition of 250 nM *E. coli* Dam. This concentration of *E. coli* Dam was therefore selected for all subsequent gel-based Dam methylation assays.

Restriction enzymes

An excess of *Bcl*I and *Xho*I were added to assays after the completion of the Dam methylation and denaturation steps, to ensure complete digestion of all plasmid DNA.

3.3.1.2 Substrate concentration

The optimum concentration of AdoMet was determined by assessing the effect of varying AdoMet concentrations on the fraction of DNA methylated (**Figure 3.8**). Full methylation of the plasmid was observed for AdoMet concentrations of 0.61 µM and above. This lower AdoMet concentration limit is approximately one tenth the *E. coli* Dam K_M^{AdoMet} (5.6 µM, Appendix Section 9.5.2) which is unsurprising due to the large excess of *E. coli* Dam (~80 times plasmid concentration) added to the assay.

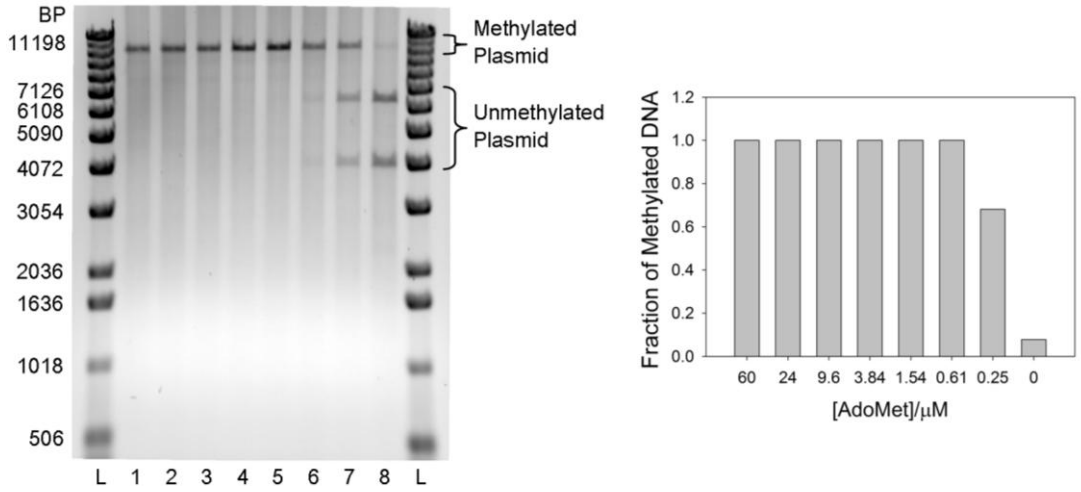

Figure 3.8 Gel-based Dam activity assay AdoMet concentration optimisation

0.8% agarose gel electrophoresis of AdoMet concentration optimisation assay (left) and fraction of methylated DNA, quantified from gel band intensity using **Equation 3.1**, for varying AdoMet concentration (right).

(L): ladder, (1-8): 60-0 µM AdoMet.

Assay conditions: 250 nM *E. coli* Dam, 3 nM plasmid (**pRL821**), 10 U μl^{-1} *Xho*I, 7.5 U μl^{-1} *Bcl*I, 0-60 µM AdoMet, 5% DMSO, 50 mM Tris, 100 mM NaCl, 10 mM $MgCl_2$, 1 mM DTT, pH 7.9. Step 1 (methylation) – total assay volume 20 µl, temperature 30 ˚C, 1 hr; Step 2 (denaturation) – total assay volume 20 µl, temperature 95 ˚C, 5 min; Step 3 (cleavage) – restriction enzymes *Xho*I and *Bcl*I added, total assay volume 22 µl, temperature 37 ˚C, 1 hr and 50 ˚C, 1 hr. Digested plasmid analysed by 0.8% agarose gel electrophoresis, bands quantified using the program ImageJ (*227*).

Ideally substrate concentrations at or close to K_M should be employed in assays for the identification of inhibitors (as discussed in Chapter 1), however in a secondary assay this is less important, as the goal of the assay is the confirmation and not initial identification of hit compounds. In the case of the gel-based methylation assay, DNA concentration is limited by the detection mode and availability of reagent and as such a concentration of 3 nM (~ one tenth K_M^{DNA} of 28 nM, Appendix Section 9.5.2) was selected to minimise reagent usage whilst maximising signal.

3.3.2 Validation

To validate the gel-based assay for the identification of Dam inhibitors and establish an optimal concentration of AdoMet for inhibition assays, a series of assays were prepared containing fixed concentrations of AdoMet and a range of AdoHcy concentrations (**Figure 3.9**).

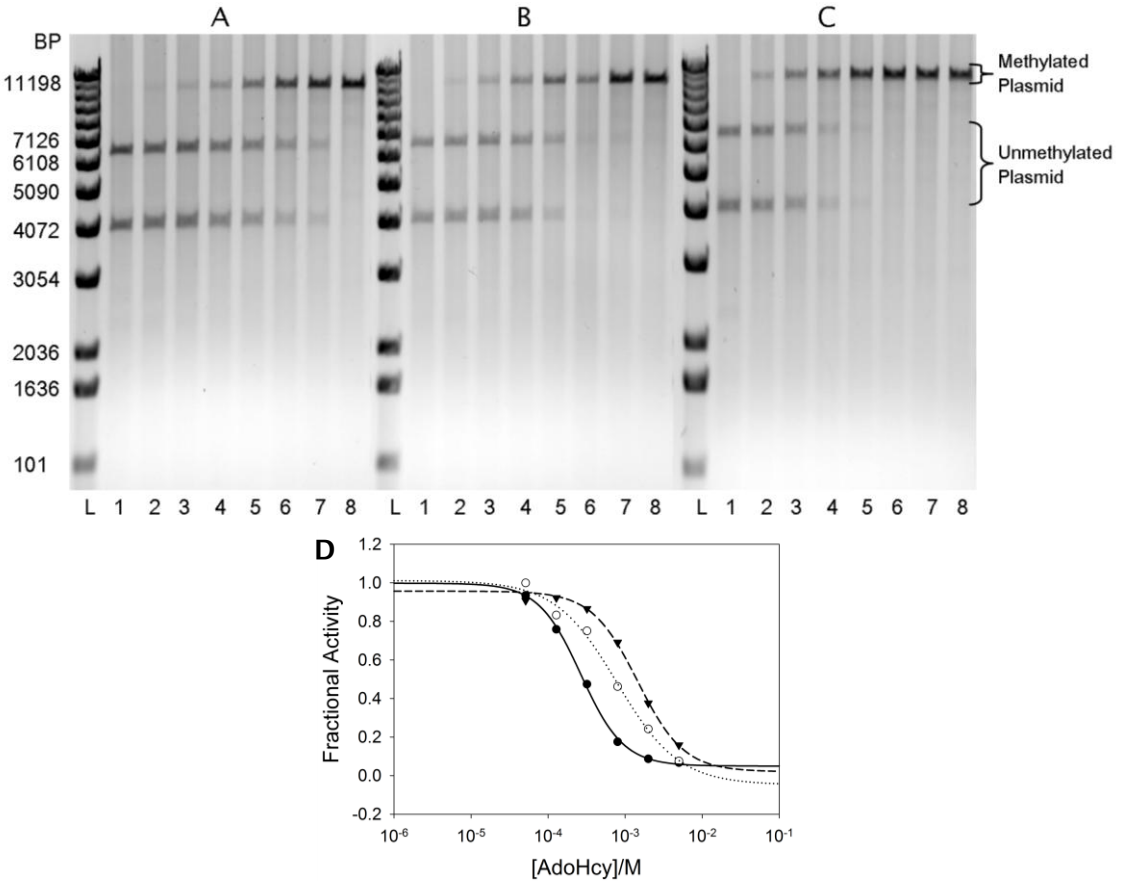

Figure 3.9 Gel-based Dam activity assay validation

A-C: 0.8% agarose gel electrophoresis of varying AdoHcy concentration with 6 (A), 24 (B) and 60 (C) µM AdoMet.

(L): ladder, (1): negative control (lacking AdoMet and AdoHcy), (2-7): 5-0.05 mM AdoHcy, (8): positive control (lacking AdoHcy).

D: Fractional activity, quantified from gel band intensity with **Equation 2.6A**, for 6 (filled circles), 24 (open circles) and 60 (triangles) µM AdoMet versus AdoHcy concentration. Data fitted to **Equation 2.6B**.

Assay conditions: 250 nM *E. coli* Dam, 3 nM plasmid (**pRL821**), 10 U μl^{-1} *Xho*I, 7.5 U μl^{-1} *Bcl*I, 0, 6, 24 or 60 µM AdoMet, 0-5 mM AdoHcy, 5% DMSO, 50 mM Tris, 100 mM NaCl, 10 mM $MgCl_2$, 1 mM DTT, pH 7.9. Step 1 (methylation) – total assay volume 20 µl, temperature 30 ˚C, 1 hr; Step 2 (denaturation) – total assay volume 20 µl, temperature 95 ˚C, 5 min; Step 3 (cleavage) – restriction enzymes *Xho*I and *Bcl*I added, total assay volume 22 µl, temperature 37 ˚C, 1 hr and 50 ˚C, 1 hr. Digested plasmid analysed by 0.8% agarose gel electrophoresis, bands quantified using the program ImageJ (*227*).

Increasing AdoMet concentration from 6 to 60 μM had little effect on the positive control assays (lacking AdoHcy), as would be expected based on the results of the AdoMet concentration optimisation. An effect on the inhibition of Dam by AdoHcy, however, was observed, with increased concentrations of AdoMet leading to a decrease in inhibition, as would be expected for an AdoMet-competitive inhibitor such as AdoHcy. An AdoMet concentration of 6 μM (~ equal to *E. coli* Dam K_M^{AdoMet}) was therefore selected for inhibition assays.

It should be noted however that at an AdoMet concentration of 6 μM, IC_{50}^{AdoHcy} was determined as 267 μM, much higher than the reported K_i^{AdoHcy} for *E. coli* Dam of 41.6 ± 10.4 (*105*). This is most likely due to the low concentration of DNA used in the gel-based assay and care should therefore be taken when interpreting results, which should ideally be used purely for the confirmation of inhibitory activity, and not for the determination of kinetic parameters.

3.4 Real-time break light cytosine methyltransferase activity assay

Off-target effects can induce unacceptable levels of toxicity, often leading to the failure of potential drug candidates. It is therefore important that the selectivity of HTS hits is established at an early stage, reducing the potential for attrition in the latter stages of the drug development process and thus minimising costs (*228*). The lack of a functionally similar DNA adenine-*N*6 methyltransferase enzyme in humans makes Dam an attractive target for the development of selective antimicrobials (*42*). However the abundance of other AdoMet-dependant methyltransferases in humans gives rise to other possible sources of toxic off-target effects.

The human DNA cytosine-*C*5 methyltransferases are functionally similar to Dam. The methyltransferases have two common substrates (DNA and AdoMet) but different DNA recognition sites and nucleotide targets. To assess the selectivity of compounds identified as Dam inhibitors through HTS, the principles of the real-time break light Dam activity assay have been utilised for the development of an activity assay for the human cytosine-*C*5 methyltransferase DNMT1 (**Figure 3.10** (*172*)).

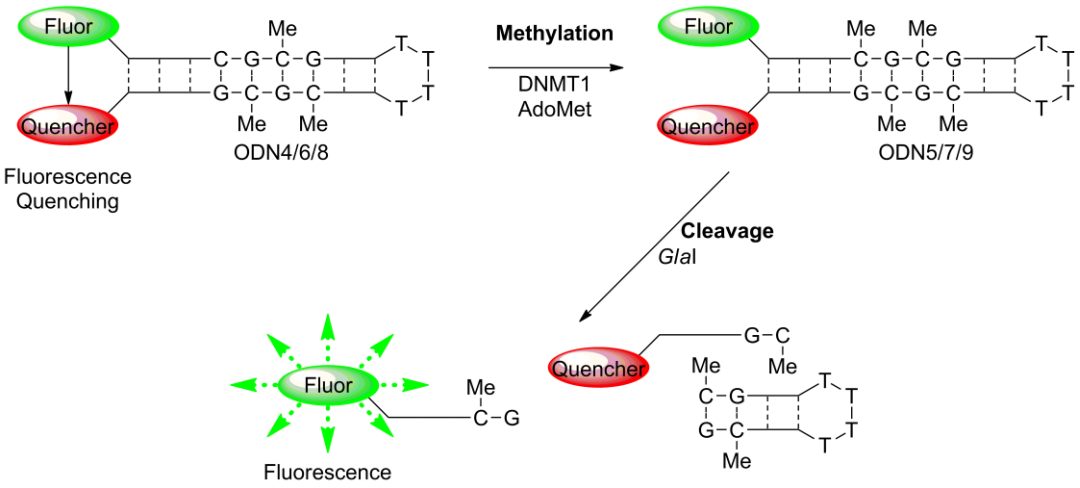

Figure 3.10 Real-time break light DNMT1 activity assay
A partially methylated break light oligonucleotide substrate (ODN4/6/8) containing a CG methylation site is fully methylated by DNMT1 (ODN5/7/9), making it a substrate for the restriction enzyme *Gla*I. Cleavage by *Gla*I results in the separation of fluorophore (Cy3/fluorescein) and quencher (dabcyl) and a subsequent proportional increase in fluorescence.

3.4.1 Optimisation

3.4.1.1 Buffer

Previous optimisation of the real-time break light DNMT1 activity assay has been completed by Dr R.J. Wood (*172*), with the optimum buffer conditions determined as [100 mM Tris, 5 mM magnesium chloride, 1 mM DTT, 0.1 mg ml^{-1} BSA, pH 7.5]. Sodium chloride concentration was not previously optimised for DNMT1 and so the effect of increasing sodium chloride concentration on DNMT1 activity was determined (**Figure 3.11**), with the optimum concentration identified as 12.5 mM.

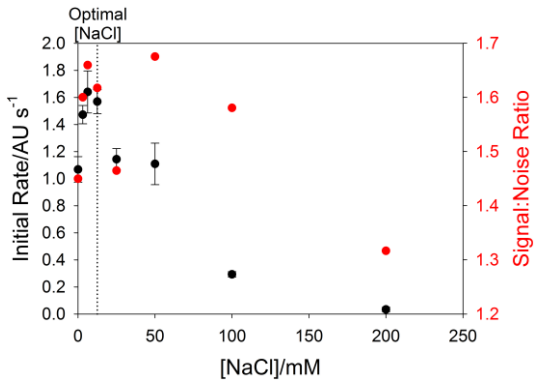

Figure 3.11 DNMT1 activity assay sodium chloride concentration optimisation
Background subtracted initial rate of methylation by DNMT1 (black) and signal:noise ratio (red).
Assay conditions: 25 nM DNMT1, 0.0125 U μl^{-1} *Gla*I, 250 nM partially methylated oligonucleotide (ODN8), 0 or 20 µM AdoMet, 0-200 mM NaCl, 100 mM Tris, 5 mM $MgCl_2$, 0.1 mg ml^{-1} BSA, 1 mM DTT, 5% glycerol, pH 7.5. Total assay volume 20 µl, in 384 well plate, gain 100, temperature 37 ˚C.

3.4.1.2 Oligonucleotide substrate design

Initial DNMT1 activity assays were carried out using break light oligonucleotide probes labelled with the fluorophore Cy3 and the quencher dabcyl. To minimise reagent costs Cy3 was replaced with the more economically viable fluorophore fluorescein (**Figure 3.12**).

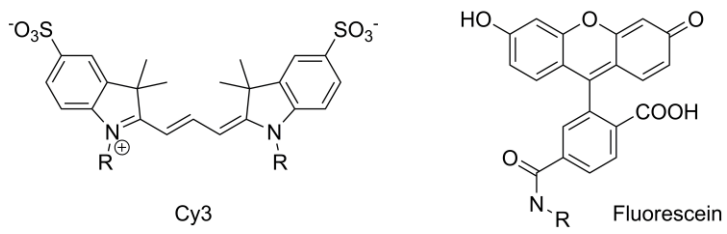

Figure 3.12 Structures of the fluorophores Cy3 and fluorescein

In addition to altering the fluorophore, oligonucleotides with CG-rich and CG-poor recognition site flanking sequences were investigated to determine the optimal substrate for DNMT1 (**Table 3.2**).

Table 3.2 DNMT1 activity assay oligonucleotides

Oligonucleotide*	Fluorophore	Stem Length#	%CG Character†	Recognition site and flanking bases‡
ODN4/5	Cy3	14 bp	57%	TAT**GC**GCA
ODN6/7	Fluorescein	14 bp	57%	TAT**GC**GCA
ODN8/9	Fluorescein	14 bp	57%	TAG**GC**GCC

* Partially methylated/fully methylated.

Length of the hairpin stem duplex (i.e. a 20 base hairpin with a 4 base loop would have an 8 base pair (bp) stem).

† Number of C or G bases in the hairpin stem/total bases in the hairpin stem.

‡ DNMT1 GC recognition site in **bold red**.

Initial *Gla*I activity assays carried out with the fully methylated fluorescein labelled oligonucleotide ODN7, showed a change in the product formation time course compared to experiments where the equivalent Cy3 oligonucleotide (ODN5) was used (**Figure 3.13A**). A "bi-phasic" change in fluorescence over time was observed for the fluorescein labelled oligonucleotide, whereas a steady decrease in rate over time was observed for the Cy3 labelled oligonucleotide.

Further analysis of the oligonucleotide equilibration period prior to the addition of *Gla*I showed the fluorescein labelled oligonucleotide to undergo two equilibration processes, the first over approximately fifteen minutes, and the second over approximately thirty minutes (**Figure 3.13B**). The drop in fluorescence observed between equilibration points 1 and 2 appeared to correlate with the bi-phasic behaviour observed in the assay time course for the fluorescein labelled oligonucleotide, raising the possibility that the two phenomena are connected.

Oligonucleotide melting profiles were obtained for the partially methylated fluorescein labelled oligonucleotide (ODN6), which showed the hairpin to have two different melting temperatures (T_m's), at 80 and 50 °C (**Figure 3.14**). This result suggests that the oligonucleotide has at least two stable forms at assay temperature (37 °C), with the effect observed in **Figure 3.13B** possibly due to equilibration between these forms.

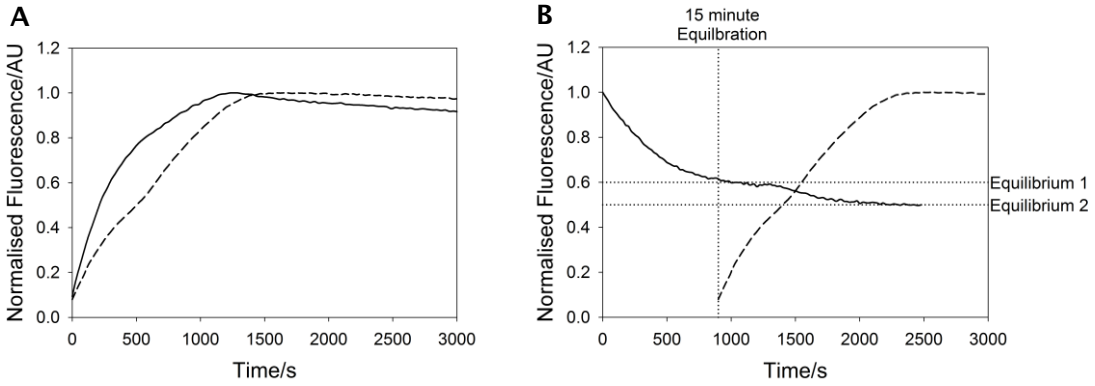

Figure 3.13 Comparison of *Gla*I assay time courses for Cy3 and fluorescein labelled fully methylated oligonucleotide substrates

A: Normalised fluorescence against time plots for Cy3 (solid line) and fluorescein (dashed line) labelled oligonucleotide substrates.

B: Normalised fluorescence against time plots for fluorescein labelled oligonucleotide extended equilibration (solid line) and assay time course after standard 15 minute equilibration (dashed line).

Assay conditions: 0.05 U μl^{-1} *Gla*I, 250 nM fully methylated oligonucleotide (ODN5 – solid line or ODN7 – dashed line), 20 µM AdoMet, 12.5 mM NaCl, 100 mM Tris, 5 mM $MgCl_2$, 0.1 mg ml^{-1} BSA, 1 mM DTT, 5% glycerol, pH 7.5. Total assay volume 20 µl, in 384 well plate, gain 133 or 110, temperature 37 °C.

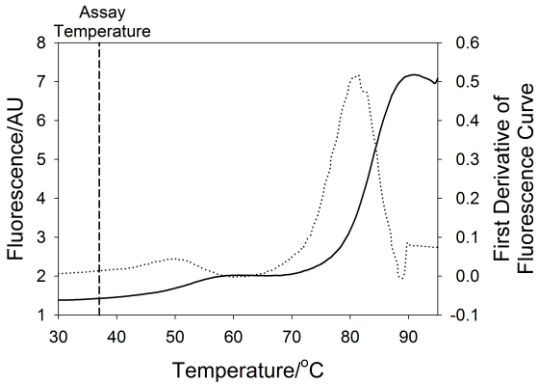

Figure 3.14 Fluorescein labelled oligonucleotide melting profile

Fluorescence versus temperature melting profile, and first derivative of melting profile showing melting temperatures at 80 and 50 °C.

Assay conditions: 250 nM partially methylated oligonucleotide (ODN6), 12.5 mM NaCl, 100 mM Tris, 5 mM $MgCl_2$, 0.1 mg ml^{-1} BSA, 1 mM DTT, pH 7.5. Total assay volume 20 µl.

The reason for the difference in the behaviour of the Cy3 (ODN5) and fluorescein (ODN7) labelled oligonucleotides is unclear. Both substrates are of the same length and sequence, making the only variation the fluorescent label located at the 5' end of

the oligonucleotide. This may suggest that the Cy3 fluorescent dye is stabilising the hairpin form, thus reducing the time for equilibration to occur. However, another possible explanation is that a similar effect does occur for the Cy3 labelled oligonucleotide, but that the change in fluorescence observed is much smaller than for the fluorescein labelled oligonucleotide and thus not as readily detected. The latter of these two theories is supported by the low quantum yield of Cy3 (0.09 in Tris buffer (*229*)) compared to fluorescein (0.92 in water (*230*)). The reinstatement of the Cy3 labelled oligonucleotide to circumvent this issue was therefore not implemented due to cost and the potential risk of experiencing a similar, unobservable, equilibration effect.

Whilst the bi-phasic behaviour observed for the fluorescein labelled oligonucleotide is not ideal, the overall effect on assay quality can be minimised by the application of an extended equilibration step prior to assay initiation. To limit the evaporation of reagents over the duration of the assay this equilibration step was set at thirty minutes, approximately equal to the second equilibration phase (**Figure 3.13B**).

The effect of DNA recognition site flanking sequence on enzyme activity was assessed by monitoring the assay time courses for partially methylated oligonucleotides ODN6 and ODN8 (**Figure 3.15A** and **B**). Whilst the signal obtained for the full assay was similar for the two substrates, ODN6 showed a much lower negative signal (for assays lacking AdoMet), as reflected by the signal:noise ratios (**Figure 3.15A** and **B**, red line).

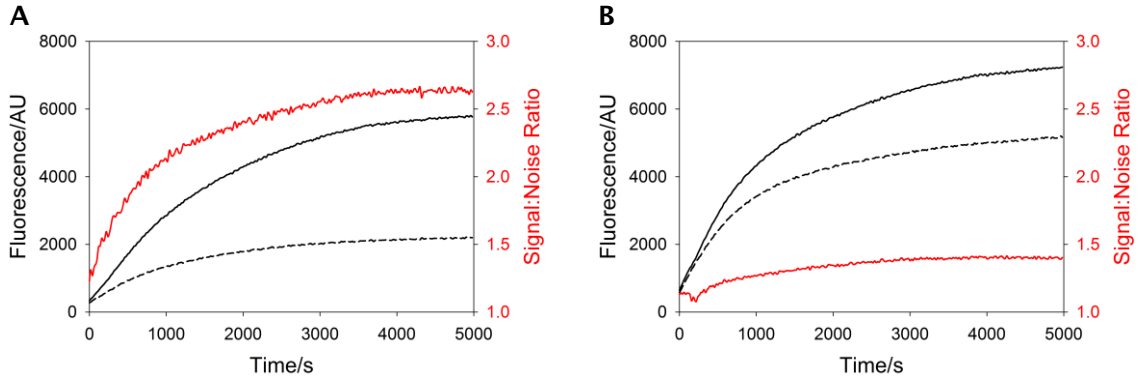

Figure 3.15 Comparison of DNMT1 assay time courses for fluorescein labelled partially methylated oligonucleotide substrates

Fluorescence against time plots for positive (solid line) and negative (lacking AdoMet, dashed line) DNMT1 activity assays for ODN6 (A) and ODN8 (B). Signal:noise ratio shown in red.

Assay conditions: 25 nM DNMT1, 0.0125 U μl^{-1} *Gla*I, 250 nM partially methylated oligonucleotide (A: ODN6 or B: ODN8), 0 or 20 µM AdoMet, 12.5 mM NaCl, 100 mM Tris, 5 mM $MgCl_2$, 0.1 mg ml^{-1} BSA, 1 mM DTT, 5% glycerol, pH 7.5. Total assay volume 20 µl, in 384 well plate, gain 110, temperature 37 ˚C.

The results of the DNMT1 assays show that a better signal:noise ratio was obtained for the oligonucleotide with the less CG-rich flanking sequences (ODN6). In addition, *Gla*I activity assays conducted with the partially and fully methylated oligonucleotides (ODN6/7 and 8/9) showed that non-specific cleavage of the partially methylated substrate was higher for ODN8 than ODN6, suggesting that in this instance, increasing the CG-richness of the flanking sequences decreases *Gla*I specificity (**Figure 3.16**). As such, ODN6 was selected as the optimum substrate for the DNMT1 activity assay.

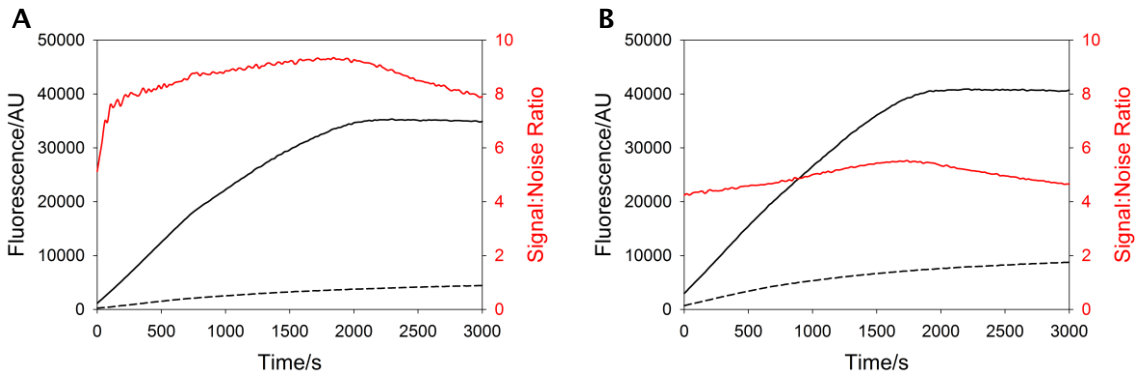

Figure 3.16 Comparison of *Gla*I assay time courses for fluorescein labelled partially and fully methylated oligonucleotide substrates

Fluorescence against time plots for fully (solid line) and partially (dashed line) methylated oligonucleotides ODN6/7 (A) and ODN8/9 (B). Signal:noise ratio shown in red.

Assay conditions: 0.05 U μl^{-1} *Gla*I, 250 nM partially or fully methylated oligonucleotide (A: ODN6/7 or B: ODN8/9), 12.5 mM NaCl, 100 mM Tris, 5 mM $MgCl_2$, 0.1 mg ml^{-1} BSA, 1 mM DTT, 5% glycerol, pH 7.5. Total assay volume 20 µl, in 384 well plate, gain 110, temperature 37 ˚C.

3.4.1.3 Plate reader

Detection of fluorescence for the real-time break light DNMT1 activity assay could be carried out using a Tecan Safire[II] or a BMG Polarstar Omega microplate reader. The variation in assay signal across and down a 384 well plate was assessed for both readers, with 16 positive and 8 negative (lacking AdoMet) control assays placed on either side of the plate. The initial rate of the positive controls divided by the average of the positive controls was plotted against row position for the first and last column of the plate (**Figure 3.17**), and showed minimal difference between the two readers. Assays read in the BMG reader had a CV of 10.5% for the positive controls compared with 14.5% for the Tecan reader, and the Z'-value across the plate was 0.40 for the BMG reader compared with 0.34 for the Tecan. The BMG reader was therefore selected for subsequent DNMT1 activity assays due to the observed production of more reproducible and accurate results.

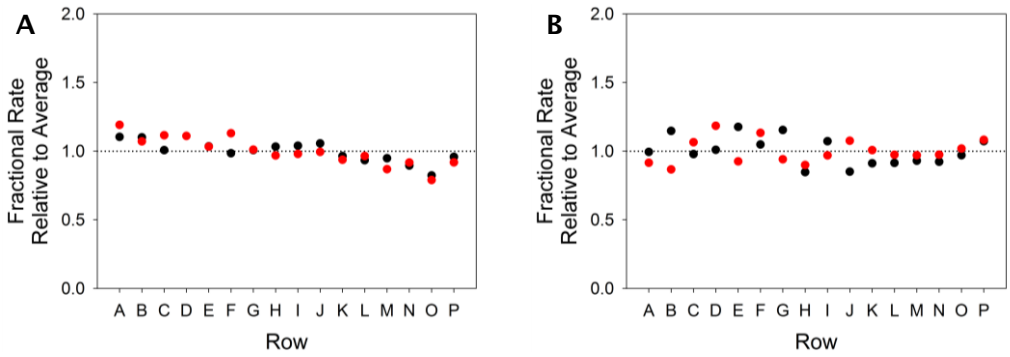

Figure 3.17 Comparison of DNMT1 assay reproducibility for different plate readers
Fractional rate relative to the average initial rate of assays placed in column 1 (black) and 24 (red) of a 384 well plate. Plate read in Tecan Safire^{II} (A) or BMG Polarstar Omega (B) plate reader.
Assay conditions: 25 nM DNMT1, 0.05 U µl^{-1} *Gla*I, 250 nM partially methylated oligonucleotide (ODN6), 0 or 20 µM AdoMet, 12.5 mM NaCl, 100 mM Tris, 5 mM $MgCl_2$, 0.1 mg ml^{-1} BSA, 1 mM DTT, 5% glycerol, pH 7.5. Total assay volume 20 µl, in 384 well plate, gain 110 (A) or 1550 (B), temperature 37 ˚C.

3.4.1.4 Enzyme concentrations

The optimum concentration of the restriction enzyme *Gla*I to be added to the DNMT1 activity assay was determined by monitoring the apparent initial rate over a range of *Gla*I concentrations (**Figure 2.14**).

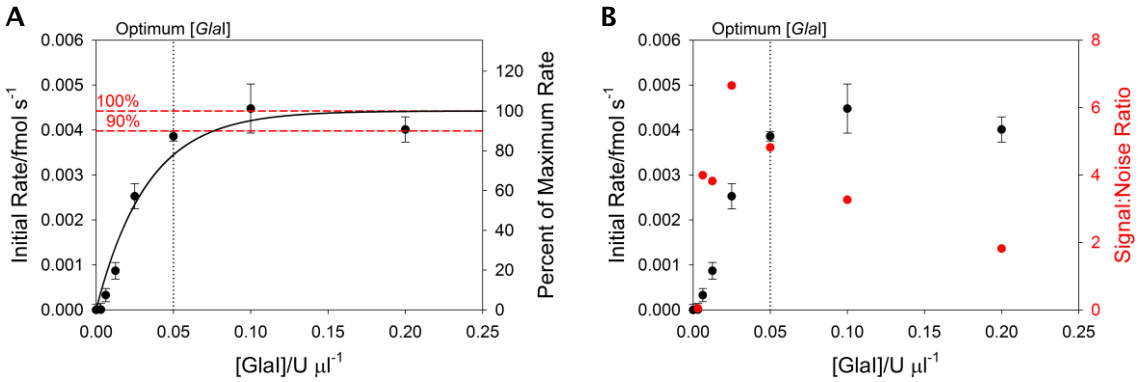

Figure 3.18 DNMT1 activity assay *Gla*I concentration optimisation
A: Background subtracted initial rate of methylation by DNMT1. Data fitted to an exponential rise to a maximum of the form f=a*(1-exp(-b*x)), where a = maximum rate.
B: Background subtracted initial rate of methylation by DNMT1 (black) and signal:noise ratio (red).
Assay conditions: 25 nM DNMT1, 0-0.2 U µl^{-1} *Gla*I, 250 nM partially methylated oligonucleotide (ODN6), 0 or 20 µM AdoMet, 12.5 mM NaCl, 100 mM Tris, 5 mM $MgCl_2$, 0.1 mg ml^{-1} BSA, 1 mM DTT, 5% glycerol, pH 7.5. Total assay volume 20 µl, in 384 well plate, gain 1550, temperature 37 ˚C.

Maximum rate was obtained at approximately 0.15 U μl^{-1} *Gla*I, however a rapid decrease in signal:noise was observed from 0.025 U μl^{-1} *Gla*I. To maintain a viable screening window a slightly lower concentration of 0.05 U μl^{-1} *Gla*I was therefore selected, at which approximately 87% of the maximum rate and a signal:noise ratio of 4.8 were achieved.

The effective assay range was established by assessing the effect of increasing DNMT1 concentration on initial rate of methylation (**Figure 2.15**). A line of best fit of the form $f=y_0+a*x$ fitted through data points from 0 to 25 nM showed the upper assay limit to be approximately 25 nM DNMT1, approximately one-tenth of the DNA concentration added to the assay.

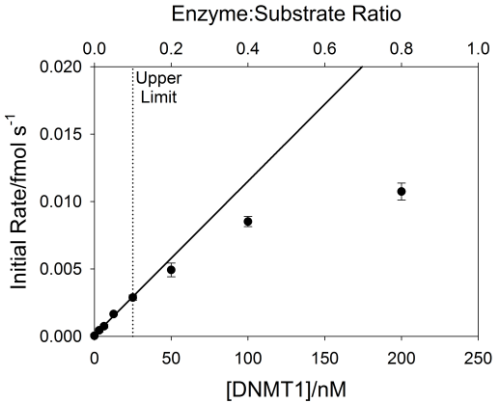

Figure 3.19 DNMT1 activity assay effective assay range
Background subtracted initial rate of methylation by DNMT1. Data fitted to a linear equation of the form $f=y_0+a*x$, where y_0 = the y-axis intercept and a = the line gradient. Assay conditions: 0-200 nM DNMT1, 0.05 U μl^{-1} *Gla*I, 250 nM partially methylated oligonucleotide (ODN6), 0 or 20 µM AdoMet, 12.5 mM NaCl, 100 mM Tris, 5 mM $MgCl_2$, 0.1 mg ml^{-1} BSA, 1 mM DTT, 5% glycerol, pH 7.5. Total assay volume 20 µl, in 384 well plate, gain 1550, temperature 37 ˚C.

3.4.1.5 Substrate concentrations

Reported values for DNMT1 K_M^{DNA} range from 4.6 µM for unmethylated DNA to 10.8 µM for hemimethylated DNA (*231*). Attempts at determining K_M^{DNA} using the real-time break light DNMT1 activity assay were inconclusive due to the equilibration effect observed previously (Section 3.4.1.2). Whilst a thirty minute equilibration was adequate for lower concentrations of DNA (up to 250 nM), increasing the DNA concentration further extends the required equilibration time, leading to a re-emergence of the bi-phasic time courses at higher DNA concentrations, and a decrease in the observed rates. Increasing equilibration time led to problems with reagent evaporation, and the addition of mineral oil to prevent this could not be satisfactorily implemented using

the available technology. It was therefore not possible to determine K_M^{DNA} for DNMT1 using the real-time break light assay and a maximum DNA concentration of 250 nM was applied to all subsequent DNMT1 activity assays.

The K_M^{AdoMet} was investigated under conditions where DNA concentration was potentially limiting in order to avoid the effects of oligonucleotide equilibration seen at higher concentrations of DNA. Initial rates of methylation were determined for a range of AdoMet concentrations and data were fitted to a hyperbola of the form f=a*x/(b+x). Values for V_{max} (a) and K_M (b) were 0.565 ± 0.007 fmol s^{-1} and 3.25 ± 0.12 µM respectively. The value of K_M^{AdoMet} determined using the real-time break light DNMT1 activity assay compares well with the previously reported value of 3.4 µM (*231*), suggesting that the low concentration of DNA used in the assay does not affect the affinity of DNMT1 for AdoMet.

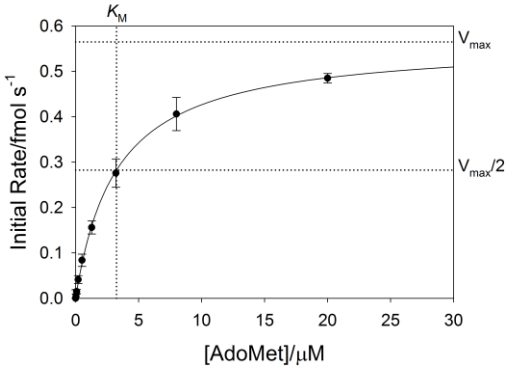

Figure 3.20 Graphical determination of DNMT1 K_M^{AdoMet}
Initial rate versus concentration of AdoMet. Data fitted to **Equation 2.4B**.
Assay conditions: 25 nM DNMT1, 0.05 U $µl^{-1}$ *Gla*I, 250 nM partially methylated oligonucleotide (ODN6), 0-20 µM AdoMet, 12.5 mM NaCl, 100 mM Tris, 5 mM $MgCl_2$, 0.1 mg ml^{-1} BSA, 1 mM DTT, 5% glycerol, pH 7.5. Total assay volume 20 µl, in 384 well plate, gain 1550, temperature 37 ˚C.

3.4.2 Validation

The screening window of the real-time break light DNMT1 activity assay was assessed over a series of four positive and four negative (lacking AdoMet) control assays. The limited availability of both enzymes required for the assay made a more valid assessment over more data points unfeasible. The results of this limited test showed the assay screening window to be acceptable, with a Z'-value of 0.51 obtained.

Validation of the assay for the identification of inhibitors and the determination of IC_{50} values was achieved by assessing the affect of the known inhibitor AdoHcy on enzyme activity. Two separate experiments, in which AdoMet concentration was held equal to K_M^{AdoMet}, found IC_{50}^{AdoHcy} to be 0.941 ± 0.076 µM, and 0.419 ± 0.076 µM, giving an average of 0.680 ± 0.369 µM, which compares well with IC_{50} values reported in the literature (*131, 232*). Experiments to determine K_i^{AdoHcy} were not carried out due to the limited availability of both DNMT1 and *Gla*I.

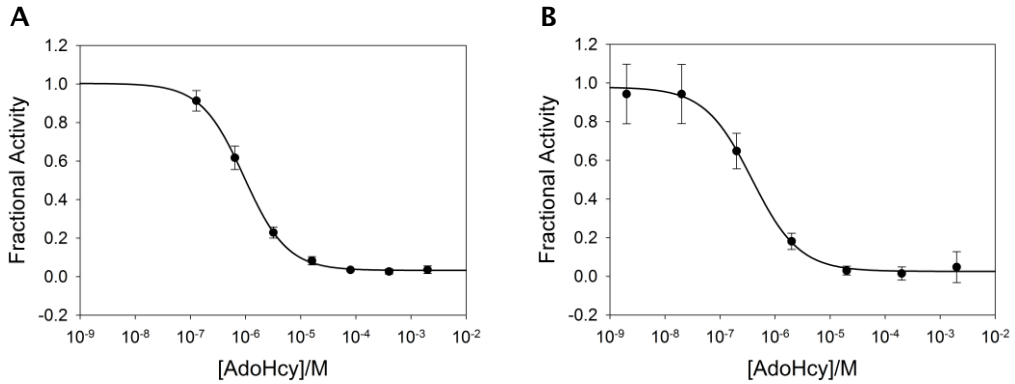

Figure 3.21 DNMT1 activity assay AdoHcy IC_{50} determination
Fractional activity, calculated using **Equation 2.6A** versus concentration of AdoHcy for experiment 1 (A) and 2 (B). Data fitted to **Equation 2.6B**.
25 nM DNMT1, 0.05 U μl^{-1} *Gla*I, 250 nM partially methylated oligonucleotide (ODN6), 0 or 3 µM AdoMet, 0-2 mM AdoHcy, 5% DMSO, 12.5 mM NaCl, 100 mM Tris, 5 mM $MgCl_2$, 0.1 mg ml^{-1} BSA, 1 mM DTT, 5% glycerol, pH 7.5. Total assay volume 20 µl, in 384 well plate, gain 1250, temperature 37 °C.

3.5 Fluorescence anisotropy assay

The substrate inhibition effect observed when increasing DNA concentrations above the apparent K_M^{DNA} for Dam makes the analysis of DNA concentration dependant effects with the real-time break light Dam activity assay difficult. In light of these issues an alternative assay format was developed to probe the binding interaction between Dam and DNA using fluorescence anisotropy (**Figure 3.22**).

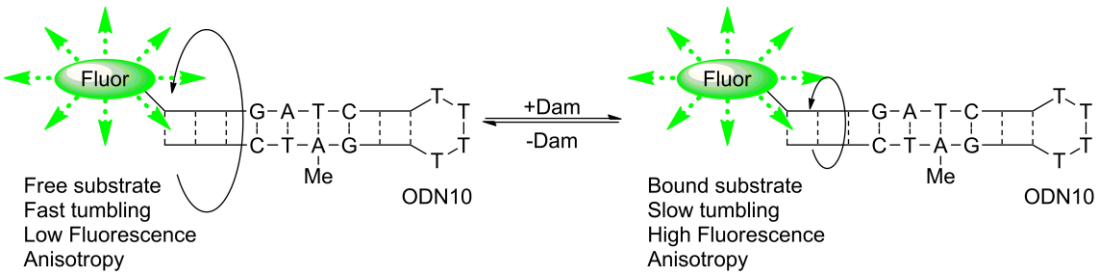

Figure 3.22 Fluorescence anisotropy assay
A hemimethylated oligonucleotide substrate (ODN10) containing a GATC methylation site is bound by Dam resulting in an increase in the observed fluorescence anisotropy of the fluorophore (fluorescein).

Excitement of a fluorophore by polarised light results in the emission of light polarised as a function of fluorescence lifetime and rotational diffusion, with the intensity of the fluorescence emitted typically measured parallel and perpendicular to the plane of the excited light. The degree to which the parallel and perpendicular fluorescence intensities vary from each other gives a measure of how quickly the fluorophore is tumbling in solution, and is generally measured as fluorescence polarisation or fluorescence anisotropy, which can be calculated with **Equation 3.2A** and **B** respectively (*233, 234*).

A: $$P = \frac{I^{\parallel} - I^{\perp}}{I^{\parallel} + I^{\perp}}$$

B: $$A = \frac{I^{\parallel} - I^{\perp}}{I^{\parallel} + 2I^{\perp}}$$

Equation 3.2 Fluorescence polarisation (A) and anisotropy (B)
Where P = polarisation, A = anisotropy, $I^{\parallel}$ = parallel fluorescence intensity and $I^{\perp}$ = perpendicular fluorescence intensity.

Fluorophores covalently attached to small ligands, such as short oligonucleotides or peptides, rotate rapidly in solution, emitting mostly depolarised light when excited by a polarised light source. Binding of a small labelled ligand to a larger receptor, such as an enzyme, significantly reduces the rotational speed of the fluorophore, leading to the emission of a greater proportion of polarised light (*234*). The degree of polarisation can be measured as anisotropy, which can be used to calculate the fraction of a labelled ligand bound by an unlabelled receptor using **Equation 3.3A** (*233*). The anisotropy of the labelled ligand in the free and bound states are determined by fitting a plot of anisotropy against receptor concentration to a ligand binding calibration curve (**Equation 3.3B**) (*235*). Finally, dissociation constants for ligand:receptor binding interactions can be determined by fitting a plot of fraction of substrate bound versus receptor concentration to **Equation 3.3C** (*233*).

A: $$F_B = \frac{A_{obs} - A_F}{A_B - A_{obs}\ Q + A_{obs} - A_F}$$

B: $$A_{obs} = A_F + \frac{A_F - A_B}{1 + \left(\frac{[R]}{x_0}\right)^h}$$

C: $$F_B = \frac{K_D + [L]_T + [R] - \sqrt{K_d + [L]_T + [R]^2 - [L]_T + [R]}}{2[L]_T}$$

Equation 3.3 Fraction of substrate bound in a fluorescence anisotropy experiment (A), ligand binding calibration curve (B) and determination of equilibrium dissociation constant (C)

Where F_B = fraction of labelled substrate bound, A_{obs} = observed anisotropy of the solution, A_F and A_B = anisotropy of the free and bound labelled substrate (as calculated by **Equation 3.1B**), Q = the ratio of the fluorescence intensities of the free and bound labelled substrates, [R] = receptor concentration, x_0 = receptor concentration at F_B = 0.5, h = the Hill coefficient, K_D = the equilibrium dissociation constant for the ligand:receptor complex, $[L]_T$ = total ligand concentration and $[R]_T$ = total receptor concentration.

Fluorescence anisotropy can also be used to study the inhibition of ligand:receptor binding through competition binding experiments, in which increasing concentrations of inhibitor are added to a fixed concentration of labelled ligand and unlabelled receptor. If the inhibitor competes with the labelled ligand for the receptor a decrease in anisotropy will be observed with increasing inhibitor concentration. In cases where

the equilibrium dissociation constant (K_D) is known and a ligand binding calibration curve has been plotted, competition binding constants can be determined by fitting a plot of the fraction of substrate bound versus inhibitor concentration to **Equation 3.4** (*233*).

$$F_B = \frac{2\sqrt{d^2 - 3e}\,\cos\left(\frac{\theta}{3}\right) - d}{3K_D + 2\sqrt{d^2 - 3e}\,\cos\left(\frac{\theta}{3}\right) - d}$$

$$d = K_D + K_{Dc} + [I] + [L]_T - [R]_T$$

$$e = [L]_T - [R]_T\ K_D + [I] - [R]_T\ K_{Dc} + K_D K_{Dc}$$

$$\theta = \arccos\left[\frac{-2d^3 + 9de - 27f}{2\sqrt{d^{2-3e}\ ^3}}\right]$$

$$f = -K_D K_{Dc}[R]_T$$

Equation 3.4 Determination of competition binding constant

Where F_B = fraction of labelled substrate bound (calculated from **Equation 3.3A** and **B**), K_D = the dissociation constant for the substrate:receptor complex, K_{Dc} = the competition binding constant for the inhibitor:receptor complex, $[L]_T$ = total ligand concentration and $[R]_T$ = total receptor concentration.

3.5.1 Optimisation

3.5.1.1 Non-specific binding

Non-specific binding and aggregation of the labelled substrate can severely impede fluorescence anisotropy readings, with labelled ligand concentration showing a non-linear relationship to fluorescence anisotropy. Reduction of these effects can be achieved through the addition of additives such as BSA and detergent (*236, 237*). Decreasing the surface:volume ratio can also help reduce non-specific binding, by minimising interactions between the labelled ligand and the reaction vessel.

Initial experiments examined the effects of buffer system and assay volume on fluorescence anisotropy over a range of fluorescently labelled DNA (substrate) concentrations, as shown in
Figure 3.23.

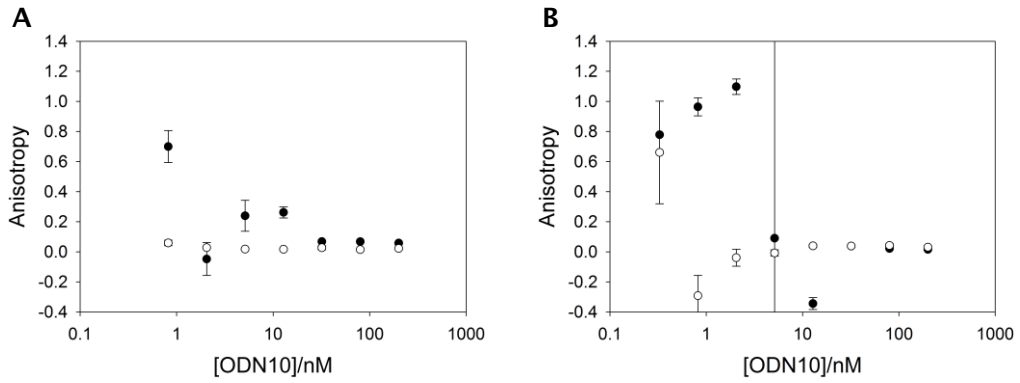

Figure 3.23 Optimisation of the fluorescence anisotropy assay buffer system and assay volume

Background corrected anisotropy versus labelled oligonucleotide concentration in 96 (A) and 384 (B) well plates. Anisotropy measured in H_2O (filled circles) or real-time break light Dam activity assay buffer[7] (open circles).

Assay conditions: 0-200 nM hemimethylated oligonucleotide (ODN10), buffer as stated above. Total assay volume 100 (A) or 20 (B) µl, in 96 (A) or 384 (B) well plate, gain 1450/1445 (A) or 1519/1518 (B), 25 ˚C.

[7] Real-time break light Dam activity assay buffer: [20 mM Tris, 80 mM NaCl, 8 mM $MgCl_2$, 1 mM DTT, 0.1 mg ml^{-1} BSA, 5% glycerol, pH 7.9].

Addition of the detergent Tween-20 to assays prepared in the real-time break light Dam activity assay buffer in 96 well plates led to little change in non-specific binding, with a linear relationship between labelled ligand concentration and fluorescence anisotropy observed down to 10 nM oligonucleotide with and without Tween-20 (**Figure 2.24**). Although a slight increase in anisotropy was observed below 10 nM on the addition of Tween-20, the detergent was included in further assays to reduce the potential for increased aggregation and non-specific binding on enzyme addition.

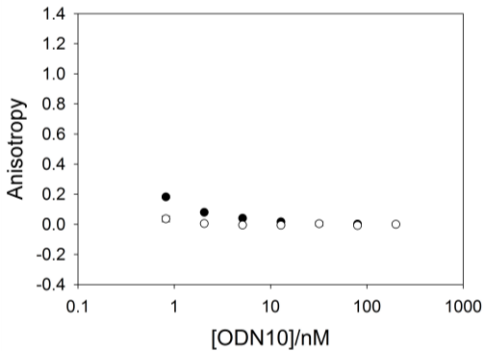

Figure 3.24 Fluorescence anisotropy assay optimisation of buffer additives
Background corrected normalised anisotropy versus labelled oligonucleotide concentration with (filled circles) and without (open circles) Tween-20. Anisotropy values normalised to minimum anisotropy = 0.
Assay conditions: 0-200 nM hemimethylated oligonucleotide (ODN10), 0.1% Tween-20, 20 mM Tris, 80 mM NaCl, 8 mM $MgCl_2$, 1 mM DTT, 0.1 mg ml^{-1} BSA, 5% glycerol, pH 7.9. Total assay volume 100 µl, in 96 well plate, gain 1450/1445, 25 ˚C.

3.5.1.2 Enzyme stability

Stability experiments carried out with *Y. pestis* and *E. coli* Dam (Section 3.3.1.1 and Chapter 2, Section 2.3.3.3) show both enzymes to undergo inactivation over extended assay time courses at 30 ˚C, with *E. coli* Dam stability approximately double that of *Y. pestis* Dam. Assessment of the effect of this inactivation process on fluorescence anisotropy signal was achieved by monitoring assays containing *Y. pestis* Dam and *E. coli* Dam over time. A control experiment was also prepared containing a thermally stable Dam from the thermophile *Pyrococcus horikoshii* (expressed and purified by J.E. Harmer).

For the thermally stable *P. horikoshii* Dam anisotropy remained relatively constant over time, however for both *E. coli* and *Y. pestis* Dam anisotropy decreased over time, with a faster rate of decay observed for *Y. pestis* Dam (**Figure 3.25A**). The addition of AdoHcy resulted in the stabilisation of initial anisotropy signals over the lifetime of the experiment (**Figure 3.25B**), suggesting that AdoHcy has a stabilising effect on the Dam:DNA complex.

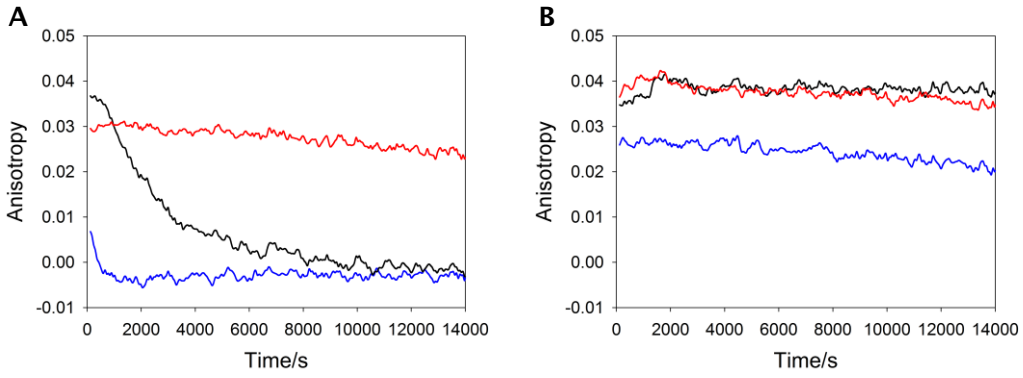

Figure 3.25 Effect of enzyme stability on anisotropy
Background subtracted anisotropy over time for *Y. pestis* (blue line) *E. coli* (black line) and *P. horikoshii* (red line) Dam in the absence (A) and presence (B) of AdoHcy.
Assay conditions: 0 or 500 nM Dam, 0 or 50 nM hemimethylated oligonucleotide (ODN10), 0 (A) or 2 (B) mM AdoHcy, 5% DMSO, 0.1% Tween-20, 20 mM Tris, 80 mM NaCl, 8 mM $MgCl_2$, 1 mM DTT, 0.1 mg ml^{-1} BSA, 5% glycerol, pH 7.9. Total assay volume 100 µl, in 96 well plate, gain 2181/2212, 30 ˚C.

The loss of anisotropy observed for *E. coli* and *Y. pestis* Dam in the absence of AdoHcy suggest that the Dam:DNA complex is dissociating over time, possibly due to inactivation of the enzyme. The rates of complex dissociation and inactivation are faster for *Y. pestis* Dam, consistent with a model in which enzyme inactivation leads to complex dissociation. These findings imply that Dam:DNA binding is regulated by the presence of the methyl donor AdoMet (in this case an AdoMet mimic, AdoHcy), which is in agreement with literature reports that AdoMet facilitates the formation of a specific Dam:DNA complex (*99, 101, 105*).

Although *P. horikoshii* Dam shows better stability in the absence of AdoHcy than *E. coli* Dam, the latter shares a much higher percentage sequence identity (70.5% versus 31.4%) with *Y. pestis* Dam. *E. coli* Dam was therefore selected for use in fluorescence anisotropy assays due to its increased similarity to *Y. pestis* Dam.

3.5.1.3 Substrate concentrations

A fixed concentration of the fluorescently labelled ligand at a concentration close to K_D for the ligand:receptor complex (if known) is typically used for fluorescence anisotropy and polarisation experiments (*234*). Coffin *et al.* have reported a fluorescence polarisation method for assessing the binding of *E. coli* Dam in which they employed 20 nM labelled substrate, with K_D^{DNA} values of 84 and 101 nM obtained in the presence of 50 µM sinefungin (*103, 104*). The use of a similar concentration of DNA in this case would therefore be valid, as K_M^{DNA} for *E. coli* Dam was determined as 28 nM with the

real-time break light Dam activity assay (Appendix Section 9.5.2), and non-specific binding has been shown to be minimised at ODN10 concentrations of 10 nM and above (Section 3.5.1.1).

Formation of a stable substrate:receptor complex for the determination of fluorescence anisotropy often requires the removal of a secondary substrate or co-factor to prevent turnover of substrate and subsequent product release. For a bi-substrate mechanism this process is relatively simple, with the unlabelled substrate removed from solution. As Dam has been shown to follow an ordered bi-bi mechanism in which AdoMet binds prior to the formation of a specific Dam:DNA complex (*99, 101, 105*), the removal of AdoMet could affect the observed K_D values. In addition, investigations into the affect of enzyme inactivation on anisotropy have shown that the addition of AdoHcy induces stabilisation (**Figure 3.25B**). Experiments were therefore prepared with and without AdoHcy, in order to assess the effect on both K_D and enzyme stability.

3.5.2 Validation

Validation of the fluorescence anisotropy experiment was achieved by comparison of K_D^{DNA} values for *E. coli* Dam binding the hemimethylated hairpin ODN10 to K_D^{DNA} values reported in the literature. Anisotropy was monitored for assays containing a range of *E. coli* Dam concentrations, a fixed concentration of fluorescently labelled oligonucleotide (ODN10) and either 0 or 200 µM AdoHcy. Data were analysed using **Equation 3.3A-C** and K_D^{DNA} was determined as 141.5 ± 13.3 nM in the absence of AdoHcy, and 77.2 ± 7.5 nM in the presence of AdoHcy. R^2 values for the fitting of data to **Equation 3.3C** were 0.997 and 0.977 respectively.

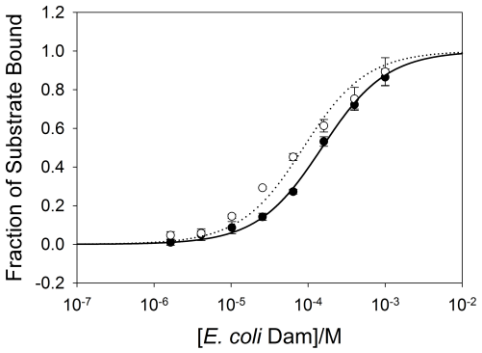

Figure 3.26 Determination of *E. coli* Dam K_D^{DNA} from fluorescence anisotropy
Fraction of substrate bound calculated using **Equation 3.3A** and **B** versus *E. coli* Dam concentration in the absence (filled circles, solid line) and presence (open circles, dotted line) of AdoHcy. Data fitted to **Equation 3.3C** to determine K_D.
Assay conditions: 0-1000 nM Dam, 0 or 20 nM hemimethylated oligonucleotide (ODN10), 0 or 200 µM AdoHcy, 5% DMSO, 0.1% Tween-20, 20 mM Tris, 80 mM NaCl, 8 mM $MgCl_2$, 1 mM DTT, 0.1 mg ml^{-1} BSA, 5% glycerol, pH 7.9. Total assay volume 100 µl, in 96 well plate, gain 2315/2366, 25 ˚C.

The values of K_D^{DNA} compare well with those determined previously (84 and 101 nM (*103, 104*)), and the addition of AdoHcy appears to increase binding affinity approximately 2-fold. The fluorescence anisotropy assay therefore represents a viable method for studying Dam:DNA interactions and the effect of inhibitors on these interactions.

3.5.3 DpnI fluorescence anisotropy assay

To further investigate the substrate inhibition effects observed in the real-time break light Dam activity assay (Chapter 2, Section 2.3.6.2) the fluorescence anisotropy was adapted for monitoring the binding of the coupled restriction enzyme *Dpn*I to hemi- and fully methylated DNA substrates. As a type II restriction enzyme, *Dpn*I requires magnesium ions for catalytic activity, the trapping of the DNA:*Dpn*I complex can therefore be achieved by omitting magnesium chloride from the assay buffer. It should however be noted that some type II restriction enzymes require magnesium ions to facilitate specific binding, and results should therefore be interpreted carefully (*214, 238*).

Initial experiments were carried out to determine K_D^{DNA} for both the hemi- (ODN10) and fully (ODN11) methylated substrates, with *Dpn*I shown to have a higher affinity for fully methylated DNA over hemimethylated DNA, even in the absence of magnesium ions (**Figure 3.27**). Comparisons of K_M^{DNA} and K_D^{DNA} show that whilst the values for fully methylated DNA are approximately the same, the values for hemimethylated DNA differ greatly, with K_M^{DNA} approximately 8 times K_D^{DNA} (**Table 3.3**).

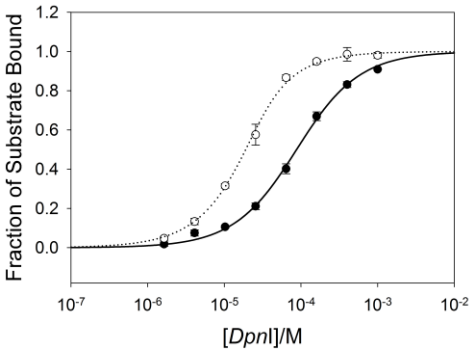

Figure 3.27 Determination of *Dpn*I K_D^{DNA} from fluorescence anisotropy
Fraction of substrate bound calculated using **Equation 3.3A** and **B** versus *Dpn*I concentration for hemimethylated (filled circles, solid line) and fully methylated (open circles, dotted line) DNA. Data fitted to **Equation 3.3C** to determine K_D.
Assay conditions: 0-1000 nM *Dpn*I, 0 or 20 nM hemimethylated (ODN10) or fully methylated (ODN11) oligonucleotide, 0.1% Tween-20, 20 mM Tris, 80 mM NaCl, 1 mM DTT, 0.1 mg ml^{-1} BSA, 5% glycerol, pH 7.9. Total assay volume 100 µl, in 96 well plate, gain 2120/2145, 25 ˚C.

Table 3.3 *Dpn*I kinetic parameters for hemimethylated and fully methylated DNA

Kinetic Parameter	Hemimethylated DNA	Fully methylated DNA
K_M/nM	653 ± 27	14.1 ± 2.3
k_{cat}/s^{-1}	0.0228 ± 0.0009	0.668 ± 0.028
K_D/nM	77.8 ± 3.6	9.02 ± 0.63

As determined from **Figure 2.21** and **Figure 3.27**.

To probe the substrate binding effect observed for the real-time break light Dam activity assay, a competition binding experiment was prepared to determine the effects of increasing concentrations of unlabelled hemimethylated substrate on the binding of *Dpn*I to the labelled fully methylated substrate. Fraction of substrate bound was calculated using the ligand binding calibration curve constructed for **Figure 3.27** (fully methylated DNA) and a plot of fraction of substrate bound against unlabelled hemimethylated DNA concentration was fitted to **Equation 3.4A** to determine the competition binding constant.

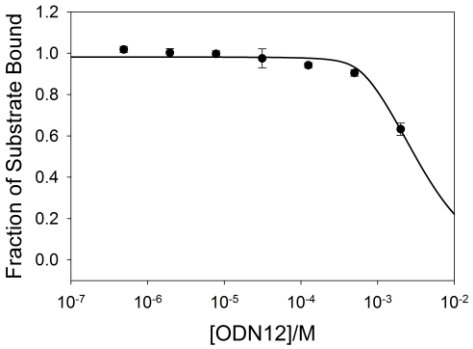

Figure 3.28 Hemimethylated DNA competition binding curve for *Dpn*I
Fraction of substrate bound calculated using **Equation 3.3A** and **B** (ligand binding curve as for **Figure 3.27**, fully methylated DNA) versus ODN12 concentration. Data fitted to **Equation 3.4** to determine competition binding constant.
Assay conditions: 500 nM *Dpn*I, 0-1000 nM unlabelled hemimethylated oligonucleotide (ODN12), 0 or 20 nM labelled fully methylated oligonucleotide (ODN11), 0.1% Tween-20, 20 mM Tris, 80 mM NaCl, 1 mM DTT, 0.1 mg ml^{-1} BSA, 5% glycerol, pH 7.9. Total assay volume 100 µl, in 96 well plate, gain 2120/2145, 25 ˚C.

Addition of an excess of hemimethylated DNA to a fully methylated DNA:*Dpn*I complex resulted in partial displacement of the fully methylated DNA from *Dpn*I, with a competition binding constant of 49.4 ± 5.3 nM (**Figure 3.28**). In the real-time break light Dam activity assay, high concentrations of hemimethylated DNA are therefore likely to lead to the preferential binding of *Dpn*I to the hemi- rather than the fully

methylated substrate, with the low k_{cat} of *Dpn*I for the hemimethylated substrate resulting in the formation of a pseudo-dead-end complex. *Dpn*I is then released only by the relatively slow non-specific cleavage of the hemi-methylated substrate (**Table 3.3**, **Figure 3.29**).

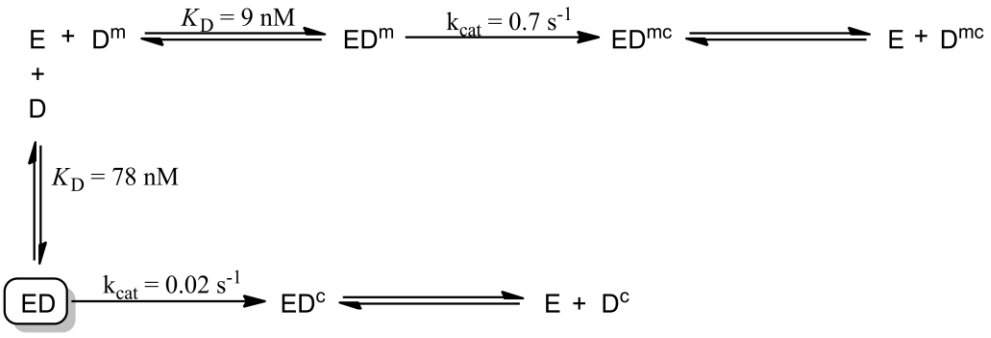

Figure 3.29 Sequestration of *Dpn*I by hemimethylated DNA
Where E = *Dpn*I, D^m = fully methylated DNA, ED^m = *Dpn*I:fully methylated DNA complex, ED^{mc} = *Dpn*I:cleaved fully methylated DNA complex, D^{mc} = cleaved fully methylated DNA, D = hemimethylated DNA, ED = *Dpn*I:hemimethylated DNA complex, ED^c = *Dpn*I:cleaved hemimethylated DNA complex, D^c = cleaved hemimethylated DNA. Pseudo-dead-end ED complex boxed.

The apparent substrate inhibition observed in the real-time break light Dam activity assay is therefore probably due to the sequestration of the coupling enzyme (*Dpn*I) by the substrate for the primary enzyme (hemimethylated DNA). Whilst increasing the concentration of *Dpn*I added to the assay would alleviate this problem, the associated increase in non-specific cleavage would severely reduce the screening window by decreasing the signal:noise ratio. Limiting DNA concentrations in the real-time break light Dam activity assay to concentrations close to K_M^{DNA} for Dam is therefore the best way to alleviate this effect.

3.6 In culture Dam activity assays

A major factor in the success of drug candidates is compound bioavailability, i.e. the rate and extent to which the active ingredient or moiety is absorbed and becomes available at the site of action. Efforts within the pharmaceutical industry to better assess and understand the pharmacokinetic properties of lead compounds, has led to a significant reduction in the rate of attrition due to poor bioavailability in recent years (*239*). Cell permeability is a significant contributor to the bioavailability of a compound, and can be assessed in simple culture based assays.

For a bacterial target such as Dam, the ability of a compound to permeate the bacterial cell and reach the target of interest unhindered by efflux pumps or degradation can be assessed by monitoring the effect of the compound on the intrecellular activity of the biological target. The viability of *dam* knockout *E. coli* strains and the wide-spread availability of non-pathogenic laboratory strains of *E. coli* make the bacterium ideal for use as a model system.

The methylation state of *E. coli* cells grown in media supplemented with an *in vitro* inhibitor can be compared with control assays prepared with no inhibitor, with the percentage of methylated adenine providing a measure of Dam activity. Both genomic and plasmid DNA can be assessed, with *N*6-methyladenine concentration quantified by gel-based methods using methylation sensitive restriction-digest, or by HPLC-based analysis of individual nucleotide concentrations. In addition to measuring the effect of *in vitro* inhibitors on the in cell methylation of adenine, off-target toxicity can also be assessed by monitoring *E. coli* growth curves.

3.6.1 In culture gel-based plasmid methylation activity assay

An in culture activity assay was designed utilising the previously discussed gel-based methylation assay format (Section 3.3). *E. coli* were transformed with a plasmid containing a methylation sensitive restriction site and cultured in media supplemented with or without an *in vitro* inhibitor. The degree of plasmid methylation was then measured by restriction digest analysis, with results visualised by agarose gel electrophoresis (**Figure 3.30**).

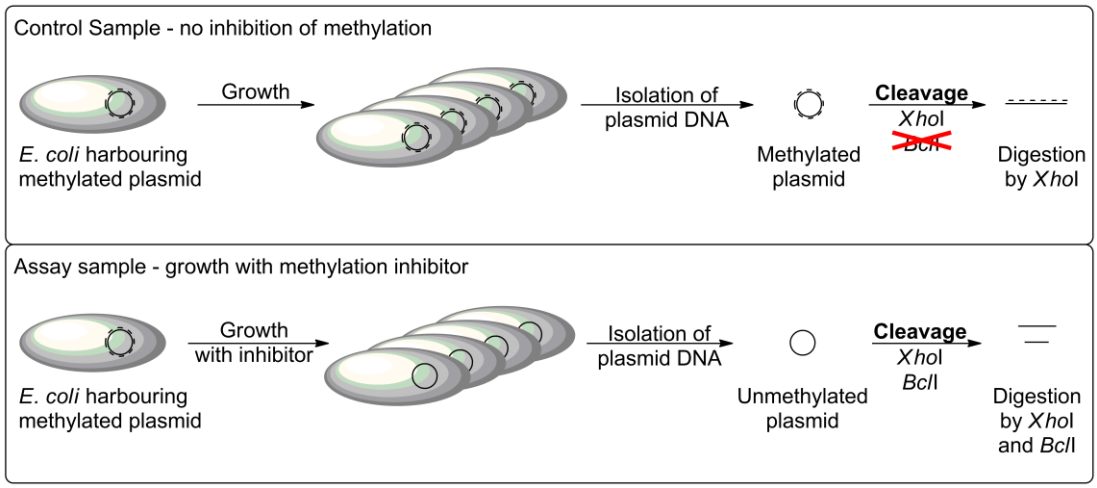

Figure 3.30 In culture gel-based plasmid methylation assay

A plasmid harboured by *E. coli* cells is methylated and isolated plasmid DNA is protected from Dam cleavage. In the presence of a cell-permeable Dam inhibitor methylation is blocked and isolated plasmid is cleaved by both *Xho*I and *Bcl*I. Results are detectable by agarose gel electrophoresis, where a single band represents an unmethylated plasmid, three bands represent a partially methylated plasmid, and two bands represent an unmethylated plasmid.

3.6.1.1 Optimisation of assay volume

Minimisation of compound quantity required per assay was achieved by minimising cell culture volume. Assays containing the *dam* knockout *E. coli* strain ER2925 transformed with plasmid **pRL821** (**Figure 3.5**) were prepared in 12 well microplates containing 1-4 ml of culture medium and the amount of plasmid isolated after 15 hrs was quantified by agarose gel electrophoresis after digestion with the methylation sensitive restriction enzyme *Bcl*I.

Plots of OD_{600} and plasmid DNA concentration after 15 hrs against cell culture volume (**Figure 3.31A** and **B**) showed both to decrease with increasing volume. This is most likely due to a decrease in culture aeration with increasing volume. An assay volume of 1 ml was therefore selected as optimal for methylation assays to minimise reagent costs and maximise plasmid yield.

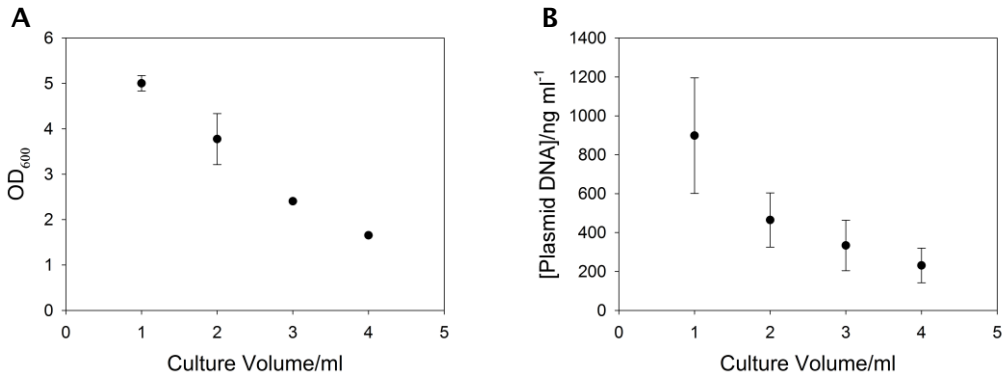

Figure 3.31 In culture gel-based plasmid methylation assay volume optimisation
A: OD_{600} at 15 hrs for **pRL821** transformed ER2925 cultures of 1-4 ml volume.
B: Plasmid DNA concentration for plasmid isolated from cultures of 1-4 ml volume grown for 15 hrs.
Assay conditions: 1, 2, 3 or 4 ml 2YT media, 100 µg ml^{-1} ampicillin, 1% innoculum of ER2925 harbouring **pRL821**. Total assay volume 1-4 ml, temperature 37 ˚C, orbital shaking at 200 rpm for 5 out of every 10 min. Plasmid isolated after 15 hrs and digested with 7.5 U $µl^{-1}$ *Bcl*I, 1 hr, 50 ˚C. Digested plasmid analysed by 0.8% agarose gel electrophoresis, bands quantified using the program ImageJ (*227*).

3.6.1.2 Optimisation of assay end-point

The optimal time for plasmid isolation was identified by monitoring the growth of **pRL821** transformed *E. coli* TOP10 and ER2925. Stationary growth was reached after approximately 10 hrs, with ER2925 cells growing to a lower final OD_{600} than TOP10 cells (**Figure 3.32**). Plasmid was isolated after 5 hrs and digested with the restriction enzymes *Xho*I and *Bcl*I. Plasmid isolated from the Dam^+ strain (TOP10) gave a single band on the agarose gel, consistent with complete methylation of **pRL821**, whereas plasmid isolated from the Dam^- strain (ER2925) gave two bands, consistent with no methylation of **pRL821**.

To ensure plasmid isolation was timed to occur during the exponential growth phase, an assay end-point of 5 hrs was selected. This corresponded to approximately half way through exponential growth. Plasmid DNA isolated after 5 hrs was of a high enough concentration to be readily analysed by restriction digest and agarose gel electrophoresis, with the assessment of plasmids grown in Dam$^+$ and Dam$^-$ *E. coli* strains validating the assay as a method for identifying Dam inhibition.

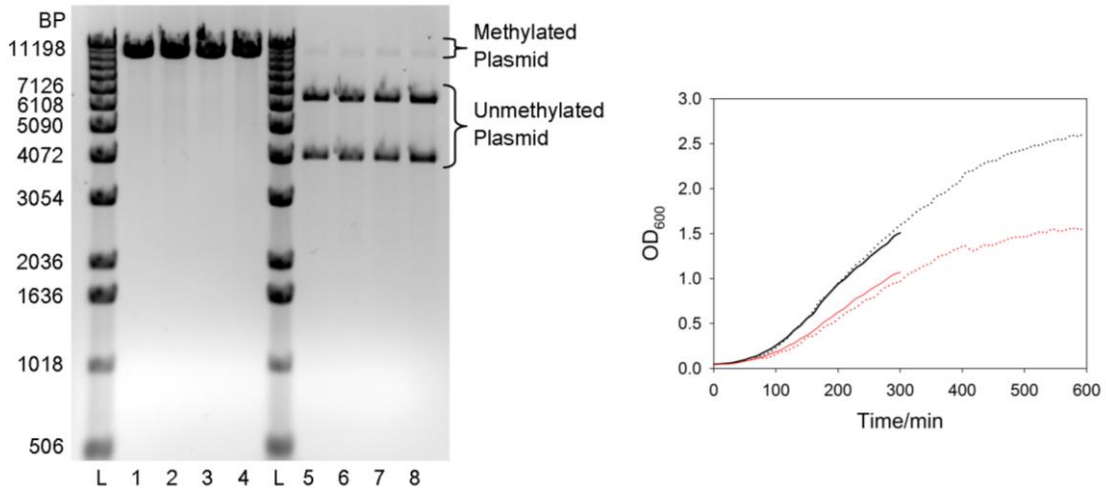

Figure 3.32 In culture gel-based plasmid methylation assay end-point optimisation
0.8% agarose gel electrophoresis of analytical digests of plasmids isolated from TOP10 (1-4) and ER2925 (5-8) *E. coli* after 5 hrs (left) and OD_{600} versus time for TOP10 (black) and ER2925 (red) *E. coli* monitored over 5 (solid lines) or 10 (dotted line) hours.
(L): ladder, (1-4): *E. coli* TOP10, (5-8): *E. coli* ER2925.
Assay conditions: 1 ml 2YT media, 100 µg ml^{-1} ampicillin, 5% DMSO, ER2925 or TOP10 harbouring **pRL821** to a final OD_{600} of 0.05. Total assay volume 1 ml, temperature 37 ˚C, orbital shaking at 400 rpm for 5 out of every 10 min. Plasmid isolated after 5 hrs and digested with 10 U µl^{-1} *Xho*I, 1 hr, 37 ˚C and 7.5 U µl^{-1} *Bcl*I, 1 hr, 50 ˚C. Digested plasmid analysed by 0.8% agarose gel electrophoresis, bands quantified using the program ImageJ (*227*).

3.6.1.3 Growth curve analysis

A possible limitation of this assay is that a small proportion remains active but is stil sufficient to catalyse the total methylation of the plasmid substrate, and so partial inhibition may not be detectable by this method. However, growth curves for an isogenic pair of Dam$^+$ and Dam$^-$ *E. coli* (BW25113 and JW3350-2) show that a lack of Dam depresses cell growth (**Figure 3.33**). A decrease in *E. coli* growth in the presence of an inhibitor may therefore be a useful indicator of Dam inhibition, and by association, cell permeability.

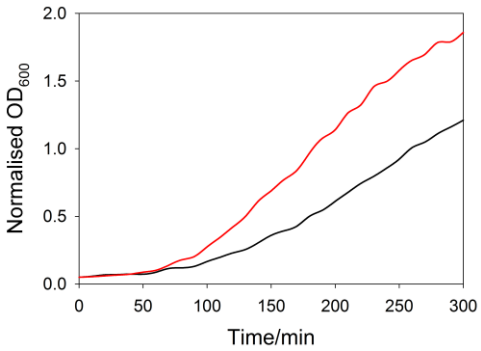

Figure 3.33 Growth curves for isogenic Dam$^+$ and Dam$^-$ *E. coli* strains

OD_{600} normalised to a start OD_{600} of 0.05 against time for BW25113 (black) and JW3350-2 (red) *E. coli* monitored over 5 hours.

Assay conditions: 1 ml 2YT media, 0 (BW25113) and 10 (JW3350-2) µg ml^{-1} kanamycin, 5% DMSO, *E. coli* BW25113 or JW3350-2 to a final OD_{600} of 0.05. Total assay volume 1 ml, temperature 37 ˚C, orbital shaking at 180 rpm for 5 out of every 10 min.

3.6.2 In culture HPLC-based genomic DNA methylation assay

A second in culture methylation assay was developed to assess the methylation state of genomic DNA, again using *E. coli* as a model system. Genomic DNA isolated from *E. coli* cells cultured in media supplemented with an *in vitro* inhibitor is digested with Nuclease P1, isolated from *Penicillium citrinum*. The resulting 2'-deoxyribonucleotide monophosphates (dNMPs) can then be quantified by HPLC analysis (**Figure 3.34**).

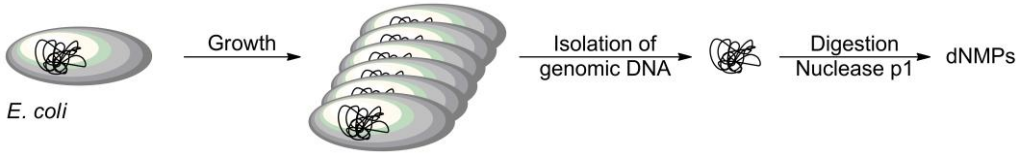

Figure 3.34 In culture HPLC-based genomic DNA methylation assay
Genomic DNA is isolated from *E. coli* cells cultured in media supplemented with an *in vitro* Dam inhibitor. Genomic DNA is isolated and digested with Nuclease P1, the concentrations of the resulting dNMPs are determined by HPLC.

Digestion of genomic DNA into dNMPs can be easily achieved with the addition of Nuclease P1 to denatured genomic DNA samples. The subsequent application of an ion-pairing methodology allows the dNMPs to be separated with good resolution on a reverse-phase HPLC column, through the addition of an ion-pairing reagent, N,N-dimethylhexylamine (DMHA), to column chromatography wash buffers (**Figure 3.35**) (*240*).

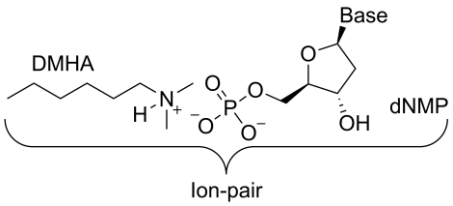

Figure 3.35 Ion-pairing interaction between DMHA and a dNMP

3.6.2.1 Optimisation of genomic DNA isolation and HPLC buffer gradient

E. coli genomic DNA was isolated from overnight cultures of BW25113 (Dam^+) and JW3350-2 (Dam^-) with a Qiagen Gentra Puregene Yeast/Bacteria kit as per the manufacturer's instructions. Heat denatured DNA was then digested with nuclease P1 and analysed by HPLC. Initial results showed impurities in the HPLC trace of the genomic DNA samples relative to a set of standards (**Figure 3.36A**). Further optimisation showed these impurities to be removed by modifying the genomic DNA isolation procedure. Inclusion of an extended RNA digestion step, in which an excess of RNase A and T1 were added to samples (Section 8.3.4.4), dramatically improved

purity, suggesting that the impurities observed were nucleotide monophosphates (**Figure 3.36B**).

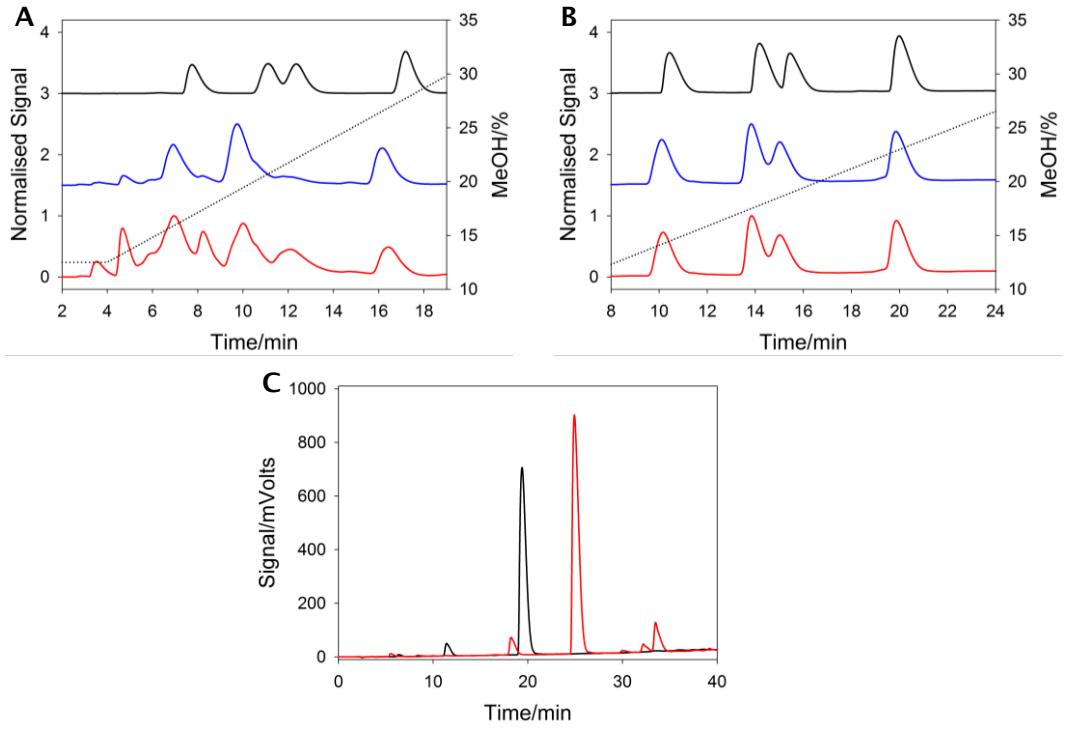

Figure 3.36 Genomic DNA isolation and HPLC buffer gradient optimisation
A and B: HPLC trace of genomic DNA digests following isolation as per manufacturer's instructions (A) and with extended RNase digest (B). dNMP standards (black line): 2'-deoxycytidine-5'-monophosphate (10.4 min), 2'-deoxyguanosine-5'-monophosphate (14.2 min), 2'-thymidine-5'-monophosphate (15.5 min), 2'-deoxyadenosine-5'-monophosphate (33.4). Genomic DNA isolated from *E. coli* BW25113 (Dam^+) (blue line) and *E. coli* JW3350-2 (Dam^-) (red line). MeOH gradient 1 (A) and 2 (B) shown as dotted black line. Signal normalised to maximum = 1 for each trace.
C: HPLC trace of dNMP standards 2'-deoxyadenosine-5'-monophosphate (black line) and 2'-deoxy-*N*6-methyladenosine-5'-monophosphate (red line).
Assay conditions: A – gradient 1, 12.5-42.5% MeOH over 26 min, 80 µl injection, 100 µM dNMP standards. B and C – gradient 2, 8.75-42.5% MeOH over 38 min, 80 µl injection, 100 µM dNMP standards.

The HPLC buffer gradient was optimised to improve resolution between individual dNMP peaks, with an increase in the length of the gradient from 12.5-42.5% MeOH over 26 minutes (gradient 1, **Figure 3.36A**) to 8.75-42.5% MeOH over 38 min (gradient 2, **Figure 3.36B**) resulting in enhanced resolution. The resolution between the 2'-deoxyadenosine-5'-monophosphate (dAMP) and the 2'-deoxy-*N*6-methyladenosine-5'-monophosphate (dmAMP) peaks was also assessed to confirm that the two dNMPs could be completely resolved (**Figure 3.36C**).

3.6.2.2 Determination of detection limits

A dmAMP standard was serial diluted and analysed by HPLC. Peak areas were integrated to determine area, and background subtracted peak areas were plotted against dmAMP concentration to determine the detection limit for the assay (**Figure 3.37**). Fitting a straight line of the form $f=y_0+a*x$ to the data showed the x-axis intercept to be at 0.317 µM, correlating to a dmAMP detection limit of 25.4 pmoles. This plot can also be used as a calibration curve, with the gradient (772851 area units/µM) linking integrated peak area and dmAMP concentration.

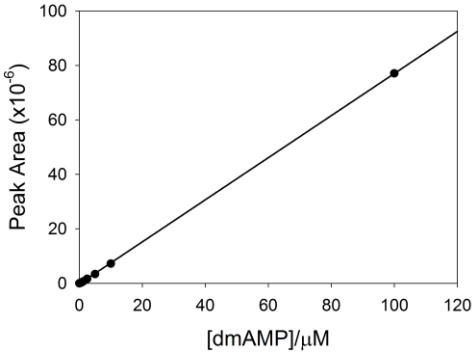

Figure 3.37 Determination of in culture HPLC-based genomic DNA methylation assay detection limit

Background subtracted peak areas against dmAMP concentration. Data fitted to a linear equation of the form $f=y_0+a*x$, where y_0 = the y-axis intercept and a = the line gradient.

Assay conditions: HPLC gradient of 8.75-42.5% MeOH over 38 min, 80 µl injection, 0-100 µM dmAMP standard.

An estimated 2% of adenine bases are methylated in *E. coli* (*241*), therefore, assuming an equal ratio of the four unmethylated bases and an average dNMP molecular weight of 325 g mol^{-1}, the minimum amount of genomic DNA required for the detection of dmAMP is 1.65 µg. Approximately 15 times this amount of DNA (25 µg) is purified on average from 0.5 ml of gram-negative bacteria culture using the Qiagen Gentra Puregene Yeast/Bacteria kit. This experiment therefore suggests that in principle, it should be possible to quantify the extent of *N*6-adenine methylation in cultures of *E. coli* grown in media supplemented with or without an *in vitro* inhibitor.

3.7 Summary

Counter-screening and hit confirmation assays have been developed to permit the elimination of false positives which inhibit *Dpn*I, intercalate DNA, or interfere with assay signal. A selectivity assay has also been developed for the human cytosine DNA methyltransferase DNMT1 to eliminate relatively non-specific hits with potentially toxic off-target effects due to non-selective modes of inhibition. The introduction of assays employing plasmid and genomic DNA substrates has enabled the effect of inhibitors on Dam to be assessed with substrate closer to those naturally methylated by Dam, whilst in culture assays have been developed to determine the ability of compounds to permeate cells and inhibit intracellular Dam.

The development of a fluorescence anisotropy assay for the investigation of enzyme-DNA binding interactions has ensured that investigation of the effect of inhibitors on such interactions is unhindered by the apparent substrate inhibition observed at concentrations of DNA above K_M in the real-time break light Dam activity assay. The fluorescence anisotropy assay has also provided further insight into the mechanism of this effect, with the sequestration of the coupling enzyme *Dpn*I by the substrate for the primary enzyme being identified as the likely mechanism of the inhibition observed.

4 High-throughput Screening

4.1 Introduction

Previous HTS campaigns for the identification of Dam inhibitors have included an *in silico* screen of the NCI/DTP open access library (*151*), a 50,000-compound small molecule library screen (*149*), and a genetic selection screen of a cyclic peptide library (*150*). Dam inhibitors were identified from all three screens, with the 50,000-compound small molecule library yielding the most potent compounds (57 compounds with IC_{50} values of 25 μM or less).

The majority of pharmaceutical companies involved in drug discovery have their own in house compound libraries. Academic research facilities however are generally reliant on external resources, which can be both time-consuming and costly. Open access repositories, such as the NCI/DTP open chemical repository (http://dtp.cancer.gov), represent a rich source of compounds available at minimal cost to the researcher, making HTS accessible to the wider scientific community.

A random library approach to HTS was initially adopted for this project, with the specific aim of identifying lead compounds which could later be incorporated into a rational design approach. The development of a real-time break light Dam activity assay and its subsequent optimisation for HTS enabled compounds to be screened in a high-throughput format, with secondary assays available for hit confirmation and the assessment of selectivity, potency and mode of action. The calculation of Z'-values throughout HTS allowed assay quality to be monitored, whilst defining the screening window for the identification of hits.

The following chapter describes the HTS of two compound libraries, and the subsequent biochemical characterisation of hits identified from each screen.

4.2 The Developmental Therapeutics Program library

A 3,082-compound library was obtained from the NCI/DTP open chemical repository in plated form for screening. Of the compounds selected: 221 originated from a natural product derived set, and were selected based on their structural diversity and availability; 1,974 were selected based on the identification of diverse pharmacophores using the Chem-X program (Chemical Design, Oxford); 827 were selected to represent a broad range of human tumour cell growth inhibition patterns; and 60 were selected from compounds inducing unusual patterns of cell line sensitivity and resistance in the DTP human tumour cell line assay (*242*).

Screening conditions were selected based on the optimisation of the real-time break light Dam activity assay, as discussed in Chapter 2, and are presented in **Table 4.1**, below. Further information on HTS set-up can be found in Appendix Section 9.7.

Table 4.1 DTP library screening conditions

Parameter	**Screening Conditions**
Buffer	[20 mM Tris, 80 mM sodium chloride, 8 mM magnesium chloride, 1 mM DTT, 0.1 mg ml^{-1} BSA, 5% glycerol, pH 7.9]
Substrate concentrations	Hemimethylated oligonucleotide ODN1 = 10 nM AdoMet = 25 µM
Enzyme concentrations	*Y. pestis* Dam = 1 nM *Dpn*I = 2 nM
Compound concentration	25 µM
Final DMSO concentration	5%
Volume	20 µl (384 well plate)
Assays/set*	96 (80 compounds, 16 controls#)
Temperature	30 ˚C

* Assays/set refers to the total number of assays to be run at one time.

8 positive (lacking library compound) and 8 negative (lacking library compound and AdoMet).

4.2.1 Dam Screen

The 3,082-compound DTP library was screened in duplicate against *Y. pestis* Dam with the real-time break light Dam activity assay. Hits were identified as compounds with initial rates falling outside three standard deviations from the positive control average in both the initial and duplicate screens. Compounds identified as hits in only one screen, with a CV in initial rate over both screens of 5% or less, were classed as weak borderline hits and discarded. Compounds identified as hits in only one screen, with an initial rate CV over both screens of greater than 5% were re-tested.

A total of 242 potential hits were identified in the initial and duplicate screens. Of these, 33 were classed as borderline hits and a further 63 were eliminated by a triplicate screen, giving a final total of 146 screening hits and a hit rate of 4.7%. Assay reproducibility and quality during screening was assessed by measuring the activity of over 300 control assays, with the results showing the assay to be highly reproducible (CV ~10%) with a good to excellent screening window (Z'-value ~0.65) and low non-specific activity (**Table 4.2**).

Table 4.2 Statistical analysis of assay reproducibility and quality during HTS

	CV*	Non-specific Activity#	Z'-value†
Initial Screen‡	10.5 ± 3.5%	5.46 ± 1.93%	0.63 ± 0.12
Duplicate Screen‡	9.07 ± 2.43%	3.85 ± 1.12%	0.69 ± 0.08

* Calculated from the average and standard deviation of the positive controls using **Equation 2.1**.

Calculated from the average of the positive and negative controls using **Equation 4.1**.

† Calculated from the average and standard deviation of the positive and negative controls using **Equation 2.2**, given to 2 decimal places.

‡ Data from 39 sets of 8 positive and 8 negative controls.

$$\frac{\mu_{c-}}{\mu_{c+}} \times 100$$

Equation 4.1 Non-specific activity

Where μ_{c-} = the average of the negative controls and μ_{c+} = the average of the positive controls.

4.2.2 Counter-screening

4.2.2.1 DpnI

Elimination of false positives and non-selective inhibitors, with activity against the coupling enzyme *Dpn*I, was achieved by screening the 146 hits identified from the real-time break light Dam activity assay in triplicate against *Dpn*I. Compounds found to inhibit *Dpn*I by greater than three standard deviations from the average of the positive controls in two or more screens were eliminated, leaving a total of 26 compounds.

4.2.2.2 FID

The remaining 26 compounds were screened in an FID assay to assess their ability to displace thiazole orange from DNA. Compounds found to decrease fluorescence by greater than three standard deviations from the average of the positive controls in a single concentration point assay were eliminated, leaving a total of six viable hits (**Figure 4.1**).

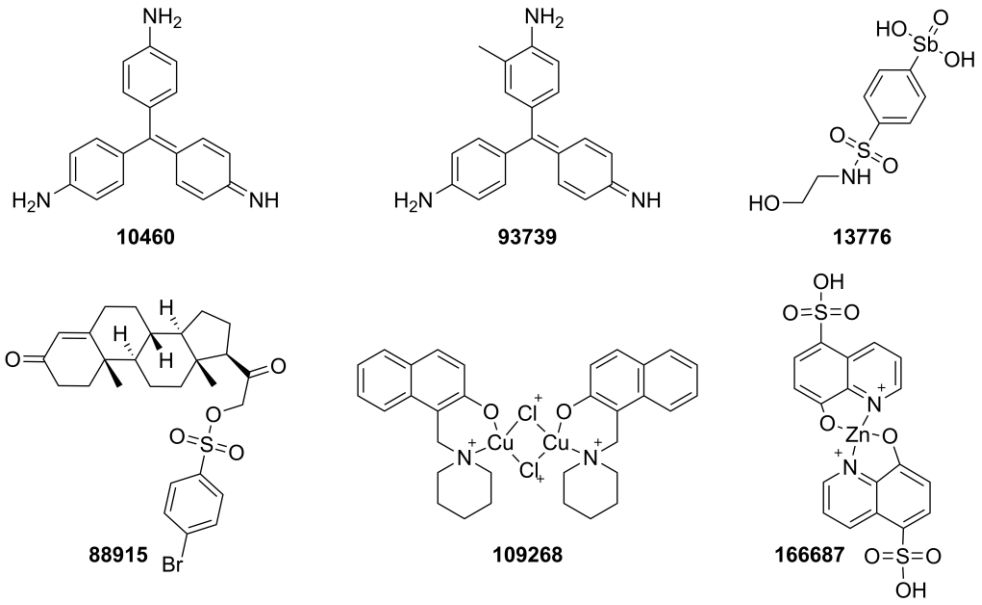

Figure 4.1 Structures of the DTP library hits

Structures of viable hits from screening and counter-screening. Number in bold = DTP NSC identifier.

4.2.3 Hit Validation

4.2.3.1 Extended FID assays

FID assays were prepared at a range of compound concentrations to identify any partial or weak DNA intercalation activity. The closely related compounds **10460** and **93739** were shown to displace thiazole orange at higher concentrations than employed in the FID counter-screen and were discarded (**Figure 4.2**). In addition, compound **109268** was found to be poorly soluble under assay conditions, with precipitate visible to the naked eye when assays were prepared in colourless reaction vessels, **109268** was therefore also discarded as an unsuitable lead.

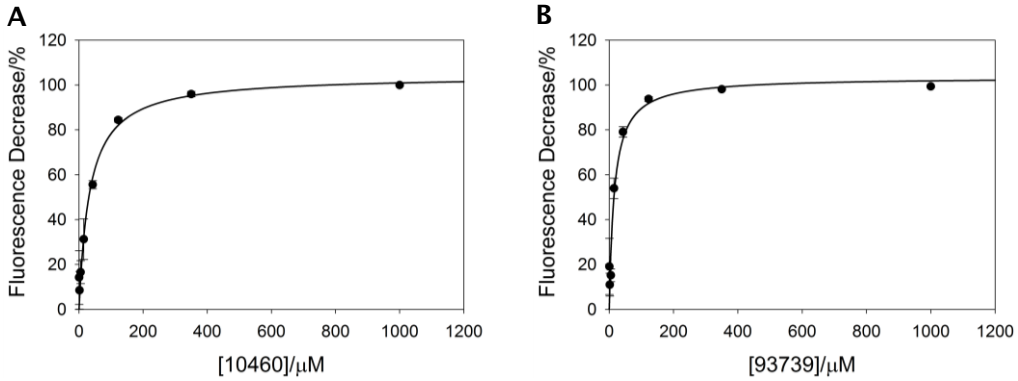

Figure 4.2 Fluorescent intercalator displacement by compounds **10460** and **93739**
Increasing concentration of compounds **10460** (A) and **93739** (B) plotted against percentage fluorescence decrease relative to a positive control. Data fitted to a hyperbola of the form f=a*x/(b+x).
Assay conditions: 100 nM unlabelled unmethylated oligonucleotide (ODN3), 500 nM thiazole orange, 0-1000 μM compound, 10% DMSO, 100 mM Tris, 100 mM NaCl, pH 7.9. Total assay volume 20 μl, in 384 well plate, gain 255, 25 ˚C.

4.2.3.2 Purity

FID assays of compound **88915** were inconclusive due to interference from background fluorescence in the sample. The chemical structure of **88915** is not consistent with the observed spectral properties; the purity of the sample was therefore investigated by TLC. Separation of four different compounds was achieved in 100% methanol, suggesting the presence of at least three impurities in compound **88915**. Whilst the separation of the various components may be possible, the limited availability (milligram quantities) of **88915** makes the identification of the active component extremely difficult, consequently the compound was discarded.

4.2.3.3 Compound 166687

Compound **166687** (bis(8-hydroxyquinoline-5-sulfonic acid) zinc(II)) is comprised of two molar equivalents of 8-hydroxy-quinoline-5-sulphonic acid (HQSA) bound to a central zinc ion. Each component of the complex was assayed alongside **166687**, at a range of concentrations against *Y. pestis* Dam and *Dpn*I, in order to determine IC_{50} values. The IC_{50} of **166687** was determined as 25.9 ± 5.0 μM for Dam and 96.4 ± 23.3 μM for *Dpn*I, however HQSA was found to have no inhibitory effect on either enzyme, whilst the IC_{50} of zinc chloride was determined as 9.79 ± 1.52 μM for Dam and 17.5 ± 3.21 μM for *Dpn*I (**Figure 4.3**).

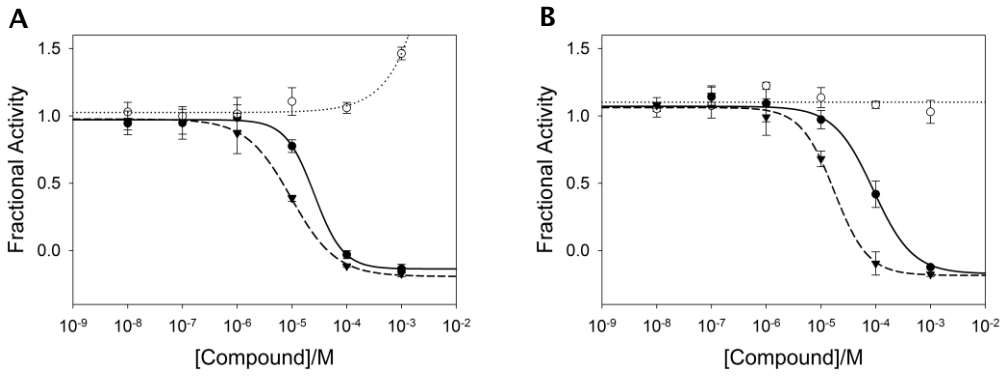

Figure 4.3 IC_{50} Dam and *Dpn*I determinations for **166687**, HQSA and zinc chloride
Fractional activity, calculated using **Equation 2.6A** versus concentration of **166687** (filled circles), HQSA (open circles) and zinc chloride (filled triangles) for Dam (A) and *Dpn*I (B). Data fitted to **Equation 2.6B** for **166687** (solid line), HQSA (dotted line) and zinc chloride (dashed line).
Assay conditions: 0.3 or 0 nM *Y. pestis* Dam, 2 nM or 12.5 pM *Dpn*I, 3.5 nM hemimethylated oligonucleotide (ODN1) or 15 nM fully methylated oligonucleotide (ODN2), 0 or 16 μM AdoMet, 0-1000 μM compound, 5% DMSO, 20 mM Tris, 80 mM NaCl, 8 mM $MgCl_2$, 1 mM DTT, 0.1 mg ml^{-1} BSA, 5% glycerol, pH 7.9. Total assay volume 20 μl, in 384 well plate, gain 190 or 170, 30 ˚C.

The decrease in IC_{50} for zinc chloride over **166687** and the lack of inhibition by HQSA suggests that the inhibition observed for **166687** was due to the release of zinc ions in solution, and not to the overall complex. Divalent zinc ions have a radius of approximately 0.74 Å, similar to that of divalent magnesium ions (0.71 Å) (*243*), which are required for the catalytic activity of *Dpn*I (*244*). The inhibition of *Dpn*I by zinc ions may therefore be due to competitive binding at the catalytic site, blocking the binding of magnesium ions and preventing DNA cleavage. The important role of zinc in many cellular processes (*245*) and the inhibitory effect on *Dpn*I suggest that **166687** would be a poor lead, and as such the compound was excluded from further investigations.

4.2.4 Compound 13776

The potency of the remaining compound, (4-(*N*-(2-hydroxyethyl)sulfamoyl)phenyl) stibonic acid (**13776**) was determined for both *Y. pestis* Dam and *Dpn*I. The IC_{50} value for *Y. pestis* Dam was found to be 3.26 ± 1.14 μM and for *Dpn*I the value was greater than the detection limit of the experiment (10 μM) (**Figure 4.4**). Although an IC_{50} was not determined for *Dpn*I, some inhibition is observed (**Figure 4.4**); however, the potency of the compound for *Y. pestis* Dam is clearly higher, suggesting some selectivity for Dam over *Dpn*I.

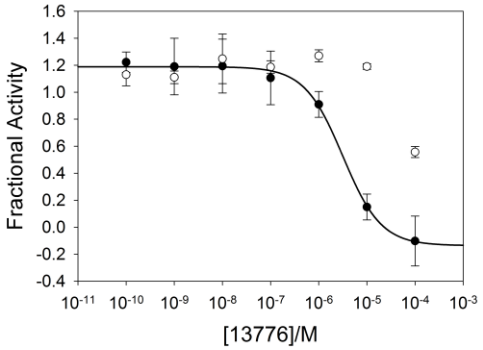

Figure 4.4 IC_{50}^{13776} determination for Dam and *Dpn*I

Fractional activity, calculated using **Equation 2.6A**, versus concentration of **13776** for Dam (filled circles) and *Dpn*I (open circles). Data fitted to **Equation 2.6B** for Dam.

Assay conditions: 0.3 or 0 nM *Y. pestis* Dam, 2 nM or 12.5 pM *Dpn*I, 3.5 nM hemimethylated oligonucleotide (ODN1) or 15 nM fully methylated oligonucleotide (ODN2), 0 or 16 μM AdoMet, 0-1000 μM compound, 5% DMSO, 20 mM Tris, 80 mM NaCl, 8 mM $MgCl_2$, 1 mM DTT, 0.1 mg ml^{-1} BSA, 5% glycerol, pH 7.9. Total assay volume 20 μl, in 384 well plate, gain 190 or 170, 30 ˚C.

4.3 The University of Cincinnati library

An alternative approach to minimising cost whilst maximising the potential for identifying a suitable lead, is to use *in silico* screening methods to reduce large compound libraries to small focussed sets. By employing a pharmacophore-based screening approach Dr M. Bodkin (Lilly, UK) was able to "cherry-pick" 3,193 compounds with structural similarities to AdoMet and adenine from the University of Cincinnati's drug discovery library (>250,000 compounds). Due to availability a total of 2,445 of these compounds were obtained and employed in a second HTS campaign for the identification of *Y. pestis* Dam inhibitors.

HTS conditions were re-assessed following the DTP library screen and substrate concentrations were reduced by 20% in order to conduct screening at concentrations closer to K_M whilst maintaining an acceptable screening window. In addition, compound concentration was increased from 25 to 50 µM to increase hit rates and improve the possibility of identifying a viable lead. A Z'-value of 0.68 was determined under the re-optimised assay conditions (**Table 4.3**), close to the value of 0.71 determined under the previous HTS conditions.

Table 4.3 University of Cincinnati library screening conditions

Parameter	Screening Conditions
Buffer	[20 mM Tris, 80 mM sodium chloride, 8 mM magnesium chloride, 1 mM DTT, 0.1 mg ml^{-1} BSA, 5% glycerol, pH 7.9]
Substrate concentrations	Hemimethylated oligonucleotide ODN1 = 8 nM AdoMet = 20 µM
Enzyme concentrations	*Y. pestis* Dam = 1 nM *Dpn*I = 2 nM
Compound concentration	50 µM
Final DMSO concentration	5%
Volume	20 µl (384 well plate)
Assays/set*	96 (80 compounds, 16 controls[#])
Temperature	30 °C

* Assays/set refers to the total number of assays to be run at one time.

[#] 8 positive (lacking library compound) and 8 negative (lacking library compound and AdoMet).

4.3.1 Dam screen

The *in silico* enriched University of Cincinnati library was screened in duplicate against *Y. pestis* Dam and hits were identified as described in Section 4.2.1. Hits identified in either the initial or duplicate screen were carried through for counter-screening and validation, giving a total of 102 potential hits (69 of which were identified in both screens), and a hit rate of 4.2%, comparable to that of the DTP library screen.

The reproducibility and quality of the assay were assessed by monitoring control assays, with an average CV, Z'-value and non-specific activity of 12.4%, 0.59 and 2.44% determined respectively (**Table 4.4**). Compared with the DTP library the CV is slightly higher and the non-specific activity and Z'-value are both slightly lower, as would be expected due to the decrease in substrate concentrations. However, the values obtained are still indicative of a highly reproducible assay with a low background and good screening window.

Table 4.4 Statistical analysis of assay reproducibility and quality during HTS II

	CV*	**Non-specific Activity#**	**Z'-value†**
Initial Screen‡	11.8 ± 3.6%	2.51 ± 0.46%	0.60 ± 0.11
Duplicate Screen‡	12.9 ± 4.2%	2.37 ± 0.61%	0.57 ± 0.13

* Calculated from the average and standard deviation of the positive controls using **Equation 2.1**.

Calculated from the average of the positive and negative controls using **Equation 4.1**.

† Calculated from the average and standard deviation of the positive and negative controls using **Equation 2.2** given to 2 decimal places.

‡ Data from 31 sets of 8 positive and 8 negative controls.

4.3.2 Counter-screening

4.3.2.1 DpnI

Due to the decreased concentration of DNA employed in the Dam screen a second *Dpn*I concentration optimisation was completed (**Figure 4.5**). An upper *Dpn*I concentration limit of 25 pM was identified, as with the previous optimisation (Chapter 3, Section 3.2.1). However, to maximise assay signal, *Dpn*I concentration was increased to this upper limit (25 pM) for the University of Cincinnati library coupling enzyme counter-screen.

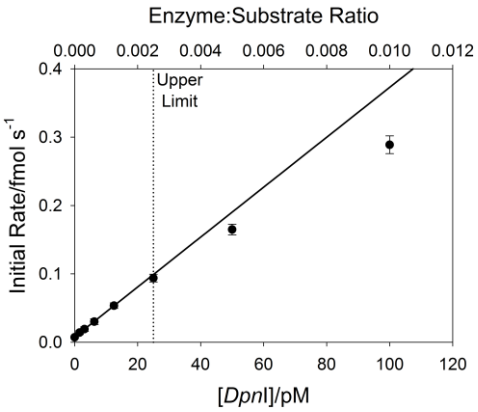

Figure 4.5 *Dpn*I counter-screen effective assay range II

Background subtracted initial rate of cleavage by *Dpn*I. Data points from 0-12.5 pM *Dpn*I fitted to a linear equation of the form $f=y_0+a*x$.

Assay conditions: 0-100 pM *Dpn*I, 8 nM fullymethylated oligonucleotide (ODN2), 5% DMSO, 20 mM Tris, 80 mM NaCl, 8 mM $MgCl_2$, 1 mM DTT, 0.1 mg ml^{-1} BSA, 5% glycerol, pH 7.9. Total assay volume 20 µl, in 384 well plate, gain 170, temperature 30 ˚C.

The 102 hits identified in the Dam screen were counter-screened in duplicate against *Dpn*I, identifying a total of 69 compounds which inhibited the coupling enzyme by 50% or more in either screen. These false positives and non-selective inhibitors were eliminated, leaving a total of 33 compounds.

4.3.2.2 FID

An FID screen of the remaining 33 compounds found 13 to significantly decrease thiazole orange fluorescence relative to a positive control (i.e. by greater than three standard deviations from the average of the positive controls), suggesting DNA intercalation activity. The DNA intercalators were discarded, leaving a total of 20 viable hits.

4.3.3 Hit validation

Of the 20 viable hits remaining after counter-screening, 9 were available to purchase commercially. Due to the limited quantities of library compounds available from the University of Cincinnati, and to ensure that compounds were pure and of the correct structure, only those available commercially were selected for further analysis (**Figure 4.6**).

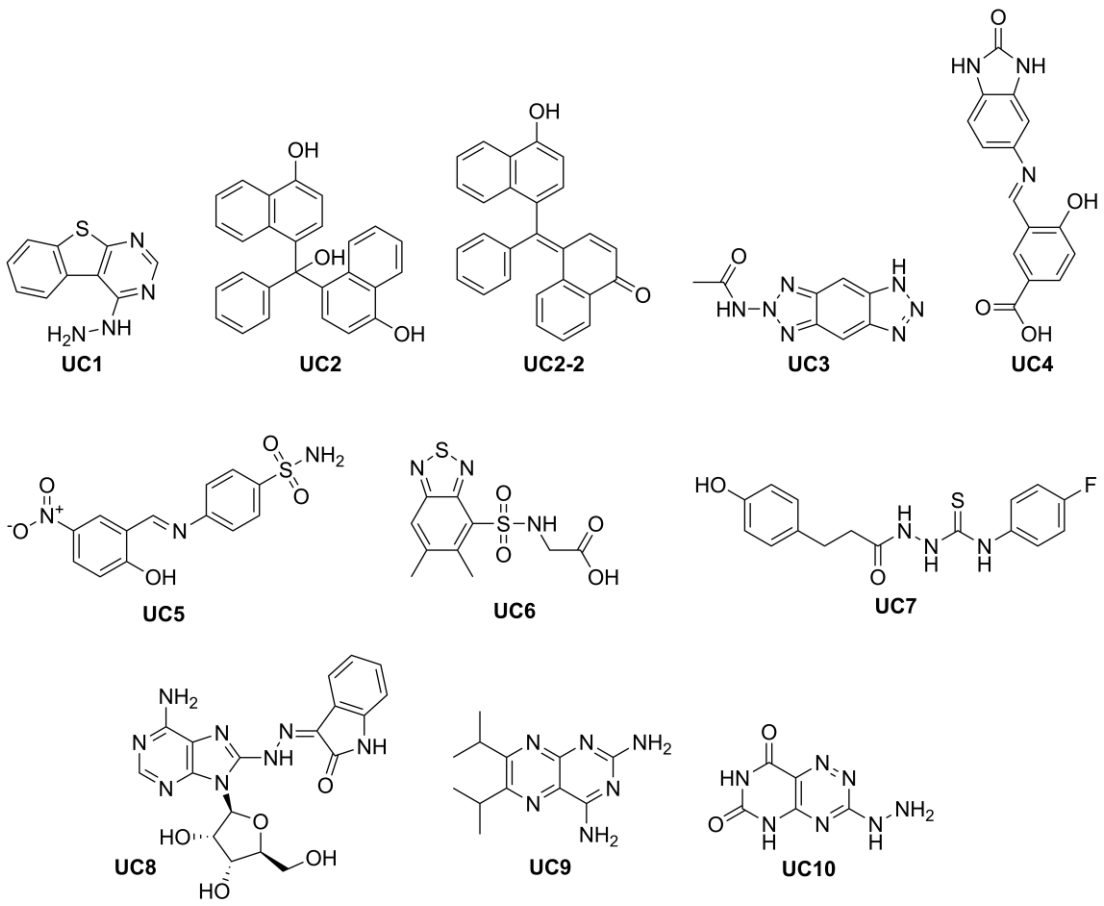

Figure 4.6 Structures of the University of Cincinnati library hits

Structures of the commercially available viable hits from the University of Cincinnati library screen. Compound **UC2** was purchased in both the hydrated (**UC2**) and unsaturated (**UC2-2**) forms.

4.3.3.1 Confirmation of activity

Confirmation of the activity of the 11 purchased University of Cincinnati library hits (**UC1**-**10** and **UC2-2**) was achieved by assessing their activity against *E. coli* Dam in the gel-based Dam methylation assay. Plasmid **pRL821** was incubated with *E. coli* Dam and 2 mM of each compound, the effects on methylation were then assessed by restriction digest and visualised by agarose gel electrophoresis. Controls containing no AdoMet (negative), 2 mM AdoHcy (inhibition), and no compound (positive) were also prepared.

The results (**Figure 3.9**) showed compounds **UC2**, **UC2-2**, **UC3**, **UC4**, **UC5** and **UC10** to strongly inhibit *E. coli* Dam at 2 mM, compounds **UC1**, **UC7** and **UC8** to weakly inhibit *E. coli* Dam at 2 mM, and compounds **UC6** and **UC9** to have no effect on *E. coli* Dam methylation.

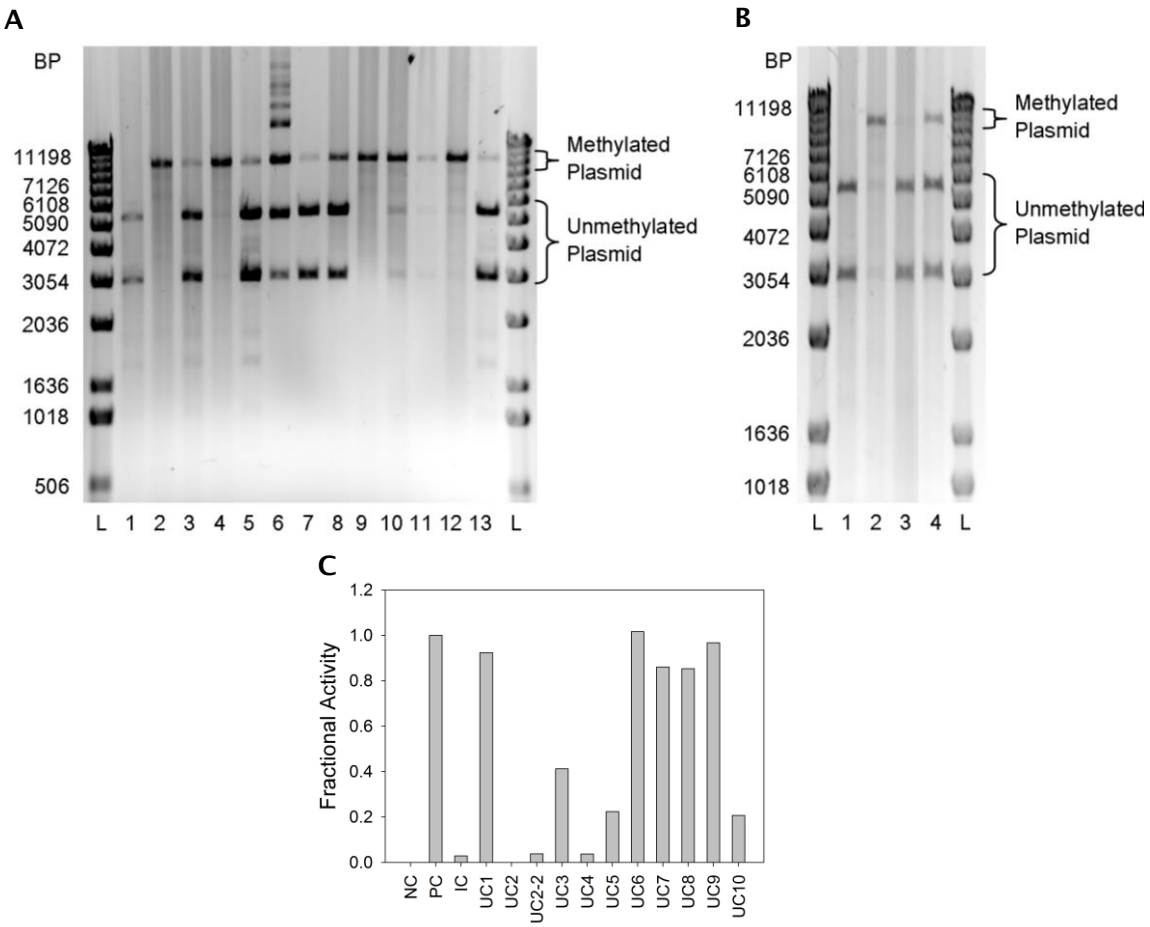

Figure 4.7 Gel-based Dam activity assay of the University of Cincinnati library hits

A and B: 0.8% agarose gel electrophoresis of Dam activity assay restriction digest for **UC1-9** and **UC2-2** (A) and UC10 (B).

(L): ladder, (1): negative control (lacking AdoMet), (2): positive control (lacking compound), (3): inhibition control (with AdoHcy), (4-12 A): **UC1-9**, (13 A): **UC2-2**, (4 B): **UC10**.

C: Fractional activity quantified from gel band intensity with **Equation 2.6A**.

Assay conditions: 250 nM *E. coli* Dam, 3 nM plasmid (**pRL821**), 10 U μl^{-1} *Xho*I, 7.5 U μl^{-1} *Bcl*I, 0 or 6 µM AdoMet, 0 or 2 mM compound, 5% DMSO, 50 mM Tris, 100 mM NaCl, 10 mM $MgCl_2$, 1 mM DTT, pH 7.9. Step 1 (methylation) – total assay volume 20 µl, temperature 30 ˚C, 1 hr; Step 2 (denaturation) – total assay volume 20 µl, temperature 95 ˚C, 5 min; Step 3 (cleavage) – restriction enzymes *Xho*I and *Bcl*I added, total assay volume 22 µl, temperature 37 ˚C, 1 hr and 50 ˚C, 1 hr. Digested plasmid analysed by 0.8% agarose gel electrophoresis, bands quantified using the program ImageJ (*227*).

The complete lack of inhibition observed for compounds **UC6** and **UC9** suggest that they are inactive against Dam, whereas all other compounds tested showed some inhibitory activity. Also of interest is the result of the restriction digest for the assay containing **UC3**, which showed a number of bands correlating to molecular weights greater than that of the linearised plasmid (10 664 base pairs). The reason for this is not clear at present, however it may suggest some covalent or non-covalent crosslinking of DNA strands in the presence of **UC3**, resulting in DNA fragments of greater molecular weight.

4.3.3.2 Potency and selectivity

The IC_{50} values for University of Cincinnati library hits **UC1-10** and **UC2-2** were determined against Dam and *Dpn*I to assess potency and selectivity. Although compounds **UC6** and **UC9** showed no inhibition in the gel-based Dam methylation assay, they were included in potency and selectivity assays to confirm the previous negative result. Dam and *Dpn*I activity was evaluated over a range of compound concentrations and fractional activity versus compound concentration plots were fitted to **Equation 2.6B** to determine IC_{50} (**Table 4.5**).

Table 4.5 Potency and selectivity of University of Cincinnati library hits **UC1-10** and **UC2-2**

Compound	**Dam IC_{50}* µM**	**DpnI IC_{50}* µM**	**Selectivity#**
UC1	1840 ± 41	>2000	-
UC2	74.1 ± 0.7	183 ± 26	2.5
UC2-2	61.2 ± 20.0	116 ± 19	1.9
UC3	150 ± 26	562 ± 95	3.8
UC4	80.5 ± 1.5	221 ± 3	2.7
UC5	306 ± 38	673 ± 11	2.2
UC6	>2000	>2000	-
UC7	>2000	>2000	-
UC8	159 ± 9	107 ± 23	0.67
UC9	>2000	>2000	-
UC10	-	-	-

Assay conditions and data handling as stated for **Figure 4.4**.

* Average of fitting to two sets of triplicate data, error stated is the standard deviation.

Calculated as *Dpn*I IC_{50}/Dam IC_{50} and given to 2 significant figures

The potency of **UC10** could not be established for either Dam or *Dpn*I due to the high background fluorescence of the compound at the wavelengths used for the activity assays. However the close structural similarities between 3-hydrazinylpyrimido[4,5-e][1,2,4]triazine-6,8(5*H*,7*H*)-dione (**UC10**) and the bacterial toxin toxoflavin (**Figure 4.8**), which forms the basis for a range of antibiotic compounds (*246, 247*), suggests that further development of **UC10** would be highly unlikely to result in the identification of a selective Dam inhibitor.

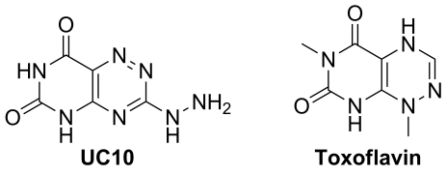

Figure 4.8 Structures of **UC10** and toxoflavin

With the exception of **UC8**, compounds which showed little or no activity in the gel-based assay were found to have high IC_{50} values, confirming minimal inhibition of Dam by compounds **UC1**, **UC6**, **UC7** and **UC9**. Compound **UC8** was poorly soluble under the conditions of the gel-based Dam activity assay, affecting the concentration of DNA loaded onto the gel, and making the accurate assessment of band intensities difficult. The most potent Dam inhibitors, compounds **UC2** and **UC2-2** have similar IC_{50} values of 74 and 61 μM respectively, suggesting that both compounds are behaving in a similar way in solution, as would be expected in aqueous media[8]. Other IC_{50} values for Dam range from 81 μM for **UC4** to 306 μM for **UC5**, with selectivity ratios ranging from 1.9 for **UC2-2** to 3.8 for **UC3**.

These results show that all of the University of Cincinnati library hits tested are relatively weak Dam inhibitors with limited selectivity and as such are unlikely to be good leads. In addition the imine compounds **UC4** and **UC5** have been shown to undergo hydrolysis to their respective aldehyde and amine components in solution, with the active component in both cases identified as the aldehyde. Such compounds would therefore make poor leads for drug development, regardless of potency and selectivity.

[8] From this point forwards the more potent of the two compounds, **UC2-2**, was used for assessment purposes.

4.3.4 In culture activity of hits

4.3.4.1 Restriction digest analysis of genomic DNA from Yersinia culture

In parallel with hit validation the activity of the University of Cincinnati compounds in bacterial cell culture was assessed by Dr M.I. Richards (dstl, Porton Down, UK). *Y. pseudotuberculosis*, a close relative of *Y. pestis* which can be handled at a lower level of containment, was used to assess the ability of the compounds to penetrate *Yersinia* spp. cells. Genomic DNA isolated from *Y. pseudotuberculosis* cell cultures grown in the presence of each inhibitor[9] was analysed by restriction digest, and the results visualised by agarose gel electrophoresis. Restriction by *Sau*3AI, which cleaves both methylated and unmethylated GATC sites, was used as a control to confirm the presence of GATC sites in the genomic DNA, whilst restriction by *Mbo*I indicated the presence of unmethylated DNA, and restriction by *Dpn*I indicated by the presence of fully methylated DNA.

All genomic DNA samples were degraded by both *Sau*3AI and *Dpn*I, indicating the presence of methylated DNA. In addition, five samples, those grown in the presence of **UC1**, **UC2-2**, **UC6**, **UC9** and **UC10**, were also restricted by *Mbo*I, indicating the presence of unmethylated DNA. These results suggest that compounds **UC1**, **UC2-2**, **UC6**, **UC9** and **UC10** penetrate *Y. pseudotuberculosis* cells and partially inhibit Dam, leading to the formation of both unmethylated and fully methylated DNA.

The weak potencies observed for compounds **UC1**, **UC6** and **UC9** against *Y. pestis* Dam would seem to suggest that the decrease in methylation observed in cell culture is due to off-target effects, or that the compounds are metabolised to a more active form in the cell.

4.3.4.2 Gel-based plasmid methylation assay

The in culture activity of compounds **UC1**-**UC9**[10] against Dam was assessed using the gel-based plasmid methylation assay. The results showed none of the compounds to inhibit the methylation of plasmid **pRL821** in *E. coli* TOP10 at a concentration of 500 μM. OD_{600} was used to monitor *E. coli* growth during the experiment and the average of two growth curves obtained in the presence of each compound and a control containing no compound, are shown in **Figure 4.9**.

[9] Compounds **UC7** and **UC8** had not been tested by restriction digest analysis of genomic DNA isolated from *Yersinia* culture at the time of writing this thesis.

[10] Compound **UC10** was not available for testing at the time the gel-based plasmid methylation assay was conducted.

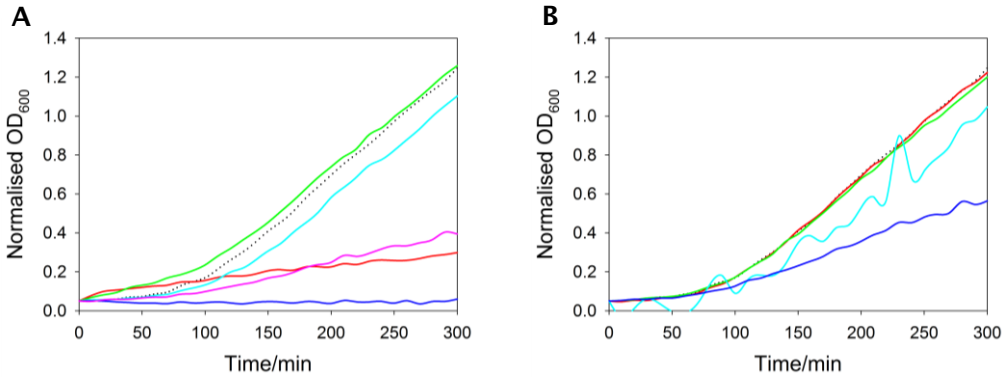

Figure 4.9 *E. coli* growth curves in the presence of **UC1-9**

OD_{600} normalised to a start OD_{600} of 0.05 against time for *E. coli* TOP10 grown in the presence of **UC1-5** (A) and **UC6-9** (B). Positive control (lacking compound) shown as dotted black line (A and B). **UC1** (A, red line), **UC2-2** (A, green line), **UC3** (A, cyan line), **UC4** (A, blue line), **UC5** (A, pink line), **UC6** (B, red line), **UC7** (B, green line), **UC8** (B, cyan line), **UC9** (B, blue line).

Assay conditions: 1 ml 2YT media, *E. coli* TOP10 to a final OD_{600} of 0.05. Total assay volume 1 ml, temperature 37 ˚C, orbital shaking at 180 rpm for 5 out of every 10 min.

Experiments with isogenic Dam^+ and Dam^- strains have shown a lack of Dam methylation in *E. coli* to lead to a decrease in the rate of bacterial cell growth (Chapter 3, Section 3.6.1.3). As *dam* knockout mutants of *E. coli* are still viable a significant decrease in growth rate in the presence of an inhibitor is likely to be indicative of an off-target toxic effect. Compounds **UC1**, **UC4**, **UC5** and **UC9**, which significantly decreased the rate of *E. coli* TOP10 growth relative to a positive control, are therefore likely to be affecting cellular processes in addition to/other than Dam methylation. The lack of a decrease in growth rate for *E. coli* TOP10 grown in the presence of compounds **UC2-2**, **UC6** and **UC7** relative to the positive control sample suggests that these compounds have little or no effect on Dam methylation in the cell, either due to a lack of cellular penetration, compound breakdown within the cell, or poor potency.

The slight decrease in the growth rate of *E. coli* TOP10 in the presence of compounds **UC3** and **UC8** compared to the positive control implies that these compounds may be penetrating the cell and inhibiting Dam methylation. However a poorly resolved growth curve was obtained for **UC8** (**Figure 4.9B**) due to insufficient compound solubility, which may also account for the observed effect.

4.3.4.3 HPLC-based genomic DNA methylation assay

Compounds found to penetrate *Y. pseudotuberculosis* and affect the methylation of genomic DNA whilst showing no toxicity in *E. coli* TOP10 were also assessed using the HPLC-based genomic DNA methylation assay. Within error no decrease in the ratio of

dmAMP:dAMP was observed for *E. coli* BW25113 grown in the presence of 500 µM **UC2-2**, **UC6** or **UC10**, relative to a positive control (lacking compound) (**Figure 4.10A**). In addition, plots of OD_{600} over time show no decrease in the rate of *E. coli* BW25113 growth in the presence of any of the compounds (**Figure 4.10B**), suggesting little if any Dam inhibition.

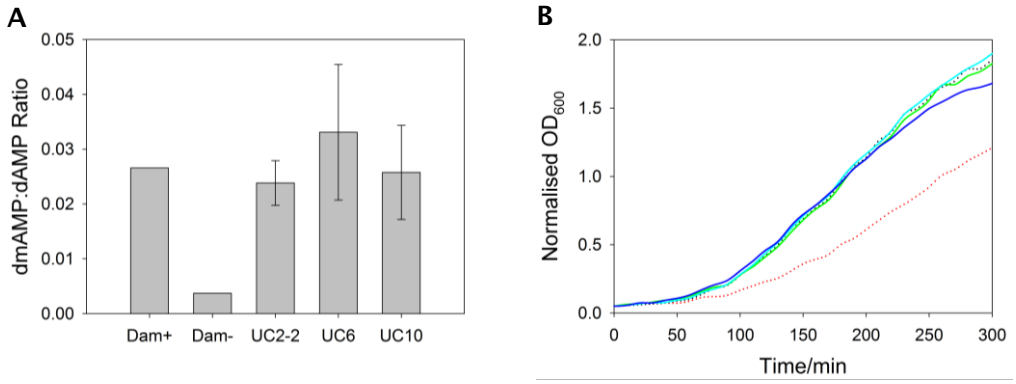

Figure 4.10 Ratio of methylated to unmethylated adenine (A) and *E. coli* growth curves in the presence of **UC2-2**, **UC6** and **UC10** (A).

A: Average ratio of dmAMP:dAMP peaks calculated from the peak areas of an HPLC trace of digested genomic DNA isolated from one culture of *E. coli* BW25113 (Dam^+) or JW3350-2 (Dam^-) (Dam^+ and Dam^- controls) or two separate cultures of *E. coli* BW25113 (Dam^+) grown in the presence of **UC2-2**, **UC6** or **UC10**.

B: OD_{600} normalised to a start OD_{600} of 0.05 against time for *E. coli* BW25113 (Dam^+) grown in the presence of **UC2-2** (green line), **UC6** (cyan line) and **UC10** (blue line), positive control (lacking compound, dotted black line) and negative control (*E. coli* JW3350-2 (Dam^-), dotted red line).

Assay conditions: 1 ml 2YT media, 0 (BW25113) and 10 (JW3350-2) µg ml^{-1} kanamycin, 5% DMSO, 0 or 500 µM compound, *E. coli* BW25113 (Dam^+) or JW3350-2 (Dam^-) to a final OD_{600} of 0.05. Total assay volume 1 ml, temperature 37 °C, orbital shaking at 180 rpm for 5 out of every 10 min, cells harvested by centrifugation at 5 hrs, genomic DNA isolated and digested to dNMPs for HPLC analysis. HPLC gradient 8.75-42.5% MeOH over 38 min, 80 µl sample injection.

The HPLC-based genomic DNA methylation assay displays a low level of sensitivity for changes in methylation, with only complete inhibition of Dam methylation, as observed for the Dam^- control sample, clearly distinguishable from the fully methylated Dam^+ control sample. Therefore, although the results of this assay suggest that at 500 µM compounds **UC2-2**, **UC6** and **UC10** do not fully inhibit Dam methylation in *E. coli*, partial inhibition cannot be ruled out.

4.4 Summary

Of the 146 compounds identified as hits in the DTP library screen, 140 were eliminated by counter-screening against *Dpn*I inhibition and DNA intercalation, leaving a total of six viable hits, and a hit rate after counter-screening of 0.2%. A further five compounds were discarded during purity and potency analysis, leaving one viable hit, the stibonic acid **13776**.

The University of Cincinnati library screen yielded 102 potential hits, with 82 of these eliminated during counter-screening, leaving a total of 20 compounds and giving a hit rate of 0.8%. Of the 20 remaining compounds only half were investigated further due to limited compound availability, with none of the tested compounds showing high levels of either potency or selectivity.

Due to differences in the concentration of library compounds screened and the cut-off limits used to select hits, the two screens cannot be directly compared. However, trends apparent across both screens include the identification of a high percentage of false positives (96% of the initial DTP library hits and 80% of the initial University of Cincinnati library hits) eliminated during counter-screening, resulting in low final hit rates (0.2% and 0.8%).

A low hit rate is not unexpected for a random library screen, with a previous HTS campaign to identify Dam inhibitors from a random library of 50,000 compounds yielding a 0.7% hit rate (*149*). The lack of a significant increase in hit rate for the *in silico* enriched library however is disappointing, and would appear to suggest that in this case there is little difference in the chance of identifying an inhibitor from an *in silico* enriched library or a random library of a similar size. There are relatively few examples in the literature where high-throughput and *in silico* screens have been directly compared, however in the few studies that have been reported a significantly higher hit rate has been achieved through virtual screening than through traditional HTS methods (*248*). The failure of *in silico* screening to identify a greater number of hits than HTS in this case could be due to a wide range of reasons including the specific *in silico* method used, the quality of the crystal structure used to inform *in silico* screening, and the size and chemical diversity of the library sampled.

The high false positive rate observed for both libraries is most likely an artefact of the *in vitro* screening assay methodology. The most common false positives identified in HTS are compounds which form aggregates under HTS conditions (promiscuous binders), compounds which interfere with the assay or detection method, and

compounds with reactive functionalities (*249*). Fortunately the majority of such compounds can be eliminated at an early stage with the application of counter-screens and validation assays, as implemented in this case.

Of the hits identified from both screens the most potent, the stibonic acid **13776**, was identified from the DTP library. None of the hits identified showed high selectivity for Dam over *Dpn*I, however **13776** exhibited a greater potency for Dam than *Dpn*I under IC_{50} assay conditions. Compound **13776** was therefore selected for further analysis, which will be discussed in detail in the following chapter.

5 Stibonic Acids

5.1 Introduction

The use of antimony is widespread: as an alloy in the manufacturing of solder, lead storage batteries, sheet and pipe metal, and castings; as an oxide in the formulation of fire-retardant plastics, rubbers, textiles, paper, and paints; as a trisulfide in the production of explosives, pigments and glass; and as a therapeutic agent for the treatment of the parasitic diseases leishmaniasis and schistosomiasis. Antimony toxicity, arising from therapeutic or occupational exposure, can induce severe respiratory, gastrointestinal and cardiovascular effects, and both antimony trioxide and antimony trisulfide have been implicated as carcinogens (*250*). Despite this, pentavalent antimonials such as sodium stibogluconate and meglumine antimoniate (**Figure 5.1**), which generally elicit less severe side effects than their trivalent counterparts, remain the drugs of choice for the treatment of both visceral and cutaneous leishmaniasis (*251, 252*).

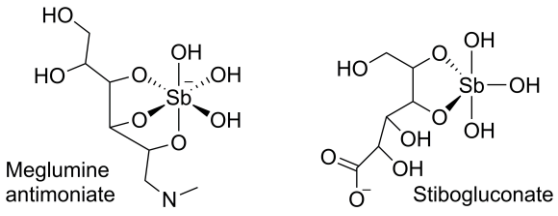

Figure 5.1 Proposed structures of meglumine antimoniate and stibogluconate
As determined by negative electrospray ionisation mass spectrometry in aqueous solution.
Source – reference (*253*).

Although pentavalent antimony (Sb^{V}) has been used in the treatment of leishmaniasis for over 50 years, its mechanism of action is still poorly understood. Amongst the models proposed for the mechanism of action of pentavalent antimonials are a prodrug model, in which Sb^{V} is reduced to the active trivalent form (Sb^{III}) intracellularly, and an intrinsic activity model, in which Sb^{V} has intrinsic antileishmanial activity, with DNA topoisomerases suggested as potential sites of action (*253, 254*).

Topoisomerase inhibition has been observed for the pentavalent animonial arylstibonic acids, with the Stivers group reporting the inhibition of both human and poxvirus topoisomerase I by a series of arylstibonic acids obtained from the DTP open access repository (*255, 256*). Arylstibonic acids have also been identified as inhibitors of other

DNA binding proteins, including human apurinic/apyrimidinic endonuclease (*257*) and CCAAT-enhancer-binding protein (*258*), as well exhibiting potent anti-HIV activity by inhibiting the interaction between human immunodeficiency virus type 1 gp120 and CD4 cells (*259*).

The identification of arylstibonic acids as inhibitors of additional protein targets and the toxicity associated with antimonial therapeutics raises serious questions regarding the selectivity and suitability of such compounds as drug candidates. The likelihood of the arylstibonic acid identified from the DTP library screen (compound **13776**) proving to be a successful lead compound for drug development is therefore relatively small. However, further assessment of the inhibitory effect observed for Dam in the presence of the stibonic acid **13776** may prove highly informative, helping to improve understanding of both the mode of action of pentavalent antimonials, and the effect of Dam inhibition on cellular processes.

5.2 Structure activity relationships

5.2.1 Sublibrary screening

5.2.1.1 Stibonic acid sublibrary

To investigate the role of the stibonic acid group in the activity of **13776** a sublibrary of arylstibonic acids and other antimonial compounds (**Figure 5.2**) was obtained from the DTP open access repository and screened against *Y. pestis* Dam. Of the 38 additional compounds screened 17 were found to inhibit Dam by more than three standard deviations from the average of the positive controls at a concentration of 25 μM. No inhibition was observed for the non-stibonic acid antimonials.

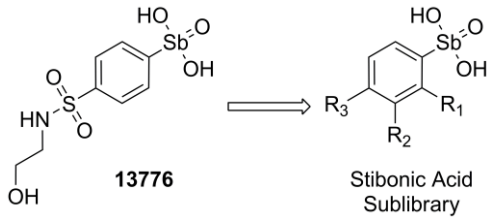

Figure 5.2 Arylstibonic acid sublibrary

Individual structures of the arylstibonic acid sublibrary and additional antimonial compounds are included in Appendix Section 9.7.2.1.

5.2.1.2 Phosphonic acid sublibrary

In discussing the inhibition of human apurinic/apyrimidinic endonuclease by arylstibonic acids Seiple *et al.* suggested that arylstibonic acids may act as DNA phosphate backbone mimics (*257*). A similar inhibitory effect might therefore be expected for phosphonic acids. To test this hypothesis an arylphosphonic acid sublibrary was obtained from the DTP open access repository and screened against *Y. pestis* Dam.

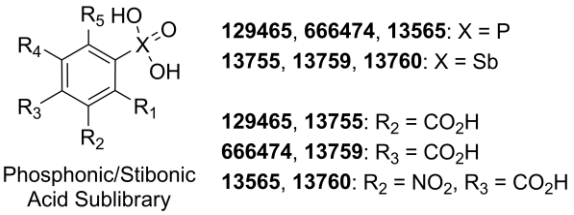

Figure 5.3 Analogous arylstibonic and arylphosphonic acids

Individual structures of the arylphosphonic sublibrary are included in Appendix Section 9.7.2.2.

No inhibition of *Y. pestis* Dam was observed for the 41 arylphosphonic acids at 25 μM, and testing of three arylphosphonic acids with analogous structures to three active

arylstibonic acids (**Figure 5.3**) over an extended concentration range (0.001 to 1000 μM) revealed no effect on Dam activity up to a concentration of 1 mM. Whilst these results do not rule out the possibility of stibonic acids acting as phosphate backbone mimics they do show that replacement of the stibonic acid moiety with an isostere of similar size and chemical composition results in a total loss of activity, suggesting that inhibitory activity is dependent on the stibonic acid.

5.2.2 Potency

The *Y. pestis* Dam IC_{50} values for the 18 arylstibonic acid Dam inhibitors were determined over a compound concentration range of 0.001 to 1000 μM (**Table 5.1**, **Figure 5.2**). The highest ranking compounds were found to be those with a carbonyl or sulfonyl functional group in the *meta* or *para* positions, with the *meta*-substituted compounds showing a slightly greater potency than their *para*- or *ortho*-substituted analogues where available. Of the arylstibonic acid compounds tested, substituent groups were ranked in the following order of potency: sulfonic acid > carboxylic acid ≈ ester > amide. The increase in potency in this series is relatively small and unlikely to be due purely to an ionic effect. However, the trends observed are consistent with the carbonyl/sulfonyl oxygen atom acting as a hydrogen-bond acceptor. The increase in potency observed for *meta*-substituted compounds over their *para*- and *ortho*-substituted analogues may indicate a more favourable positioning of this hydrogen bond acceptor.

Table 5.1 Potency of the stibonic acid hits against *Y. pestis* Dam

Compound ID*	R_1	R_2	R_3	Y. pestis Dam IC_{50} nM#
13746	H	H	SO_3H	16.4 ± 4.5
15578	H	H	CH_2SO_3H	43.1 ± 15.9
13771	H	CO_2CH_3	H	65.5 ± 22.2
13759	H	CO_2H	H	75.9 ± 11.8
15584	H	$CO_2C_2H_5$	H	87.8 ± 9.2
13755	H	NO_2	CO_2H	119 ± 20
13760	H	H	CO_2H	125 ± 20
15583	H	H	$CO_2C_2H_5$	214 ± 75
13778	H	$C_2H_4CO_2H$	H	247 ± 72
13765	H	$CONH_2$	H	288 ± 126
13793	H	H	$C_3H_6CO_2C_2H_5$	488 ± 75
13782	H	$CONHC_2H_4OH$	H	742 ± 83
15575	H	H	$CONH_2$	1,020 ± 140
15577	H	H	CH_3	1,320 ± 700
13758	CO_2H	H	H	2,850 ± 890
13776	H	H	$SO_2NHC_2H_4OH$	3,260 ± 1,140
13745	H	H	OH	7,250 ± 1,150
25176	H	H	NH_2	>10,000‡

* DTP NSC identifier. Compounds ranked by *Y. pestis* Dam IC_{50}.

Error is the standard error of measurement from a triplicate IC_{50} determination.

‡ IC_{50} was greater than the detection limit of the experiment (10,000 nM).

5.2.3 Selectivity

5.2.3.1 Against DpnI

The selectivity of the arylstibonic acid Dam inhibitors against *Dpn*I was assessed by comparing IC_{50} values determined for *Y. pestis* Dam and *Dpn*I. Experiments were carried out under conditions where substrate concentrations were held approximately equal to K_M, allowing a rough approximation to be made to K_i and IC_{50} values for the two separate enzymes to be compared. The selectivity of each compound for *Y. pestis* Dam over *Dpn*I is tabulated as a selectivity ratio in **Table 5.2**, below.

Table 5.2 Selectivity of the stibonic acid hits for *Y. pestis* Dam over *Dpn*I

Compound ID*	R_1	R_2	R_3	Selectivity Ratio[#]
13746	H	H	SO_3H	22 ± 10
15578	H	H	CH_2SO_3H	2.9 ± 1.1
13771	H	CO_2CH_3	H	26 ± 12
13759	H	CO_2H	H	25 ± 14
15584	H	$CO_2C_2H_5$	H	30 ± 11
13755	H	NO_2	CO_2H	7.8 ± 2.8
13760	H	H	CO_2H	3.1 ± 0.9
15583	H	H	$CO_2C_2H_5$	12 ± 6
13778	H	$C_2H_4CO_2H$	H	5.4 ± 1.9
13765	H	$CONH_2$	H	24 ± 11
13793	H	H	$C_3H_6CO_2C_2H_5$	3.5 ± 0.9
13782	H	$CONHC_2H_4OH$	H	0.16 ± 0.03
15575	H	H	$CONH_2$	[‡]
15577	H	H	CH_3	2.4 ± 1.4
13758	CO_2H	H	H	[‡]
13776	H	H	$SO_2NHC_2H_4OH$	[‡]
13745	H	H	OH	[‡]
25176	H	H	NH_2	[†]

* DTP NSC identifier. Compounds ranked by *Y. pestis* Dam IC_{50}.

[#] *Dpn*I IC_{50}/*Y. pestis* Dam IC_{50} given to 2 significant figures, error is the combined standard error of measurement from each triplicate IC_{50} determination.

[‡] *Dpn*I IC_{50} was greater than the detection limit of the experiment (10,000 nM).

[†] *Dpn*I and *Y. pestis* Dam IC_{50} was greater than the detection limit of the experiment (10,000 nM).

A single compound, **13782**, was found to be selective for *Dpn*I over *Y. pestis* Dam, with the remaining compounds showing selectivity ratios of between 2.4 and 30 (where calculation of a ratio was possible). These results show that, in addition to being more potent than their *para*- or *ortho*- substituted counterparts, the *meta*-substituted compounds have a greater selectivity for *Y. pestis* Dam. Also of interest is the apparent decrease in selectivity observed when the distance between a carbonyl or sulfonyl substituent and the benzene ring is increased.

5.2.3.2 Against DNMT1

The selectivity of 15[11] of the arylstibonic acid Dam inhibitors was also assessed by screening each compound against the human cytosine methyltransferase DNMT1. The results showed all but three compounds to inhibit DNMT1 by greater than 50% at a concentration of 25 μM. The three compounds showing less than 50% inhibition of DNMT1 were also weak *Y. pestis* Dam inhibitors, ranked 13th, 16th and 17th out of 18 in order of potency. These findings strongly suggest that the arylstibonic acids are non-selective, inhibiting DNA binding proteins in an indiscriminate manner.

[11] Compounds **13758**, **15577**, **15578** were unavailable for testing at this time.

5.3 Mode of Inhibition Characterisation

5.3.1 Inhibitory constants

To improve our understanding of the non-selective inhibition displayed by the arylstibonic acids, their mode of action was assessed. The apparent K_i values of the original DTP libray hit, **13776**, and the most potent arylstibonic acid, 4-stibonobenzenesulfonic acid (**13746**) were determined with respect to DNA and AdoMet. Lineweaver-Burk plots revealed a competitive mode of action for both **13776** and **13746** with respect to the hemimethylated oligonucleotide ODN1 (**Figure 5.5A** and **C**), and noncompetitive modes of action with respect to AdoMet (**Figure 5.5B** and **D**).

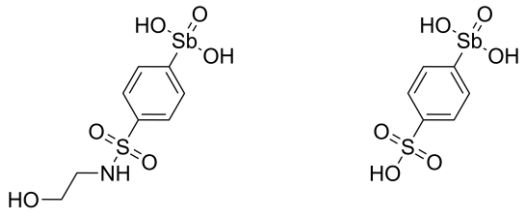

Figure 5.4 Structures of the original HTS hit **13776** and the most potent sublibrary hit **13746**

K_i and αK_i values were calculated by fitting replots of y-axis intercept and gradient against inhibitor concentration to **Equation 2.8B** and **C** respectively (**Table 5.3**). The determined modes of inhibition are in agreement with those revealed by the Lineweaver-Burk plots, and in both cases K_i values determined for varying AdoMet concentration are higher than those determined for varying DNA concentration. The variation in K_i is likely due to the addition of insufficient DNA for pseudo-first order kinetics to be observed. Due to the substrate inhibition effects observed at higher DNA concentrations further experiments at higher concentrations of DNA were not attempted.

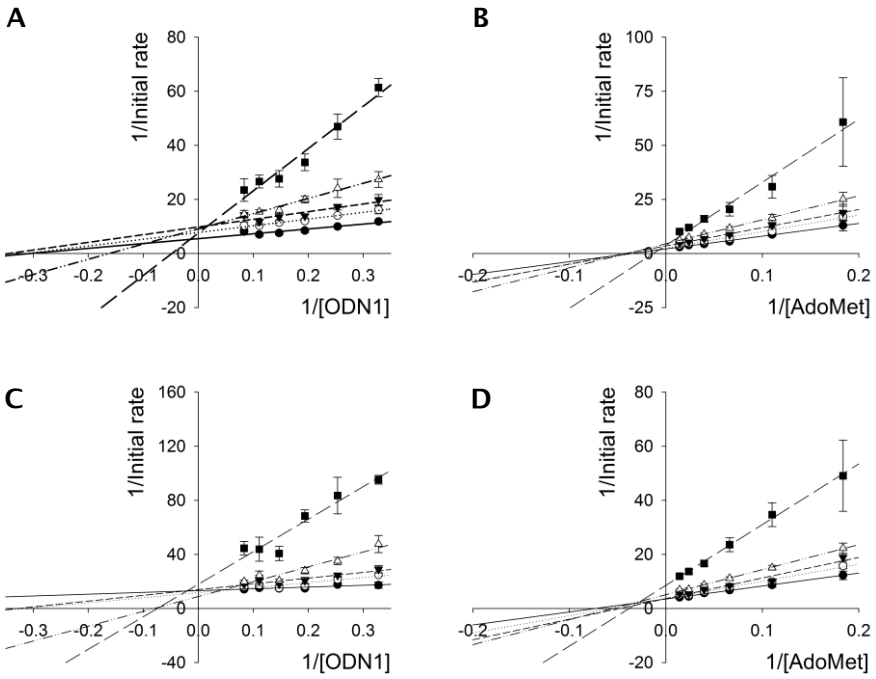

Figure 5.5 Lineweaver-Burk plots for compounds **13776** and **13746**

A and B: Plots of 1/initial rate at 0 (filled circles), 0.77 (open circles), 1.92 (filled triangles), 4.80 (open triangles), and 12.00 (filled squares) μM **13776** against 1/DNA concentration (A) or 1/AdoMet concentration (B).

C and D: Plots of 1/initial rate at 0 (filled circles), 6.14 (open circles), 15.36 (filled triangles), 38.40 (open triangles), and 96.00 (filled squares) nM **13746** against 1/DNA concentration (C) or 1/AdoMet concentration (D).

Data fitted globally to **Equation 2.8A**.

Assay conditions: 0.3 (A and C) or 1 (B and D) nM *Y. pestis* Dam, 2 nM *Dpn*I, 3.1-12 (A and C) or 10 (B and D) nM hemimethylated oligonucleotide (ODN1), 0, 160 (A and C) or 5.4-70 (B and D) μM AdoMet, 0-12 μM **13776** or 0-96 nM **13746**, 5% DMSO, 20 mM Tris, 80 mM NaCl, 8 mM $MgCl_2$, 1 mM DTT, 0.1 mg ml^{-1} BSA, 5% glycerol, pH 7.9. Total assay volume 20 μl, in 384 well plate, gain 190, 30 ˚C.

Table 5.3 Inhibition constants for compounds **13776** and **13746**

Compound	Variable substrate	K_i	αK_i	Mode of inhibition
13776	DNA	0.960 ± 0.036 μM	179 ± 119 μM	Competitive
	AdoMet	2.59 ± 0.07 μM	22.7 ± 3.2 μM	Noncompetitive
13746	DNA	6.46 ± 0.07 nM	234 ± 31 nM	Competitive
	AdoMet	25.1 ± 2.3 nM	58.8 ± 0.3 nM	Noncompetitive

Errors given are the standard errors of fit.

5.3.2 Fluorescence anisotropy competition binding

Further probing of the DNA competitive mode of action observed was achieved by monitoring the effect of compounds **13776** and **13746** on the binding of *E. coli* Dam to DNA. Competition binding constants (K_{Dc}) were determined by fitting plots of fraction of compound bound versus substrate concentration to **Equation 3.4** for experiments prepared with and without AdoHcy (**Figure 3.28**, **Table 5.4**).

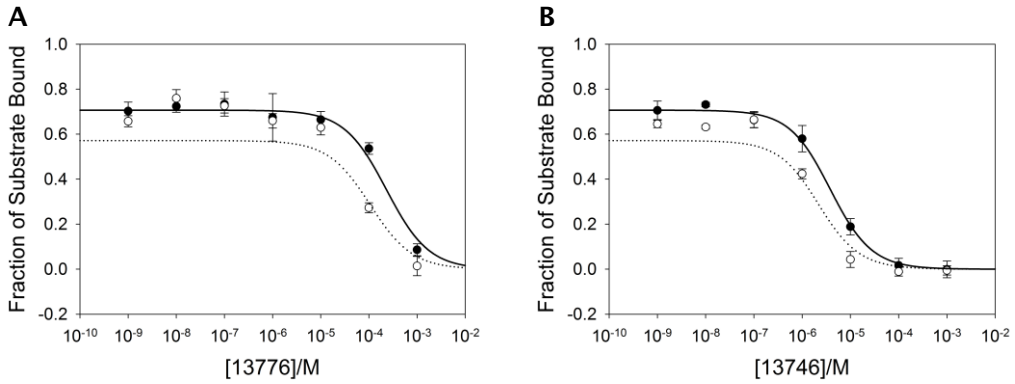

Figure 5.6 Competition binding curves for compounds **13776** and **13746**

Fraction of substrate bound calculated using **Equation 3.3A** and **B** (ligand binding curves as for **Figure 3.26**) versus **13776** (A) or **13746** (B) concentration in the absence (open circles, dotted line) and presence (filled circles, solid line) of AdoHcy. Data fitted to **Equation 3.4**.

Assay conditions: 200 nM *E. coli* Dam, 0-1000 µM compound **13776** (A) or **13746** (B), 0 or 100 µM AdoHcy, 0 or 20 nM labelled hemimethylated oligonucleotide (ODN10), 0.1% Tween-20, 20 mM Tris, 80 mM NaCl, 8 mM $MgCl_2$, 1 mM DTT, 0.1 mg ml^{-1} BSA, 5% glycerol, pH 7.9. Total assay volume 100 µl, in 96 well plate, gain 2315/2366, 25 °C.

Table 5.4 Competition binding constants for compounds **13776** and **13746**

Compound	Second Ligand	K_{Dc}* µM	R^2
13776	None	43.9 ± 32.2	0.899
	AdoHcy	64.8 ± 4.7	0.989
13746	None	0.859 ± 0.352	0.979
	AdoHcy	1.04 ± 0.01	0.998

* Competition binding constant calculated using **Equation 3.4**.

Errors shown are the standard errors of fit.

Compounds **13776** and **13746** were found to fully displace DNA from *E. coli* Dam in solution, both in the absence and presence of AdoHcy, confirming a DNA competitive mode of inhibition. Addition of AdoHcy had little effect on K_{Dc}, with the slightly

increased R^2 values for these experiments possibly reflecting the collection of more accurate data due to the stabilisation of Dam induced by AdoHcy. Competition binding constants were higher than the values of K_i determined for each inhibitor, although the order of potency remains the same, with **13746** showing a greater affinity for Dam than **13776**.

5.3.3 Oligonucleotide melting curves

The identification of arylstibonic acids as inhibitors of multiple DNA binding proteins (*255-258*) raises question about both their selectivity and mode of action. To investigate complex formation between DNA and arylstibonic acids as a potential cause of enzyme inhibition, DNA duplex melting profiles were assessed in the absence and presence of compounds **13776** and **13746**. Melting temperature (T_m) was calculated as the maximum of the first derivatives of fluorescence versus temperature plots for varying concentrations of **13776** and **13746** (**Table 5.5**).

Table 5.5 DNA melting temperatures for varying arylstibonic acid concentration

Compound	**Compound Concentration µM**	**T_m °C**
None	-	78.4 ± 0.2
13776	25	78.5 ± 0.2
	10	78.5 ± 0.2
	1	78.4 ± 0.2
13746	25	78.4 ± 0.2
	10	78.2 ± 0.1
	1	78.5 ± 0.0

T_m's determined as the average maximum of the first derivatives of triplicate fluorescence versus temperature plots for hemimethylated oligonucleotide ODN1. Errors are the standard deviation of triplicate measurements.
Assay conditions: 100 nM hemimethylated oligonucleotide (ODN1), 0, 1, 10 or 25 µM **13776** or **13746**, 5% DMSO, 20 mM Tris, 80 mM NaCl, 8 mM $MgCl_2$, 1 mM DTT, 0.1 mg ml^{-1} BSA, pH 7.9. Total assay volume 20 µl, in LightCycler capillaries, 30-90 °C.

No significant difference in T_m was observed on addition of either **13776** or **13746** to solutions containing the hemimethylated hairpin oligonucleotide ODN1. Whilst not conclusive proof, the lack of a change in T_m combined with the lack of intercalation observed in the FID assay would suggest that no complex is formed between the arylstibonic acids and DNA. This fits well with literature reports, which have found Sb^V to form complexes in solution with ribonucleotides, but not deoxyribonucleotides (*260*).

5.3.4 Aggregation

An alternative possible cause of non-selective inhibition is the formation of arylstibonic aggregates which may act as promiscuous binders (*199*). The addition of detergent to HTS assays has been suggested as a method by which to identify and eliminate such compounds (*237*, *261*). The addition of Tween-20 (0.1%) to fluorescence anisotropy competition binding experiments did not lead to a loss of inhibitory action by compounds **13776** or **13746** (Section 5.3.2). However in order to fully assess the effect of detergent on the potency of the arylstibonic acids the IC_{50} of **13746** was determined in the presence of 0.1% Tween-20 and compared to an experiment containing no detergent was added.

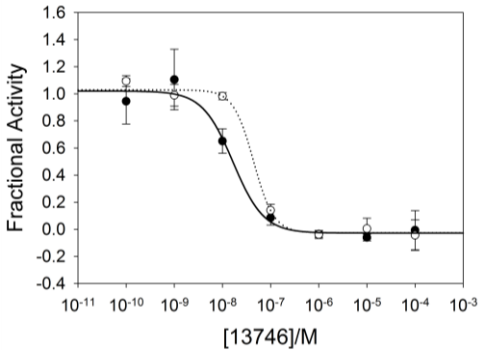

Figure 5.7 Comparison of IC_{50}^{13746} with and without detergent
Fractional activity, calculated using **Equation 2.6A** versus concentration of **13746** with (open circles) and without (filled circles) detergent. Data fitted to **Equation 2.6B**.
Assay conditions: 0.3 or 0 nM *Y. pestis* Dam, 2 nM *Dpn*I, 3.5 nM hemimethylated oligonucleotide (ODN1), 0 or 16 µM AdoMet, 0-100 µM **13746**, 5% DMSO, 0 or 0.1% Tween-20, 20 mM Tris, 80 mM NaCl, 8 mM $MgCl_2$, 1 mM DTT, 0.1 mg ml^{-1} BSA, 5% glycerol, pH 7.9. Total assay volume 20 µl, in 384 well plate, gain 190, 30 °C.

IC_{50} was determined as 44.5 ± 13.7 nM when assays were supplemented with 0.1% Tween-20, compared to 16.4 ± 4.5 nM in a separate experiment where no detergent was added. Ryan *et al.* Suggest that the addition of 36% of the critical micellular concentration (CMC) of Tween-20 (approximately 0.025% v/v) is sufficient to eliminate the effects of promiscuous inhibition (*237*). The small change in IC_{50} observed on addition of 0.1% Tween-20 is therefore unlikely to be indicative of promiscuous binding, implying that the arylstibonic acids do not cause inhibition through aggregation.

5.4 In culture activity

The activity of the arylstibonic acids in *Y. pseudotuberculosis* cell culture was assessed by Dr M.I. Richards (dstl, Porton Down, UK). Genomic DNA was isolated from cultures of *Y. pseudotuberculosis* grown in the presence of each of the arylstibonic acid Dam inhibitors and a selection of inactive arylstibonic acids. Isolated DNA was then analysed by restriction digest with *Sau*3AI (to confirm the presence of GATC sites), *Mbo*I (to identify unmethylated DNA), and *Dpn*I (to identify methylated DNA). The results of the restriction digests were visualised by agarose gel electrophoresis and a single compound, (3-((2-hydroxyethyl)carbamoyl)phenyl)stibonic acid (**13782**), was found to cause the partial inhibition of DNA methylation in bacterial cell culture, as evidenced by the degradation of genomic DNA by both *Mbo*I and *Dpn*I (**Figure 5.8**).

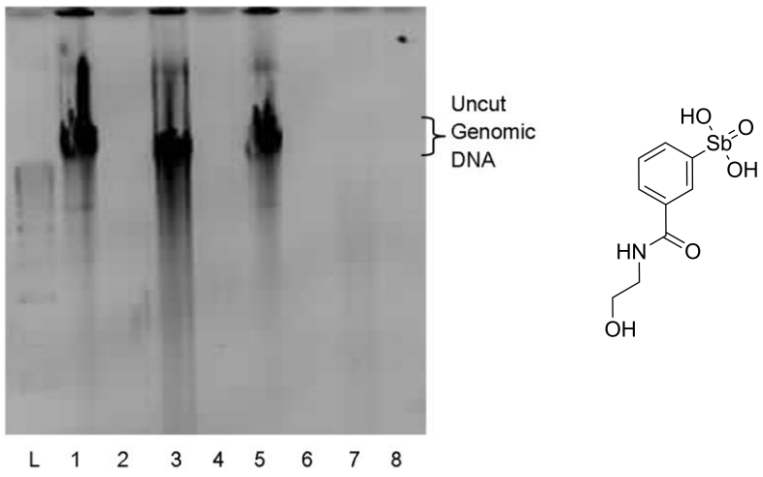

Figure 5.8 Restriction digest of *Y. pseudotuberculosis* genomic DNA grown in the presence of compound **13782**

1% agarose gel electrophoresis of *Y. pseudotuberculosis* genomic DNA digest (left) and the structure of compound **13782** (right).

(L): ladder, (1-4): genomic DNA isolated from *Y. pseudotuberculosis* grown in the presence of an inactive control compound, (5-8): genomic DNA isolated from *Y. pseudotuberculosis* grown in the presence of **13782**, (1 and 5): uncut genomic DNA, (2 and 6): *Dpn*I digested genomic DNA, (3 and 7): *Mbo*I digested genomic DNA, (4 and 8): *Sau*3AI digested genomic DNA.

5.4.1 Compound 13782

Assessment of the methylation state of genomic DNA isolated from *Y. pseudotuberculosis* cell culture showed arylstibonic acid **13782** to be able to penetrate cells and partially inhibit DNA methylation. Compound **13782** has been identified as a potent inhibitor of both Dam and the restriction enzyme *Dpn*I *in vitro*, with a Dam:*Dpn*I selectivity ratio of 0.7, suggesting that **13782** would make a poor drug candidate. However the mechanism by which **13782** is able to penetrate *Yersinia* cells and inhibit DNA methylation and the effect of this inhibition on other cellular processes is of interest and may help to direct further drug discovery efforts.

5.4.1.1 Toxicity

Dam is not essential for the viability of *Y. pestis* (*40*), and so the inhibition of Dam by should not have a detrimental effect on the growth of *Y. pestis* cells. To assess the toxicity of **13782**, *Y. pestis* cells were cultured in the presence of **13782** by Dr M.I. Richards (dstl, Porton Down, UK) and their growth monitored by OD_{600}. Comparison of growth curves for inhibited and control cultures of *Y. pestis* showed **13782** to have little effect on *Y. pestis* growth (**Figure 5.9**), suggesting that the compound does not elicit off-target toxicity. Further evidence of the lack of toxicity displayed by the arylstibonic acids can be found in the publicly available DTP AIDS antiviral screening data (available online at http://dtp.nci.nih.gov), which tested eleven of the arylstibonic acid Dam inhibitors (including **13782**) for toxicity against human CEM cells and found all to have EC_{50} values of greater than 30 μM (the detection limit of the experiment).

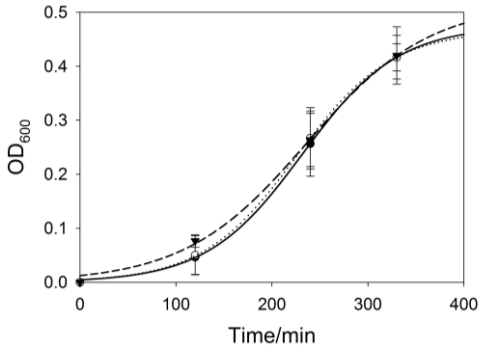

Figure 5.9 *Y. pestis* growth curves in the presence of **13782**

OD_{600} against time for *Y. pestis* grown in the presence of **13782** (filled triangles, dashed line), DMSO (filled circles, solid line), or no additives (open circles, dotted line). Data fitted to a sigmod of the form $y = a/(1+\exp(-(x-x_0)/b))$.

5.4.1.2 mRNA profiling

The effect of **13782** on gene expression was assessed by Dr T.S. Milne (dstl, Porton Down, UK) via microarray mRNA profiling of duplicate RNA samples isolated from *Y.*

pestis cultures grown in the presence of **13782**, and control cultures grown in the absence of **13782**. Statistical analysis of profiling data showed a total of 91 *Y. pestis* open reading frames (ORFs) to have undergone statistically significant (greater than 1.3-fold) up- or down-regulation in the presence of **13782** (see Appendix Section 9.8 for further details). Down-regulated *Y. pestis* genes included ORFs encoding proteins involved in iron acquisition, type III secretion, DNA repair and response to universal stress. Among the genes affected by **13782** mediated inhibition are those involved in the Yersiniabactin (Ybt) iron uptake system and the type III secretion system encoded by the Yop virulon. These results are encouraging as they correlate well with reports in the literature, which have shown both the Ybt and type III secretion systems to be involved in the pathogenicity of *Yersinia* spp. (*262, 263*).

5.4.1.3 Activity of re-synthesised compound 13782

Due to the promising activity shown by compound **13782** in *Y. pestis*, the compound was synthesised by Dr G. Hobley using the method of Englert and Sweeting (*264*). HPLC analysis of both resynthesised compound **13782** (**GH13782**) and **13782** showed the latter to contain a mixture of two components, only one of which was present in the re-synthesised sample, and *Y. pestis* Dam IC_{50} determinations showed **GH13782** to have a significantly lower potency than **13782** (**Figure 5.10**).

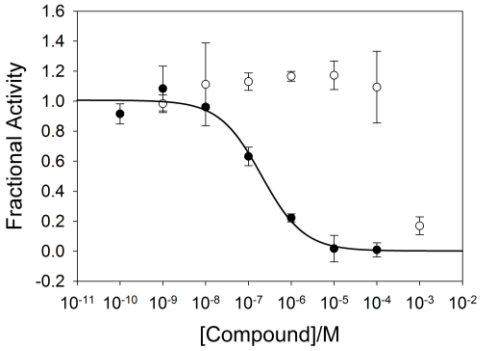

Figure 5.10 IC_{50}^{13782} and $IC_{50}^{GH13782}$ for *Y. pestis* Dam
Fractional activity, calculated using **Equation 2.6A** versus concentration of **13782** (filled circles, solid line) and **GH13782** (open circles). Data fitted to **Equation 2.6B** for **13782**. Assay conditions: 0.3 nM *Y. pestis* Dam, 2 nM *Dpn*I, 3.5 nM hemimethylated oligonucleotide (ODN1), 0 or 16 µM AdoMet, 0-100 or 0-1000 µM compound, 5% DMSO, 20 mM Tris, 80 mM NaCl, 8 mM $MgCl_2$, 1 mM DTT, 0.1 mg ml^{-1} BSA, 5% glycerol, pH 7.9. Total assay volume 20 µl, in 384 well plate, gain 190, 30 ˚C.

The minimal potency displayed by **GH13782** suggested that the activity of **13782** may be due to the second component visible by HPLC, and that the presence of a small amount of this contaminant or break-down product in the re-synthesised sample may

be responsible for the inhibition of *Y. pestis* Dam observed at 1 mM **GH13782**. The components of **13782** were separated by reverse phase chromatography, fractions collected, concentrated, and tested for activity against *Y. pestis* Dam.

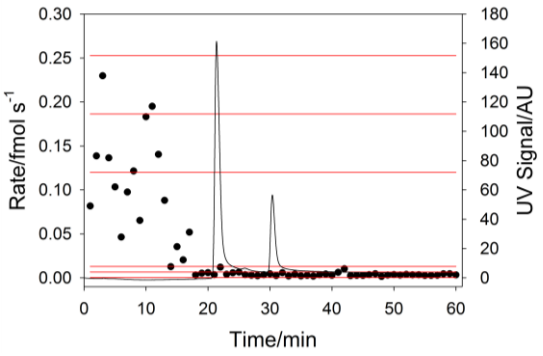

Figure 5.11 HPLC trace of **13782** and activity of concentrated fractions
HPLC trace of **13782** (black line) and activity of concentrated HPLC fractions (filled circles). Positive and negative control averages and plus/minus three standard deviations shown as red lines.
Assay conditions: HPLC gradient 0-100% 0.1 M ammonium acetate over 20 min followed by 100% ammonium acetate over 40 min, 2 ml fractions collected every minute. Freeze-dried fractions were resuspended in 20 µl H_2O and assayed under the following conditions 0.3 nM *Y. pestis* Dam, 2 nM *Dpn*I, 3.5 nM hemimethylated oligonucleotide (ODN1), 0 or 16 µM AdoMet, 25% compound, 20 mM Tris, 80 mM NaCl, 8 mM $MgCl_2$, 1 mM DTT, 0.1 mg ml^{-1} BSA, 5% glycerol, pH 7.9. Total assay volume 20 µl, in 384 well plate, gain 190, 30 ˚C.

Complete inhibition was observed from 18 minutes, corresponding to the point at which ammonium acetate concentration reaches 100%. Subsequent assays showed *Y. pestis* Dam to be fully inhibited by 0.1 M ammonium acetate, rendering the HPLC method used inadequate for this purpose. Further attempts at isolating the active component of **13782** have to date proved futile.

5.5 Summary

Basic SARs for compounds related to HTS hit **13776** have been investigated by screening sublibraries of arylstibonic and arylphosphonic acids. A total of 17 additional arylstibonic acid, and no arylphosphonic acid, Dam inhibitors were identified, suggesting that the stibonic acid group is required for activity. Some minor SAR trends were observed for the arylstibonic acids, with *meta*-substituted compounds showing both increased selectivity for Dam over *Dpn*I and increased potency compared to their *ortho*- and *para*-substituted analogues. Compounds with a carbonyl or sulfonyl group located directly adjacent to the aromatic ring also showed improved selectivity for Dam.

None of the arylstibonic acids tested showed high levels of selectivity for Dam over *Dpn*I, and all but the weakest Dam inhibitors were also shown to inhibit the human DNA methyltransferase DNMT1 by greater than 50% at a concentration of 25 μM. This lack of selectivity is perhaps unsurprising in light of the identification of arylstibonic acids as inhibitors of other DNA-binding proteins. However, further experiments have shown a promiscuous mode of inhibition by aggregation or binding to DNA to be unlikely, suggesting a common mode of action for the inhibition of DNA-binding proteins which is yet to be determined.

The identification of a compound with in cell activity (**13782**) has allowed us to study the effect of the arylstibonic acids on gene expression, with the results of an mRNA profiling study showing genes involved in pathogenesis to be down-regulated. Whether this effect is purely due to the inhibition of Dam or a combination of effects is unclear, however no effects on *Y. pestis* growth were observed, suggesting that **13782** exhibits little or no bacterial toxicity.

Resynthesis of **13782** and HPLC analysis of both **13782** and resynthesised compound **GH13782** have shown the original compound to comprise of two components, only one of which is present in **GH13782**. Further analysis showed **GH13782** to exhibit weak activity against *Y. pestis* Dam in both *in vitro* and preliminary in culture assays. These findings suggest that an active component is common to both samples, but present at much higher concentrations in **13782**. Whether this active component is a break-down product or a contaminant is yet to be elucidated, and the development of an HPLC method compatible with the *in vitro* testing of Dam activity could prove to be a key step in this process.

6 Bisubstrate Analogues

6.1 Introduction

Analogues of the methyl donor AdoMet have been widely explored as methyltransferase inhibitors (*114-121*), however poor levels of selectivity have been observed for such compounds due to the extensive use of AdoMet in enzymatic reactions (*265*). To improve the selectivity of AdoMet analogue methyltransferase inhibitors a bisubstrate approach has been applied in which the structural features of AdoMet are combined with those of the methylation target. Examples of methyltransferases targeted using this approach include COMTs (*136, 137*), bacterial DNA methyltransferases (*142*), HMTs (*134*), mycolic acid methyltransferases (*141*), and PRMTs (*135*). A range of synthetic methodologies have been applied to the development of bisubstrate methyltransferase inhibitors, with AdoMet modified at various positions, as shown in **Figure 6.1**.

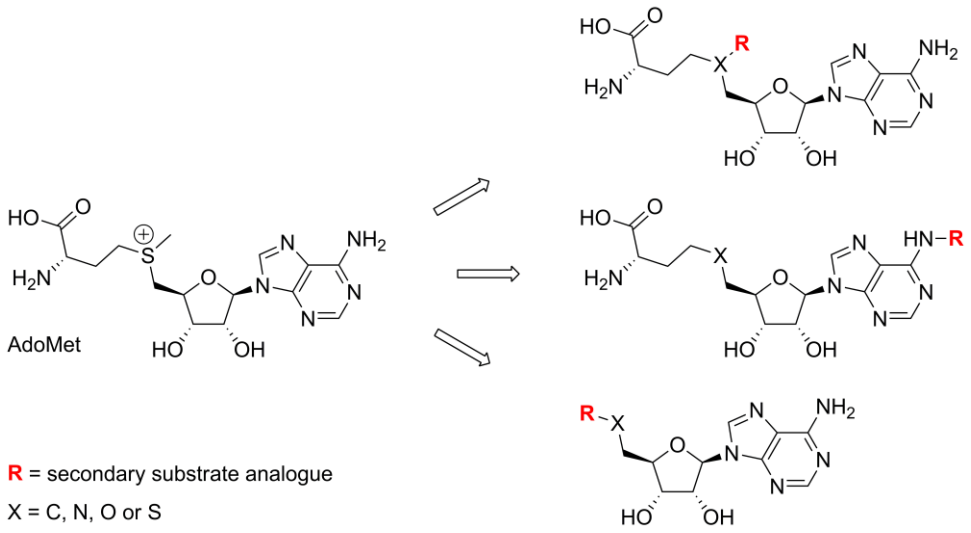

Figure 6.1 Modification of AdoMet for the development of bisubstrate methyltransferase inhibitors

A reductive amination strategy has been applied as a means of synthesising a series of bisubstrate Dam inhibitors from an amine AdoMet analogue scaffold and an aldehyde adenine analogue, based on the methods of Wahhab *et al.* (*266*). A similar technique has been successfully applied to the development of bisubstrate PRMT inhibitors (*135*), demonstrating the validity of such an approach. Inhibitors were designed to mimic the methylation transition state by linking an adenine analogue to the sulfonyl (or equivalent) moiety of an AdoMet analogue (**Figure 6.2**).

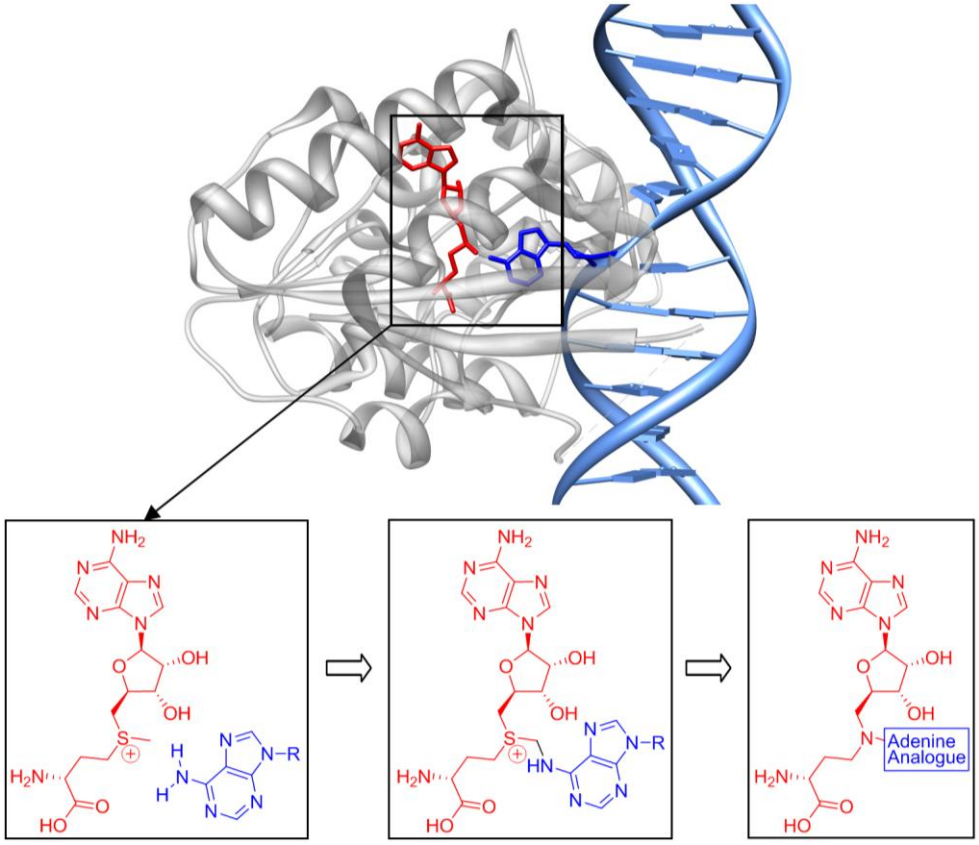

Figure 6.2 Design of bisubstrate Dam inhibitors

Structure of T4 Dam in complex with sinefungin (red) and DNA (blue) and combination of AdoMet (red) and adenine (blue) to form a bisubstrate inhibitor.

Protein image created using pdb file 1YFL molecule E with the program UCSF Chimera (*77*).

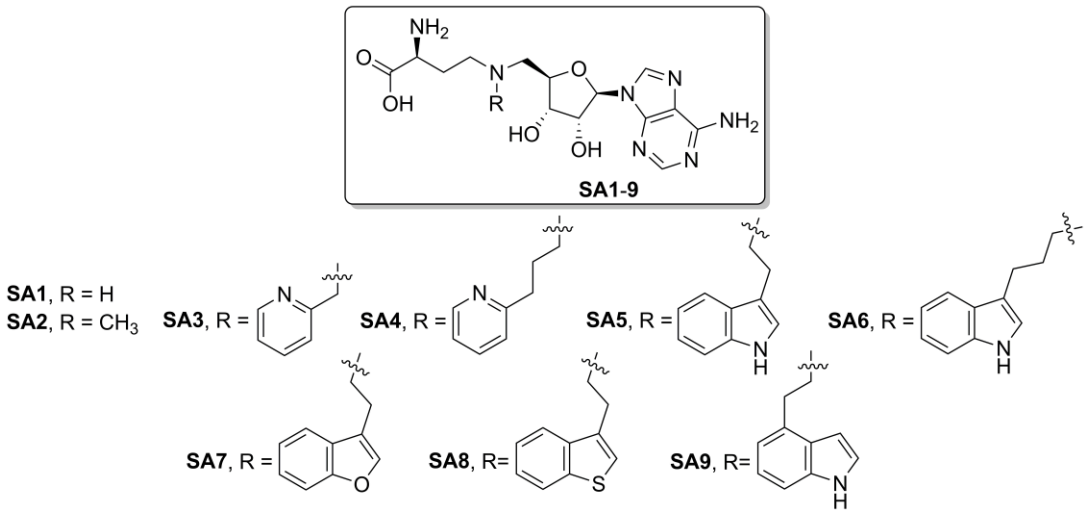

Figure 6.3 The bisubstrate Dam inhibitor library

A small library of 9 bisubstrate Dam inhibitors (**Figure 6.3**) were prepared by Dr G. Hobley as described in reference (*267*). The following chapter describes the *in vitro* evaluation of the potency, selectivity and mode of action of these compounds.

6.2 Hit Validation

6.2.1 Potency

Y. pestis Dam IC_{50} values were determined for the 9-compound bisubstrate inhibitor library and AdoHcy over a concentration range of 0 to 2000 μM and ranked in terms of potency (**Table 5.1**). Substitution of the amine AdoMet analogue scaffold with a pyridine ring led to a loss of activity compared to control analogues **SA1** and **2**. Whereas substitution by an indole, benzofuran or benzothiophene ring system led to an increase in activity over the control compounds, with the analogues substituted with an indole ring at the *C*3-position showing IC_{50} values comparable to that of AdoHcy.

Table 6.1 Potency of the bisubstrate inhibitors against *Y. pestis* Dam

Compound ID*	**Adenine Analogue Substituent**	**Y. pestis Dam IC_{50} μM#**
AdoHcy	-	11.9 ± 4.8
SA5	$CH_2CH_2C_7H_5NH$	12.3 ± 0.8
SA6	$CH_2CH_2CH_2C_7H_5NH$	13.1 ± 2.7
SA8	$CH_2CH_2C_7H_5S$	28.9 ± 8.9
SA9	$CH_2CH_2C_7H_5NH$	31.3 ± 13.0
SA7	$CH_2CH_2C_7H_5O$	39.2 ± 2.6
SA1	H	84.0 ± 20.9
SA2	CH_3	237 ± 68.0
SA3	$CH_2C_5H_4N$	> 250‡
SA4	$CH_2CH_2CH_2C_5H_4N$	> 250‡

* Compounds ranked by *Y. pestis* Dam IC_{50}.

Average ± standard deviation of two independent triplicate assay sets.

‡ IC_{50} was greater than the detection limit of the experiment (250 μM).

6.2.2 Confirmation of activity

The activity of the bisubstrate analogues with *Y. pestis* Dam IC_{50} values of less than 250 μM was confirmed by assessing their activity against *E. coli* Dam in the gel-based methylation assay. Plasmid **pRL821** was incubated with *E. coli* Dam and 2 mM of compounds **SA1**, **2** and **5**-**9**, and restriction digest was used to determine the methylation state of the plasmid after incubation. The results were then visualised by agarose gel electrophoresis (**Figure 3.9**). Control assays were also prepared containing no AdoMet (negative), 2 mM AdoHcy (inhibition), and no compound (positive). Inhibition of *E. coli* Dam was observed for all of the bisubstrate analogues tested, confirming **SA1**, **2** and **5**-**9** as Dam inhibitors.

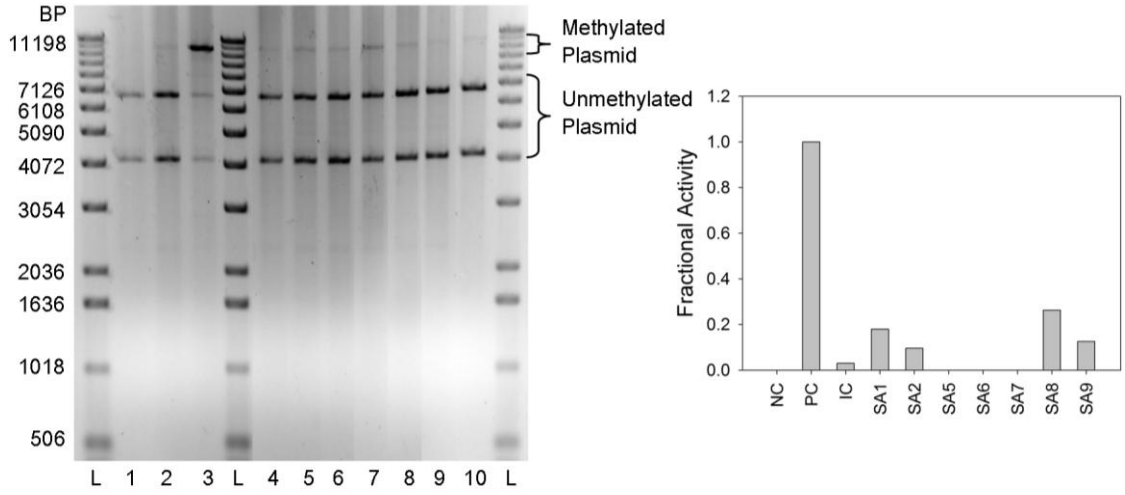

Figure 6.4 Gel-based Dam activity assay of the active bisubstrate inhibitors

A: 0.8% agarose gel electrophoresis of Dam activity assay restriction digest for **SA1**, **2** and **5**-**9**.

(L): ladder, (1): negative control (lacking AdoMet), (2): inhibition control (with AdoHcy), (3): positive control (lacking compound), (4): **SA1**, (5): **SA2**, (6): **SA7**, (7): **SA8**, (8): **SA9**, (9): **SA5**, (10): **SA6**.

C: Fractional activity, quantified from gel band intensity with **Equation 2.6A**.

Assay conditions: 250 nM *E. coli* Dam, 3 nM plasmid (**pRL821**), 10 U μl^{-1} *Xho*I, 7.5 U μl^{-1} *Bcl*I, 0 or 6 μM AdoMet, 0 or 2 mM compound, 5% DMSO, 50 mM Tris, 100 mM NaCl, 10 mM $MgCl_2$, 1 mM DTT, pH 7.9. Step 1 (methylation) – total assay volume 20 μl, temperature 30 ˚C, 1 hr; Step 2 (denaturation) – total assay volume 20 μl, temperature 95 ˚C, 5 min; Step 3 (cleavage) – restriction enzymes *Xho*I and *Bcl*I added, total assay volume 22 μl, temperature 37 ˚C, 1 hr and 50 ˚C, 1 hr. Digested plasmid analysed by 0.8% agarose gel electrophoresis, bands quantified using the program ImageJ (*227*).

6.3 Selectivity

6.3.1 Against DpnI

IC_{50} values were determined for each compound against *Dpn*I, and compared to the previously determined *Y. pestis* Dam IC_{50} values. Substrate concentrations for all IC_{50} experiments were held in the region of K_M, allowing IC_{50} to be roughly approximated to K_i and IC_{50} values for the two different enzymes to be compared. The selectivity ratio (*Dpn*I IC_{50}/*Y. pestis* Dam IC_{50}) for each of the active inhibitors is tabulated below (**Table 6.2**).

Table 6.2 Selectivity of the bisubstrate inhibitors for *Y. pestis* Dam over *Dpn*I

Compound ID*	Adenine Analogue Substituent	Selectivity Ratio#
AdoHcy	-	‡
SA5	$CH_2CH_2C_7H_5NH$	3.8 ± 1.0
SA6	$CH_2CH_2CH_2C_7H_5NH$	4.1 ± 2.5
SA8	$CH_2CH_2C_7H_5S$	4.5 ± 1.3
SA9	$CH_2CH_2C_7H_5NH$	2.1 ± 1.3
SA7	$CH_2CH_2C_7H_5O$	6.3 ± 3.4
SA1	H	‡
SA2	CH_3	‡

* Compounds ranked by *Y. pestis* Dam IC_{50}.

*Dpn*I IC_{50}/*Y. pestis* Dam IC_{50} given to 2 significant figures, error is the combined standard deviation from each pair of triplicate IC_{50} determinations.

‡ *Dpn*I IC_{50} was greater than the detection limit of the experiment (250 nM).

Whilst control analogues **SA1** and **2** show no affinity for *Dpn*I at the concentrations tested the more potent compounds, **SA5**-**9**, were all identified as *Dpn*I inhibitors with minimal selectivity shown for *Y. pestis* Dam. The lack of *Dpn*I inhibition displayed by the control compounds suggests that this lack of selectivity is caused by the addition of the adenine analogue substituent to the amine AdoMet analogue scaffold.

6.3.2 Against DNMT1

The bicyclic, heteroaromatic ring substituted analogues **SA5**-**9** display similar levels of potency for *Y. pestis* Dam, and similar levels of selectivity for *Y. pestis* Dam over *Dpn*I, a single analogue, the benzothiophene substituted **SA8**, was therefore selected for further analysis. Assessment of the effect of adding an adenine-like moiety to an AdoMet analogue on *Y. pestis* Dam and DNMT1 IC_{50} was assessed for **SA8** and the methylated control **SA2** (**Figure 6.5**, **Table 6.3**).

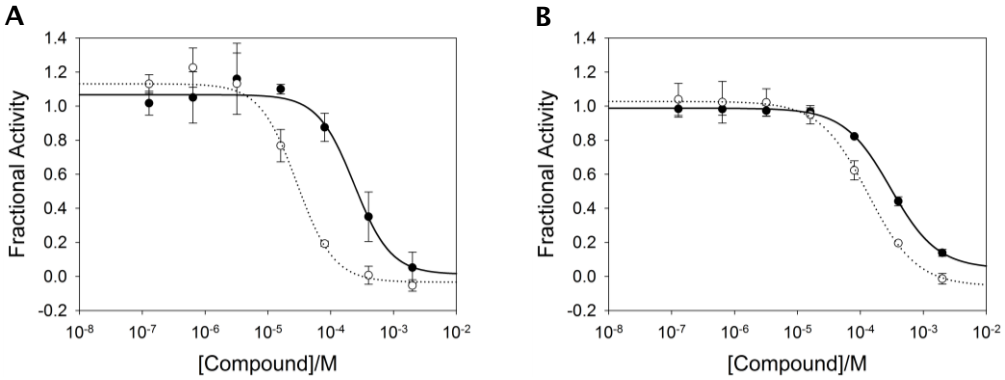

Figure 6.5 Comparison of IC_{50}^{SA2} and IC_{50}^{SA8} for *Y. pestis* Dam and DNMT1

Fractional activity, calculated using **Equation 2.6A** versus concentration of **SA2** (filled circles, solid line) and **SA8** (open circles, dotted line) for Dam (A) and DNMT1 (B). Data fitted to **Equation 2.6B**.

Assay conditions (A): 0.3 nM *Y. pestis* Dam, 2 nM *Dpn*I, 3.5 nM hemimethylated oligonucleotide (ODN1), 0 or 3 μM AdoMet, 0-2000 μM compound, 5% DMSO, 20 mM Tris, 80 mM NaCl, 8 mM $MgCl_2$, 1 mM DTT, 0.1 mg ml^{-1} BSA, 5% glycerol, pH 7.9. Total assay volume 20 μl, in 384 well plate, gain 190, 30 ˚C.

Assay conditions (B): 25 nM DNMT1, 0.05 U μl^{-1} *Gla*I, 250 nM partially methylated oligonucleotide (ODN6), 0 or 16 μM AdoMet, 0-2000 μM compound, 5% DMSO, 100 mM Tris, 12.5 mM NaCl, 5 mM $MgCl_2$, 1 mM DTT, 0.1 mg ml^{-1} BSA, 5% glycerol, pH 7.9. Total assay volume 20 μl, in 384 well plate, gain 1250, 37 ˚C.

Table 6.3 Comparison of IC_{50}^{SA2} and IC_{50}^{SA8} for *Y. pestis* Dam and DNMT1

Compound ID	Adenine Analogue Substituent	Y. pestis Dam IC_{50} μM	DNMT1 IC_{50} μM*
SA2	CH_3	237 ± 68	302 ± 29
SA8	$CH_2CH_2C_7H_5NH$	28.9 ± 8.9	132 ± 9
Potency Ratio#		8.2 ± 3.5	2.3 ± 0.3

* $IC_{50}^{SA2}/IC_{50}^{SA8}$ given to 2 significant figures, error is the combined standard error of measurement from each triplicate IC_{50} determination.

An increase in potency was observed for both *Y. pestis* Dam and DNMT1 upon addition of the benzothiophene group; however the increase for *Y. pestis* Dam was approximately four times that for DNMT1. This result implies that the incorporation of an adenine analogue moiety into bisubstrate Dam inhibitors increases their selectivity for Dam over cytosine-specific methyltransferases such as DNMT1.

6.4 Mode of Inhibition Characterisation

6.4.1 Inhibitory constants

The apparent K_i values of the benzothiophene analogue (**SA8**) were determined by assessing the effect of varying substrate and **SA8** concentration on *Y. pestis* Dam activity. Lineweaver-Burk plots were used to determine mode of action with respect to each substrate (**Figure 6.6**), and K_i values were calculated by fitting replots of y-axis intercept and gradient against inhibitor concentration to **Equation 2.8B** and **C** respectively (**Table 6.4**).

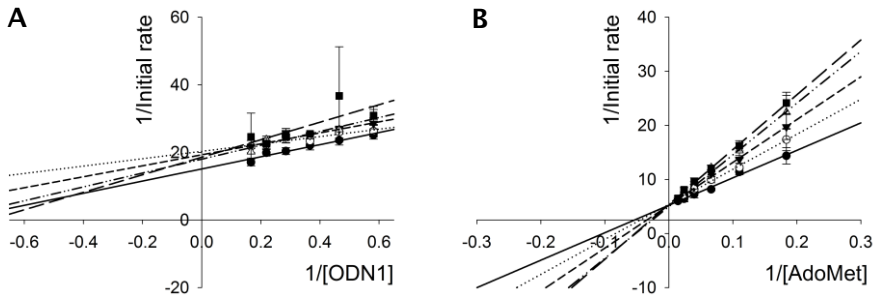

Figure 6.6 Lineweaver-Burk plots for compound SA8

A and B: Plots of 1/initial rate at 0 (filled circles), 11.7 (open circles), 19.4 (filled triangles), 32.4 (open triangles), and 54.0 (filled squares) µM **SA8** against 1/DNA concentration (A) or 1/AdoMet concentration (B).

Data fitted globally to **Equation 2.8A**.

Assay conditions: 0.3 (A) or 1 (B) nM *Y. pestis* Dam, 2 nM *Dpn*I, 3.1-12 (A) or 10 (B) nM hemimethylated oligonucleotide (ODN1), 0, 160 (A) or 5.4-70 (B) µM AdoMet, 0-54 µM **SA8**, 5% DMSO, 20 mM Tris, 80 mM NaCl, 8 mM $MgCl_2$, 1 mM DTT, 0.1 mg ml^{-1} BSA, 5% glycerol, pH 7.9. Total assay volume 20 µl, in 384 well plate, gain 190, 30 ˚C.

Table 6.4 Inhibition constants for compound **SA8**

Compound	Variable substrate	K_i µM	αK_i µM	Mode of inhibition
SA8	DNA	65.0 ± 33.4	572 ± 966	Noncompetitive
	AdoMet	57.6 ± 12.2	> 10,000	Competitive

Errors given are the standard errors of fit.

The Lineweaver-Burk plots showed **SA8** to have a competitive mode of inhibition with respect to AdoMet, and a noncompetitive mode of inhibition with respect to DNA. However the variable DNA concentration plot is ill-defined, with large standard errors

of fit associated with K_i and αK_i values calculated from gradient and y-axis intercept replots, possibly due to the substrate inhibition effect observed at concentrations of DNA above *Y. pestis* Dam K_M. The K_i calculated with respect to AdoMet, 57.6 ± 12.2 μM, is therefore likely to represent a more realistic value.

As an AdoMet analogue compound **SA2** is also likely to possess an AdoMet competitive mode of inhibition. However the determination an inhibitory constant using the real-time Dam activity assay was not possible for this compound due to its relatively weak affinity for *Y. pestis* Dam.

6.4.2 Fluorescence anisotropy

6.4.2.1 Fluorescence anisotropy competition binding

The effect of the bisubstrate analogue inhibitors on the interaction between *Y. pestis* Dam and DNA was assessed through fluorescence anisotropy competition binding experiments. The addition of up to 2 mM of the benzothiophene (**SA8**) or methyl (**SA2**) substituted analogues to assays containing 200 nM *E. coli* Dam and 20 nM DNA had little effect on fluorescence anisotropy. Whilst this results implies that neither **SA8** or **SA2** affect the overall binding affinity of Dam for DNA, the affect of the bisubstrate inhibitors on the binding of the flipped adenine base to the active site pocket has not been established.

6.4.2.2 Stabilisation of the Dam:DNA complex

Previous experiments (Chapter 3, Section 3.5.1.2) have shown the AdoMet analogue AdoHcy to have a stabilising effect on the *E. coli* Dam:DNA complex. The effect of bisubstrate inhibitor (**SA8**) and the methylated AdoMet analogue control (**SA 2**) on the lifetime of the *E. coli* Dam:DNA complex was therefore assessed to determine whether this stabilisation also occurs in the presence of an amine AdoMet analogue or a bisubstrate amine AdoMet analogue. The results (**Figure 6.7**) showed compound **SA2** to induce partial stabilisation of the enzyme:DNA complex compared to the controls (with AdoHcy and lacking compound), and compound **SA8** to induce minimal stabilisation. Suggesting that **SA2**, **SA8** and AdoHcy have different Dam binding modes resulting in different levels of stabilisation of the enzyme:DNA complex.

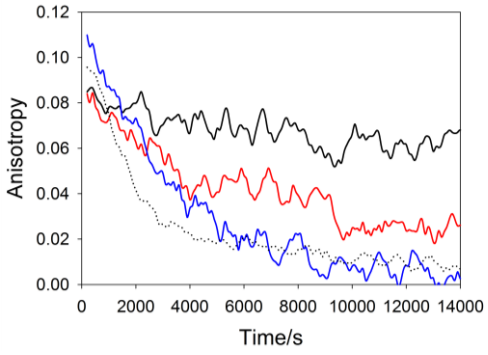

Figure 6.7 Effect of AdoHcy, **SA2** and **SA8** on Dam:DNA complex stability

Background subtracted averaged anisotropy over time for *Y. pestis* Dam:DNA supplemented with AdoHcy (black line), **SA2** (red line), **SA8** (blue line) and a control (black dotted line) lacking compound.

Assay conditions: 0 or 500 nM Dam, 0 or 50 nM hemimethylated oligonucleotide (ODN10), 0 or 2 mM compound, 5% DMSO, 0.1% Tween-20, 20 mM Tris, 80 mM NaCl, 8 mM $MgCl_2$, 1 mM DTT, 0.1 mg ml^{-1} BSA, 5% glycerol, pH 7.9. Total assay volume 100 µl, in 96 well plate, gain 2478/2624, 30 ˚C.

6.5 Summary

The activity of the AdoMet amine analogue **SA2** against *Y. pestis* Dam demonstrates the validity of a nitrogen centred scaffold as a starting point for developing Dam inhibitors. However comparison of the IC_{50} values of the AdoHcy amine analogue **SA1** and AdoHcy, shows that the substitution of sulfur for nitrogen results in an 8-fold decrease in potency, highlighting the need for the continued development of alternative AdoMet analogue scaffolds.

Replacement of the amino methyl substituent with a hydrogen substituent, as in compound **SA1**, resulted in a 3-fold increase in potency, whilst replacement by a substituent containing a single heteroaromatic ring (**SA3** and **4**) resulted in a loss of potency, suggesting that the inhibitor is bound to a confined pocket. However, substitution of the nitrogen centred scaffold by a bicyclic heteroaromatic ring (**SA5**-**9**) led to an increase in potency over both the methyl- and hydrogen-substituted analogues, implying that compounds **SA5**-**9** employ an alternative binding conformation to compounds **SA1**-**4**.

Increasing the length of the linker between the bicyclic heteroaromatic substituent and the nitrogen of the AdoMet analogue scaffold from two to three carbons had little effect on potency, suggesting a certain degree of flexibility within the binding site accommodating the adenine mimic. Attempts at probing this binding interaction by varying the heteroatom have shown a slight decrease in potency when nitrogen is substituted for oxygen or sulfur, and a minor decrease in potency when the point of attachment is moved from the *C*3 to the *C*4 position.

The selectivity of the bisubstrate inhibitors for *Y. pestis* Dam over *Dpn*I was surprisingly poor considering the total lack of affinity shown by *Dpn*I for the AdoMet analogue AdoHcy. Activity against *Dpn*I has therefore been attributed to the adenine analogue substituent. Selectivity for *Y. pestis* Dam over DNMT1 is also poor, however in this case the addition of an adenine analogue substituent led to an increase in potency for Dam compared to a control compound containing a methyl substituent (**SA2**). The bisubstrate nature of these inhibitors suggests that the development of analogues with a greater degree of selectivity for Dam over both *Dpn*I and DNMT1 can be achieved by modifying both the AdoMet and adenine analogue portions of the inhibitors.

Mode of inhibition characterisation showed bisubstrate inhibitor **SA8** to have a competitive mode of action with respect to AdoMet and a K_i of 57.6 ± 12.2 μM. Mode of inhibition with respect to DNA was not fully resolved, however fluorescence

anisotropy competition binding studies revealed no displacement of *E. coli* Dam from DNA by either **SA2** or **SA8**. Extended fluorescence anisotropy assays revealed that **SA2** partially stabilised the Dam:DNA complex, whereas no stabilisation effect was observed in the presence of compound **SA8**.

The interaction between the bisubstrate inhibitors and Dam has been probed further by the crystallisation of *E. coli* Dam in complex with AdoHcy and compound **SA8** (carried out by J.E. Harmer). Resolution of these crystal structures has shown binding of analogues containing the bicyclic heteroaromatic substituent to be accommodated by a conformational change in the protein backbone involving tryptophan 10 (**Figure 6.8**).

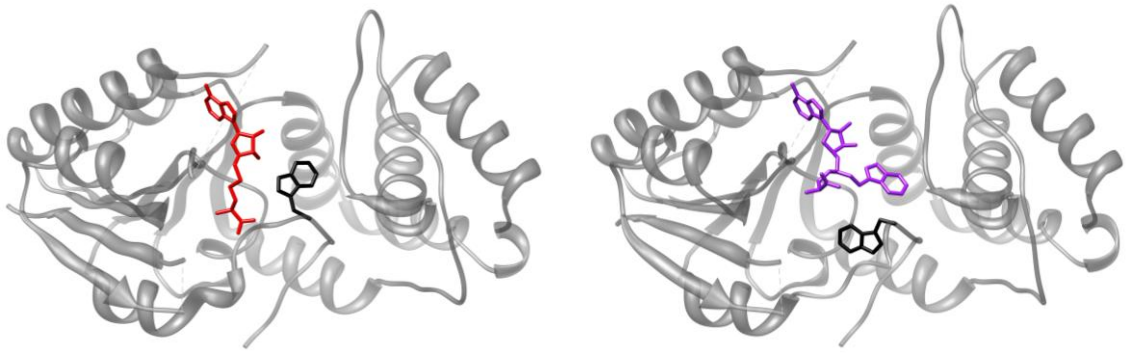

Figure 6.8 AdoHcy and **SA8** in complex with *E. coli* Dam
Structure of *E. coli* Dam in complex with AdoHcy (red) or bisubstrate inhibitor **SA8** (purple). Tryptophan 10 shown in black.
Protein image created with the program UCSF Chimera (*77*).

Accommodation of the adenine-like moiety of bisubstrate inhibitor **SA8** requires a conformational shift in the protein backbone of *E. coli* Dam. No such change occurs on binding AdoHcy or the amine AdoMet analogue **SA2**, indicating that the lack of stabilisation induced by bisubstrate inhibitor **SA8** in fluorescence anisotropy assays is a direct result of this shift. The lack of displacement observed in competition binding studies implies that binding **SA8** does not decrease the affinity of *E. coli* Dam for DNA. The lack of stabilisation induced by **SA8** therefore suggests that *E. coli* Dam is destabilised by the conformational change in the protein backbone, resulting in enzyme denaturation and the subsequent release of DNA.

7 Conclusions and Further Work

7.1 Conclusions

A real-time coupled enzyme assay for monitoring the activity of the bacterial *N*6-adenine methyltransferase Dam has been developed and optimised for HTS, to facilitate the identification of *Y. pestis* Dam inhibitors. Careful optimisation has resulted in a robust and highly reproducible assay, capable of tolerating up to 50% inhibition of the coupling enzyme *Dpn*I, and identifying all modalities of reversible inhibition with minimal bias.

Assays for the validation and characterisation of screening hits have also been developed including: *Dpn*I activity and FID counter-screens designed to eliminate false positives and non-selective compounds which inhibit the coupling enzyme, intercalate DNA, or interfere with assay signal; an alternative Dam activity assay, in which the methylation state of a plasmid incubated with *E. coli* Dam is determined by restriction digest and agarose gel electrophoresis visualisation, designed to validate hits not eliminated through counter-screening; an activity assay for the human cytosine methyltransferase DNMT1, designed to assess the selectivity of validated hits; gel- and HPLC-based in culture assays designed to determine the ability of compounds to permeate bacterial cells and reach the target of interest, unhindered by efflux pumps or degradation; IC_{50} and K_i assays designed to determine the potency and mode of inhibition of viable leads; and fluorescence anisotropy assays designed to probe the effect of compounds on the Dam-DNA binding interaction.

7.1.1 HTS

Two libraries were selected for HTS, the first, a 3,082 compound library from the NCI/DTP open access repository, and the second, a 2,445 compound *in silico* enriched library selected from the University of Cincinnati's drug discovery compound collection (>250,000 compounds) based on structural similarities to AdoMet and adenine. Both libraries were screened in duplicate, with control assays used to monitor assay quality and consistency. The average CV, non-specific activity and Z'-value for each screen is tabulated below (**Table 4.2**) with overall averages calculated over 140 data sets illustrating the high levels of reproducibility and robustness achieved with the real-time break light Dam activity assay during HTS.

Table 7.1 Statistical analysis of assay reproducibility and quality during HTS

Library	Screen[‡]	CV*	Non-specific Activity[#]	Z'-value[†]
DTP	Initial[‡]	10.5 ± 3.5%	5.46 ± 1.93%	0.63 ± 0.12
	Duplicate[‡]	9.07 ± 2.43%	3.85 ± 1.12%	0.69 ± 0.08
University of Cincinnati	Initial[§]	11.8 ± 3.6%	2.51 ± 0.46%	0.60 ± 0.11
	Duplicate[§]	12.9 ± 4.2%	2.37 ± 0.61%	0.57 ± 0.13
	AVERAGE[§]	**11.1 ± 1.7%**	**3.55 ± 1.44%**	**0.63 ± 0.05**

* Calculated from the average and standard deviation of the positive controls using **Equation 2.1**.

[#] Calculated from the average of the positive and negative controls using **Equation 4.1**.

[†] Calculated from the average and standard deviation of the positive and negative controls using **Equation 2.2**, given to 2 decimal places.

[‡] DTP library screen data calculated from 39 sets of 8 positive and 8 negative controls, University of Cincinnati library screen data calculated from 39 sets of 8 positive and 8 negative controls.

[§] Average of each screen ± standard deviation.

Whilst a significant number of hits were initially identified from both screens, a high percentage of these (96 and 80% for the DTP and University of Cincinnati libraries respectively) were eliminated as false positives during counter-screening, with post-counter-screening hit rates similar for both HTS campaigns. The failure of *in silico* screening to improve HTS results in this case is inconsistent with reported examples, in which the benefits of *in silico* enrichment have been documented (*248*) with possible causes including the specific *in silico* screening method applied, the quality of the crystal structure used to inform *in silico* screening, and the size and chemical diversity of the library sampled.

Of the six DTP library hits and 10 University of Cincinnati library hits investigated further, only one compound, the stibonic acid **13776**, was found to exhibit modest (low micromolar) potency against *Y. pestis* Dam, whilst displaying some selectivity for *Y. pestis* Dam over the coupling enzyme *Dpn*I. Although an additional 10 compounds identified as hits in the University of Cincinnati library screen were not investigated further, the likelihood of identifying a viable lead from these compounds is minimal as none inhibited *Y. pestis* Dam by greater than 50% at 50 μM, and all showed some activity against the coupling enzyme *Dpn*I.

Examples of hit rates from other fluorescence-based HTS campaigns range from around 0.1 to 1% (*268-270*), at least 500-times the rate observed in this study (a single lead from a total of 5,527 compounds represents a final hit rate of 0.0002%). Possible reasons for this low hit rate include poor sampling of chemical diversity in library selection, a high false-negative rate, or the application of a more rigorous counter-screening process.

7.1.2 Stibonic acids

Sublibrary screening of compounds analogous to HTS hit **13776** identified a further 17 arylstibonic acids with activity against *Y. pestis* Dam. Investigation of basic SARs revealed that replacement of the stibonic acid moiety with an isosteric phosphonic acid group led to a total loss of activity. Of the compounds tested substituent groups were ranked in the following order of potency: sulfonic acid > carboxylic acid ≈ ester > amide, with the *meta*-substituted compounds showing a slightly greater potency than their *para*- and *ortho*-substituted analogues where available. The minimal increases in potency observed are consistent with the carbonyl/sulfonyl oxygen atom acting as a hydrogen-bond acceptor which is positioned more favourably in the *meta*- substituted compounds.

Poor levels of selectivity were observed for the arylstibonic acids against both the coupling enzyme *Dpn*I and the human cytosine methyltransferase DNMT1, which, in light of the identification of arylstibonic acids as inhibitors of other DNA binding proteins (*255-258*), suggests that the arylstibonic acids have a non-selective, DNA-competitive mode of action. However, the disruption of protein-protein interactions by arylstibonic acids has also been reported (*259*), raising the possibility that inhibition arises from nonspecific compound-protein interactions.

Kinetic characterisation of the initial DTP library hit (**13776**) and the most potent inhibitor (**13746**) against Dam revealed a DNA-competitive mode of action, with K_i values calculated as 960 ± 36 and 6.46 ± 0.07 nM for **13776** and **13746** respectively. Whilst fluorescence anisotropy experiments showed both compounds to completely displace a hemimethylated hairpin oligonucleotide substrate from *E. coli* Dam. These findings, combined with the negative results of compound aggregation and oligonucleotide melting temperature experiments, suggest that the arylstibonic acids are binding to the surface of the protein and blocking the formation of a Dam:DNA complex. A similar phenomenon has been reported for Sb^{III} species, which have been shown to form stable complexes with intracellular thiols (*271*).

Of the 17 arylstibonic acids found to be active against Dam *in vitro* a single compound, **13782**, was found to be active in *Yersinia* spp. cell culture. Cell growth and restriction digest experiments showed **13782** to be capable of penetrating *Yersinia* cells and partially inhibiting methylation, whilst having no toxic effect on cell growth. In addition, mRNA profiling experiments have shown **13782** to induce a statistically significant change in a total of 91 *Y. pestis* ORFs, including the Ybt and type III secretion systems, both of which are involved in the pathogenicity of *Yersinia* spp. (*262, 263*). Unfortunately attempts at resynthesising **13782** have resulted in minimal

success, with re-synthesised compound **GH13782** displaying only weak potency against *Y. pestis* Dam ($IC_{50}^{GH13782}$ > 100 μM, compared with IC_{50}^{13782} = 742 ± 83 nM). HPLC analysis of both **13782** and **GH13782** have identified a second component present only in the original sample, whilst the activity of **GH13782** in cell culture suggests that this secondary component may be a break-down product, the formation of which is catalysed more readily *in vivo*.

7.1.3 Bisubstrate analogues

The *in vitro* evaluation of a series of bisubstrate compounds designed to mimic both the methyl donor AdoMet, and the methyl acceptor adenine, has established that the size of the adenine analogue substituent directly affects compound potency. Comparison of the inhibitor AdoHcy and the analogous bisubstrate inhibitor (**SA1**) revealed that substitution of sulfur for nitrogen results in a significant but not total loss of activity, demonstrating the viability of an amine AdoMet analogue scaffold for the development of bisubstrate inhibitors. Substitution of the hydrogen atom of **SA1** with a methyl group led to a 3-fold decrease in potency, whilst substitution by a more bulky substituent, containing a single heteroaromatic ring, led to an even greater loss of potency.

In contrast, substitution by a bicyclic heteroaromatic ring led to an increase in potency, with the indole substituted analogues **SA5** and **SA6** exhibiting similar levels of potencies to that of AdoHcy. Examination of the crystal structure of *E. coli* Dam bound to both AdoHcy and the benzothiophene substituted analogue **SA8** revealed that the bulky bicyclic heteroaromatic ring was accommodated by a conformational change in the protein backbone. Fluorescence anisotropy analysis of *E. coli* Dam and DNA in the presence of **SA8** and AdoHcy showed that the methyl donor product stabilised the enzyme-DNA complex, whilst **SA8** did not. This result suggests that either the conformational change induced by **SA8** is destabilising to the protein:DNA complex, or that AdoHcy (and AdoMet) induces a conformational change that stabilises the complex.

Selectivity analysis showed the addition of a bicyclic heteroaromatic ring substituent to decrease the affinity of the analogues for DNMT1, whilst increasing their affinity for *Dpn*I. In addition, kinetic characterisation of the benzothiophene analogue (**SA8**) identified an AdoMet-competitive mode of action. These findings imply that both selectivity and potency can be improved by modifying the AdoMet and adenine analogues independently, with the AdoMet analogue substituent controlling selectivity against other adenine binding proteins, and the adenine analogue substituent controlling selectivity against other AdoMet binding proteins.

7.2 Further Work

7.2.1 Identification of inhibitors

The low hit rate observed for both HTS campaigns suggests that the identification of a viable lead would require the screening of a significantly larger number of compounds. Whilst *in silico* screening would enable large libraries to be screened quickly and relatively inexpensively, this methodology has to date proved unsuccessful as a means of identifying potent and selective Dam inhibitors. A fragment-based screening approach would allow a diverse range of chemical space to be sampled without screening large numbers of compounds, thus minimising both cost and development time. In addition a fragment-based approach is ideal for probing targets with multiple binding pockets, such as Dam, with the development of an efficient and reliable crystallisation system for *E. coli* Dam facilitating the location of binding sites for active compounds.

An initial fragment-based screening campaign has been implemented by J.E. Harmer, with the Maybridge 1,000-compound RO3 fragment library screened at high concentration (~1 mM) to identify weak binders. Crystallisation of *E. coli* Dam with screening hits is currently being undertaken to establish binding sites, with future work hopefully involving the linking of weak inhibitors binding different pockets to form a more potent amalgamated compound.

7.2.2 Characterisation of inhibitors

The real-time break light Dam activity assay has proved efficient at identifying and ranking Dam inhibitors, however some issues have arisen due to the coupled nature of the assay. Specifically the inhibition of the coupled enzyme by the primary enzyme substrate has led to difficulties in establishing mode of inhibition with respect to DNA concentration. To overcome this issue a fluorescence anisotropy DNA binding assay was developed to monitor Dam-DNA binding interactions. Whilst this assay has enabled the direct assessment of DNA-competitive inhibition, AdoMet-, and flipped adenine-competitive inhibition cannot probed so readily.

A fluorescence anisotropy AdoMet binding assay could be applicable not only to the identification and characterisation of Dam inhibitors, but also to the identification and characterisation of inhibitors of other AdoMet-dependant methyltransferases. As such, a fluorescent AdoMet analogue (**SA10**) has been synthesised by Dr G. Hobley (**Figure 7.1**). Initial experiments have shown **SA10** to inhibit *Y. pestis* Dam with an IC_{50} of 77.6 ± 32.6 μM, implying that the compound binds Dam, despite the addition of the bulky coumarin group. Further work is now required to determine whether **SA10** could be used as a fluorescent probe for monitoring Dam-AdoMet binding interactions.

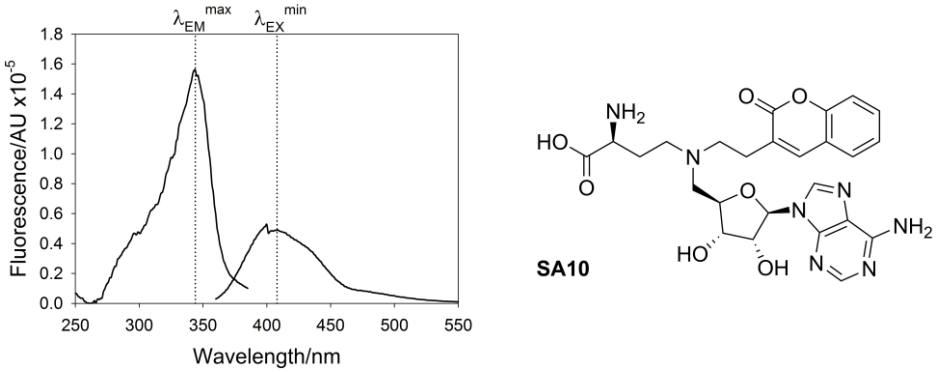

Figure 7.1 Structure and fluorescence spectra of AdoMet analogue **SA10**
Where λ_{EX}^{max} = maximum excitation wavelength and λ_{EM}^{max} = maximum emission wavelength.

Probing the flipped adenine binding pocket has previously been achieved by monitoring the fluorescence of the adenine analogue 2AP in stopped flow fluorescence experiments (*93*). Adaptation of this method could provide a third direct binding interaction assessment, with the effect of inhibitors on the binding of flipped adenine to the active site pocket monitored by changes in the fluorescence of 2AP.

7.2.3 Hit-to-lead progression

7.2.3.1 Stibonic acids

Further investigation of the stibonic acid Dam inhibitors requires identification of the active component of the in cell inhibitor **13782**. Initially this may be achieved through the development of alternative HPLC methods compatible with Dam activity assays. In parallel with this other antimonial compounds, such as the anti-leishmaniasis drugs meglumine antimoniate and stibogluconate, could be tested both *in vitro* and in cell culture and their effects compared with those of the stibonic acid Dam inhibitors. Attempts at elucidating binding mode by crystallising *E. coli* Dam in the presence of the stibonic acids have to date been unsuccessful, however structural analysis of the protein in the presence of inhibitor could prove invaluable, with alternative methods such as circular dichroism (CD) spectroscopy providing insight into both the mode of action and binding site of these compounds.

7.2.3.2 Bisubstrate analogues

Analysis of the bisubstrate analogue series showed the addition of an adenine-like moiety to increase selectivity for Dam over DNMT1, but reduce selectivity for Dam over *Dpn*I. Further bisubstrate analogue libraries should therefore focus on both the AdoMet and the adenine moieties. To achieve this, a fragment-based approach could be used to screen separate libraries of adenine and AdoMet analogues, with crystallisation used to identify the most efficient way of linking the two components. The identification of a more appropriate sulfur atom substitute is also required, and could potentially be achieved using an *in silico* approach to model the properties of potential replacement groups, with the ease of synthesising such compounds also carefully considered.

7.2.4 Investigating the stability of Dam

Experiments have shown *Y. pestis* Dam to be thermally less stable than *E. coli* Dam, which is in turn less stable than the thermophillic *P. horikoshii* Dam. A similar result has been observed for wild-type *S. typhimurium* Dam and a *C*-terminal deletion mutant, suggesting that temperature sensitivity is related to the *C*-terminus of the Dam protein (*272*). Alignment of all four sequences (**Figure 2.4**) shows the longest and shortest *C*-terminals to correlate respectively to the most (*P. horikoshii*) and least (*Y. pestis*) thermally stable Dams.

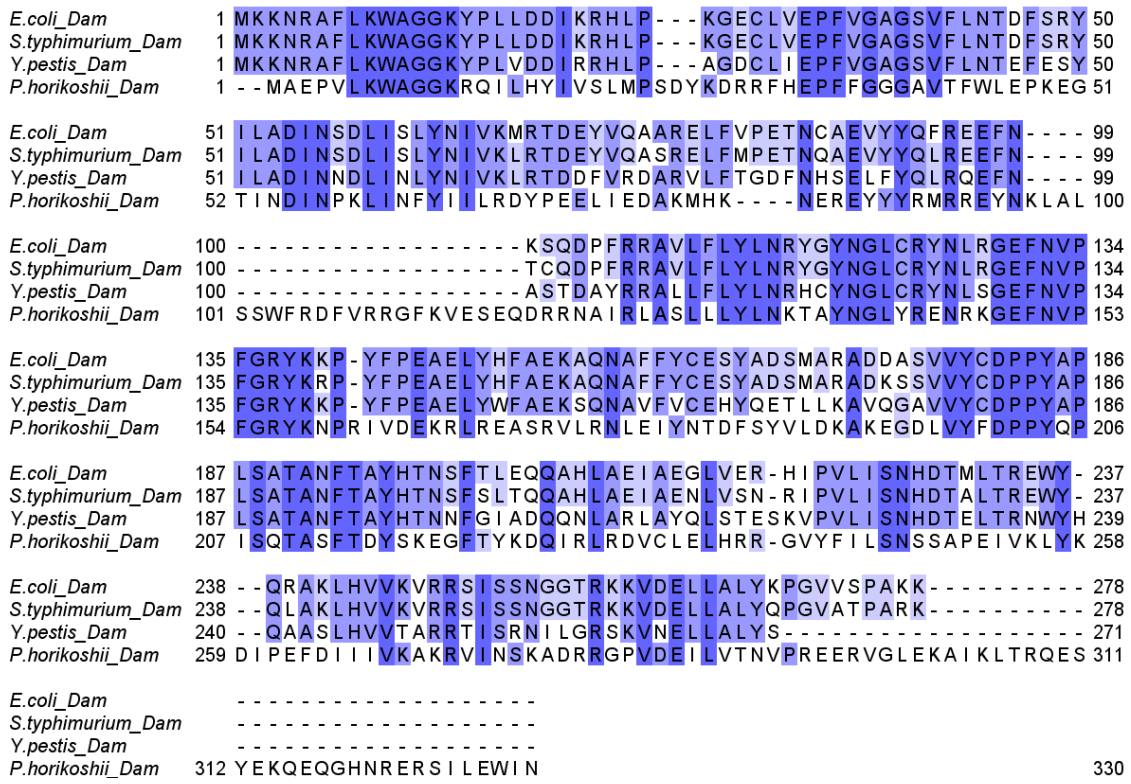

Figure 7.2 Alignment of *Y. pestis*, *E. coli*, *S. typhimurium* and *P. horikoshii* Dam
Calculated with the ClustalW algorithm using the program Jalview (*95, 96*). 100% identity shown in blue.

Additionally fluorescence anisotropy experiments revealed that DNA was released over time from the Dam:DNA complex in the absence of AdoHcy for both *Y. pestis* and *E. coli* Dam. This result suggests that the protein undergoes a time-dependant change which leads to the release of DNA. A possible reason for this behaviour is that the binding of Dam to DNA must be tightly regulated to prevent the blocking of methylated GATC sites by Dam. The specific binding of the protein to DNA would therefore occur only in the presence of the methyl donor AdoMet, as previously observed in crystallographic studies of both *E. coli* and T4 Dam (*91, 97, 98*). Additionally, in the absence of DNA the protein may unfold, with the rate of unfolding

mediated by both temperature and the *C*-terminus. Such temperature-dependant denaturation may have a role in controlling the concentration of Dam within the cell, thus circumventing the potentially toxic effects of Dam overexpression.

Investigation of this effect could be achieved through the study of further *C*-terminal deletion mutants, and the crystallisation of Dams with *C*-terminals of differing lengths, with and without substrates. Although the lack of a published substrate-free Dam structure suggests that the crystallisation of the enzyme without substrates is difficult, giving further weight to the theory that the protein unfolds in the absence of substrates. Probing of this unfolding interaction may be possible through a more dynamic technique such as CD spectroscopy.

8 Experimental

8.1 Materials

Chemicals

AdoMet hydrochloride, AdoHcy, thiazole orange and standard dNMPs were purchased from Sigma Aldrich (Dorset, UK); dmAMP was purchased from AtdBio (Hampshire, UK); DTT, BSA and antibiotics were purchased from Melford Laboratories (Suffolk, UK); polyacrylamide-bis polyacrylamide (30% w/v, 37:5:1) and Bacto agar were purchased from Fisher Scientific (Leicestershire, UK); Bacto tryptone and yeast extract for culture media were purchased from Oxoid (Hampshire, UK); Chelating Fast Flow resins were purchased from GE Healthcare (Buckinghamshire, UK).

All other chemicals were of the highest quality available and purchased from Sigma Aldrich or Fisher Scientific.

Compound libraries

The DTP library, stibonic acid sublibrary and phosphonic sublibrary were obtained from the NCI/DTP open chemical repository (http://dtp.cancer.gov); the University of Cincinnati library was obtained from the University of Cincinnati; Compounds **UC1**- **10** were re-sourced from Acros Organics (Fisher Scientific), Ambinter (Orléans, France), ChemBridge (San Diego, USA), Maybridge (Fisher Scientific) and Sigma Aldrich; the bisubstrate analogue library was synthesised by Dr G. Hobley at the University of Southampton.

Consumables

12 well clear sterile suspension plates with lids, 96 well half area black microplates and 384 well low volume black HiBase microplates were purchased from Greiner Bio-One (Gloucestershire, UK); Biomek P20 and P250 robotic tips were purchased from Beckman Coulter (Buckinghamshire, UK); LightCycler capillaries were purchased from Roche (West Sussex, UK); sterile filters were purchased from Millipore (Hertfordshire, UK); Wizard Plus SV Minipreps Plasmid DNA Purification System was purchased from Promega (Hampshire, UK); Gentra Puregene Yeast/Bacteria kit was purchased from Qiagen (West Sussex, UK).

E. coli Strains

E. coli strains GM43 (CGSC# 5127, Marinus M.G.), GM2929 (CGSC# 7080, Marinus M.G.), BW25113 (CGSC# 7636, Wanner, B.L.) and JW3350-2 (CGSC# 11675, the Keio collection) were obtained from the Yale *E. coli* genetic stock centre; *E. coli* ER2925 was purchased from New England Biolabs (Hertfordshire, UK); E. coli TOP10 was purchased from Invitrogen (Paisley, UK).

Enzymes

Restriction enzymes *Bcl*I, *Dpn*I, *Mbo*I, *Nco*I and *Xho*I were purchased from New England Biolabs; His-tagged *Dpn*I and *Y. pestis* Dam were prepared by M.D. Maynard-Smith and J.C. McKelvie and kept in frozen stocks at the University of Southampton; His-tagged *P. horikoshii* and *E. coli* Dam were prepared by J.E. Harmer and kept in frozen stocks at the University of Southampton; DNMT1 was a kind gift from Cancer Research Technologies (London, UK); *Gla*I was purchased from SibEnzyme (Siberia, Russia); Nuclease P1 was purchased from Sigma-Aldrich; RNaseA and T1 were purchased from Roche.

Oligonucleotides

Oligonucleotides ODN1-12 were purchased from AtdBio.

Plasmids

E. coli GM43 harbouring plasmid **pMMS/4958/59** was prepared by M.D. Maynard-Smith and kept in frozen stocks at the University of Southampton; plasmids **pRJW/4213/07** and **pRL821** were prepared by Dr R.J. Wood and Dr R. Leonardi respectively and kept in frozen stocks at the University of Southampton; plasmid **pBAD/HisA** was purchased from Invitrogen.

8.2 Equipment

Automated assay preparation

Assays were prepared in 96 or 384 well plates using a Beckman Coulter Biomek 3000 laboratory automation workstation at room temperature.

Centrifugation

Samples were centrifuged at 4 °C in a Sorval Evolution RC centrifuge fitted with an SLC-6000 or an SLA-1500 rotor or a Heraeus Multifuge 1-R fitted with a Highconic rotor. Small volumes (< 1.5 ml) were centrifuged in a bench top microcentrifuge at room temperature.

Computer software

Data analysis was carried out using Microsoft Excel and MathWorks MATLAB; Graphs were plotted using Systat SigmaPlot 11; Protein structures were visualised with UCSF Chimera (*77*); Gel bands were quantified using ImageJ (*227*); Alignments, percentage identity and neighbour joining trees were calculated with Jalview (*95, 96*); Chemical structures were drawn with CambridgeSoft ChemDraw Ultra 12.

DNA melting profile analysis

A carousel-based Roche LightCycler 1.5 system was used to measure DNA melting profiles over temperature ranges of 30-95 °C.

Fluorescence spectroscopy

Fluorescence measurements were recorded in a Tecan Safire^2 or BMG POLARstar Omega microplate reader and fluorescence anisotropy experiments were carried out in a BMG POLARstar Omega microplate reader. The following measurement parameters were applied unless otherwise stated:

Tecan Safire^2 microplate reader – Z-Position of 9,300 µm for 96 well plates or 12 000 µm for 384 well plates, integration time of 20 µs, 0 s between each movement and reading, no shaking between data collections.

BMG POLARstar Omega microplate reader – Integration time of 20 µs, 0 s between each movement and reading, no shaking between data collections.

Excitation and emission wavelengths, bandwidths, gain and temperature are stated for each experimental method.

FPLC

A GE Healthcare FPLC System maintained at 4 ˚C was used for all protein purifications.

HPLC analysis

A Gilson system workcenter including 321 pumps and 234 Gilson autoinjector was connected to a Shimadzu RF-10Axl fluorimeter and a Gilson UV/Vis-155 detector, and used for HPLC analysis at room temperature.

Incubations

Bacterial plate cultures were grown in a Gallenkamp Economy Incubator Size 2 (37 ˚C, overnight). Bacterial liquid cultures were incubated in a New Brunswick Scientific Innova 4400 Incubator Shaker (37 ˚C, 180 rpm), or a BMG POLARstar Omega microplate reader (37 ˚C, with double orbital shaking).

pH determination

A Mettler Delta 340 pH meter in conjunction with a Mettler Toledo Inlab 413 Combination Electrode was used for pH measurements. This equipment was calibrated at pH 4.0–7.0 or pH 7.0–10.0 before use and stored in 3 M potassium chloride.

UV-Vis spectroscopy

UV absorbance measurements were recorded with a Thermo Electron Biomate 3 spectrophotometer and UV spectra were recorded with BMG POLARstar Omega microplate reader.

8.3 General Methods

8.3.1 Microbiological Methods

Standard sterile techniques were used during all microbiological experiments. Sterilisation of growth media and heat stable solutions was achieved with a PriorClave autoclave (121 °C, 25 min). Heat labile solutions (antibiotics and arabinose) were sterilised by filtration through 0.22 µm filters.

Growth media were supplemented with antibiotics (dependant on specific cell strain antibiotic resistance) of the following concentrations:
ampicillin, 100 µg ml^{-1}
kanamycin, 10 µg ml^{-1}
chloramphenicol 30 µg ml^{-1}

8.3.1.1 The rubidium chloride method for making competent cells

2YT media (100 ml) was inoculated with overnight cultures of *E. coli* (1 ml). The resulting culture was incubated with shaking (37 °C, 180 rpm) until an OD_{600} of ~0.6 was reached. Cultures were then cooled on ice (<4 °C, 10 min) and cells harvested by centrifugation (2 x 50 ml, 4 °C, 4000 rpm, 10 min). The supernatant was decanted and the centrifuge tubes inverted to remove excess liquid (4 °C, 1 min). Cell pellets were resuspended in TBFI (10 ml, 4 °C) and recovered by centrifugation (2 x 10 ml, 4 °C, 4000 rpm, 10 min). The supernatant was decanted and the centrifuge tubes inverted to remove excess liquid (4 °C, 2 min). Cell pellets were resuspended in TBFII (1.5 ml, 4 °C) and aliquots (100 µl) flash frozen on dry ice and stored at -80 °C until required.

8.3.1.2 Transformation

Plasmid solution (1 µl, <4 °C) was added with gentle mixing to an aliquot of thawed (<4 °C) competent cells and the cells incubated on ice (<4 °C, 30-40 min). Cells were then heat shocked (42 °C, 45 s) before being returned to the ice (<4 °C, 2 min). SOC media (250 µl, 37 °C) was added to the heat shocked cells which were then incubated with shaking (37 °C, 180 rpm, 1 hr). Antibiotic (dependant on the cell strain used) supplemented 2YT media plates (37 °C) were spread with transformed cell solution (100 µl) and incubated (37 °C, overnight). Plates were sealed and stored at 4 °C for up to 8 weeks.

8.3.1.3 Preparation of glycerol freezes

Overnight culture of *E. coli*, prepared by inoculation of 2YT media with a single colony picked from an agar plate, was mixed with sterile glycerol (70%) in a 4:1 ratio and aliquots were stored at -80 °C until required.

8.3.1.4 Isolation of plasmid DNA

E. coli cells were harvested from cultures by centrifugation (1-10 ml, 4 °C, 4000 rpm, 10 min) and plasmid DNA was isolated using the Promega Wizard Plus SV Minipreps Plasmid DNA Purification System, as per the manufacturer's instructions. Plasmid DNA was eluted from the purification column with sterile water (50-100 µl) and stored at -20 °C until required.

8.3.1.5 Isolation of genomic DNA

E. coli cells were harvested from cultures by centrifugation (1 ml, 13,200 rpm, 5 min) and genomic DNA was isolated using the Qiagen Gentra Puregene Yeast/Bacteria Kit, as per the manufacturer's instructions, with the exception of the RNase digestion step which was modified to digestion (37 °C, 30 min) with RNase A/T1 solution (0.5 µg μl^{-1} /50 U μl^{-1}, 20 µl). Genomic DNA was eluted from the purification column with sterile water (100 µl) and stored at -20 °C until required.

8.3.1.6 Analytical digests

The analytical digest solution described below (**Table 8.1**) was prepared and incubated at the optimal temperature[12] (typically 37 °C, 1 hr). The results were analysed by 0.8 or 1% agarose gel electrophoresis with ethidium bromide staining.

Table 8.1 Analytical digest solution

Component	Final Concentration	Quantity
Plasmid DNA (100-500 ng μl^{-1})	50-250 ng μl^{-1}	5 µl
NEBuffer1-4[12] (10x)	1x	1 µl
BSA[13] (1 mg μl^{-1})	0.1 mg μl^{-1}	1 µl
Restriction enzyme(s) (5-20 U μl^{-1})	0.25-1 U μl^{-1}	0.5 µl (per enzyme)
Sterile Water		To a final volume of 10 µl

8.3.1.7 Determination of protein concentration by Bradford Assay

Protein concentration was assayed using the method of Bradford (*211*). Bradford reagent (1 ml) was added to a protein sample (20 µl) and incubated (5 min, room temperature). Absorbance at 595 nm (OD_{595}) was measured, and the sample diluted if OD_{595} exceeded 1.0. Calibration curves were prepared from BSA standards and used to convert OD_{595} to protein concentration.

[12] Optimal buffer and temperature conditions for each restriction enzyme were selected using the NEBuffer Activity Chart (available online at http://www.neb.com).

[13] BSA was only added when recommended by the manufacturer.

8.3.1.8 SDS-PAGE

15% SDS-PAGE gels were prepared by mixing the components described in **Table 8.2** and **Table 8.3** respectively, with the resolving gel (~4 ml) poured first and allowed to set (~45 min) before pouring of the stacking gel (~1.5 ml).

Table 8.2 15% SDS-PAGE resolving gel

Component	Final Concentration	Quantity
Acrylamide/bis acrylamide (30%)	15%	2.5 ml
Tris (pH 8.8, 1.5 M)	0.4 M	1.3 ml
SDS (10%)	0.1%	50 µl
Ammonium persulfate (10%)	0.1%	50 µl
TEMED	0.04%	2 µl
Deionised Water		1.1 ml
Total Volume		**5 ml**

Table 8.3 5% SDS-PAGE stacking gel

Component	Final Concentration	Quantity
Acrylamide/bis acrylamide (30%)	5%	333 µl
Tris (pH 6.8, 1 M)	0.2	400 µl
SDS (10%)	0.1%	20 µl
Ammonium persulfate (10%)	0.1%	20 µl
TEMED	0.1%	2 µl
Deionised Water		1.23 ml
Total Volume		**2 ml**

Samples were prepared by mixing protein solution in a 1:1 ratio with 2x SDS-PAGE loading buffer and denaturing (95 °C, 5 min). Samples (15 µl) were then loaded onto the gel and electrophoresis was carried out (200 V, in 1x SDS-PAGE running buffer). Gels were stained with coomassie brilliant blue and destained in destain solution (12-48 hrs) before imaging.

8.3.1.9 Small scale protein expression studies

An overnight *E. coli* starter culture (1 ml) was used to inoculate 2YT media (100 ml) supplemented with antibiotic (dependant on cell strain). The culture was incubated with shaking (37 °C, 180 rpm) and OD_{600} monitored. At an OD_{600} of 0.6 cells were induced by the addition of sterile arabinose solution (20% w/v, 1 ml). Cells were then

incubated with shaking (37 °C, 180 rpm), with a samples (1 ml) removed every hour for analysis. Cells from samples were immediately harvested by centrifugation (10,000 rpm, 10 min) and the supernatant discarded. Cell pellets were then analysed by SDS-PAGE (Section 8.3.1.8).

8.3.1.10 Large scale protein expression

An overnight *E. coli* starter culture (12.5 ml) was used to inoculate 2YT media (1.25 L) supplemented with antibiotic (dependant on cell strain). The culture was incubated with shaking (37 °C, 180 rpm) and OD_{600} monitored. At an OD_{600} of 0.6 cells were induced by the addition of sterile arabinose solution (20% w/v, 1.25 ml) and cultures were incubated with shaking (37 °C, 180 rpm). Cells were harvested by centrifugation (4 °C, 7000 rpm, 30 min) and stored at -80 °C until required. Time of harvesting was dependant on expression studies and growth monitoring, and is stated for each large scale growth described.

8.3.1.11 Purification of His-tagged protein

Frozen cell pellet (10 g) was resuspended in ice cold low imidazole buffer (30 ml, <4 °C, 10 min). Lysozyme (5-15 mg) was added and the resuspension mixture stirred on ice (<4 °C, 15 min). The solution was then sonicated on ice (<4 °C, 20 x 10 s with 10 s rest). Protein concentration was determined by Bradford Assay, as described in Section 0, and if a concentration of <20 mg ml^{-1} was observed sonication was repeated as before. The lysate was then centrifuged (4 °C, 14000 rpm, 30 min) to precipitate cell debris, and the resulting supernatant loaded (4 ml min^{-1}) onto a Ni-NTA sepharose column with a bed volume of 10 ml. The column was then washed with low imidazole buffer (4 ml min^{-1}, 150 ml). Elution of His-tagged protein was achieved with a 0-100% step to high imidazole buffer. Eluted fractions containing protein (determined by Bradford assay as before) were pooled and desalted by dialysis (2 x 500 ml, 30 min) into storage buffer and stored at -80 °C until required.

8.3.2 Real-time break light enzyme activity assay methods

8.3.2.1 Real-time break light Dam activity assay

The activity of *Y. pestis* or *E. coli* Dam was measured in triplicate (unless otherwise stated) in Greiner 96 well half area black microplates with a total assay volume of 100 µl, or Greiner 384 well low volume black HiBase microplates with a total assay volume of 20 µl, maintained at 30 °C. Assays were prepared as described below using a Biomek 3000 laboratory automation workstation (unless otherwise stated) and fluorescence changes were recorded in a Tecan Safire^2 microplate reader with 10 readings per well (each measurement), measurement parameters were as described previously (Section 8.2). Excitation was set at 486 nm (5 nm bandwidth) and emission at 518 nm (10 nm bandwidth). Microplate reader gain was as stated per experiment.

Assays containing buffer A or B supplemented with AdoMet and hemimethylated oligonucleotide ODN1 were equilibrated in a Tecan Safire^2 (30 °C, 10 min) prior to initiation with ice-cold *Y. pestis* Dam and *Dpn*I in buffer A or B. An average background fluorescence was determined over 5 readings prior to initiation and subtracted from the fluorescence of initiated assays, monitored over 2000-4000 s. Initial rate of fluorescence change was determined as the gradient of the first ten background subtracted data points or as the maximum differential of a moving average taken over 5 background subtracted data points. Rate of change of fluorescence was converted to initial rate of reaction using calibration plots, prepared as described in Appendix Section 9.4.1, and non-specific background changes in fluorescence were accounted for by subtracting a negative control (lacking AdoMet) where appropriate.

8.3.2.2 Real-time break light DpnI activity assay

The activity of *Dpn*I was measured in triplicate (unless otherwise stated) in Greiner 96 well half area black microplates with a total assay volume of 100 µl, or Greiner 384 well low volume black HiBase microplates with a total assay volume of 20 µl, maintained at 30 °C. Assays were prepared as described below using a Biomek 3000 laboratory automation workstation (unless otherwise stated) and fluorescence changes were recorded in a Tecan Safire^2 microplate reader with 10 readings per well (each measurement), measurement parameters were as described previously (Section 8.2). Excitation was set at 486 nm (5 nm bandwidth) and emission at 518 nm (10 nm bandwidth). Microplate reader gain was as stated per experiment.

Assays containing buffer A or B supplemented with hemimethylated oligonucleotide ODN1 or fully methylated oligonucleotide ODN2 were equilibrated in a Tecan Safire^2 (30 °C, 10 min) prior to initiation with ice-cold *Dpn*I in buffer A or B. An average background fluorescence was determined over 5 readings prior to initiation and subtracted from the fluorescence of initiated assays, monitored over 2000-4000 s.

Initial rate of fluorescence change was determined as the gradient of the first ten background subtracted data points or as the maximum differential of a moving average taken over 5 background subtracted data points. Rate of change of fluorescence was converted to initial rate of reaction using calibration plots, prepared as described in Appendix Section 9.4.1, and non-specific background changes in fluorescence were accounted for by subtracting a negative control (lacking *Dpn*I) where appropriate.

8.3.2.3 Real-time break light cytosine methyltransferase activity assay

The activity of DNMT1 was measured in triplicate (unless otherwise stated) in Greiner 384 well low volume black HiBase microplates, with a total assay volume of 20 µl, maintained at 37 °C. Assays were prepared as described below using a Biomek 3000 laboratory automation workstation and fluorescence changes were recorded in a Tecan Safire^2 or BMG POLARstar Omega microplate reader with 10 readings per well (each measurement), measurement parameters were as described previously (Section 8.2). For the Tecan Safire^2 excitation was set at 486 nm (5 nm bandwidth) and emission at 518 nm (10 nm bandwidth), and for the BMG POLARstar Omega excitation was set at 490 nm (5 nm bandwidth) and emission at 520 nm (5 nm bandwidth). Microplate reader gain was as stated per experiment.

Assays containing buffer C supplemented with AdoMet and partially methylated oligonucleotide ODN4/6/8 were equilibrated in a Tecan Safire^2 or BMG POLARstar Omega (37 °C, 10-30 min) prior to initiation with DNMT1 and *Gla*I in buffer D. An average background fluorescence was determined over 5 readings prior to initiation and subtracted from the fluorescence of initiated assays, monitored over 2000-6000 s. Initial rate of fluorescence change was determined as the gradient of background subtracted data collected between 500 and 1000 s (allowing for a slight lag phase). Rate of change of fluorescence was converted to initial rate of reaction using calibration plots, prepared as described in Appendix Section 9.4.2, and non-specific background changes in fluorescence were accounted for by subtracting a negative control (lacking AdoMet) where appropriate.

8.3.2.4 Real-time break light GlaI activity assay

The activity of *Gla*I was measured in triplicate (unless otherwise stated) in Greiner 384 well low volume black HiBase microplates, with a total assay volume of 20 µl, maintained at 37 °C. Assays were prepared as described below using a Biomek 3000 laboratory automation workstation and fluorescence changes were recorded in a Tecan Safire^2 or BMG POLARstar Omega microplate reader with 10 readings per well (each measurement), measurement parameters were as described previously (Section 8.2).

For the Tecan Safire^2 excitation was set at 486 nm (5 nm bandwidth) and emission at 518 nm (10 nm bandwidth), and for the BMG POLARstar Omega excitation was set at 490 nm (5 nm bandwidth) and emission at 520 nm (5 nm bandwidth). Microplate reader gain was as stated per experiment.

Assays containing buffer C supplemented with partially methylated oligonucleotide ODN4/6/8 or fully methylated oligonucleotide ODN5/7/9 were equilibrated in a Tecan Safire^2 or BMG POLARstar Omega (37 °C, 10-30 min) prior to initiation with *Gla*I in buffer D. An average background fluorescence was determined over 5 readings prior to initiation and subtracted from the fluorescence of initiated assays, monitored over 2000-6000 s. Initial rate of fluorescence change was determined as the gradient of background subtracted data collected between 500 and 1000 s (allowing for a slight lag phase). Rate of change of fluorescence was converted to initial rate of reaction using calibration plots, prepared as described in Appendix Section 9.4.2, and non-specific background changes in fluorescence were accounted for by subtracting a negative control (lacking *Gla*I) where appropriate.

8.3.2.5 Determination of K_M from real-time break light activity assays

Enzyme activity was determined as described in Sections 8.3.2.1, 8.3.2.2 and 8.3.2.3 for assays supplemented with substrates at a range of concentrations (one fixed, one variable). Control assays lacking AdoMet (negative) were also prepared. Plots of initial rate versus substrate concentration were fitted to **Equation 2.4B** to determine K_M.

8.3.2.6 High-throughput screening

Sets of 96 assays were prepared as described in Sections 8.3.2.1 and 8.3.2.3 in Greiner 384 well low volume black HiBase microplates, with a total assay volume of 20 µl. Assays were supplemented with library compounds dissolved in DMSO or ammonium carbonate, and control assays lacking library compound, but supplemented with DMSO or ammonium carbonate (positive) or lacking library compound and AdoMet, but supplemented with DMSO or ammonium carbonate (negative) were also prepared. The Z'-value for each assay set (80 compounds and 16 controls) was calculated using **Equation 2.2** and hits were classified as those compounds falling outside 3 standard deviations from the average of the positive control.

8.3.2.7 Determination of IC_{50} from real-time break light activity assays

Enzyme activity was determined as described in Sections 8.3.2.1, 8.3.2.2 and 8.3.2.3 for assays supplemented with inhibitor at a range of concentrations. Control assays lacking library compound, but supplemented with DMSO or ammonium carbonate (positive) or lacking library compound and AdoMet, but supplemented with DMSO or ammonium carbonate (negative) were also prepared. Fractional activity was calculated

using **Equation 2.6A** and a plot of fractional activity against inhibitor concentration was fitted to **Equation 2.6**B to determine IC_{50}.

8.3.2.8 Determination of K_i from real-time break light activity assays

Enzyme activity was determined in duplicate as described in Sections 8.3.2.1 and 8.3.2.3 for assays supplemented with inhibitor at a range of concentrations and substrates at a range of concentrations (one fixed, one variable). Control assays lacking inhibitor, but supplemented with DMSO (positive) or lacking inhibitor and AdoMet, but supplemented with DMSO (negative) were also prepared. Lineweaver-Burk plots of reciprocal rate and substrate concentration data for each inhibitor concentration were globally fitted to **Equation 2.8A** to determine K_M^{app} and V_{max}^{app}. Re-plots of y-axis intercept and gradient against inhibitor concentration were then fitted to **Equation 2.8B** and **C** to determine K_i and αK_i respectively from the negative of the x-axis intercepts.

8.3.3 Counter-screening assay methods

8.3.3.1 DpnI counter-screen

Sets of 96 assays were prepared as described in Section 8.3.2.2 in Greiner 384 well low volume black HiBase microplates, with a total assay volume of 20 µl. Assays were supplemented with library compounds dissolved in DMSO and control assays lacking library compound, but supplemented with DMSO (positive) or lacking library compound and *Dpn*I, but supplemented with DMSO (negative) were also prepared. The Z'-value for each assay set (80 compounds and 16 controls) was calculated using **Equation 2.2** and hits (non-*Dpn*I inhibitors) were classified as those compounds falling within 3 standard deviations from the average of the positive control or those compounds inhibiting *Dpn*I by less than 50% compared to the average of the positive controls.

8.3.3.2 Fluorescent intercalator displacement (FID) counter-screen

The relative percentage of fluorescent intercalator displacement was measured in triplicate (unless otherwise stated) in Greiner 384 well low volume black HiBase microplates, with a total assay volume of 20 µl, maintained at room temperature (~25 °C). Assays were prepared as described below using a Biomek 3000 laboratory automation workstation and fluorescence changes were recorded in a Tecan Safire^2 microplate reader with 10 readings per well (each measurement) and measurement parameters were as described previously (Section 8.2). Excitation was set at 504 nm (5 nm bandwidth) and emission at 527 nm (5 nm bandwidth). Microplate reader gain was as stated per experiment.

Assays containing buffer D supplemented with hemimethylated unlabelled oligonucleotide ODN3, thiazole orange and DMSO (5%) were equilibrated in a Tecan Safire^2 (~25 °C, 5 min). Library compound and DMSO (5%) were then added and assays were equilibrated in a Tecan Safire^2 (~25 °C, 30 min). An average of 10 end-point fluorescence readings were then taken and percentage fluorescence decrease was calculated relative to an average of three positive controls (lacking library compound) using **Equation 8.1**.

$$\text{Percentage fluorescence decrease} = \left(\frac{\mu_S}{\mu_{C+}}\right) \times 100$$

Equation 8.1 Percentage fluorescence decrease

Where μ_s = assay fluorescence signal and μ_{c+} = average of the positive control assay fluorescence signals.

8.3.4 Additional assay and characterisation methods

8.3.4.1 Fluorescence anisotropy assay

Fluorescence anisotropy was measured in triplicate (unless otherwise stated) in Greiner 96 well half area black microplates, with a total assay volume of 100 µl, maintained at 25-30 °C. Assays were prepared as described below using a Biomek 3000 laboratory automation workstation and fluorescence changes were recorded in a BMG POLARstar Omega microplate reader with 10 readings per well (each measurement), measurement parameters were as described previously (Section 8.2). Excitation was set at 490 nm (5 nm bandwidth) and dual emission at 520 nm (5 nm bandwidth). Microplate reader gain for emission channels A and B was as stated per experiment.

Assays containing buffer B or E supplemented with hemimethylated oligonucleotide ODN10 or fully methylated oligonucleotide ODN11 were equilibrated in a BMG POLARstar Omega (25 °C, 10 min) prior to initiation with ice-cold enzyme in buffer B or E. The parallel and perpendicular fluorescein emission of initiated assays was monitored over 2000-14000 s. Control assay containing no enzyme or DNA (background) and no enzyme (negative) were also prepared. Fluorescence anisotropy was calculated from background subtracted parallel and perpendicular fluorescence using **Equation 3.2B**.

Determination of K_D from fluorescence anisotropy assays

Assays were prepared as described above and supplemented with Tween-20 and a range of enzyme concentrations. Fluorescence anisotropy was plotted against enzyme concentration and fitted to a ligand binding calibration curve (**Equation 3.3B**) to determine the anisotropy of the bound and free labelled ligand. This data was then used to convert fluorescence anisotropy to fraction of substrate bound using **Equation 3.3A**, and fraction of substrate bound was plotted against enzyme concentration and fitted to **Equation 3.3C** to determine K_D.

Determination of competition binding constants from fluorescence anisotropy assays

Assays were prepared as described above and supplemented with Tween-20 and a range of inhibitor concentrations. Fluorescence anisotropy was converted to fraction of substrate bound using **Equation 3.3A** and the anisotropy of the bound and free labelled ligand determined from a ligand binding calibration curve (as above). A plot of fraction of substrate bound against inhibitor concentration was then fitted to **Equation 3.4** to determine K_{Dc}.

8.3.4.2 Determination of oligonucleotide melting profiles

Oligonucleotide melting profiles were measured in triplicate (unless otherwise stated) in Roche LightCycler capillaries, with a total assay volume of 20 µl, over a temperature range of 30-95 °C. Fluorescence changes at an emission wavelength of 530 nm were recorded in a Roche LightCycler with using the following program:

Step	Temperature °C	Rate of change °C s^{-1}	Step Time min
Denature	30-95	1	5
Anneal	95-30	0.017	65
Hold	30	-	10
Melt	30-95	0.017	65
Cool	95-30	1	10

Fluorescence versus time data was differentiated, with T_m calculated from the maxima of annealing data or the minima of melting data.

8.3.4.3 Gel-based Dam methylation assay

Unmethylated plasmid **pRL821** was prepared by transforming methylated **pRL821** into competent cells of the Dam⁻ *E. coli* strain ER2925 (prepared as described in Section 8.3.1.1) following the protocol described in Section 8.3.1.2. Unmethylated plasmid was then isolated from overnight cultures of ER2925 harbouring plasmid **pRL821** as described in Section 8.3.1.4.

Methylation assays were prepared by supplementing NEBuffer 3 with unmethylated plasmid **pRL821**, *E. coli* Dam, AdoMet, DMSO and library compound in a final volume of 20 µl. Control assays containing no compound (positive) and no AdoMet (negative) were also prepared in some cases. Assays were incubated in an Eppendorf Mastercycler Gradient thermal cycler (30 °C, 1 hr), the restriction enzymes *Bcl*I (15 U ul^{-1}, 1 µl) and *Xho*I (20 U ul^{-1}, 1 µl) were then added and assays incubated (37 °C, 1 hr followed by 50 °C, 1 hr). The results were analysed by 0.8% agarose gel electrophoresis with ethidium bromide staining, and quantified with the program ImageJ (*227*).

8.3.4.4 In culture gel-based plasmid methylation assay

Plasmid **pRL821** was transformed into competent *E. coli* TOP10 cells (prepared as described in Section 8.3.1.1) following the protocol described in Section 8.3.1.2. Overnight cultures of TOP10 harbouring plasmid **pRL821** were used to inoculate 2YT media (1 ml) supplemented with inhibitor and DMSO to an initial OD_{600} of 0.05. Positive control assays containing no compound were also prepared. Assays were prepared in

Greiner 12 well clear sterile suspension plates with lids and maintained in a BMG POLARstar Omega (37 ˚C, with double orbital shaking). OD_{600} was monitored and cells were harvested after 5 hours. Plasmid DNA was isolated from harvested cells as described in Section 8.3.1.4 and the plasmid methylation state was analysed as described in Section 8.3.4.3.

8.3.4.5 In culture HPLC-based genomic DNA methylation assay

Overnight cultures of *E. coli* BW25113 were used to inoculate 2YT media (1 ml) supplemented with inhibitor and DMSO to an initial OD_{600} of 0.05. Control assays containing DMSO were also prepared and inoculated with *E. coli* BW25113 (positive control) or JW3350-2 (negative inhibition control). Assays were prepared in Greiner 12 well clear sterile suspension plates with lids and maintained in a BMG POLARstar Omega (37 ˚C, with double orbital). OD_{600} was monitored and cells were harvested after 5 hours. Genomic DNA was isolated as described in Section 8.3.1.5 and dNMPs were excised by heat denaturation (90 ˚C, 10 min) followed by rapid cooling (4 ˚C, 1 min) and digestion (50 ˚C, 4 hrs) with nuclease P1 solution (3 μg μl^{-1}, 4 μl). Nuclease P1 was inactivated by heat denaturation (90 ˚C, 10 min) followed by centrifugation (5 min, 13,200 rpm) to remove debris. dNMP solution (80 μl) or dNMP standard solution (prepared by dissolving dNMP standards in water) was injected onto a Gemini 5u C18 110A column, washed with HPLC buffer A [pH 7, 5 mM DMHA, 5% MeOH] (4 min, 0.8 ml min^{-1}) and eluted with a gradient of HPLC buffer B [pH 7, 5 mM DMHA, 80% MeOH] as described for each experiment.

8.4 Experimental for Chapter 2

8.4.1 Large scale growth and purification of His-tagged DpnI

8.4.1.1 Large scale DpnI growth

Large scale growths of *E. coli* GM43 harbouring the *Dpn*I expression plasmid **pMMS/4958/59** were carried out as described in Section 8.3.1.10, with cells harvested after 4 or 3 hours.

8.4.1.2 DpnI purification

Purification of His-tagged *Dpn*I was carried out as described in Section 8.3.1.11, with the low imidazole buffer supplemented with PMSF (1 mM) and a Roche protease inhibitor tablet.

8.4.1.3 Determination of DpnI activity

The activity of purified *Dpn*I was determined using the real-time break light *Dpn*I activity assay, as described in Section 8.3.2.2. Assays were prepared by hand in 96 well plates in a total volume of 100 µl using conditions as described below:

Component/Parameter	Amount/Value
Gain setting	100
Buffer	A
Substrate(s)	300 nM ODN1 or 2 25 µM AdoMet
Enzyme(s)	0.8 (ODN1) or 0.08 (ODN2) nM *Dpn*I

8.4.2 Large scale growth and purification of His-tagged Y. pestis Dam

8.4.2.1 Large scale Y. pestis Dam growth

Large scale growths of *E. coli* ER2925 and GM2929 harbouring the *Y. pestis* Dam expression plasmid **pRJW/4958/59** were carried out as described in Section 8.3.1.10, with cells harvested once growth had reached the stationary phase (290 minutes for GM2929 cells and 320 minutes for ER2925 cells).

8.4.2.2 Y. pestis Dam purifications

Purification of His-tagged *Y. pestis* Dam was carried out as described in Section 8.3.1.11, with the low imidazole buffer supplemented with Triton-X (0.05%) for the second purification.

8.4.2.3 Determination of Y. pestis Dam activity

The activity of purified *Y. pestis* Dam was determined using the real-time break light Dam activity assay, as described in Section 8.3.2.1. Assays were prepared by hand in 96 well plates in a total volume of 100 µl using conditions as described below:

Component/Parameter	Amount/Value
Gain setting	130
Buffer	A
Substrate(s)	30 nM ODN1 25 µM AdoMet
Enzyme(s)	2 nM *Y. pestis* Dam 0.8 nM *Dpn*I

8.4.3 Optimisation of the real-time break light Dam activity assay

8.4.3.1 Buffer conditions

Dam and *Dpn*I activity assays were prepared by hand in 96 well plates in a total volume of 100 µl, as described in Sections 8.3.2.1 and 8.3.2.2, with the components of assay buffer B varied to determine the optimal buffer conditions. Assay conditions were as described below for each assay format:

*Dpn*I activity assay

Component/Parameter	Amount/Value
Gain setting	130
Buffer	B
Varied buffer components	NaCl (0-150 mM) $MgCl_2$ (0-30 mM)
Substrate(s)	30 nM ODN1 or 2 25 µM AdoMet
Enzyme(s)	0.8 nM *Dpn*I

Dam activity assay

Component/Parameter	Amount/Value
Gain setting	130
Buffer	B
Varied buffer components	NaCl (0-150 mM) $MgCl_2$ (0-30 mM)
Substrate(s)	30 nM ODN1 25 µM AdoMet
Enzyme(s)	2 nM *Y. pestis* Dam 0.8 nM *Dpn*I

8.4.3.2 Assay temperature

Dam activity assays were prepared by hand in 96 well plates in a total volume of 100 µl, as described in Section 8.3.2.1 with enzyme and assay solutions incubated at 28, 30, 32, 34, 38 and 40 °C prior to initiation and during the assay. Conditions were as described below:

Component/Parameter	Amount/Value
Gain setting	130
Buffer	A
Substrate(s)	10 nM ODN1 25 µM AdoMet
Enzyme(s)	1 nM *Y. pestis* Dam 0.8 nM *Dpn*I

8.4.3.3 Enzyme concentration

Dam activity assays were prepared in 384 well plates in a total volume of 20 µl, as described in Section 8.3.2.1. With *Dpn*I concentration varied to determine the optimal amount of coupled enzyme, and *Y. pestis* Dam concentration varied to determine the linear range of the assay. Assay conditions were as described below:

Component/Parameter	Amount/Value
Gain setting	170
Buffer	B
Substrate(s)	10 nM ODN1 25 µM AdoMet
Enzyme(s)	1 or 0-4 nM *Y. pestis* Dam 0-4 or 2 nM *Dpn*I

8.4.3.4 Enzyme stability

Y. pestis Dam was incubated with oligonucleotide ODN1, AdoMet or no substrates in an Eppendorf Mastercycler Gradient thermal cycler (30 °C, 0-1600 s), the remaining assay components were then added and *Y. pestis* Dam activity determined as described in Section 8.3.2.1. Assays were prepared in 384 well plates in a total volume of 20 µl using conditions as described below:

Component/Parameter	Amount/Value
Gain setting	170
Buffer	B
DMSO	5%
Substrate(s)	10 nM ODN1
	25 µM AdoMet
Enzyme(s)	1 nM *Y. pestis* Dam
	2 nM *Dpn*I

8.4.3.5 Effect of compound library solvent

Dam activity assays were prepared in 384 well plates in a total volume of 20 µl, as described in Section 8.3.2.1 and supplemented with 0-10% DMSO. Assay conditions were as described below:

Component/Parameter	Amount/Value
Gain setting	170
Buffer	B
DMSO	0-10%
Substrate(s)	10 nM ODN1
	25 µM AdoMet
Enzyme(s)	1 nM *Y. pestis* Dam
	2 nM *Dpn*I

8.4.3.6 Assay volume

Dam activity assays were prepared in 96 or 384 well plates in a total volume of 20 or 100 µl, as described in Section 8.3.2.1. A total of 36-48 positive and 36-48 negative control assays were prepared for each experiment and used to calculate Z'-values (**Equation 2.2**). Assay conditions were as described below:

Component/Parameter	Amount/Value
Gain setting	120 (96 well) or 170 (384 well)
Buffer	B
DMSO	5%
Substrate(s)	10 nM ODN1 25 µM AdoMet
Enzyme(s)	1 nM *Y. pestis* Dam 2 nM *Dpn*I

8.4.3.7 Substrate concentrations

Experiments to determine *Y. pestis* Dam K_M^{AdoMet} and K_M^{DNA}, and *Dpn*I K_M^{DNA} were prepared in 384 well plates in a total volume of 20 µl as described in Section 8.3.2.5. Assay conditions were as described below for each experiment:

Y. pestis Dam K_M^{AdoMet}

Component/Parameter	Amount/Value
Gain setting	170
Buffer	B
DMSO	5%
Substrate(s)	10 nM ODN1 0-200 µM AdoMet
Enzyme(s)	1 nM *Y. pestis* Dam 2 nM *Dpn*I

Y. pestis Dam K_M^{DNA}

Component/Parameter	Amount/Value
Gain setting	170
Buffer	B
DMSO	5%
Substrate(s)	3-30.5 nM ODN1 25, 50 or 100 µM AdoMet
Enzyme(s)	0.3 nM *Y. pestis* Dam 2 nM *Dpn*I

*Dpn*I K_M^{DNA}

Component/Parameter	Amount/Value
Gain setting	170
Buffer	B
DMSO	5%
Substrate(s)	0-1000 nM ODN1 or 0-250 nM ODN2
Enzyme(s)	2 nM (ODN1) or 12.5 pM (ODN2) *Dpn*I

Substrate concentrations for HTS

Dam activity assays were prepared in 96 well plates in a total volume of 100 µl, as described in Section 8.3.2.1. A total of 8 positive and 8 negative control assays were prepared at a range of DNA and AdoMet concentrations and used to calculate Z'-values (**Equation 2.2**). Assay conditions were as described below:

Component/Parameter	Amount/Value
Gain setting	130
Buffer	B
Substrate(s)	3-34 nM ODN1 12.5 or 25 µM AdoMet
Enzyme(s)	1 nM *Y. pestis* Dam 2 nM *Dpn*I

8.4.3.8 Y. pestis Dam IC_{50}^{AdoHcy}

Assays were prepared in 384 well plates in a total volume of 20 µl as described in Section 8.3.2.7. Assay conditions were as described below:

Component/Parameter	Amount/Value
Gain setting	190
Buffer	B
DMSO	5%
Inhibitor	0-1000 µM AdoHcy
Substrate(s)	3.5 nM ODN1 16 µM AdoMet
Enzyme(s)	0.3 nM *Y. pestis* Dam 2 nM *Dpn*I

8.5 Experimental for Chapter 3

8.5.1 Optimisation of the real-time break light DpnI activity assay

8.5.1.1 Enzyme concentration

*Dpn*I activity assays were prepared in 384 well plates in a total volume of 20 µl, as described in Section 8.3.2.2. With *Dpn*I concentration varied to determine the linear range of the assay. Assay conditions were as described below:

Component/Parameter	Amount/Value
Gain setting	170
Buffer	B
DMSO	5%
Substrate(s)	10 nM ODN2
Enzyme(s)	0-100 pM *Dpn*I

8.5.2 Optimisation of the gel-based Dam methylation assay

8.5.2.1 Enzymes

Stability

E. coli Dam stability was determined as described in Section 8.4.3.4. Assays were prepared in 384 well plates in a total volume of 20 µl using conditions as described below:

Component/Parameter	Amount/Value
Gain setting	170
Buffer	B
DMSO	5%
Substrate(s)	25 nM ODN1 12 µM AdoMet
Enzyme(s)	1 nM *E. coli* Dam 10 nM *Dpn*I

Concentration

Gel-based Dam methylation assays were prepared in a total assay volume of 20 µl as described in Section 8.3.4.3, with assay conditions as described below:

Component/Parameter	Amount/Value
DMSO	5%
Substrate(s)	6 nM unmethylated **pRL821** 60 µM AdoMet
Enzyme(s)	62.5-250 nM *E. coli* Dam

8.5.2.2 Substrate concentration

Gel-based Dam methylation assays were prepared in a total assay volume of 20 µl as described in Section 8.3.4.3, with assay conditions as described below:

Component/Parameter	Amount/Value
DMSO	5%
Substrate(s)	3 nM unmethylated **pRL821** 0-60 µM AdoMet
Enzyme(s)	250 nM *E. coli* Dam

8.5.2.3 Inhibition with AdoHcy

Gel-based Dam methylation assays were prepared in a total assay volume of 20 µl as described in Section 8.3.4.3, with assay conditions as described below:

Component/Parameter	Amount/Value
DMSO	5%
Inhibitor	0-5 mM AdoHcy
Substrate(s)	3 nM unmethylated **pRL821** 0, 6, 24 or 60 µM AdoMet
Enzyme(s)	250 nM *E. coli* Dam

8.5.3 Optimisation of the real-time break light cytosine methyltransferase activity assay

8.5.3.1 Buffer conditions

DNMT1 activity assays were prepared in 384 well plates in a total volume of 20 µl, as described in Sections 8.3.2.3 and 8.3.2.4, with sodium chloride concentration varied to determine the optimal buffer conditions. Assay conditions were as described below:

Component/Parameter	Amount/Value
Microplate reader	Tecan Safire^2
Gain setting	100
Varied buffer component	NaCl (0-200 mM)
Substrate(s)	250 nM ODN8 20 µM AdoMet
Enzyme(s)	25 nM DNMT1 0.0125 U µl^{-1} *Gla*I

8.5.3.2 Oligonucleotide substrate

GlaI activity I

*Gla*I activity assays were prepared in 384 well plates in a total volume of 20 µl, as described in Section 8.3.2.4, with assay conditions as described below:

Component/Parameter	Amount/Value
Microplate reader	Tecan Safire^2
Gain setting	100
Substrate(s)	250 nM ODN5 or ODN7 20 µM AdoMet
Enzyme(s)	0.05 U µl^{-1} *Gla*I

Melting profiles

Assays were prepared in assay buffer C and supplemented with partially methylated oligonucleotide ODN6 (250 nM), melting profiles were then determined as described in Section 8.3.4.2.

DNMT1 activity

DNMT1 activity assays were prepared in 384 well plates in a total volume of 20 µl, as described in Section 8.3.2.3, with assay conditions as described below:

Component/Parameter	Amount/Value
Microplate reader	Tecan Safire^2
Gain setting	110
Substrate(s)	250 nM ODN6 or ODN8 20 µM AdoMet
Enzyme(s)	25 nM DNMT1 0.0125 U µl^{-1} *Gla*I

GlaI activity II

*Gla*I activity assays were prepared in 384 well plates in a total volume of 20 µl, as described in Section 8.3.2.4, with assay conditions as described below:

Component/Parameter	Amount/Value
Microplate reader	Tecan Safire^2
Gain setting	110
Substrate(s)	250 nM ODN6, ODN7, ODN8 or ODN9 20 µM AdoMet
Enzyme(s)	0.05 U µl^{-1} *Gla*I

8.5.3.3 Plate reader

DNMT1 activity assays were prepared in 384 well plates in a total volume of 20 µl, as described in Section 8.3.2.3. Fluorescence measurements were recorded in a Tecan Safire^2 at a gain setting of 110 or a BMG POLARstar Omega at a gain setting of 1550, with assay conditions as described below:

Component/Parameter	Amount/Value
Substrate(s)	250 nM ODN6 20 µM AdoMet
Enzyme(s)	25 nM DNMT1 0.05 U µl^{-1} *Gla*I

8.5.3.4 Enzyme concentration

DNMT1 activity assays were prepared in 384 well plates in a total volume of 20 µl, as described in Section 8.3.2.3, and fluorescence measurements were recorded in a BMG POLARstar Omega. *Gla*I concentration was varied to determine the optimal amount of coupled enzyme, and DNMT1 concentration was varied to determine the linear range of the assay. Assay conditions were as described below:

Component/Parameter	Amount/Value
Gain setting	1550
Substrate(s)	250 nM ODN6
	20 µM AdoMet
Enzyme(s)	25 or 0-200 nM DNMT1
	0-0.2 or 0.05 U μl^{-1} *Gla*I

8.5.3.5 DNMT1 K_M^{AdoMet}

DNMT1 activity assays were prepared in 384 well plates in a total volume of 20 µl, as described in Section 8.3.2.3, and fluorescence measurements were recorded in a BMG POLARstar Omega. Assay conditions were as described below:

Component/Parameter	Amount/Value
Gain setting	1550
Substrate(s)	250 nM ODN6
	0-20 µM AdoMet
Enzyme(s)	25 nM DNMT1
	0.05 U μl^{-1} *Gla*I

8.5.3.6 DNMT1 IC_{50}^{AdoMet}

DNMT1 activity assays were prepared in 384 well plates in a total volume of 20 µl, as described in Section 8.3.2.3, fluorescence measurements were recorded in a BMG POLARstar Omega. Assay conditions were as described below:

Component/Parameter	Amount/Value
Gain setting	1250
DMSO	5%
Inhibitor	0-2 mM AdoHcy
Substrate(s)	250 nM ODN6 0-20 µM AdoMet
Enzyme(s)	25 nM DNMT1 0.05 U μl^{-1} *Gla*I

8.5.4 Optimisation of the fluorescence anisotropy assay

8.5.4.1 Non-specific binding

Buffer

Assays were prepared in 96 or 384 well plates in a total volume of 100 or 20 µl, as described in Section 8.3.4.1. Assay conditions were as described below:

Component/Parameter	Amount/Value
Gain settings (A/B)	1450/1445 (96 well) or 1519/1518 (384 well)
Buffer	Water or B
Substrate(s)	0-200 nM ODN10
Enzyme(s)	none

Detergent

Assays were prepared in 96 well plates in a total volume of 100, as described in Section 8.3.4.1. Assay conditions were as described below:

Component/Parameter	Amount/Value
Gain settings (A/B)	1450/1445
Buffer	B
Detergent	0 or 0.1% Tween-20
Substrate(s)	0-200 nM ODN10
Enzyme(s)	none

8.5.4.2 Enzyme stability

Assays were prepared in 96 well plates in a total volume of 100, as described in Section 8.3.4.1. Assay conditions were as described below:

Component/Parameter	Amount/Value
Gain settings (A/B)	1450/1445
Temperature	30 ˚C
Buffer	B supplemented with 0.1% Tween-20
Substrate(s)	50 nM ODN10
Enzyme(s)	500 nM *Y. pestis*, *E. coli* or *P. horikoshii* Dam

8.5.4.3 E. coli Dam K_D^{DNA}

Assays were prepared in 96 well plates in a total volume of 100 µl, as described in Section 8.3.4.1. Assay conditions were as described below:

Component/Parameter	Amount/Value
Gain settings (A/B)	1450/1445
Buffer	B supplemented with 0.1% Tween-20
Substrate(s)	20 nM ODN10 0 or 200 µM AdoHcy
Enzyme(s)	0-1000 nM *E. coli* Dam

8.5.4.4 DpnI K_D^{DNA}

Assays were prepared in 96 well plates in a total volume of 100 µl, as described in Section 8.3.4.1. Assay conditions were as described below:

Component/Parameter	Amount/Value
Gain settings (A/B)	2120/2145
Buffer	E supplemented with 0.1% Tween-20
Substrate(s)	20 nM ODN10 or ODN11
Enzyme(s)	0-1000 nM *Dpn*I

8.5.4.5 DpnI hemimethylated DNA competition binding constant

Assays were prepared in 96 well plates in a total volume of 100 µl, as described in Section 8.3.4.1. Assay conditions were as described below:

Component/Parameter	Amount/Value
Gain settings (A/B)	2120/2145
Buffer	E supplemented with 0.1% Tween-20
DMSO	5%
Inhibitor	0-1000 ODN12
Substrate(s)	20 nM ODN11
Enzyme(s)	500 nM *Dpn*I

8.5.5 Optimisation of the in culture gel-based plasmid methylation assay

8.5.5.1 Assay volume

Cultures of ER2925 harbouring **pRL821** were prepared in 1, 2, 3 and 4 ml of 2YT media as described in Section 8.3.4.4 and supplemented with DMSO (5%). Plasmid DNA was isolated after 15 hrs and digested with *Bcl*I (7.5 U μl^{-1}, 1 hr, 50 °C) the results were analysed by 0.8% agarose gel electrophoresis and concentration determined by quantification of bands with the program ImageJ (*227*).

8.5.5.2 Assay end-point

Cultures of ER2925 harbouring **pRL821** supplemented with DMSO (5%) were prepared as described in Section 8.3.4.4.

8.5.5.3 Growth curve analysis

2YT media (1 ml) was inoculated with *E. coli* BW25113 and JW3350-2 from overnight cultures to a start OD_{600} of 0.05. Assays were prepared in Greiner 12 well clear sterile suspension plates with lids, maintained in a BMG POLARstar OMEGA (37 °C, with double orbital shaking), and OD_{600} was monitored.

8.5.6 Optimisation of the in culture HPLC-based genomic DNA methylation assay

8.5.6.1 Genomic DNA isolation

Genomic DNA was isolated from overnight cultures of *E. coli* BW25113 and JW3350-2 as described in Section 8.3.1.5 with the RNase digestion step as per manufacturer's instructions (RNase A, 4 U μl^{-1}, 1.5 µl) or as described in Section 8.3.1.5 (RNase A/T1 solution, 0.5 µg μl^{-1} /50 U μl^{-1}, 20 µl).

8.5.6.2 HPLC buffer gradient

Genomic DNA (Section 8.5.6.1) was then digested and analysed as described in Section 8.3.4.5, with an HPLC gradient of 10-50% HPLC buffer B over 26 min or 5-50% HPLC buffer B over 38 min.

8.5.6.3 Detection limits

A serial dilution of dmAMP was prepared in water and analysed by HPLC as described in Section 8.3.4.5, with an HPLC gradient of 5-50% HPLC buffer B over 38 min. HPLC peak areas were integrated to determine area and plotted against dAMP concentration to determine the upper and lower assay detection limits.

8.6 Experimental for Chapter 4

8.6.1 High-throughput screen of the DTP library

8.6.1.1 Dam screen

The DTP library was diluted in DMSO (100%) to a concentration of 500 μM and screened against *Y. pestis* Dam as described in Section 8.3.2.6 using the assay conditions listed below:

Component/Parameter	Amount/Value
Gain setting	170
Temperature	30 ˚C
Buffer	B
DMSO	5%
Library compound concentration	25 μM
Substrate(s)	10 nM ODN1 25 μM AdoMet
Enzyme(s)	1 nM *Y. pestis* Dam 2 nM *Dpn*I

8.6.1.2 Counter-screening

DpnI

Hits from the DTP library screen were screened against *Dpn*I as described in Section 8.3.3.1 using the assay conditions listed below:

Component/Parameter	Amount/Value
Gain setting	170
Temperature	30 ˚C
Buffer	B
DMSO	5%
Library compound concentration	25 μM
Substrate(s)	10 nM ODN2
Enzyme(s)	12.5 pM *Dpn*I

FID

Compounds inhibiting *Dpn*I by less than three standard deviations from the average of the positive controls were screened for DNA intercalation activity as described in Section 8.3.3.2 using the assay conditions listed below:

Component/Parameter	Amount/Value
Gain setting	255
Temperature	25 ˚C
Buffer	D
DMSO	10%
Thiazole orange concentration	500 nM
Library compound concentration	5 µM
Substrate(s)	100 nM ODN3

8.6.1.3 Extended FID assays

Assays were prepared as described in Section 8.3.3.2 using the assay conditions listed below:

Component/Parameter	Amount/Value
Gain setting	255
Temperature	25 ˚C
Buffer	D
DMSO	10%
Thiazole orange concentration	2.5 µM
Library compound concentration	0-1000 µM
Substrate(s)	500 nM ODN3

8.6.1.4 Purity analysis

TLC analysis of compound **88915** was achieved with using following solvent systems: 100% hexane; 75% hexane, 25% ethylacetate; 50% hexane, 50% ethylacetate; 50% ethylacetate, 50% methanol; 100% methanol; and 70% DCM, 30% methanol.

8.6.1.5 Potency

Y. pestis Dam and *Dpn*I IC_{50} were determined in duplicate from assays prepared in 384 well plates in a total volume of 20 µl as described in Section 8.3.2.7. Assays were carried out in duplicate using conditions as described below for each enzyme:

Y. pestis Dam

Component/Parameter	Amount/Value
Gain setting	190
Temperature	30 ˚C
Buffer	B
DMSO	5%
University of Cincinnati library hit	0-2000 µM
Substrate(s)	3.5 nM ODN1 16 µM AdoMet
Enzyme(s)	0.3 nM *Y. pestis* Dam 2 nM *Dpn*I

*Dpn*I

Component/Parameter	Amount/Value
Gain setting	190
Temperature	30 ˚C
Buffer	B
DMSO	5%
University of Cincinnati library hit	0-2000 µM
Substrate(s)	14 nM ODN2
Enzyme(s)	12.5 pM *Dpn*I

8.6.2 High-throughput screen of the University of Cincinnati library

8.6.2.1 Dam screen

The University of Cincinnati library was diluted in DMSO (100%) to a concentration of 1 mM and screened against *Y. pestis* Dam as described in Section 8.3.2.6 using the assay conditions listed below:

Component/Parameter	Amount/Value
Gain setting	170
Temperature	30 ˚C
Buffer	B
DMSO	5%
Library compound concentration	50 µM
Substrate(s)	8 nM ODN1 20 µM AdoMet
Enzyme(s)	1 nM *Y. pestis* Dam 2 nM *Dpn*I

8.6.2.2 Counter-screening

DpnI

Hits from the University of Cincinnati library screen were screened against *Dpn*I as described in Section 8.3.3.1 using the assay conditions listed below:

Component/Parameter	Amount/Value
Gain setting	170
Temperature	30 ˚C
Buffer	B
DMSO	5%
Library compound concentration	50 µM
Substrate(s)	8 nM ODN2
Enzyme(s)	25 pM *Dpn*I

FID

Compounds inhibiting *Dpn*I by less than 50% compared to the average of the positive controls were screened for DNA intercalation activity as described in Section 8.3.3.2 using the assay conditions listed below:

Component/Parameter	Amount/Value
Gain setting	255
Temperature	25 ˚C
Buffer	D
DMSO	10%
Thiazole orange concentration	500 nM
Library compound concentration	5 µM
Substrate(s)	100 nM ODN3

8.6.2.3 Hit validation

Gel-based Dam methylation assays were prepared in a total assay volume of 20 µl as described in Section 8.3.4.3, with assay conditions as described below:

Component/Parameter	Amount/Value
DMSO	5%
University of Cincinnati library hits	2 mM
Substrate(s)	3 nM unmethylated **pRL821** 6 µM AdoMet
Enzyme(s)	250 nM *E. coli* Dam

8.6.2.4 Potency

Y. pestis Dam and *Dpn*I IC_{50} were determined in duplicate from assays prepared in 384 well plates in a total volume of 20 µl as described in Section 8.3.2.7. Assays were carried out in duplicate using conditions as described below for each enzyme:

Y. pestis Dam

Component/Parameter	Amount/Value
Gain setting	190
Temperature	30 ˚C
Buffer	B
DMSO	5%
University of Cincinnati library hit	0-2000 µM
Substrate(s)	3.5 nM ODN1 16 µM AdoMet
Enzyme(s)	0.3 nM *Y. pestis* Dam 2 nM *Dpn*I

*Dpn*I

Component/Parameter	Amount/Value
Gain setting	190
Temperature	30 ˚C
Buffer	B
DMSO	5%
University of Cincinnati library hit	0-2000 µM
Substrate(s)	14 nM ODN2
Enzyme(s)	12.5 pM *Dpn*I

8.6.2.5 In culture activity

Restriction digest analysis of genomic DNA from Yersinia culture

Experiments were carried out at dstl Porton Down under containment level 2. Overnight cultures of *Y. pseudotuberculosis* were used to inoculate LB broth (10 ml) supplemented with University of Cincinnati library hit (20 µg ml^{-1}) and DMSO (0.025%). Cultures were incubated with shaking (28 ˚C, overnight) and genomic DNA was isolated as described in Section 8.3.1.5 as per the manufacturer's instructions only. Isolated genomic DNA was then analysed by restriction with *Mbo*I, *Sau*3AI or *Dpn*I (4 hrs, 37 ˚C) and results were analysed by 0.7% agarose gel electrophoresis with ethidium bromide staining.

In culture gel-based plasmid methylation assay

Assays supplemented with University of Cincinnati library hit (500 μM) were prepared and analysed as described in Section 8.3.4.4.

In culture HPLC-based genomic DNA methylation assay

Assays supplemented with University of Cincinnati library hit (500 μM) were prepared and analysed as described in Section 8.3.4.5, using an HPLC gradient of 5-50% HPLC buffer B over 38 min.

8.7 Experimental for Chapter 5

8.7.1 Sublibrary screening

8.7.1.1 Stibonic acid sublibrary

The stibonic acid sublibrary was diluted in DMSO (100%) to a concentration of 500 µM and screened against *Y. pestis* Dam as described in Section 8.3.2.6 using the assay conditions listed below:

Component/Parameter	Amount/Value
Gain setting	170
Temperature	30 °C
Buffer	B
DMSO	5%
Sublibrary compound concentration	25 µM
Substrate(s)	10 nM ODN1 25 µM AdoMet
Enzyme(s)	1 nM *Y. pestis* Dam 2 nM *Dpn*I

8.7.1.2 Phosphonic acid sublibrary

The phosphonic acid sublibrary was diluted in ammonium carbonate (25 mM) to a concentration of 500 µM and screened against *Y. pestis* Dam as described in Section 8.3.2.6 using the assay conditions listed below:

Component/Parameter	Amount/Value
Gain setting	170
Temperature	30 °C
Buffer	B
Ammonium carbonate	1.25 mM
Sublibrary compound concentration	25 µM
Substrate(s)	10 nM ODN1 25 µM AdoMet
Enzyme(s)	1 nM *Y. pestis* Dam 2 nM *Dpn*I

8.7.2 Potency

Y. pestis Dam IC_{50} determination assays were prepared in 384 well plates in a total volume of 20 µl as described in Section 8.3.2.7, using conditions as described below:

Component/Parameter	Amount/Value
Gain setting	190
Temperature	30 ˚C
Buffer	B
DMSO	5%
Arylstibonic acid	0-100 µM
Substrate(s)	3.5 nM ODN1 16 µM AdoMet
Enzyme(s)	0.3 nM *Y. pestis* Dam 2 nM *Dpn*I

8.7.3 Selectivity

8.7.3.1 Against DpnI

*Dpn*I IC_{50} determination assays were prepared in 384 well plates in a total volume of 20 µl as described in Section 8.3.2.7, using conditions as described below:

Component/Parameter	Amount/Value
Gain setting	190
Temperature	30 ˚C
Buffer	B
DMSO	5%
Arylstibonic acid	0-100 µM
Substrate(s)	14 nM ODN2
Enzyme(s)	12.5 pM *Dpn*I

8.7.3.2 Against DNMT1

The diluted stibonic acid sublibrary (500 µM in 100% DMSO) was screened against DNMT1 as described in Section 8.3.2.6 using the assay conditions listed below:

Component/Parameter	Amount/Value
Gain setting	1250
Temperature	37 ˚C
Buffer	B
DMSO	5%
Sublibrary compound concentration	25 µM
Substrate(s)	250 nM ODN6
	3 µM AdoMet
Enzyme(s)	25 nM DNMT1
	0.05 U μl^{-1} *Gla*I

8.7.4 Mode of inhibition Characterisation

8.7.4.1 Determination of K_i^{13776} and K_i^{13746}

Assays were prepared in 384 well plates in a total volume of 20 µl as described in Section 8.3.2.8. Assay conditions were as described below for each substrate:

Variable AdoMet

Component/Parameter	Amount/Value
Gain setting	190
Buffer	B
DMSO	5%
Inhibitor	0-12 µM **13776** or 0-96 nM **13746**
Substrate(s)	10 nM ODN1 5.4-70 µM AdoMet
Enzyme(s)	1 nM *Y. pestis* Dam 2 nM *Dpn*I

Variable DNA

Component/Parameter	Amount/Value
Gain setting	190
Buffer	B
DMSO	5%
Inhibitor	0-12 µM **13776** or 0-96 nM **13746**
Substrate(s)	3.1-12 nM ODN1 160 µM AdoMet
Enzyme(s)	0.3 nM *Y. pestis* Dam 2 nM *Dpn*I

8.7.4.2 Determination of Competition binding constants

Assays were prepared in 96 well plates in a total volume of 100 µl, as described in Section 8.3.4.1. Assay conditions were as described below:

Component/Parameter	Amount/Value
Gain settings (A/B)	2315/2366
Buffer	E supplemented with 0.1% Tween-20
DMSO	5%
Inhibitor	0-1000 µM **13776** or **13746**
Substrate(s)	20 nM ODN10
Enzyme(s)	500 nM *E. coli* Dam

8.7.4.3 Oligonucleotide melting profiles

Assays were prepared in assay buffer B and supplemented with hemimethylated oligonucleotide ODN1 (100 nM), DMSO (5%) and **13776** or **13746** (0, 1, 10 or 25 µM). Melting profiles were then determined as described in Section 8.3.4.2.

8.7.4.4 Aggregation

Y. pestis Dam IC_{50} determination assays were prepared as described in Section 8.7.2 and supplemented with Tween-20 (0.1%).

8.7.5 In culture activity

8.7.5.1 Restriction digest analysis of genomic DNA from Yersinia culture

Assays were prepared and analysed as described in Section 8.7.5.1 and supplemented with arylstibonic acid (20 μg ml^{-1})

8.7.5.2 Toxicity of compound 13782 against Y. pestis GB

Experiments were carried out at dstl Porton Down under containment level 3. Overnight cultures of *Y. pestis* GB were used to inoculate BAB media (10 ml) supplemented with $CaCl_2$ (2.5 mM), **13782** (20 μg ml^{-1}) and DMSO (0.025%). Cultures were incubated with shaking (37 °C) and samples removed periodically for assessment of OD_{600} for the construction of growth curves.

8.7.5.3 Determination of the activity of re-synthesised 13782

IC_{50}^{13782}

Y. pestis Dam IC_{50} determination assays were prepared as described in Section 8.7.2 and supplemented with re-synthesised **13782**.

HPLC analysis

Compound **13782** (~1 mg) was dissolved in sodium carbonate solution (1%, 50 μl) and injected onto a Hamilton pRP-X100 anion exchange column, washed with water and eluted with a gradient of HPLC buffer C [pH 9, 0.1 M ammonium acetate] (0-100%, 20 min) and washed with HPLC buffer C (40 min). Collected fractions (60 x 2 ml) were freeze-dried and resuspended in water (20 μl). *Y. pestis* Dam activity was then determined as described in Section 8.3.2.1, with assays prepared in 384 well plates and supplemented with freeze-dried/resuspended HPLC fraction. Assay conditions were as described below:

Component/Parameter	Amount/Value
Gain setting	170
Buffer	B
DMSO	5%
Freeze-dried/resuspended HPLC fraction	5 μl
Substrate(s)	10 nM ODN1 25 μM AdoMet
Enzyme(s)	1 nM *Y. pestis* Dam 2 nM *Dpn*I

8.8 Experimental for Chapter 6

8.8.1 Validation

8.8.1.1 Potency

Y. pestis Dam IC_{50} determination assays were prepared in 384 well plates in a total volume of 20 µl as described in Section 8.3.2.7, using conditions as described below:

Component/Parameter	Amount/Value
Gain setting	190
Temperature	30 ˚C
Buffer	B
DMSO	5%
Bisubstrate analogue	0-2000 µM
Substrate(s)	3.5 nM ODN1 16 µM AdoMet
Enzyme(s)	0.3 nM *Y. pestis* Dam 2 nM *Dpn*I

8.8.1.2 Confirmation of activity

Gel-based Dam methylation assays were prepared in a total assay volume of 20 µl as described in Section 8.3.4.3, with assay conditions as described below:

Component/Parameter	Amount/Value
DMSO	5%
Bisubstrate analogue	2 mM
Substrate(s)	3 nM unmethylated **pRL821** 6 µM AdoMet
Enzyme(s)	250 nM *E. coli* Dam

8.8.2 Selectivity

8.8.2.1 Against DpnI

*Dpn*I IC_{50} determination assays were prepared in 384 well plates in a total volume of 20 µl as described in Section 8.3.2.7, using conditions as described below:

Component/Parameter	Amount/Value
Gain setting	190
Temperature	30 ˚C
Buffer	B
DMSO	5%
Bisubstrate analogue	0-2000 µM
Substrate(s)	14 nM ODN2
Enzyme(s)	12.5 pM *Dpn*I

8.8.2.2 Against DNMT1

DNMT1 IC_{50} determination assays were prepared in 384 well plates in a total volume of 20 µl as described in Section 8.3.2.7, using conditions as described below:

Component/Parameter	Amount/Value
Gain setting	1250
Temperature	37 ˚C
Buffer	C
DMSO	5%
Bisubstrate analogue	0-2000 µM
Substrate(s)	250 nM ODN6
	3 µM AdoMet
Enzyme(s)	25 nM DNMT1
	0.05 U $µl^{-1}$ *Gla*I

8.8.3 Mode of inhibition

8.8.3.1 Determination of K_i^{SA8}

Assays were prepared in 384 well plates in a total volume of 20 µl as described in Section 8.3.2.8. Assay conditions were as described below for each substrate:

Variable AdoMet

Component/Parameter	Amount/Value
Gain setting	190
Buffer	B
DMSO	5%
Inhibitor	0-54 µM **SA8**
Substrate(s)	10 nM ODN1 5.4-70 µM AdoMet
Enzyme(s)	1 nM *Y. pestis* Dam 2 nM *Dpn*I

Variable DNA

Component/Parameter	Amount/Value
Gain setting	190
Buffer	B
DMSO	5%
Inhibitor	0-54 µM **SA8**
Substrate(s)	3.1-12 nM ODN1 160 µM AdoMet
Enzyme(s)	0.3 nM *Y. pestis* Dam 2 nM *Dpn*I

8.8.3.2 Determination of Competition binding constants

Assays were prepared in 96 well plates in a total volume of 100 µl, as described in Section 8.3.4.1. Assay conditions were as described below:

Component/Parameter	Amount/Value
Gain settings (A/B)	2315/2366
Buffer	E supplemented with 0.1% Tween-20
DMSO	5%
Inhibitor	0-2000 µM **SA8** or **SA2**
Substrate(s)	20 nM ODN10
Enzyme(s)	500 nM *E. coli* Dam

8.8.3.3 Stabilisation of the Dam:DNA complex

Assays were prepared in 96 well plates in a total volume of 100, as described in Section 8.3.4.1. Assay conditions were as described below:

Component/Parameter	Amount/Value
Gain settings (A/B)	2478/2624
Temperature	30 ˚C
Buffer	B supplemented with 0.1% Tween-20
DMSO	5%
Inhibitor	2 mM **SA8** or **SA2**
Substrate(s)	50 nM ODN10
Enzyme(s)	500 nM *E. coli* Dam

8.9 Media and buffers

8.9.1 Competent cell buffers

TBFI (pH 5.8)

Reagent	Final Concentration	Quantity
Potassium acetate	30 mM	0.588 g
Rubidium Chloride	100 mM	2.42 g
Calcium Chloride	10 mM	0.294 g
Manganese Chloride	50 mM	2.0 g
Glycerol	15% (v/v)	30 ml
Sterile Water		To a final volume of 200 ml

TBFII (pH 6.5)

Reagent	Final Concentration	Quantity
MOPS	10 mM	0.21 g
Rubidium Chloride	10 mM	0.121 g
Calcium Chloride	75 mM	1.1 g
Glycerol	15% (v/v)	15 ml
Sterile Water		To a final volume of 100 ml

8.9.2 SDS-PAGE buffers, stains and destains

1x SDS-PAGE loading buffer

Reagent	Final Concentration	Quantity
Tris.HCl (pH 6.8, 0.2 M)	50 mM	2.5 ml
DTT	0.1 mM	15.4 mg
SDS	2% (w/v)	200 mg
Bromophenol Blue	0.1% (w/v)	10 mg
Glycerol	10% (v/v)	1 ml
Deionised Water		To a final volume of 10 ml

1x Tris-Glycine electrophoresis buffer

Reagent	Final Concentration	Quantity
Tris Base	25 mM	3.02 g
Glycine	250 mM	18.8 g
SDS	0.1% (w/v)	1 g
Deionised Water		To a final volume of 1 L

SDS-PAGE gel stain

Reagent	Final Concentration	Quantity
Coomassie Brilliant Blue		0.25 g
Methanol	45% (v/v)	45 ml
Glacial Acetic Acid	10% (v/v)	10 ml
Deionised Water		To a final volume of 10 ml

SDS-PAGE gel destain

Reagent	Final Concentration	Quantity
Methanol	5% (v/v)	50 ml
Glacial Acetic Acid	7.5% (v/v)	75 ml
Deionised Water		To a final volume of 1 L

8.9.3 Purification buffers

8.9.3.1 DpnI purification buffers

Low imidazole *Dpn*I purification buffer (pH 7.4)

Reagent	Final Concentration	Quantity
Tris	50 mM	Acid: 6.61 g Base: 0.97 g
Sodium chloride	400 mM	23.4 g
Imidazole	50 mM	3.40 g
β-mercaptoethanol	5 mM	350 µl
Glycerol	10% (w/v)	100 g
Deionised Water		To a final volume of 1 L

High imidazole *Dpn*I purification buffer (pH 7.4)

Reagent	Final Concentration	Quantity
Tris	50 mM	Acid: 6.61 g Base: 0.97 g
Sodium chloride	400 mM	23.4 g
Imidazole	500 mM	34.0 g
β-mercaptoethanol	5 mM	350 µl
Glycerol	10% (w/v)	100 g
Deionised Water		To a final volume of 1 L

*Dpn*I storage buffer (pH 7.4)

Reagent	Final Concentration	Quantity
Tris	10 mM	Acid: 1.32 g Base: 0.19 g
Sodium chloride	400 mM	23.4 g
EDTA	0.1 mM	29 mg
DTT	1 mM	154 mg
Glycerol	50% (w/v)	500 g
Deionised Water		To a final volume of 1 L

8.9.3.2 Y. pestis Dam purification buffers

Low imidazole *Y. pestis* Dam purification buffer (pH 9)

Reagent	Final Concentration	Quantity
Tris	50 mM	Acid: 0.76 g Base: 5.47 g
Sodium chloride	300 mM	17.5 g
Imidazole	50 mM	3.40 g
β-mercaptoethanol	5 mM	350 µl
Glycerol	10% (w/v)	100 g
Deionised Water		To a final volume of 1 L

High imidazole *Y. pestis* Dam purification buffer (pH 9)

Reagent	Final Concentration	Quantity
Tris	50 mM	Acid: 0.76 g Base: 5.47 g
Sodium chloride	300 mM	17.5 g
Imidazole	500 mM	34.0 g
β-mercaptoethanol	5 mM	350 µl
Glycerol	10% (w/v)	100 g
Deionised Water		To a final volume of 1 L

Y. pestis Dam storage buffer (pH 7.5)

Reagent	Final Concentration	Quantity
Tris	50 mM	Acid: 6.35 g Base: 1.18 g
Sodium chloride	200 mM	11.7 g
EDTA	0.2 mM	58 mg
DTT	2 mM	308 mg
Glycerol	20% (w/v)	200 g
Deionised Water		To a final volume of 1 L

8.9.4 Assay buffers

Assay buffer A (pH 7.9)

Reagent	Final Concentration	Quantity
Tris	20 mM	Acid: 1.95 g Base: 0.92 g
Potassium acetate	50 mM	4.91 g
Magnesium acetate	10 mM	1.42 g
Sodium chloride	20 mM	1.17 g
BSA	0.1 mg ml^{-1}	100 mg
DTT	1 mM	154 mg
Deionised Water		To a final volume of 1 L

Assay buffer B (pH 7.9)

Reagent	Final Concentration	Quantity
Tris	20 mM	Acid: 1.95 g Base: 0.92 g
Magnesium chloride.$6H_2O$	8 mM	1.63 g
Sodium chloride	80 mM	4.68 g
BSA	0.1 mg ml^{-1}	100 mg
DTT	1 mM	154 mg
Glycerol	5% (w/v)	50 g
Deionised Water		To a final volume of 1 L

Assay buffer C (pH 7.5)

Reagent	Final Concentration	Quantity
Tris	100 mM	Acid: 9.75 g Base: 4.60 g
Magnesium chloride.$6H_2O$	5 mM	1.02 g
Sodium chloride	12.5 mM	0.73 g
BSA	0.1 mg ml^{-1}	100 mg
DTT	1 mM	154 mg
Glycerol	5% (w/v)	50 g
Deionised Water		To a final volume of 1 L

Assay buffer D (pH 7.9)

Reagent	Final Concentration	Quantity
Tris	100 mM	Acid: 9.75 g Base: 4.60 g
Sodium chloride	100 mM	5.85 g
Deionised Water		To a final volume of 1 L

Assay buffer E (pH 7.9)

Reagent	Final Concentration	Quantity
Tris	20 mM	Acid: 1.95 g Base: 0.92 g
Sodium chloride	80 mM	4.68 g
BSA	0.1 mg ml^{-1}	100 mg
DTT	1 mM	154 mg
Glycerol	5% (w/v)	50 g
Deionised Water		To a final volume of 1 L

NEBuffer 3

Reagent	Final Concentration	Quantity
Tris	50 mM	Acid: 0.76 g Base: 5.47 g
Sodium chloride	100 mM	5.85 g
Magnesium chloride	10 mM	952 mg
DTT	1 mM	154 mg
Deionised Water		To a final volume of 1 L

8.9.5 HPLC buffers

HPLC buffer A (pH 7)

Reagent	Final Concentration	Quantity
DMHA	5 mM	869 µl
Methanol	5%	50 ml
Deionised Water		To a final volume of 1 L

HPLC buffer B (pH 7)

Reagent	Final Concentration	Quantity
DMHA	5 mM	869 µl
Methanol	80%	800 ml
Deionised Water		To a final volume of 1 L

HPLC buffer C (pH 9)

Reagent	Final Concentration	Quantity
Ammonium acetate	0.1 M	7.71 g
Deionised Water		To a final volume of 1 L

9 Appendix

9.1 Derivation of equations

9.1.1 Enzyme kinetics

9.1.1.1 The Michaelis-Menten equation

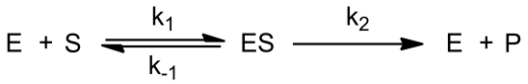

Figure 9.1 Enzyme catalysed reaction
Where E = enzyme, S = substrate, ES = enzyme-substrate complex, P = product, k_1 and k_2 = association rate constants, k_{-1} = dissociation rate constant (k_{-2} can be ignored under initial rate conditions).

The rate of change of enzyme-substrate complex concentration is given as:

9.1
$$\frac{d[ES]}{dt} = k_1[E][S]-k_{-1}[ES]-k_2[ES]$$
$$= k_1[E][S]- (k_{-1}+k_2)[ES]$$

Under steady-state approximation the rate of enzyme-substrate complex formation is equal to the rate of enzyme-substrate complex decay hence:

9.2
$$\frac{d[ES]}{dt} = -\frac{d[ES]}{dt} = 0$$

Substituting **9.2** into **9.1** gives:

9.3
$$k_1[E][S]- (k_{-1}+k_2)[ES] = 0$$
$$k_1[E][S] = (k_{-1}+k_2)[ES]$$

Rearranging **9.3** to group the rate constants gives:

9.4
$$[E][S] = \frac{k_{-1}+k_2}{k_1}[ES]$$

Where $(k_{-1}+k_2)/k_1$ is defined as the Michaelis-Menten constant (K_M) **9.4** becomes:

9.5 $[E][S] = K_M[ES]$

Total enzyme concentration ($[E]_T$) can be written as:

9.6 $[E]_T = [E]_0 = [E]+[ES]$

(where $[E]_0$ = initial enzyme concentration)

Rearranging **9.6** gives:

9.7 $[E] = [E]_0-[ES]$

Substituting **9.6** into **9.5** gives:

$$[E]_0-[ES]\ [S] = K_M[ES]$$
$$[E]_0[S]-[ES][S] = K_M[ES]$$
9.8 $$[E]_0[S] = K_M[ES]+[ES][S]$$
$$[E]_0[S] = [ES]\ K_M+[S]$$
$$[ES] = \frac{[E]_0[S]}{K_M+[S]}$$

Initial velocity (ν) is dependent on rate of product formation and can be defined as:

9.9 $\nu = k_2[ES]$

And maximum velocity (V_{max}) is the rate of product formation when all the enzyme is substrate-bound, defined as:

9.10 $$V_{max} = k_2[E]_{total}$$
$$= k_2[E]_0$$

Substituting **9.9** and **9.10** into **9.8** gives:

9.11 $$\frac{\nu}{k_2} = \frac{V_{max}[S]}{k_2\ K_M+[S]}$$

The rate constant k_2 can then be cancelled from both sides of **9.11** to give the Michaelis-Menten equation:

9.12 $$\nu = \frac{V_{max}[S]}{K_M+[S]}$$

9.1.1.2 Competitive substrate inhibition

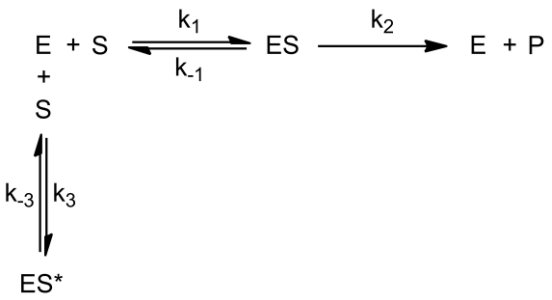

Figure 9.2 Enzyme catalysed reaction with competitive substrate inhibition
Where E = enzyme, S = substrate, ES = enzyme-substrate complex, P = product, ES* = inactive enzyme-substrate complex, k_1-k_3 = association rate constants, k_{-1} and k_{-3} = dissociation rate constants (k_{-2} can be ignored under initial rate conditions).

Where substrate binds the free enzyme to form active and inactive enzyme-substrate complexes (**Figure 9.2**) the rate of reaction can be equated to the rate of reaction in the presence of a competitive inhibitor.

The rate of change of inactive enzyme-substrate complex concentration is given as:

9.13 $$\frac{d[ES^*]}{dt} = k_3[E][S]-k_{-3}[ES^*]$$

Under steady-state approximation the rate of enzyme-substrate complex formation is equal to the rate of enzyme-substrate complex decay hence:

9.14 $$\frac{d[ES^*]}{dt} = -\frac{d[ES^*]}{dt} = 0$$

Substituting **9.13** into **9.14** gives:

$$k_3[E][S]-k_{-3}[ES^*] = 0$$

$$k_{-3}[ES^*] = k_3[E][S]$$

9.15 $$[ES^*] = \frac{k_3}{k_{-3}}[E][S]$$

$$= \frac{[E][S]}{K_{is}}$$

(where K_{is} = the substrate inhibition dissociation constant)

In this case total enzyme concentration ($[E]_T$) can be written as:

9.16 $$[E]_T = [E]_0 = [E]+[ES]+[ES^*]$$

(where $[E]_0$ = initial enzyme concentration)

Substituting **9.15** into **9.16** gives:

$$[E]_0 = [E]+[ES]+\frac{[E][S]}{K_{is}}$$

$$[E]+\frac{[E][S]}{K_{is}} = [E]_0-[ES]$$

9.17
$$[E]\left(1+\frac{[S]}{K_{is}}\right) = [E]_0-[ES]$$

$$[E]= \frac{[E]_0-[ES]}{\left(1+\frac{[S]}{K_{is}}\right)}$$

Substituting **9.17** into **9.5** gives:

$$\frac{[S]\ [E]_0-[ES]}{\left(1+\frac{[S]}{K_{is}}\right)} = K_M[ES]$$

$$[S][E]_0-[S][ES] = K_M[ES]\left(1+\frac{[S]}{K_{is}}\right)$$

9.18
$$[S][E]_0 = K_M[ES]\left(1+\frac{[S]}{K_{is}}\right)+[S][ES]$$

$$[S][E]_0 = [ES]\left[K_M\left(1+\frac{[S]}{K_{is}}\right)+[S]\right]$$

$$[ES] = \frac{[S][E]_0}{K_M\left(1+\frac{[S]}{K_{is}}\right)+[S]}$$

Substituting **9.9** and **9.10** into **9.18** and cancelling rate constant k_2 from both sides gives the substrate inhibition equation:

9.19
$$\nu = \frac{V_{max}[S]}{K_M\left(1+\frac{[S]}{K_{is}}\right)+[S]}$$

9.1.1.3 Reversible inhibition

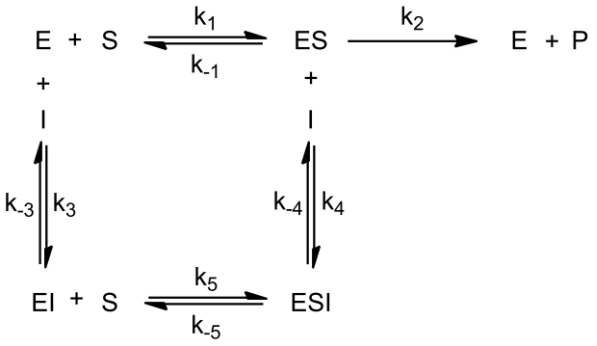

Figure 9.3 Reversible enzyme inhibition

Where E = enzyme, S = substrate, I = inhibitor, ES = enzyme-substrate complex, EI = enzyme-inhibitor complex, ESI = enzyme-substrate-inhibitor complex, P = product, k_1-k_5 = association rate constants, k_{-1} and k_{-3}-k_{-5} = dissociation rate constants (k_{-2} can be ignored under initial rate conditions).

Rate equations for reversible competitive, noncompetitive and uncompetitive inhibition (**Figure 9.3**) can be derived in a similar way to competitive substrate inhibition, as described in the previous Section. Derivations for each inhibitor modality are detailed below.

Competitive reversible inhibition

The rate of change of enzyme-inhibitor complex concentration is given as:

9.20 $$\frac{d[EI]}{dt} = k_3[E][I]-k_{-3}[EI]$$

Under steady-state approximation the rate of enzyme-substrate complex formation is equal to the rate of enzyme-substrate complex decay hence:

9.21 $$\frac{d[EI]}{dt} = -\frac{d[EI]}{dt} = 0$$

Substituting **9.20** into **9.21** gives:

$$k_3[E][I]-k_{-3}[EI] = 0$$

$$k_{-3}[EI] = k_3[E][I]$$

9.22 $$[EI] = \frac{k_3}{k_{-3}}[E][I]$$

$$= \frac{[E][I]}{K_i}$$

(where K_i = the inhibitory dissociation constant)

In this case total enzyme concentration ($[E]_T$) can be written as:

9.23 $[E]_T = [E]_0 = [E]+[ES]+[EI]$

(where $[E]_0$ = initial enzyme concentration)

Substituting **9.22** into **9.23** gives:

$$[E]_0 = [E]+[ES]+\frac{[E][I]}{K_i}$$

$$[E]+\frac{[E][I]}{K_i} = [E]_0-[ES]$$

9.24
$$[E]\left(1+\frac{[I]}{K_i}\right) = [E]_0-[ES]$$

$$[E]= \frac{[E]_0-[ES]}{\left(1+\frac{[I]}{K_i}\right)}$$

Substituting **9.24** into **9.5** gives:

$$\frac{[S]\ [E]_0-[ES]}{\left(1+\frac{[I]}{K_i}\right)} = K_M[ES]$$

$$[S][E]_0-[S][ES] = K_M[ES]\left(1+\frac{[I]}{K_i}\right)$$

9.25
$$[S][E]_0 = K_M[ES]\left(1+\frac{[I]}{K_i}\right)+[S][ES]$$

$$[S][E]_0 = [ES]\left[K_M\left(1+\frac{[I]}{K_i}\right)+[S]\right]$$

$$[ES] = \frac{[S][E]_0}{K_M\left(1+\frac{[I]}{K_i}\right)+[S]}$$

Substituting **9.9** and **9.10** into **9.25** and cancelling rate constant k_2 from both sides gives the competitive inhibition rate equation:

9.26
$$\nu = \frac{V_{max}[S]}{K_M\left(1+\frac{[I]}{K_i}\right)+[S]}$$

(where $K_M(1+([I]/K_i)) = K_M^{app}$)

Noncompetitive reversible inhibition

The rates of change of enzyme-inhibitor and enzyme-substrate-inhibitor complex concentrations are given as:

9.20 $\frac{d[EI]}{dt} = k_3[E][I]-k_{-3}[EI]$

9.27 $\frac{d[ESI]}{dt} = k_4[ES][I]-k_{-4}[ESI]$

Under steady-state approximation the rate of complex formation is equal to the rate of complex decay hence:

9.21 $\frac{d[EI]}{dt} = -\frac{d[EI]}{dt} = 0$

9.28 $\frac{d[ESI]}{dt} = -\frac{d[ESI]}{dt} = 0$

Substituting **9.20** into **9.21** gives:

$$k_3[E][I]-k_{-3}[EI] = 0$$

$$k_{-3}[EI] = k_3[E][I]$$

9.22 $$[EI] = \frac{k_3}{k_{-3}}[E][I]$$

$$= \frac{[E][I]}{K_i}$$

(where K_i = the inhibitory dissociation constant)

And substituting **9.20** $\frac{d[EI]}{dt} = k_3[E][I]-k_{-3}[EI]$

9.27 into **9.21** $\frac{d[EI]}{dt} = -\frac{d[EI]}{dt} = 0$

9.28 gives:

$$k_4[ES][I]-k_{-4}[ESI] = 0$$

$$k_{-4}[ESI] = k_4[ES][I]$$

9.29 $$[ESI] = \frac{k_4}{k_{-4}}[ES][I]$$

$$= \frac{[ES][I]}{\alpha K_i}$$

(where K_i = the inhibitory dissociation constant and α = constant describing the degree to which inhibitor binding affects the affinity of the enzyme for substrate)

In this case total enzyme concentration ($[E]_T$) can be written as:

9.30 $[E]_T = [E]_0 = [E]+[ES]+[EI]+[ESI]$

(where $[E]_0$ = initial enzyme concentration)

Substituting **9.22** and **9.29** into **9.30** gives:

$$[E]_0 = [E]+[ES]+\frac{[E][I]}{K_i}+\frac{[ES][I]}{\alpha K_i}$$

$$[E]+\frac{[E][I]}{K_i} = [E]_0-[ES]-\frac{[ES][I]}{\alpha K_i}$$

9.31
$$[E]\left(1+\frac{[I]}{K_i}\right) = [E]_0-[ES]\left(1+\frac{[I]}{\alpha K_i}\right)$$

$$[E] = \frac{[E]_0-[ES]\left(1+\frac{[I]}{\alpha K_i}\right)}{\left(1+\frac{[I]}{K_i}\right)}$$

Substituting **9.31** into **9.5** gives:

$$\frac{[S]\left[[E]_0-[ES]\left(1+\frac{[I]}{\alpha K_i}\right)\right]}{\left(1+\frac{[I]}{K_i}\right)} = K_M[ES]$$

9.32
$$[S][E]_0-[S][ES]\left(1+\frac{[I]}{\alpha K_i}\right) = K_M[ES]\left(1+\frac{[I]}{K_i}\right)$$

$$[S][E]_0 = [ES]\left[K_M\left(1+\frac{[I]}{K_i}\right)+[S]\left(1+\frac{[I]}{\alpha K_i}\right)\right]$$

$$[ES] = \frac{[S][E]_0}{K_M\left(1+\frac{[I]}{K_i}\right)+[S]\left(1+\frac{[I]}{\alpha K_i}\right)}$$

Substituting **9.9** and **9.10** into **9.32** and cancelling rate constant k_2 from both sides gives the noncompetitive inhibition rate equation:

9.33
$$v = \frac{V_{max}[S]}{K_M\left(1+\frac{[I]}{K_i}\right)+[S]\left(1+\frac{[I]}{\alpha K_i}\right)}$$

Dividing the numerator and denominator of **9.33** by $(1+([I]/\alpha K_i))$ gives:

9.34
$$v = \frac{\frac{V_{max}}{\left(1+\frac{[I]}{\alpha K_i}\right)}[S]}{K_M\left[\frac{\left(1+\frac{[I]}{K_i}\right)}{\left(1+\frac{[I]}{\alpha K_i}\right)}\right]+[S]}$$

(where $K_M((1+([I]/K_i))/(1+([I]/\alpha K_i))) = K_M^{app}$ and $V_{max}/(1+([I]/\alpha K_i)) = V_{max}^{app}$)

Uncompetitive reversible inhibition

The rate of change of enzyme-substrate-inhibitor complex concentration is given as:

9.35 $$\frac{d[ESI]}{dt} = k_4[ES][I]-k_{-4}[ESI]$$

Under steady-state approximation the rate of complex formation is equal to the rate of complex decay hence:

9.36 $$\frac{d[ESI]}{dt} = -\frac{d[ESI]}{dt} = 0$$

Substituting **9.20** $\frac{d[EI]}{dt} = k_3[E][I]-k_{-3}[EI]$

9.27 into **9.21** $\frac{d[EI]}{dt} = -\frac{d[EI]}{dt} = 0$

9.28 gives:

$$k_4[ES][I]-k_{-4}[ESI] = 0$$

$$k_{-4}[ESI] = k_4[ES][I]$$

9.29 $$[ESI] = \frac{k_4}{k_{-4}}[ES][I]$$

$$= \frac{[ES][I]}{\alpha K_i}$$

(where K_i = the inhibitory dissociation constant and α = constant describing the degree to which inhibitor binding affects the affinity of the enzyme for substrate)

In this case total enzyme concentration ($[E]_T$) can be written as:

9.37 $[E]_T = [E]_0 = [E]+[ES]+[ESI]$

(where $[E]_0$ = initial enzyme concentration)

Substituting and **9.29** into **9.37** gives:

9.38

$$[E]_0 = [E]+[ES]+\frac{[ES][I]}{\alpha K_i}$$

$$[E]= [E]_0-[ES]\left(1+\frac{[I]}{\alpha K_i}\right)$$

Substituting **9.38** into **9.5** gives:

$$[S]\left[[E]_0-[ES]\left(1+\frac{[I]}{\alpha K_i}\right)\right]=K_M[ES]$$

$$[S][E]_0-[S][ES]\left(1+\frac{[I]}{\alpha K_i}\right)=K_M[ES]$$

9.39

$$[S][E]_0=[ES]\left[K_M+[S]\left(1+\frac{[I]}{\alpha K_i}\right)\right]$$

$$[ES]=\frac{[S][E]_0}{K_M+[S]\left(1+\frac{[I]}{\alpha K_i}\right)}$$

Substituting **9.9** and **9.10** into **9.39** and cancelling rate constant k_2 from both sides gives the uncompetitive inhibition rate equation:

9.40 $$\nu=\frac{V_{max}[S]}{K_M+[S]\left(1+\frac{[I]}{\alpha K_i}\right)}$$

Dividing the numerator and denominator of **9.40** by $(1+([I]/\alpha K_i))$ gives:

9.41 $$\nu=\frac{\frac{V_{max}}{\left(1+\frac{[I]}{\alpha K_i}\right)}[S]}{K_M\left[\frac{1}{\left(1+\frac{[I]}{\alpha K_i}\right)}\right]+[S]}$$

(where $K_M(1/(1+([I]/\alpha K_i)))=K_M^{app}$ and $V_{max}/(1+([I]/\alpha K_i))=V_{max}^{app}$)

Determination of K_i

Both competitive and uncompetitive reversible inhibition can be expressed in terms of the noncompetitive reversible inhibition rate equation:

9.34 $$\nu=\frac{\frac{V_{max}}{\left(1+\frac{[I]}{\alpha K_i}\right)}[S]}{K_M\left[\frac{\left(1+\frac{[I]}{K_i}\right)}{\left(1+\frac{[I]}{\alpha K_i}\right)}\right]+[S]}$$

For competitive inhibition, where inhibitor can only bind free enzyme, α tends towards infinity and $(1+([I]/K_i))>>(1+([I]/\alpha K_i))$. For uncompetitive inhibition, where inhibitor can only bind the enzyme-substrate complex, α tends towards 0 and $(1+([I]/\alpha K_i))>>(1+([I]/\alpha K_i))$. A general rate equation for reversible inhibition can therefore be expressed as:

9.42 $$\nu = \frac{V_{max}^{app}[S]}{K_M^{app}+[S]}$$

(where $K_M^{app} = K_M((1+([I]/K_i))/(1+([I]/\alpha K_i)))$ and $V_{max}^{app} = V_{max}/(1+([I]/\alpha K_i))$

Rearrangement of the Michaelis-Menten equation (**9.12**) gives the Lineweaver-Burk equation:

$$\begin{aligned}\frac{1}{\nu} &= \frac{K_M+[S]}{V_{max}[S]}\\ &= \frac{K_M}{V_{max}[S]}+\frac{[S]}{V_{max}[S]}\\ &= \frac{K_M}{V_{max}}\times\frac{1}{[S]}+\frac{1}{V_{max}}\end{aligned} \qquad \textbf{9.43}$$

The same rearrangement can be made for the general reversible inhibition rate equation (**9.42**) to give:

$$\frac{1}{\nu} = \frac{K_M^{app}}{V_{max}^{app}}\times\frac{1}{[S]}+\frac{1}{V_{max}^{app}} \qquad \textbf{9.44}$$

The gradients (K_M^{app}/V_{max}^{app}) and y-axis intercepts ($1/V_{max}^{app}$) of $1/\nu$ against $1/[S]$ plots can be replotted against inhibitor concentration and fitted to **9.45** and **9.46** respectively:

$$\begin{aligned}\frac{K_M^{app}}{V_{max}^{app}} &= \frac{K_M\left[\frac{\left(1+\frac{[I]}{K_i}\right)}{\left(1+\frac{[I]}{\alpha K_i}\right)}\right]}{\frac{V_{max}}{\left(1+\frac{[I]}{\alpha K_i}\right)}}\\ &= \frac{K_M\left(1+\frac{[I]}{K_i}\right)}{V_{max}}\\ &= \frac{K_M+\frac{K_M[I]}{K_i}}{V_{max}}\\ &= \frac{K_M}{V_{max}K_i}[I]+\frac{K_M}{V_{max}}\end{aligned} \qquad \textbf{9.45}$$

$$\begin{aligned}\frac{1}{V_{max}^{app}} &= \frac{1}{\frac{V_{max}}{\left(1+\frac{[I]}{\alpha K_i}\right)}}\\ &= \frac{1+\frac{[I]}{\alpha K_i}}{V_{max}}\\ &= \frac{1}{V_{max}\alpha K_i}[I]+\frac{1}{V_{max}}\end{aligned} \qquad \textbf{9.46}$$

K_i and αK_i can then be calculated from the negative of the x-axis intercept of replots fitted to **9.45** and **9.46** respectively.

The Cheng-Prusoff equation – competitive reversible inhibition

Dividing **9.26** by **9.12** gives:

$$\frac{v_i}{v_0} = \frac{V_{max}[S]}{K_M\left(\frac{1+[I]}{K_i}\right)+[S]}\frac{K_M+[S]}{V_{max}[S]}$$

$$= \frac{K_M+[S]}{K_M\left(\frac{1+[I]}{K_i}\right)+[S]} \qquad \textbf{9.47}$$

Substituting $v_i/v_0 = 0.5$ and $[I] = IC_{50}$ into **9.47** gives:

$$\frac{1}{2} = \frac{K_M+[S]}{K_M\left(\frac{1+IC_{50}}{K_i}\right)+[S]}$$

$$2K_M+2[S] = K_M+\frac{K_M IC_{50}}{K_i}+[S] \qquad \textbf{9.48}$$

$$[S]+K_M\frac{K_i}{K_M} = IC_{50}$$

$$IC_{50} = K_i\left(1+\frac{[S]}{K_M}\right)$$

The Cheng-Prusoff equation – noncompetitive reversible inhibition

Dividing **9.34** by **9.12** gives:

$$\frac{v_i}{v_0} = \frac{\frac{V_{max}}{\left(\frac{1+[I]}{\alpha K_i}\right)}[S]}{K_M\frac{\left(\frac{1+[I]}{K_i}\right)}{\left(\frac{1+[I]}{\alpha K_i}\right)}+[S]}\frac{K_M+[S]}{V_{max}[S]}$$

$$= \frac{\frac{K_M+[S]}{\left(\frac{1+[I]}{\alpha K_i}\right)}}{K_M\frac{\left(\frac{1+[I]}{K_i}\right)}{\left(\frac{1+[I]}{\alpha K_i}\right)}+[S]} \qquad \textbf{9.49}$$

$$= \frac{K_M+[S]}{K_M\left(\frac{1+[I]}{K_i}\right)+[S]\left(\frac{1+[I]}{\alpha K_i}\right)}$$

Substituting $v_i/v_0 = 0.5$ and $[I] = IC_{50}$ into **9.49** gives:

$$\frac{1}{2} = \frac{K_M+[S]}{K_M\left(\frac{1+IC_{50}}{K_i}\right)+[S]\left(\frac{1+IC_{50}}{\alpha K_i}\right)}$$

$$2K_M+2[S] = K_M+\frac{K_M IC_{50}}{K_i}+[S]+\frac{[S]IC_{50}}{\alpha K_i}$$

$$\mathbf{9.50} \qquad K_M+[S] = \frac{\alpha K_M IC_{50}+[S]IC_{50}}{\alpha K_i}$$

$$IC_{50} = \frac{\alpha K_i \ K_M+[S]}{\alpha K_M+[S]}$$

$$= \frac{K_M+[S]}{\frac{K_M}{K_i}+\frac{[S]}{\alpha K_i}}$$

The Cheng-Prusoff equation - Uncompetitive reversible inhibition

Dividing **9.41** by **9.12** gives:

$$\frac{v_i}{v_0} = \frac{\frac{V_{max}}{\left(\frac{1+[I]}{\alpha K_i}\right)}[S]}{K_M\frac{1}{\left(\frac{1+[I]}{\alpha K_i}\right)}+[S]}\frac{K_M+[S]}{V_{max}[S]}$$

$$\mathbf{9.51} \qquad = \frac{\frac{K_M+[S]}{\left(\frac{1+[I]}{\alpha K_i}\right)}}{\frac{K_M}{\left(\frac{1+[I]}{\alpha K_i}\right)}+[S]}$$

$$= \frac{K_M+[S]}{K_M+[S]\left(\frac{1+[I]}{\alpha K_i}\right)}$$

Substituting $v_i/v_0 = 0.5$ and $[I] = IC_{50}$ into **9.49** gives:

$$\frac{1}{2} = \frac{K_M+[S]}{K_M+[S]\left(\frac{1+IC_{50}}{\alpha K_i}\right)}$$

$$2K_M+2[S] = K_M+[S]+\frac{[S]IC_{50}}{\alpha K_i}$$

$$\mathbf{9.52} \qquad K_M+[S] = \frac{[S]IC_{50}}{\alpha K_i}$$

$$IC_{50} = \frac{\alpha K_i K_M+\alpha K_i[S]}{[S]}$$

$$= \alpha K_i\left(1+\frac{K_M}{[S]}\right)$$

9.1.1.4 Enzyme-inhibitor binding isotherm equation

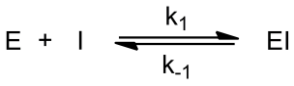

Figure 9.4 Reversible enzyme-inhibitor complex formation
Where E = enzyme, I = inhibitor, EI = enzyme-inhibitor complex, k_1 = association rate constant, k_{-1} = dissociation rate constant.

The rate of change of enzyme-inhibitor complex concentration is given as:

9.53 $$\frac{d[EI]}{dt} = k_1[E][I]-k_{-1}[EI]$$

Under steady-state approximation the rate of enzyme-substrate complex formation is equal to the rate of enzyme-substrate complex decay hence:

9.54 $$\frac{d[EI]}{dt} = -\frac{d[EI]}{dt} = 0$$

Substituting **9.53** into **9.54** gives:

9.55 $$k_1[E][I]-k_{-1}[EI] = 0$$
$$k_1[E][I] = k_{-1}[EI]$$

Rearranging **9.55** to group the rate constants gives:

9.56 $$[EI] = \frac{k_1}{k_{-1}}[E][I]$$
$$= \frac{[E][I]}{K_D}$$

(where K_D is the equilibrium dissociation binding constant (k_{-1}/k_1))

Substituting **9.10** into **9.11** gives:

9.57 $$\nu_0 = [E]_T \frac{k_{cat}[S]}{K_M+[S]}$$

(where ν_0 is the uninhibited initial rate and k_{cat} is the catalytic rate constant k_2)

In the presence of an inhibitor initial rate is proportional to the concentration of free enzyme:

9.58 $$\nu_i = [E]\frac{k_{cat}[S]}{K_M+[S]}$$

(where ν_i is the inhibited initial rate)

The fractional enzyme activity in the presence of a concentration of inhibitor can therefore be given as (**9.58**/**9.57**):

9.59 $$\frac{\nu_i}{\nu_0} = \frac{[E]}{[E]_T}$$

Substituting **9.61** into **9.59** gives:

9.60 $$\frac{\nu_i}{\nu_0} = \frac{[E]_T-[EI]}{[E]_T} = 1-\frac{[EI]}{[E]_T}$$

The concentration of free enzyme and inhibitor can be expressed as:

9.61 $[E] = [E]_T-[EI]$

9.62 $[I] = [I]_T-[EI]$

However, where [I]>>[E] **9.62** can be simplified to:

9.63 $[I] = [I]_T$

Substituting **9.61** and **9.63** into **9.56** gives:

$$[EI] = \frac{[E]_T-[EI]\ [I]_T}{K_D}$$

$$K_D[EI] = [E]_T[I]_T-[EI][I]_T$$

9.64 $$K_D[EI]+[EI][I]_T = [E]_T[I]_T$$

$$[EI] = \frac{[E]_T[I]_T}{K_D+[I]_T} = \frac{[E]_T}{1+\frac{K_D}{[I]_T}}$$

Dividing both sides of **9.64** by $[E]_T$ gives:

9.65 $$\frac{[EI]}{[E]_T} = \frac{1}{1+\frac{K_D}{[I]_T}}$$

Substituting **9.65** into **9.60** gives:

9.66 $$\frac{\nu_i}{\nu_0} = 1-\frac{1}{1+\frac{K_D}{[I]_T}}$$

Which can be rearranged to give:

9.67 $$\frac{v_i}{v_0} = \frac{1}{1+\frac{[I]_T}{K_D}}$$

Substituting the equilibrium binding constant K_D for the half maximal inhibitory constant IC_{50} gives:

9.68 $$\frac{v_i}{v_0} = \frac{1}{1+\frac{[I]_T}{IC_{50}}}$$

The binding stoichiometry of enzyme-inhibitor interactions can be accounted for by multiplying the $[I]_T/IC_{50}$ term by the Hill parameter (h) to give:

9.69 $$\frac{v_i}{v_0} = \frac{1}{1+\left(\frac{[I]_T}{IC_{50}}\right)^h}$$

9.1.2 Fluorescence anisotropy equations

$$E + S' \underset{}{\overset{K_D}{\rightleftharpoons}} ES'$$

Figure 9.5 Reversible enzyme-labelled substrate complex formation
Where E = enzyme, S' = fluorescently labelled substrate, ES'= enzyme-labelled substrate complex, K_D = equilibrium dissociation binding constant.

Observed fluorescence anisotropy (A_{obs}) represents a weighted average of the bound (A_B) and free (A_F) fluorophore and can be expressed as:

9.70 $A_{obs} = F_B A_B + F_F A_F$

(where F_B and F_F are the fraction of bound and free substrate respectively)

Including a correction factor (Q) for the ratio of bound and free fluorescence intensities, and substituting F_F for $1-F_B$, **9.70** becomes:

9.71 $$A_{obs} = \frac{QF_B A_B + F_B A_F}{1-(1-Q)F_B}$$

Rearranging **9.71** in terms of F_B gives:

$$A_{obs} - A_{obs}F_B - A_{obs}QF_B = QF_B A_B + A_F - F_B A_F$$
$$A_{obs} - F_B\ A_{obs} - A_{obs}Q = F_B\ QA_B - A_F + A_F$$
$$A_{obs} - A_F = F_B\ QA_B - A_F + F_B\ A_{obs} - A_{obs}Q$$

9.72
$$A_{obs} - A_F = F_B\ QA_B - A_F + A_{obs} - A_{obs}Q$$
$$A_{obs} - A_F = F_B\ Q\ A_B - A_{obs} - A_F + A_{obs}$$
$$F_B = \frac{A_{obs} - A_F}{Q\ A_B - A_{obs} - A_F + A_{obs}}$$

Direct binding

Binding of enzyme to labelled substrate (**Figure 9.5**) can be described as:

9.73 $$K_D = \frac{[E][S']}{[ES']}$$

The concentration of free enzyme and labelled substrate can be expressed as:

9.74 $[E] = [E]_T - [ES']$

9.75 $[S'] = [S']_T - [ES']$

Substituting **9.74** and **9.75** into **9.73** gives:

9.76
$$K_D = \frac{[E]_T-[ES'] \quad [S']_T-[ES']}{[ES']}$$
$$K_D[ES'] = [E]_T-[ES'] \quad [S']_T-[ES']$$

Which can be rearranged to give a quadratic equation:

9.77
$$0 = [E]_T-[ES'] \quad [S']_T-[ES'] \quad -K_D[ES']$$
$$= [E]_T[S']_T-[E]_T[ES']-[S']_T[ES']+[ES']^2 - K_D[ES']$$
$$=[ES']^2- [E]_T+[S']_T+K_D \ [ES']+[E]_T[S']_T$$

Solving **9.77** gives two possible solutions, only one of which has physical meaning:

9.78
$$[ES'] = \frac{[E]_T+[S']_T+K_D \ -\sqrt{[E]_T+[S']_T+K_D \ ^2-4[E]_T[S']_T}}{2}$$

Fraction of substrate bound can be expressed in terms of fraction of free substrate as:

9.79
$$F_B = 1-F_F$$
$$= 1-\frac{[S']}{[S']_T}$$

Substituting **9.75** into **9.79** gives:

9.80
$$F_B = 1-\frac{[S']}{[S']_T}$$
$$= 1-\frac{[S']_T-[ES']}{[S']_T}$$
$$= \frac{[ES']}{[S']_T}$$

Substituting **9.78** into **9.80** gives:

9.81
$$F_B = \frac{[E]_T+[S']_T+K_D \ -\sqrt{[E]_T+[S']_T+K_D \ ^2-4[E]_T[S']_T}}{2[S']_T}$$

Competitive binding

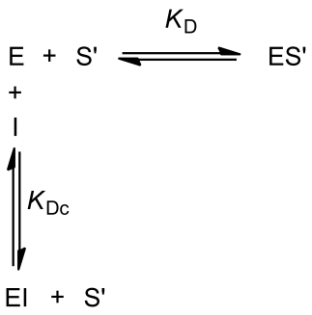

Figure 9.6 Reversible competitive inhibition of enzyme-labelled substrate complex formation

Where E = enzyme, S' = fluorescently labelled substrate, I = inhibitor, ES'= enzyme-labelled substrate complex, EI= enzyme-inhibitor complex, K_D = equilibrium dissociation binding constant, K_{Dc} = equilibrium dissociation competition binding constant.

Competitive inhibition of enzyme-labelled substrate complex formation (**Figure 9.6**) can be described by **9.73**, **9.75**, **9.79** and:

9.82 $$K_{Dc} = \frac{[E][I]}{[EI]}$$

9.83 $$[E] = [E]_T - [ES'] - [EI]$$

9.84 $$[I] = [I]_T - [EI]$$

Solving **9.73**, **9.75**, **9.79**, **9.82**, **9.83** and **9.84** for $[I]_T$ and eliminating [R], [S'], [ES'], [I] and [EI] gives the cubic equation:

9.85 $$[I]_T = \frac{\left[K_D - K_{Dc} F_B + K_{Dc} \right]\left[[S']_T F_B^2 - K_D + [S']_T + [E]_T F_B + [E]_T \right]}{1 - F_B F_B K_D}$$

Solving **9.85** for F_B gives a single physically meaning root expressed by:

9.86 $$F_B = \frac{2\sqrt{d^2 - 3e}\cos\frac{\theta}{3} - d}{3K_D + 2\sqrt{d^2 - 3e}\cos\frac{\theta}{3} - d}$$

Where:

$$d = K_D + K_{Dc} + [S']_T + [I]_T - [E]_T$$

$$e = [I]_T - [E]_T K_D + [I]_T - [E]_T K_{Dc} + K_D K_{Dc}$$

$$f = -K_D K_{Dc} [E]_T$$

$$\theta = \arccos\left| \frac{-2d^3 + 9de - 27f}{2\sqrt{d^2 - 3e^3}} \right|$$

9.2 Plasmid Maps

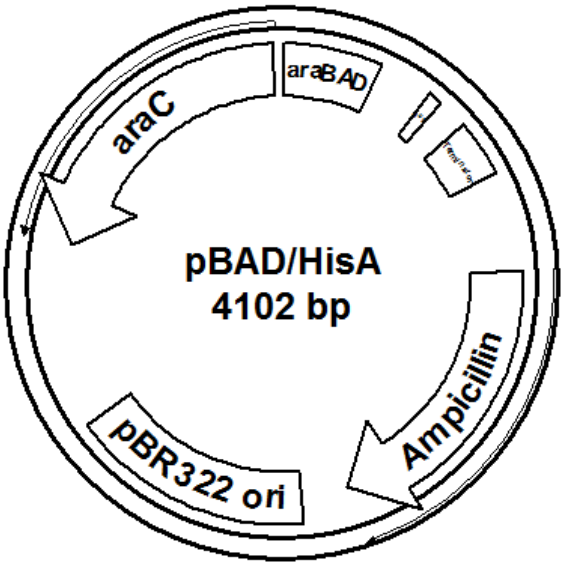

Figure 9.7 pBAD/HisA expression vector

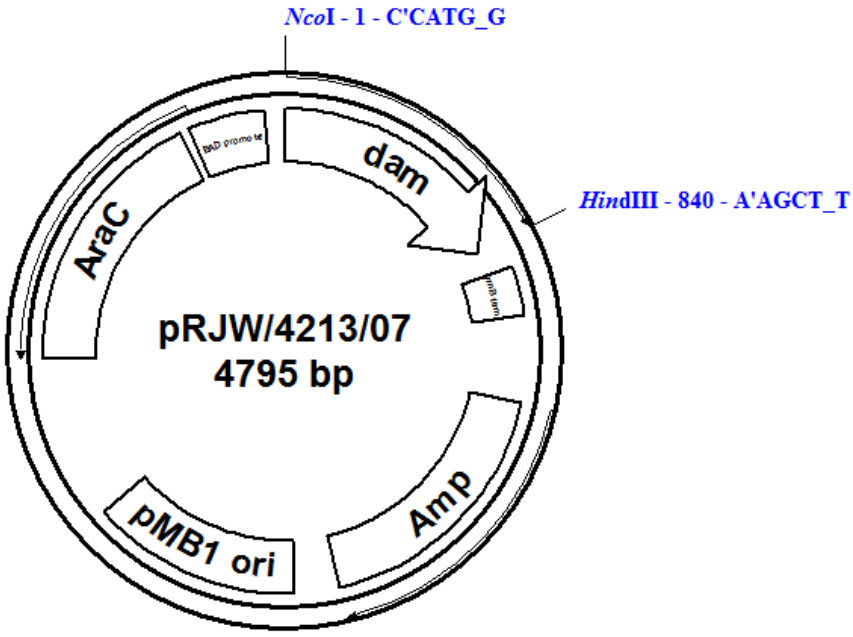

Figure 9.8 *Y. pestis* Dam expression vector

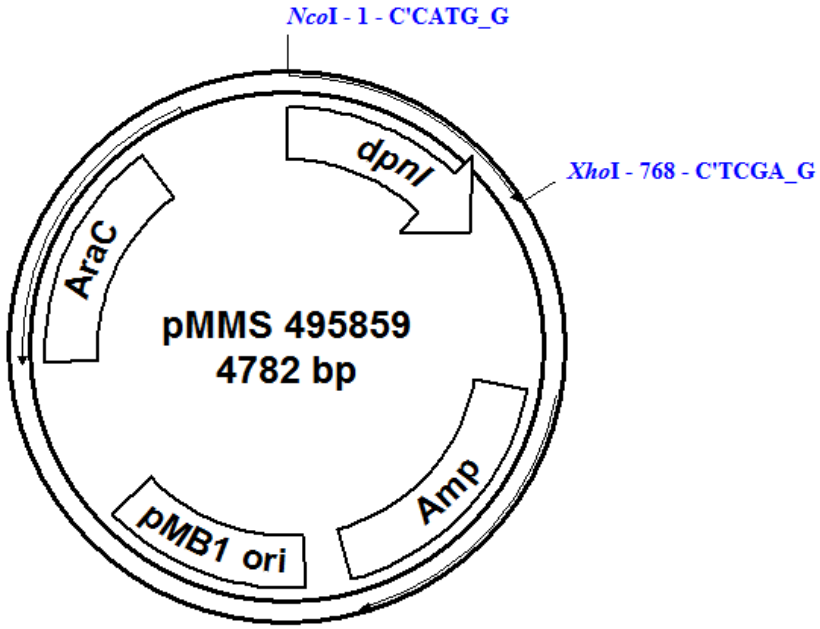

Figure 9.9 *Dpn*I expression vector

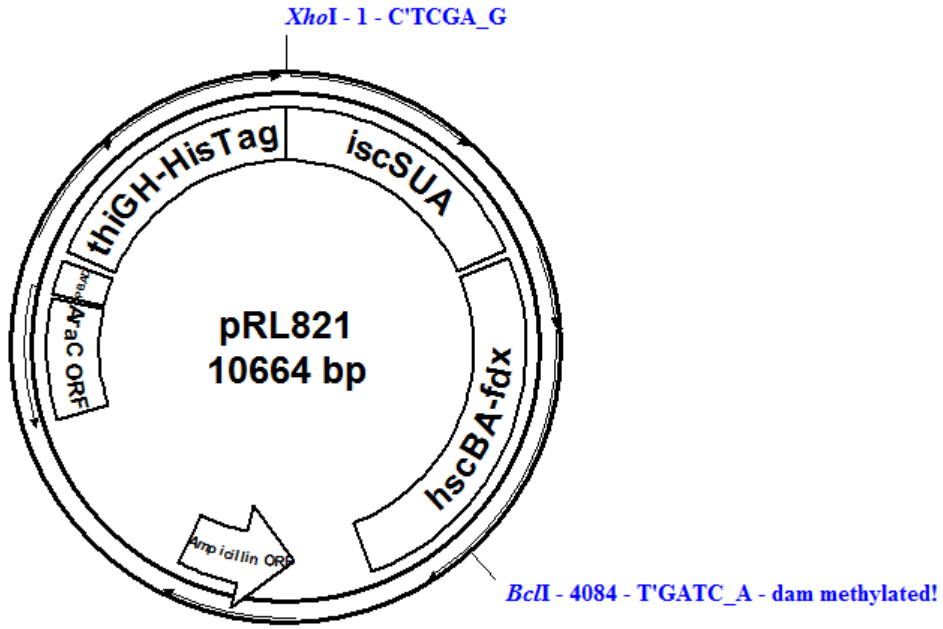

Figure 9.10 Gel-based and in culture gel-based Dam methylation assay plasmid

9.3 Oligonucleotides

(^{m}A – *N*6-methyladenine, ^{m}C – 5-methylcytosine, F – Fluorescein, Cy – Cy3, D – Dabcyl, recognition sequence in **bold**, hairpin loop in *italics*)

ODN1: F-CCG**G^{m}ATC**CAG*TTTT*CTG**GATC**CGG-D

ODN2: F-CCG**G^{m}ATC**CAG*TTTT*CTG**G^{m}ATC**CGG-D

ODN3: CCG**GATC**CAG*TTTT*CTG**GATC**CGG

ODN4: Cy-CCTAT**GCG^{m}C**ATCAG*TTTT*CTGAT**G^{m}CG^{m}C**ATAGG-D

ODN5: Cy-CCTAT**G^{m}CG^{m}C**ATCAG*TTTT*CTGAT**G^{m}CG^{m}C**ATAGG-D

ODN6: F-CCTAT**GCG^{m}C**ATCAG*TTTT*CTGAT**G^{m}CG^{m}C**ATAGG-D

ODN7: F-CCTAT**G^{m}CG^{m}C**ATCAG*TTTT*CTGAT**G^{m}CG^{m}C**ATAGG-D

ODN8: F-TATAG**GCG^{m}C**CCATG*TTTT*CATGG**G^{m}CG^{m}C**CTATA-D

ODN9: F-TATAG**G^{m}CG^{m}C**CCATG*TTTT*CATGG**G^{m}CG^{m}C**CTATA-D

ODN10: F-CCG**G^{m}ATC**CAG*TTTT*CTG**GATC**CGG-D

ODN11: F-CCG**G^{m}ATC**CAG*TTTT*CTG**G^{m}ATC**CGG-D

ODN12: CCG**G^{m}ATC**CAG*TTTT*CTG**GATC**CGG

9.4 Calibration plots

9.4.1 Real-time break light Dam and DpnI activity assays

Assays were prepared in 96 and 384 well plates in a total volume of 100 or 20 µl as described in Chapter 8, Section 8.3.2.2, and supplemented with fully methylated oligonucleotide ODN2 (0-35 nM) and *Dpn*I (0.8 nM). End point fluorescence was measured at gain settings of 100-190, and plots of end-point fluorescence against total amount of DNA at various gain settings were fitted to a linear equation of the form y = y0+a*x, where a is the fluorescence change per unit of DNA turned over.

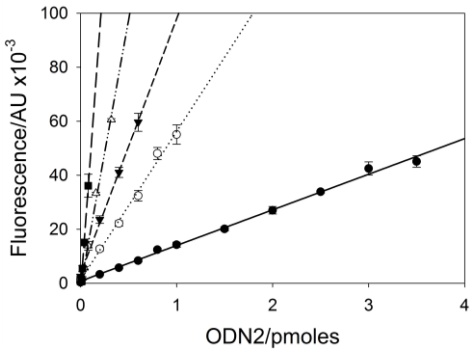

Figure 9.11 Fluorescence calibration curve I

End-point fluorescence versus amount of fully methylated oligonucleotide ODN2 for 96 well plates at gain settings of 100 (filled circles), 120 (open circles) and 120 (filled triangles), and for 384 well plates at gain settings of 150 (open triangles), 170 (filled squares) and 190 (open squares). Data fitted to a linear equation of the form y = y0+a*x.

Assay conditions: 0.8 nM *Dpn*I, 0-35 nM fully methylated oligonucleotide (ODN2), 20 mM Tris, 80 mM NaCl, 8 mM $MgCl_2$, 0.1 mg ml^{-1} BSA, 1 mM DTT, pH 7.9. Total assay volume 100 or 20 µl, in 96 or 384 well plates, gain 100-190, temperature 30 °C.

Table 9.1 Fluorescence calibration data I

Plate	Gain Setting	ΔF/fmole*	R^2
96 well	100	13.2 ± 0.4	0.996
	120	55.0 ± 1.7	0.993
	130	94.5 ± 3.1	0.999
384 well	150	86.4 ± 2.5	0.994
	170	197 ± 5	0.996
	190	483 ± 23	0.995

* Gradient (a) ± standard error of fit calculated from **Figure 9.11**

9.4.2 Real-time break light DNMT1 activity assay

Assays were prepared in 384 well plates in a total volume of 20 µl, as described in Chapter 8, Section 8.3.2.4, and supplemented with fully methylated oligonucleotide ODN7 (0-250 nM) and *Gla*I (0.25 U μl^{-1}). End point fluorescence was measured in a BMG Polarstar Omega at gain settings of 1250-1550, and plots of end-point fluorescence against total amount of DNA at various gain settings were fitted to a linear equation of the form y = y0+a*x, where a is the fluorescence change per unit amount of DNA turned over.

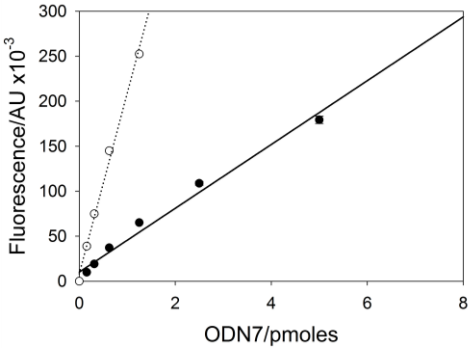

Figure 9.12 Fluorescence calibration curve II

End-point fluorescence versus amount of fully methylated oligonucleotide ODN7 at gain settings of 1250 (filled circles) and 1550 (open circles). Data fitted to a linear equation of the form y = y0+a*x.

Assay conditions: 0.25 U μl^{-1} *Gla*I, 0-250 nM fully methylated oligonucleotide (ODN7), 100 mM Tris, 12.5 mM NaCl, 5 mM $MgCl_2$, 0.1 mg ml^{-1} BSA, 1 mM DTT, pH 7.5. Total assay volume 20 µl, in 384 well plates, gain 1250-1550, temperature 37 ˚C.

Table 9.2 Fluorescence calibration data II

Plate	Gain Setting	ΔF/fmole*	R^2
384 well	1250	35.4 ± 4.6	0.982
	1550	201 ± 9	0.994

* Gradient (a) ± standard error of fit calculated from **Figure 9.12**

9.5 Optimisation of the real-time break light Dam activity assay for E. coli Dam

9.5.1 Enzyme concentration

E. coli Dam activity assays were prepared in 384 well plates in a total volume of 20 µl as described in Chapter 8, Section 8.3.2.1. Assays were maintained at 37 ˚C and supplemented with hemimethylated oligonucleotide ODN1 (200 nM), AdoMet (200 µM), *E. coli* Dam (1 nM) and *Dpn*I (0.6-20 nM). Initial rate versus *Dpn*I concentration data was fitted to an exponential rise to a maximum of the form f=a*(1-exp(-b*x)) and the optimal concentration of *Dpn*I, where 94% maximum rate was achieved, was identified as 10 nM.

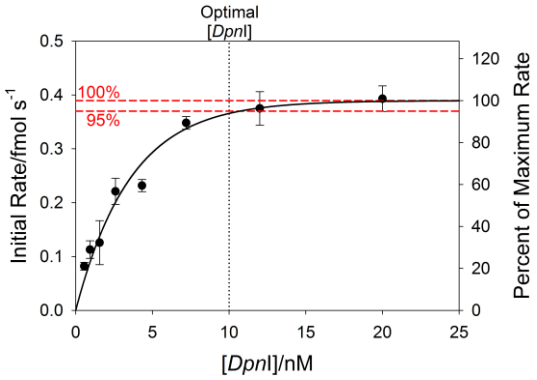

Figure 9.13 *Dpn*I concentration optimisation

Background subtracted initial rate of methylation by *E. coli* Dam. Data fitted to an exponential rise to a maximum of the form f=a*(1-exp(-b*x)), where a = maximum rate. Assay conditions: 1 nM *E. coli* Dam, 0-20 nM *Dpn*I, 200 nM hemimethylated oligonucleotide (ODN1), 25 or 0 µM AdoMet, 20 mM Tris, 80 mM NaCl, 8 mM $MgCl_2$, 1 mM DTT, 0.1 mg ml^{-1} BSA, 5% glycerol, pH 7.9. Total assay volume 20 µl, in 384 well plate, gain 150, temperature 37 ˚C.

9.5.2 Substrate concentrations

9.5.2.1 DNA

E. coli Dam K_M^{DNA} assays were prepared in 384 well plates in a total volume of 20 µl as described in Chapter 8, Section 8.3.2.5. Assays were maintained at 37 ˚C and supplemented with hemimethylated oligonucleotide ODN1 (6-200 nM), AdoMet (200 µM), DMSO (5%), *E. coli* Dam (0.5 nM) and *Dpn*I (2, 10 or 15 nM). Initial rate versus DNA concentration data was fitted globally to **Equation 2.5** with K_M and V_{max} shared, and K_M^{DNA} was identified as 28.0 ± 14.2 nM.

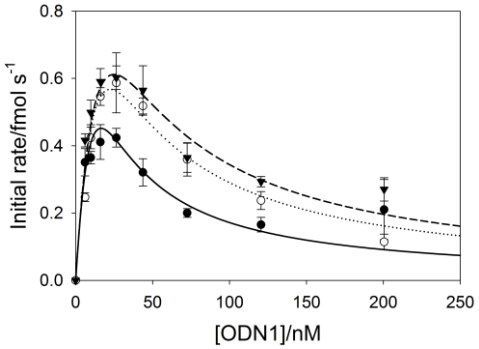

Figure 9.14 Graphical determination of *E. coli* Dam K_M^{DNA}
Background subtracted initial rate versus concentration of DNA with 2 (filled circles), 10 (open circles) or 15 (filled triangles) nM *Dpn*I. Data fitted globally to **Equation 2.5** with K_M and V_{max} shared.
Assay conditions: 0.5 nM *E. coli* Dam, 2, 10 or 15 nM *Dpn*I, 6-200 nM hemimethylated oligonucleotide (ODN1), 0 or 100 µM AdoMet, 5% DMSO, 20 mM Tris, 80 mM NaCl, 8 mM $MgCl_2$, 1 mM DTT, 0.1 mg ml^{-1} BSA, 5% glycerol, pH 7.9. Total assay volume 20 µl, in 384 well plate, gain 130, 37 ˚C.

9.5.2.2 AdoMet

E. coli Dam K_M^{AdoMet} assays were prepared in 384 well plates in a total volume of 20 µl as described in Chapter 8, Section 8.3.2.5. Assays were maintained at 37 ˚C and supplemented with hemimethylated oligonucleotide ODN1 (100 nM), AdoMet (0-100 µM), *E. coli* Dam (1 nM) and *Dpn*I (0.6-20 nM). Initial rate versus AdoMet concentration data was fitted to **Equation 2.4B** and K_M^{AdoMet} was identified as 5.56 ± 0.80 µM.

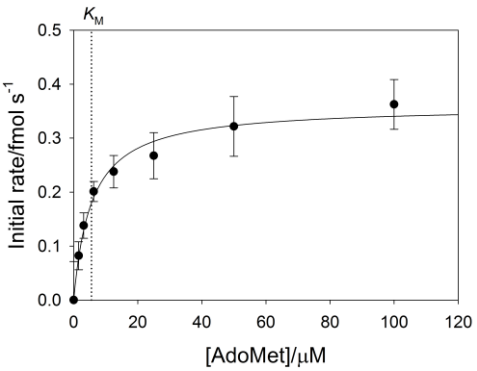

Figure 9.15 Graphical determination of *E. coli* Dam K_M^{AdoMet}

Initial rate versus concentration of AdoMet. Data fitted to **Equation 2.4B**.

Assay conditions: 1 nM *Y. pestis* Dam, 2 nM *Dpn*I, 30 nM hemimethylated oligonucleotide (ODN1), 0-200 μM AdoMet, 5% DMSO, 20 mM Tris, 80 mM NaCl, 8 mM $MgCl_2$, 1 mM DTT, 0.1 mg ml^{-1} BSA, 5% glycerol, pH 7.9. Total assay volume 20 μl, in 384 well plate, gain 130, 37 ˚C.

9.6 Assay automation

A Beckman Coulter Biomek 3000 laboratory automation workstation was used for the automated preparation of assays in 384 well plates. Automation programs (**Table 9.3**, **Table 9.4** and **Table 9.5**) were optimised to ensure rapid and efficient mixing of components was achieved.

Table 9.3 Dry well automated plate addition

Step	Parameter	Value
Prewet	Overage	5 µl
	Delay	200 ms
Mixing (prior to aspiration)	Volume	-
	Aspirate height	-
	Aspirate speed	-
	Dispense height	-
	Dispense speed	-
Aspirate	Height	-3 mm (from the liquid)
	Airgap	2 µl
	Delay	200 ms
	Speed	20 µl s^{-1}
Dispense	Delay	200 ms
	Height	0.3 mm (from the bottom)
	Speed	20 µl s^{-1}
Mixing	Volume	-
	Aspirate height	-
	Aspirate speed	-
	Dispense height	-
	Dispense speed	-
Tip touch	Height	-1 mm (from the well top)
	Speed	75% of maximum

Table 9.4 Wet well automated plate addition

Step	Parameter	Value
Prewet	Overage	5 µl
	Delay	200 ms
Mixing (prior to aspiration)	Volume	5 µl x 4
	Aspirate height	-2 mm (from the liquid)
	Aspirate speed	100 µl s^{-1}
	Dispense height	-2 mm (from the liquid)
	Dispense speed	100 µl s^{-1}
Aspirate	Height	-2 mm (from the liquid)
	Airgap	2 µl
	Delay	200 ms
	Speed	20 µl s^{-1}
Dispense	Delay	200 ms
	Height	1.5 mm (from the bottom)
	Speed	40 µl s^{-1}
Mixing	Volume	10 µl x 4
	Aspirate height	1.5 mm (from the bottom)
	Aspirate speed	100 µl s^{-1}
	Dispense height	1.5 mm (from the bottom)
	Dispense speed	100 µl s^{-1}
Tip touch	Height	-1 mm (from the well top)
	Speed	75% of maximum

Table 9.5 Automated assay initiation (enzyme addition)

Step	Parameter	Value
Prewet	Overage	5 µl
	Delay	100 ms
Mixing (prior to aspiration)	Volume	-
	Aspirate height	-
	Aspirate speed	-
	Dispense height	-
	Dispense speed	-
Aspirate	Height	-2 mm (from the liquid)
	Airgap	2 µl
	Delay	100 ms
	Speed	20 µl s^{-1}
Dispense	Delay	100 ms
	Height	2 mm (from the bottom)
	Speed	20 µl s^{-1}
Mixing	Volume	10 µl x 2
	Aspirate height	2 mm (from the bottom)
	Aspirate speed	50 µl s^{-1}
	Dispense height	2 mm (from the bottom)
	Dispense speed	50 µl s^{-1}
Tip touch	Height	-1 mm (from the well top)
	Speed	75% of maximum

9.7 HTS

9.7.1 Plate layout

384 well plates were divided into three sections and compounds were screened 80 compounds at a time with 8 positive and a negative control assays per compound set. Plate layout was as shown in **Figure 9.16**.

	1	2	3	4	5	6	7
A	+	1	2	3	4	5	
B		6	7	8	9	10	+
C	-	11	12	13	14	15	
D		16	17	18	19	20	-
E	+	21	22	23	24	25	
F		26	27	28	29	30	+
G	-	31	32	33	34	35	
H		36	37	38	39	40	-
I	+	41	42	43	44	45	
J		46	47	48	49	50	+
K	-	51	52	53	54	55	
L		56	57	58	59	60	-
M	+	61	62	63	64	65	
N		66	67	68	69	70	+
O	-	71	72	73	74	75	
P		76	77	78	79	80	-

Figure 9.16 HTS plate layout

Single assay set, three assay sets in total per 384 well plate. + = positive control assay (no library compound), - = negative control assay (no library compound, no AdoMet), 1-80 = complete assays.

9.7.2 Sublibraries

9.7.2.1 Stibonic acid sublibrary

NSC identifier shown in **bold**, for *Y. pestis* Dam screen hits, NSC identifier is shown in **red**.

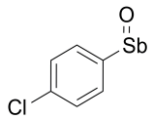

13731

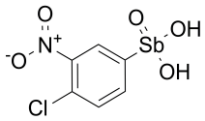

13735

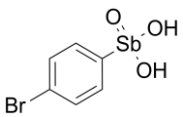

13740

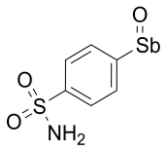

13741

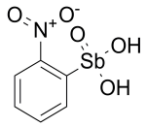

13742

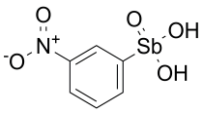

13743

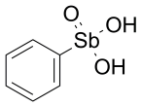

13744

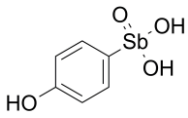

13745

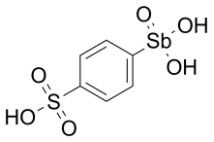

13746

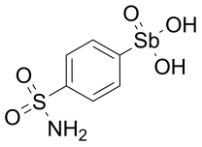

13748

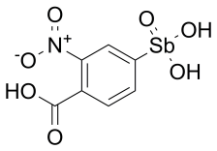

13755

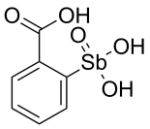

13758

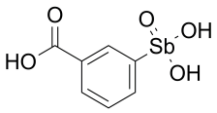

13759

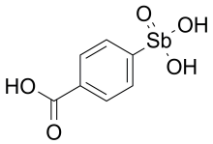

13760

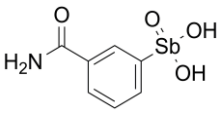

13765

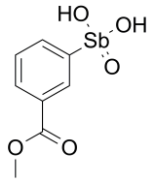

13771

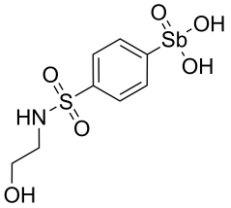

13776

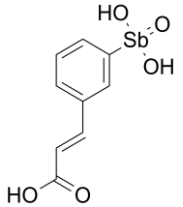

13778

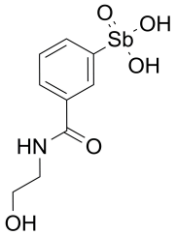

13782

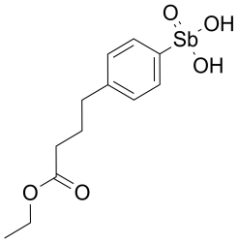

13793

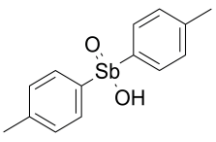

13794

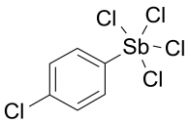

13935

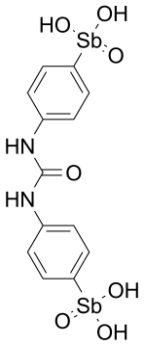

15408

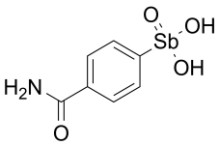

15575

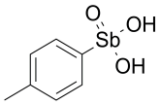

15577

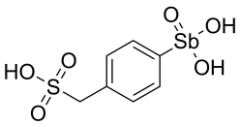

15578

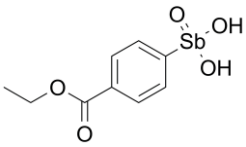

15583

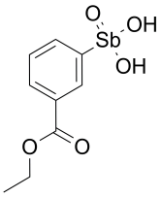

15584

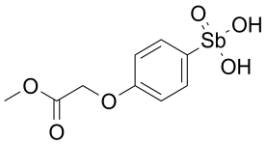

15585

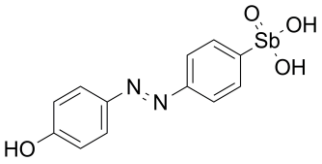

15591

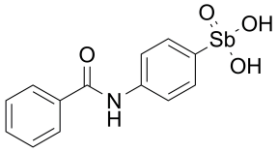

15596

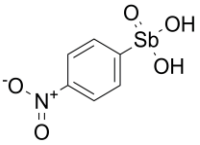

17164

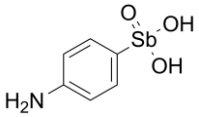

25176

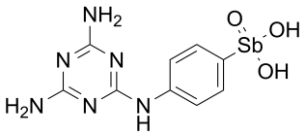

35015

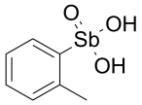

115831

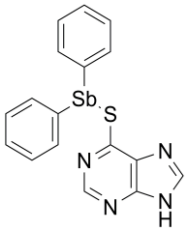

118018

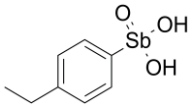

140279

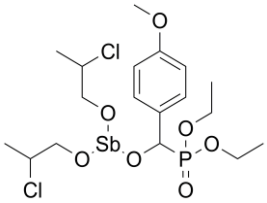

221126

9.7.2.2 Phosphonic acid sublibrary

NSC identifier shown in **bold**.

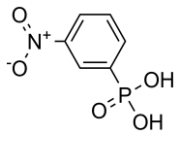

419

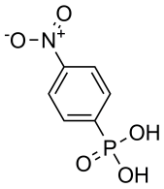

420

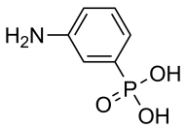

13007

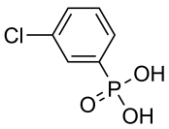

13559

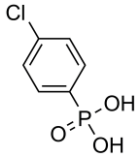

13560

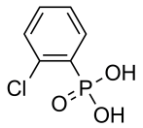

13561

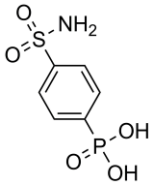

13562

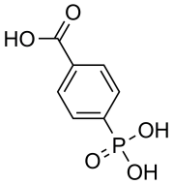

13565

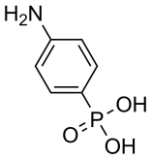

55744

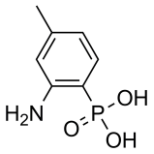

87207

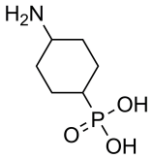

129447

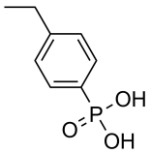

129452

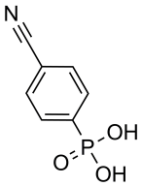

129453

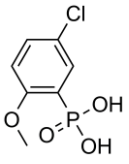

129456

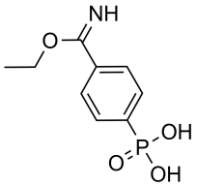

129457

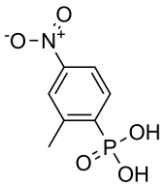

129458

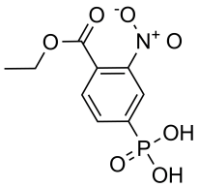

129459

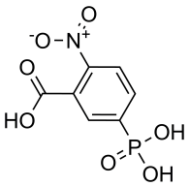

129460

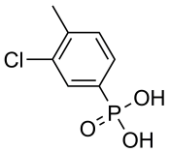

129461

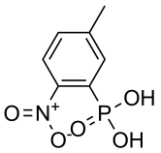

129462

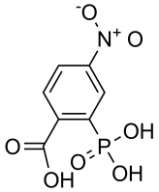

129463

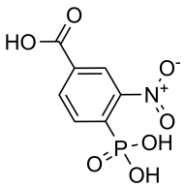

129464

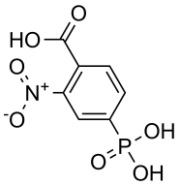

129465

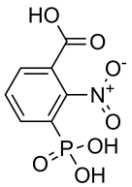

129466

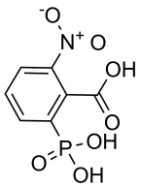

129467

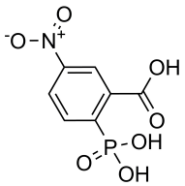

129468

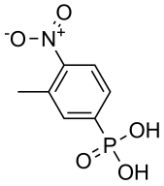

129469

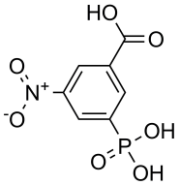

129474

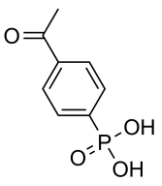

129475

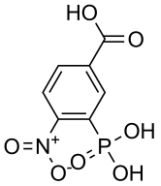

129478

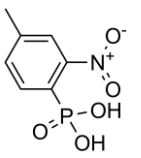

140271

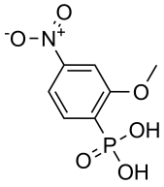

140272

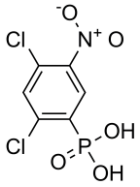

140290

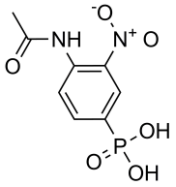

141170

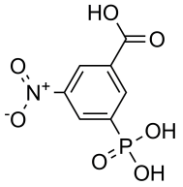

141172

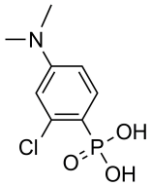

349096

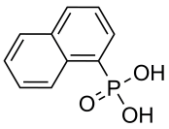

400340

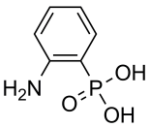

402274

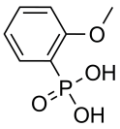

407831

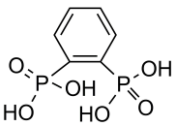

408071

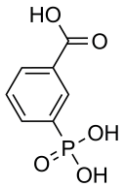

666474

9.8 mRNA profiling

Experiments were carried out at dstl Porton Down under containment level 3 by Dr M. I. Richards. Overnight cultures of *Y. pestis* GB were used to inoculate BAB media (10 ml) supplemented with $CaCl_2$ (2.5 mM), **13782** (20 µg ml^{-1}) and DMSO (0.025%). Controls lacking **13782** were also prepared. Cultures were incubated (37 °C, 180 rpm) to an OD_{590} of 0.4. Aliquots of culture (2 ml) were removed into Qiagen RNA Protect solution and mRNA extracted using the Qiagen RNeasy kit as per the manufacturer's instructions. RNA concentration was determined by nanodrop quantification and 1 mg ml^{-1} samples were prepared by ethanol precipitation followed by re-suspension with the appropriate volume of RNase-free water. Samples were stored at -80 °C until required. Hybridisations were carried out as described by Robinson *et al.* (*40*).

Whole genome microarrays based on strain CO92 were obtained from St Georges' Hospital Bacterial Microarray group at the University of London. All predicted CO92 coding sequences are represented on the microarray. Gene numbers refer to the published genome sequence annotation (*273*). Microarray slides were scanned using an Affymetrix 428 scanner (MWG Biotech, London, UK) with GenePix software. Subsequent GenePix analysis enabled spot quantification to be captured. Quantified data were loaded into Genespring 6.0 (Aglient, Cheshire, UK). Data were interpreted using the 'log of ratio' with the cross-gene error model switched off. A 2-fold difference in expression level between the wild-type and the mutant was set as the cut-off. Genes that demonstrated at least a 2-fold difference in expression level were tested by Student's t-test to determine that the difference was statistically significant. The Benjamini and Hochberg false discovery rate was used to correct for multiple testing. The results are a compilation of the gene expression profiles of three biological replicates grown on different days and two arrays of each replicate also performed on different days, resulting in a total of six arrays.

Table 9.6 *Y. pestis* genes showing >1.3-fold up-regulation during growth in the presence of compound **13782**

Gene ID	Annotation	Corrected p-value	p-value	FC Absolute*
Up-regulation				
nupC	Nucleoside permease	1.43E-03	2.28E-06	2.38
pCD1-yscJ	Putative type III secretion lipoprotein	1.21E-02	1.06E-04	2.26
YPO0473	Hypothetical protein	4.41E-03	2.11E-05	2.23
YPO2605	Conserved hypothetical protein	1.65E-03	4.59E-06	2.14
dacA	Cutative penicillin-binding protein 5	2.56E-02	4.49E-04	1.98
fabF	3-oxoacyl-[acyl-carrier-protein] synthase II	1.21E-02	9.97E-05	1.97
topA	DNA topoisomerase I	6.96E-04	8.30E-07	1.96
YPO1716	Putative transport protein	1.49E-03	3.08E-06	1.90
pCD1-27	Putative type III secretion protein	4.93E-03	2.55E-05	1.88
secD	Protein-export membrane protein SecD	2.44E-02	2.91E-04	1.88
YPO2422	Conserved hypothetical protein	2.53E-02	3.34E-04	1.81
dapX	Lipoprotein	2.53E-02	3.99E-04	1.80
prfA	Peptide chain release factor 1	7.20E-03	4.01E-05	1.78
ffh	Signal recognition particle protein	7.65E-03	4.56E-05	1.77
YPO2978	Putative membrane protein	4.13E-02	1.21E-03	1.76
YPO2875	GTP-binding protein	2.53E-02	4.17E-04	1.76
trmD	tRNA (guanine-N1)-methyltransferase	3.53E-02	8.60E-04	1.72
rpoH	RNA polymerase sigma-32 factor	2.53E-02	3.28E-04	1.69
yapA	Putative autotransporter protein	4.64E-02	1.57E-03	1.67
fabH	3-oxoacyl-[acyl-carrier-protein] synthase III	2.85E-02	5.33E-04	1.66
pCD1-sycE	Putative yopE chaperone	3.83E-02	1.04E-03	1.66

YPO2050	Conserved hypothetical protein	4.05E-02	1.18E-03	1.65
pCD1-yscX	Putative type III secretion protein	2.93E-03	1.25E-05	1.62
hemH	Ferrochelatase	3.53E-02	8.46E-04	1.60
pyrG	CTP synthase	3.83E-02	1.07E-03	1.60
YPO1575	Conserved hypothetical protein	4.97E-02	1.84E-03	1.59
ribD	Riboflavin biosynthesis protein RibD	2.22E-02	2.39E-04	1.57
cysP	Thiosulfate-binding protein	3.67E-02	9.42E-04	1.55
nadD	Putative nicotinate-nucleotide	1.21E-02	1.01E-04	1.52
purK	Phosphoribosylaminoimidazole carboxylase ATPase	4.96E-02	1.79E-03	1.52
rplM	50S ribosomal protein L13	3.53E-02	8.17E-04	1.51
nuoF	NADH dehydrogenase I chain F	3.53E-02	8.70E-04	1.51
atpI	ATP synthase protein I	1.21E-02	9.99E-05	1.51
pCD1-73c	Hypothetical protein	3.08E-02	6.01E-04	1.50
murB	UDP-N-acetylenolpyruvoylglucosamine reductase	2.53E-02	4.32E-04	1.50
tatC	Sec-independent protein translocase protein	1.71E-02	1.64E-04	1.50
mreC	Rod shape-determining protein MreC	4.67E-02	1.60E-03	1.49
speE	Spermidine synthase	2.53E-02	4.01E-04	1.45
tmk	Thymidylate kinase	2.53E-02	3.11E-04	1.40
pPMT1-85	-	3.26E-02	6.48E-04	1.36
YPO3170	Conserved hypothetical protein	4.36E-02	1.35E-03	1.35
YPO3857	Conserved hypothetical protein	3.53E-02	8.35E-04	1.32
guaC	GMP reductase	4.36E-02	1.35E-03	1.30

* Absolute fold-change.

Table 9.7 *Y. pestis* genes showing >1.3-fold down-regulation during growth in the presence of compound **13782**

Gene ID	Annotation	Corrected p-value	p-value	FCAbsolute [a]
Down-regulation				
YPO2304	Hypothetical protein	2.25E-02	2.60E-04	3.09
katA	Catalase	2.93E-03	1.26E-05	2.87
YPO1892	Putative oxidoreductase	2.53E-02	4.24E-04	2.74
YPO3279	Putative sigma 54 modulation protein	1.93E-02	1.98E-04	2.55
YPO3744	Hypothetical protein	2.25E-02	2.59E-04	2.49
YPO2675	Putative potassium channel protein	7.74E-03	4.92E-05	2.40
uspA	Universal stress protein A	1.49E-03	3.57E-06	2.39
YPO0735	Hypothetical protein	4.58E-02	1.53E-03	2.39
nrdA	Ribonucleoside-diphosphate reductase 1 alpha	1.93E-02	2.00E-04	2.34
narX	Nitrate/nitrite sensor protein	4.73E-02	1.68E-03	2.23
23s rRNA	23S ribosomal RNA	3.53E-02	8.36E-04	2.12
YPO0072	Bifunctional regulatory protein/DNA repair	3.78E-02	1.01E-03	2.06
YPO2705	Conserved hypothetical protein	2.93E-03	1.06E-05	1.99
YPO2745	Conserved hypothetical protein	3.48E-02	7.20E-04	1.97
YPO3556	Conserved hypothetical protein	3.89E-02	1.11E-03	1.97
YPO1354	Putative lipoprotein	4.29E-02	1.30E-03	1.96
YPO2935	Putative exported protein	2.93E-03	1.28E-05	1.94
YPO1536	Putative iron-siderophore transport system	4.58E-02	1.53E-03	1.90
YPO2197	Similar to *Vibrio cholerae* probable sulphate	3.06E-02	5.83E-04	1.88
frdC	Fumarate reductase hydrophobic protein	4.43E-02	1.39E-03	1.88
YPO1532	Putative siderophore biosynthetic enzyme	3.52E-02	7.42E-04	1.87
dps	Putative DNA-binding protein	3.67E-02	9.64E-04	1.87
YPO3649	Putative gamma carboxymuconolactone	4.49E-02	1.45E-03	1.87
YPO3527	Conserved hypothetical protein	4.67E-02	1.62E-03	1.84
ureE	Urease accessory protein	2.53E-02	4.06E-04	1.78

ureD	Urease accessory protein	2.67E-02	4.77E-04	1.76
YPO1736	Putative membrane protein	3.83E-02	1.06E-03	1.74
YPO0505	Conserved hypothetical protein	4.96E-02	1.80E-03	1.73
YPO1683	Conserved hypothetical protein	1.21E-02	9.99E-05	1.72
iucA	Similar to *Escherichia coli* aerobactin siderophore	4.47E-02	1.42E-03	1.72
YPO4020	Putative membrane protein	3.67E-02	9.53E-04	1.69
ybtT	*Yersiniabactin* biosynthetic protein YbtT	3.53E-02	8.61E-04	1.68
YPO0966	Putative kinase	2.83E-02	5.17E-04	1.67
YPO2672	Conserved hypothetical protein	3.60E-02	9.02E-04	1.66
16s rRNA	16S ribosomal RNA	4.71E-02	1.65E-03	1.64
napC	Cytochrome C-type protein NapC	1.30E-02	1.18E-04	1.64
YPO0273	Putative type III secretion apparatus protein	2.53E-02	4.14E-04	1.63
cueR	Putative regulatory protein	2.53E-02	3.91E-04	1.62
map	Methionine aminopeptidase	4.49E-02	1.47E-03	1.61
YPO0511a	Hypothetical protein	1.17E-02	7.93E-05	1.60
YPO1568	Hypothetical protein	3.53E-02	7.89E-04	1.58
pheT	Phenylalanyl-tRNA synthetase beta chain	4.24E-02	1.26E-03	1.52
nrdG	Anaerobic ribonucleoside-triphosphate reductase	3.83E-02	1.08E-03	1.48
YPO2846	Putitive ABC-transporter ATP-binding protein	2.53E-02	4.29E-04	1.43
YPO0265	Putative type III secretion system apparatus	3.34E-02	6.78E-04	1.38
YPO0969	Hypothetical protein	4.96E-02	1.81E-03	1.37
ssuB	Putative aliphatic sulfonates transport	2.53E-02	4.23E-04	1.37
YPO3978	Putative regulatory protein	3.53E-02	8.05E-04	1.31

* Absolute fold-change.

10 References

1. Waksman, S.A. (1947) What is an antibiotic or an antibiotic substance?, *Mycologia 39*, 565-569.
2. Davies, J., and Davies, D. (2010) Origins and evolution of antibiotic resistance, *Microbiol Mol Biol R 74*, 417-433.
3. Fleming, A. (2001) On the antibacterial action of cultures of a penicillium, with special reference to their use in the isolation of *B. influenzae*, *B World Health Organ 79*, 780-790.
4. Sykes, R. (2001) Penicillin: From discovery to product, *B World Health Organ 79*, 778-779.
5. Otten, H. (1986) Domagk and the development of the sulphonamides, *J Antimicrob Chemoth 17*, 689-696.
6. Bentley, R. (2009) Different roads to discovery; Prontosil (hence sulfa drugs) and penicillin (hence beta-lactams), *J Ind Microbiol Biot 36*, 775-786.
7. Van Epps, H.L. (2006) Rene Dubos: Unearthing antibiotics, *J Exp Med 203*, 259-259.
8. Chain, E., Florey, H.W., Gardner, A.D., Heatley, N.G., Jennings, M.A., Orr-Ewing, J., and Sanders, A.G. (1940) Penicillin as a chemotherapeutic agent, *Lancet 236*, 226-228.
9. Coates, A.R., Halls, G., and Hu, Y. (2011) Novel classes of antibiotics or more of the same?, *Brit J Pharmacol 163*, 184-194.
10. Powers, J.H. (2004) Antimicrobial drug development - the past, the present, and the future, *Clin Microbiol Infec 10 Suppl 4*, 23-31.
11. Fernandes, P. (2006) Antibacterial discovery and development - the failure of success?, *Nat Biotechnol 24*, 1497-1503.
12. Wright, G.D. (2007) The antibiotic resistome: The nexus of chemical and genetic diversity, *Nat Rev Microbiol 5*, 175-186.
13. Walsh, C., and Wright, G. (2005) Introduction: Antibiotic resistance, *Chem Rev 105*, 391-394.
14. Levy, S.B., and Marshall, B. (2004) Antibacterial resistance worldwide: Causes, challenges and responses, *Nat Med 10*, S122-129.
15. Abraham, E.P., and Chain, E. (1940) An enzyme from bacteria able to destroy penicillin, *Nature 146*, 837-837.
16. Forbes, G.B. (1949) Infection with penicillin-resistant staphylococci in hospital and general practice, *Brit Med J 2*, 569-571.
17. Alekshun, M.N., and Levy, S.B. (2007) Molecular mechanisms of antibacterial multidrug resistance, *Cell 128*, 1037-1050.
18. Iseman, M.D. (1993) Treatment of multidrug-resistant tuberculosis, *New Eng J Med 329*, 784.
19. Morar, M., and Wright, G.D. (2010) The genomic enzymology of antibiotic resistance, *Annu Rev Genet 44*, 25-51.
20. Martinez, J.L., Fajardo, A., Garmendia, L., Hernandez, A., Linares, J.F., Martinez-Solano, L., and Sanchez, M.B. (2009) A global view of antibiotic resistance, *FEMS Microbiol Rev 33*, 44-65.
21. Furuya, E.Y., and Lowy, F.D. (2006) Antimicrobial-resistant bacteria in the community setting, *Nat Rev Microbiol 4*, 36-45.
22. Walsh, C. (2000) Molecular mechanisms that confer antibacterial drug resistance, *Nature 406*, 775-781.
23. Perry, R.D., and Fetherston, J.D. (1997) *Yersinia pestis* - etiologic agent of plague, *Clin Microbiol Rev 10*, 35.
24. WHO. (2004) Human plague in 2002 and 2003, *Wkly Epidemiol Rec 79*, 301-306.
25. Schrag, S.J., and Wiener, P. (1995) Emerging infectious disease: What are the relative roles of ecology and evolution?, *Trends Ecol Evol 10*, 319-324.
26. Inglesby, T.V., Dennis, D.T., Henderson, D.A., Bartlett, J.G., Ascher, M.S., Eitzen, E., Fine, A.D., Friedlander, A.M., Hauer, J., Koerner, J.F., Layton, M., McDade, J.,

Osterholm, M.T., O'Toole, T., Parker, G., Perl, T.M., Russell, P.K., Schoch-Spana, M., and Tonat, K. (2000) Plague as a biological weapon: Medical and public health management. Working Group on Civilian Biodefense, *J Amer Med Assoc 283*, 2281-2290.

27. Frean, J.A., Arntzen, L., Capper, T., Bryskier, A., and Klugman, K.P. (1996) *In vitro* activities of 14 antibiotics against 100 human isolates of *Yersinia pestis* from a southern African plague focus, *Antimicrob Agents Ch 40*, 2646-2647.
28. Galimand, M., Guiyoule, A., Gerbaud, G., Rasoamanana, B., Chanteau, S., Carniel, E., and Courvalin, P. (1997) Multidrug resistance in *Yersinia pestis* mediated by a transferable plasmid, *New Eng J Med 337*, 677-680.
29. Guiyoule, A., Gerbaud, G., Buchrieser, C., Galimand, M., Rahalison, L., Chanteau, S., Courvalin, P., and Carniel, E. (2001) Transferable plasmid-mediated resistance to streptomycin in a clinical isolate of *Yersinia pestis*, *Emerg Infect Dis 7*, 43.
30. Hinnebusch, B.J., Rosso, M.L., Schwan, T.G., and Carniel, E. (2002) High frequency conjugative transfer of antibiotic resistance genes to *Yersinia pestis* in the flea midgut, *Mol Microbiol 46*, 349-354.
31. Galimand, M., Carniel, E., and Courvalin, P. (2006) Resistance of *Yersinia pestis* to antimicrobial agents, *Antimicrob Agents Ch 50*, 3233-3236.
32. Anisimov, A.P., and Amoako, K.K. (2006) Treatment of plague: promising alternatives to antibiotics, *J Med Microbiol 55*, 1461.
33. Cornelis, G.R., and Wolf Watz, H. (1997) The *Yersinia* Yop virulon: A bacterial system for subverting eukaryotic cells, *Mol Microbiol 23*, 861-867.
34. Chen, Y.T., Xie, J., and Seto, C.T. (2003) Peptidic-ketocarboxylic acids and sulfonamides as inhibitors of protein tyrosine phosphatases, *J Org Chem 68*, 4123-4125.
35. Xie, J., Comeau, A.B., and Seto, C.T. (2004) Squaric acids: A new motif for designing inhibitors of protein tyrosine phosphatases, *Org Lett 6*, 83-86.
36. Lee, K., Boovanahalli, S.K., Nam, K.Y., Kang, S.U., Lee, M., Phan, J., Wu, L., Waugh, D.S., Zhang, Z.Y., and No, K.T. (2005) Synthesis of tripeptides as potent *Yersinia* protein tyrosine phosphatase inhibitors, *Bioorg Med Chem Lett 15*, 4037-4042.
37. Nordfelth, R., Kauppi, A.M., Norberg, H.A., Wolf-Watz, H., and Elofsson, M. (2005) Small-molecule inhibitors specifically targeting type III secretion, *Infect Immun 73*, 3104.
38. Wren, B.W. (2000) Microbial genome analysis: Insights into virulence, host adaptation and evolution, *Nat Rev Genet 1*, 30-39.
39. Heusipp, G., Falker, S., and Schmidt, M.A. (2007) DNA adenine methylation and bacterial pathogenesis, *Int J Med Microbiol 297*, 1-7.
40. Robinson, V.L., Oyston, P.C., and Titball, R.W. (2005) A dam mutant of *Yersinia pestis* is attenuated and induces protection against plague, *FEMS Microbiol Lett 252*, 251-256.
41. Taylor, V.L., Titball, R.W., and Oyston, P.C.F. (2005) Oral immunization with a dam mutant of *Yersinia pseudotuberculosis* protects against plague, *Microbiology 151*, 1919.
42. Marinus, M.G., and Casadesus, J. (2009) Roles of DNA adenine methylation in host-pathogen interactions: mismatch repair, transcriptional regulation, and more, *FEMS Microbiol Rev 33*, 488-503.
43. Martin, J.L., and McMillan, F.M. (2002) SAM (dependent) I AM: the *S*-adenosylmethionine-dependent methyltransferase fold, *Curr Opin Struc Biol 12*, 783-793.
44. Cheng, X., and Blumenthal, R. (1999) *S-adenosylmethionine-dependent methyltransferases: Structures and functions*, World Scientific, Singapore; London.
45. Mannisto, P.T., and Kaakkola, S. (1999) Catechol-*O*-methyltransferase (COMT): Biochemistry, molecular biology, pharmacology, and clinical efficacy of the new selective COMT inhibitors, *Pharmacol Rev 51*, 593-628.
46. Tai, C.H., and Wu, R.M. (2002) Catechol-*O*-methyltransferase and Parkinson's disease, *Acta Med Okayama 56*, 1-6.

47. Ogawa, H., Gomi, T., Takusagawa, F., and Fujioka, M. (1998) Structure, function and physiological role of glycine *N*-methyltransferase, *Int J Biochem Cell B 30*, 13-26.
48. Luka, Z., Mudd, S.H., and Wagner, C. (2009) Glycine *N*-methyltransferase and regulation of *S*-adenosylmethionine levels, *J Biol Chem 284*, 22507.
49. Jones, B.L., and Kearns, G.L. (2011) Histamine: New thoughts about a familiar mediator, *Clin Pharmacol Ther 89*, 189-197.
50. Drinkwater, N., Gee, C.L., Puri, M., Criscione, K.R., McLeish, M.J., Grunewald, G.L., and Martin, J.L. (2009) Molecular recognition of physiological substrate noradrenaline by the adrenaline-synthesizing enzyme PNMT and factors influencing its methyltransferase activity, *Biochem J 422*, 463-471.
51. Gordon, N. (2010) Guanidinoacetate methyltransferase deficiency (GAMT), *Brain Dev 32*, 79-81.
52. Vance, D.E., and Vance, J.E. (2009) Physiological consequences of disruption of mammalian phospholipid biosynthetic genes, *J Lipid Res 50 Suppl*, S132-137.
53. Lee, D.Y., Teyssier, C., Strahl, B.D., and Stallcup, M.R. (2005) Role of protein methylation in regulation of transcription, *Endocr Rev 26*, 147.
54. Wolf, S.S. (2009) The protein arginine methyltransferase family: An update about function, new perspectives and the physiological role in humans, *Cell Mol Life Sci 66*, 2109-2121.
55. Paik, W.K., Paik, D.C., and Kim, S. (2007) Historical review: The field of protein methylation, *Trends Biochem Sci 32*, 146-152.
56. Dillon, S.C., Zhang, X., Trievel, R.C., and Cheng, X. (2005) The SET-domain protein superfamily: Protein lysine methyltransferases, *Genome Biol 6*, 227.
57. Smith, B.C., and Denu, J.M. (2009) Chemical mechanisms of histone lysine and arginine modifications, *Biochim Biophys Acta 1789*, 45-57.
58. Crain, P.F., and McCloskey, J.A. (1996) The RNA modification database, *Nucleic Acids Res 24*, 98.
59. Motorin, Y., and Grosjean, H. (2005) Transfer RNA modification, *eLS*.
60. Hou, Y.M., and Perona, J.J. (2010) Stereochemical mechanisms of tRNA methyltransferases, *FEBS Lett 584*, 278-286.
61. Jeltsch, A. (2002) Beyond Watson and Crick: DNA methylation and molecular enzymology of DNA methyltransferases, *Chembiochem 3*, 274-293.
62. Hattman, S. (2005) DNA-[adenine] methylation in lower eukaryotes, *Biochemistry (Moscow) 70*, 550-558.
63. Ratel, D., Ravanat, J.L., Berger, F., and Wion, D. (2006) *N*6-methyladenine: the other methylated base of DNA, *Bioessays 28*, 309-315.
64. Jones, P.A., and Takai, D. (2001) The role of DNA methylation in mammalian epigenetics, *Science 293*, 1068-1070.
65. Denis, H., Ndlovu, M.N., and Fuks, F. (2011) Regulation of mammalian DNA methyltransferases: A route to new mechanisms, *EMBO Rep*.
66. Lan, J., Hua, S., He, X., and Zhang, Y. (2010) DNA methyltransferases and methyl-binding proteins of mammals, *Acta Biochim Biophys Sin 42*, 243-252.
67. Gopalakrishnan, S., Van Emburgh, B.O., and Robertson, K.D. (2008) DNA methylation in development and human disease, *Mutat Res 647*, 30-38.
68. Issa, J.-P.J., and Kantarjian, H.M. (2009) Targeting DNA methylation, *Clin Cancer Res 15*, 3938-3946.
69. Cheng, X., and Roberts, R.J. (2001) AdoMet-dependent methylation, DNA methyltransferases and base flipping, *Nucleic Acids Res 29*, 3784-3795.
70. Buryanov, Y.I., and Shevchuk, T.V. (2005) DNA methyltransferases and structural-functional specificity of eukaryotic DNA modification, *Biochemistry (Moscow) 70*, 730-742.
71. Bheemanaik, S., Reddy, Y.V., and Rao, D.N. (2006) Structure, function and mechanism of exocyclic DNA methyltransferases, *Biochem J 399*, 177-190.
72. Roberts, R.J., and Cheng, X. (1998) Base flipping, *Annu Rev Biochem 67*, 181-198.
73. Wu, J.C., and Santi, D.V. (1987) Kinetic and catalytic mechanism of HhaI methyltransferase, *J Biol Chem 262*, 4778.

74. Pogolotti, A.L., Ono, A., Subramaniam, R., and Santi, D.V. (1988) On the mechanism of DNA-adenine methylase, *J Biol Chem 263*, 7461.
75. Casadesus, J., and Low, D. (2006) Epigenetic gene regulation in the bacterial world, *Microbiol Mol Biol R 70*, 830-856.
76. Wion, D., and Casadesus, J. (2006) *N*6-methyl-adenine: An epigenetic signal for DNA-protein interactions, *Nat Rev Microbiol 4*, 183-192.
77. Pettersen, E.F., Goddard, T.D., Huang, C.C., Couch, G.S., Greenblatt, D.M., Meng, E.C., and Ferrin, T.E. (2004) UCSF Chimera - a visualization system for exploratory research and analysis, *J Comput Chem 25*, 1605-1612.
78. Boye, E., Løbner-Olesen, A., and Skarstad, K. (2000) Limiting DNA replication to once and only once, *EMBO Rep 1*, 479-483.
79. Iyer, R.R., Pluciennik, A., Burdett, V., and Modrich, P.L. (2006) DNA mismatch repair: Functions and mechanisms, *Chem Rev 106*, 302-323.
80. Wang, T.-C., V., and Smith, K.C. (1986) Inviability of *dam recA* and *dam recB* cells of *Escherichia coli* is correlated with their inability to repair DNA double-strand breaks produced by mismatch repair, *J Bacteriol 165*, 1023.
81. Low, D.A., and Casadesus, J. (2008) Clocks and switches: Bacterial gene regulation by DNA adenine methylation, *Curr Opin Microbiol 11*, 106-112.
82. Hernday, A.D., Braaten, B.A., and Low, D.A. (2003) The mechanism by which DNA adenine methylase and papI activate the pap epigenetic switch, *Mol Cell 12*, 947-957.
83. García-Del Portillo, F., Pucciarelli, M.G., and Casadesús, J. (1999) DNA adenine methylase mutants of *Salmonella typhimurium* show defects in protein secretion, cell invasion, and M cell cytotoxicity, *Proc Natl Acad Sci USA 96*, 11578.
84. Heithoff, D.M., Sinsheimer, R.L., Low, D.A., and Mahan, M.J. (1999) An essential role for DNA adenine methylation in bacterial virulence, *Science 284*, 967-970.
85. Oza, J.P., Yeh, J.B., and Reich, N.O. (2005) DNA methylation modulates *Salmonella enterica* serovar Typhimurium virulence in *Caenorhabditis elegans*, *FEMS Microbiol Lett 245*, 53-59.
86. Watson Jr, M.E., Jarisch, J., and Smith, A.L. (2004) Inactivation of deoxyadenosine methyltransferase (dam) attenuates *Haemophilus influenzae* virulence, *Mol Microbiol 53*, 651-664.
87. Julio, S.M., Heithoff, D.M., Provenzano, D., Klose, K.E., Sinsheimer, R.L., Low, D.A., and Mahan, M.J. (2001) DNA adenine methylase is essential for viability and plays a role in the pathogenesis of *Yersinia pseudotuberculosis* and *Vibrio cholerae*, *Infect Immun 69*, 7610-7615.
88. Chen, L., Paulsen, D.B., Scruggs, D.W., Banes, M.M., Reeks, B.Y., and Lawrence, M.L. (2003) Alteration of DNA adenine methylase (Dam) activity in *Pasteurella multocida* causes increased spontaneous mutation frequency and attenuation in mice, *Microbiology 149*, 2283.
89. Erova, T.E., Pillai, L., Fadl, A.A., Sha, J., Wang, S., Galindo, C.L., and Chopra, A.K. (2006) DNA adenine methyltransferase influences the virulence of *Aeromonas hydrophila*, *Infect Immun 74*, 410.
90. Yang, Z., Horton, J.R., Zhou, L., Zhang, X.J., Dong, A., Zhang, X., Schlagman, S.L., Kossykh, V., Hattman, S., and Cheng, X. (2003) Structure of the bacteriophage T4 DNA adenine methyltransferase, *Nat Struct Biol 10*, 849-855.
91. Horton, J.R., Liebert, K., Hattman, S., Jeltsch, A., and Cheng, X. (2005) Transition from nonspecific to specific DNA interactions along the substrate-recognition pathway of dam methyltransferase, *Cell 121*, 349-361.
92. Horton, J.R., Liebert, K., Bekes, M., Jeltsch, A., and Cheng, X. (2006) Structure and substrate recognition of the *Escherichia coli* DNA adenine methyltransferase, *J Mol Biol 358*, 559-570.
93. Liebert, K., Horton, J.R., Chahar, S., Orwick, M., Cheng, X., and Jeltsch, A. (2007) Two alternative conformations of *S*-adenosyl-L-homocysteine bound to *Escherichia coli* DNA adenine methyltransferase and the implication of conformational changes in regulating the catalytic cycle, *J Biol Chem 282*, 22848-22855.

94. Malone, T., Blumenthal, R.M., and Cheng, X. (1995) Structure-guided analysis reveals nine sequence motifs conserved among DNA amino-methyl-transferases, and suggests a catalytic mechanism for these enzymes, *J Mol Biol 253*, 618-632.
95. Clamp, M., Cuff, J., Searle, S.M., and Barton, G.J. (2004) The Jalview Java alignment editor, *Bioinformatics 20*, 426-427.
96. Waterhouse, A.M., Procter, J.B., Martin, D.M., Clamp, M., and Barton, G.J. (2009) Jalview Version 2 - A multiple sequence alignment editor and analysis workbench, *Bioinformatics 25*, 1189-1191.
97. Malygin, E.G., Evdokimov, A.A., Zinoviev, V.V., Ovechkina, L.G., Lindstrom, W.M., Reich, N.O., Schlagman, S.L., and Hattman, S. (2001) A dual role for substrate *S*-adenosyl-L-methionine in the methylation reaction with bacteriophage T4 Dam DNA-[*N*6-adenine]-methyltransferase, *Nucleic Acids Res 29*, 2361-2369.
98. Liebert, K., Hermann, A., Schlickenrieder, M., and Jeltsch, A. (2004) Stopped-flow and mutational analysis of base flipping by the *Escherichia coli* Dam DNA-(adenine-*N*6)-methyltransferase, *J Mol Biol 341*, 443-454.
99. Urig, S., Gowher, H., Hermann, A., Beck, C., Fatemi, M., Humeny, A., and Jeltsch, A. (2002) The *Escherichia coli* Dam DNA methyltransferase modifies DNA in a highly processive reaction, *J Mol Biol 319*, 1085-1096.
100. Zinoviev, V.V., Evdokimov, A.A., Malygin, E.G., Schlagman, S.L., and Hattman, S. (2003) Bacteriophage T4 Dam DNA-(*N*6-adenine)-methyltransferase. Processivity and orientation to the methylation target, *J Biol Chem 278*, 7829-7833.
101. Malygin, E.G., Sclavi, B., Zinoviev, V.V., Evdokimov, A.A., Hattman, S., and Buckle, M. (2004) Bacteriophage T4Dam DNA-(adenine-*N*6)-methyltransferase. Comparison of pre-steady state and single turnover methylation of 40-mer duplexes containing two (un)modified target sites, *J Biol Chem 279*, 50012-50018.
102. Peterson, S.N., and Reich, N.O. (2006) GATC flanking sequences regulate Dam activity: Evidence for how Dam specificity may influence pap expression, *J Mol Biol 355*, 459-472.
103. Coffin, S.R., and Reich, N.O. (2009) *Escherichia coli* DNA adenine methyltransferase: Intrasite processivity and substrate-induced dimerization and activation, *Biochemistry 48*, 7399-7410.
104. Coffin, S.R., and Reich, N.O. (2009) *Escherichia coli* DNA adenine methyltransferase: The structural basis of processive catalysis and indirect read-out, *J Biol Chem 284*, 18390-18400.
105. Mashhoon, N., Carroll, M., Pruss, C., Eberhard, J., Ishikawa, S., Estabrook, R.A., and Reich, N. (2004) Functional characterization of *Escherichia coli* DNA adenine methyltransferase, a novel target for antibiotics, *J Biol Chem 279*, 52075-52081.
106. Malygin, E.G., Lindstrom, W.M., Jr., Schlagman, S.L., Hattman, S., and Reich, N.O. (2000) Pre-steady state kinetics of bacteriophage T4 dam DNA-[*N*(6)-adenine] methyltransferase: interaction with native (GATC) or modified sites, *Nucleic Acids Res 28*, 4207-4211.
107. Malygin, E.G., Lindstrom, W.M., Jr., Zinoviev, V.V., Evdokimov, A.A., Schlagman, S.L., Reich, N.O., and Hattman, S. (2003) acteriophage T4Dam (DNA-(adenine-*N*6)-methyltransferase): Evidence for two distinct stages of methylation under single turnover conditions, *J Biol Chem 278*, 41749-41755.
108. Malygin, E.G., Zinoviev, V.V., Petrov, N.A., Evdokimov, A.A., Jen-Jacobson, L., Kossykh, V.G., and Hattman, S. (1999) Effect of base analog substitutions in the specific GATC site on binding and methylation of oligonucleotide duplexes by the bacteriophage T4 Dam DNA-[*N*6-adenine] methyltransferase, *Nucleic Acids Res 27*, 1135-1144.
109. Zinoviev, V.V., Evdokimov, A.A., Gorbunov, Y.A., Malygin, E.G., Kossykh, V.G., and Hattman, S. (1998) Phage T4 DNA [*N*6-adenine] methyltransferase: Kinetic studies using oligonucleotides containing native or modified recognition sites, *Biol Chem 379*, 481-488.

110. Urieli-Shoval, S., Gruenbaum, Y., and Razin, A. (1983) Sequence and substrate specificity of isolated DNA methylases from *Escherichia coli* C, *J Bacteriol 153*, 274.
111. Lyko, F., and Brown, R. (2005) DNA methyltransferase inhibitors and the development of epigenetic cancer therapies, *J Natl Cancer I 97*, 1498.
112. Bonifácio, M.J., Palma, P.N., Almeida, L., and Soares da Silva, P. (2007) Catechol-*O*-methyltransferase and its inhibitors in Parkinson's Disease, *CNS Drug Rev 13*, 352-379.
113. Ueland, P.M. (1982) Pharmacological and biochemical aspects of *S*-adenosylhomocysteine and *S*-adenosylhomocysteine hydrolase, *Pharmacol Rev 34*, 223-253.
114. Borchardt, R.T., Huber, J.A., and Wu, Y.S. (1974) Potential inhibitors of *S*-adenosylmethionine-dependent methyltransferases. 2. Modification of the base portion of *S*-adenosylhomocysteine, *J Med Chem 17*, 868-873.
115. Borchardt, R.T., and Wu, Y.S. (1974) Potential inhibitors of *S*-adenosylmethionine-dependent methyltransferases. 1. Modification of the amino acid portion of *S*-adenosylhomocysteine, *J Med Chem 17*, 862-868.
116. Borchardt, R.T., Huber, J.A., and Wu, Y.S. (1976) Potential inhibitors of *S*-adenosylmethionine-dependent methyltransferases. 4. Further modifications of the amino acid and base portions of *S*-adenosyl-L-homocysteine, *J Med Chem 19*, 1094-1099.
117. Borchardt, R.T., and Wu, Y.S. (1975) Potential inhibitors of *S*-adenosylmethionine-dependent methyltransferases. 3. Modifications of the sugar portion of *S*-adenosylhomocysteine, *J Med Chem 18*, 300-304.
118. Borchardt, R.T., and Wu, Y.S. (1976) Potential inhibitors of *S*-adenosylmethionine-dependent methyltransferases. 5. Role of the asymmetric sulfonium pole in enzymatic binding of *S*-adenosyl-L-methionine, *J Med Chem 19*, 1099-1103.
119. Borchardt, R.T., Wu, Y.S., Huber, J.A., and Wycpalek, A.F. (1976) Potential Inhibitors of *S*-adenosylmethionine-dependent methyltransferases. 6. Structural modifications of *S*-adenosylmethionine, *J Med Chem 19*, 1104-1110.
120. Coward, J.K., Bussolotti, D.L., and Chang, C.D. (1974) Analogs of *S*-adenosylhomocysteine as potential inhibitors of biological transmethylation. Inhibition of several methylases by *S*-tubercidinylhomocysteine, *J Med Chem 17*, 1286-1289.
121. Coward, J.K., and Slisz, E.P. (1973) Analogs of *S*-adenosylhomocysteine as potential inhibitors of biological transmethylation. Specificity of the *S*-adenosylhomocysteine binding site, *J Med Chem 16*, 460-463.
122. Boeck, L.D., Clem, G.M., Wilson, M.M., and Westhead, J.E. (1973) A9145, a new adenine-containing antifungal antibiotic: fermentation, *Antimicrob Agents Ch 3*, 49.
123. Pugh, C.S., Borchardt, R.T., and Stone, H.O. (1978) Sinefungin, a potent inhibitor of virion mRNA(guanine-7-)-methyltransferase, mRNA(nucleoside-2'-)-methyltransferase, and viral multiplication, *J Biol Chem 253*, 4075-4077.
124. Fuller, R.W., and Nagarajan, R. (1978) Inhibition of methyltransferases by some new analogs of *S*-adenosylhomocysteine, *Biochem Pharmacol 27*, 1981.
125. Billich, A., and Zocher, R. (1987) *N*-Methyltransferase function of the multifunctional enzyme enniatin synthetase, *Biochemistry 26*, 8417-8423.
126. Reich, N.O., and Mashhoon, N. (1990) Inhibition of EcoRI DNA methylase with cofactor analogs, *J Biol Chem 265*, 8966-8970.
127. Schluckebier, G., Kozak, M., Bleimling, N., Weinhold, E., and Saenger, W. (1997) Differential binding of *S*-adenosylmethionine *S*-adenosylhomocysteine and Sinefungin to the adenine-specific DNA methyltransferase M.TaqI, *J Mol Biol 265*, 56-67.
128. Blanchard, P., Dodic, N., Fourrey, J.L., Lawrence, F., Mouna, A.M., and Robertgero, M. (1991) Synthesis and biological activity of sinefungin analogs, *J Med Chem 34*, 2798-2803.

129. Kumar, R., Srivastava, R., Singh, R.K., Surolia, A., and Rao, D.N. (2008) Activation and inhibition of DNA methyltransferases by *S*-adenosyl-L-homocysteine analogues, *Bioorg Med Chem 16*, 2276-2285.
130. Saavedra, O.M., Isakovic, L., Llewellyn, D.B., Zhan, L., Bernstein, N., Claridge, S., Raeppel, F., Vaisburg, A., Elowe, N., Petschner, A.J., Rahil, J., Beaulieu, N., MacLeod, A.R., Delorme, D., Besterman, J.M., and Wahhab, A. (2009) SAR around (l)-*S*-adenosyl-L-homocysteine, an inhibitor of human DNA methyltransferase (DNMT) enzymes, *Bioorg Med Chem Lett 19*, 2747-2751.
131. Isakovic, L., Saavedra, O.M., Llewellyn, D.B., Claridge, S., Zhan, L., Bernstein, N., Vaisburg, A., Elowe, N., Petschner, A.J., and Rahil, J. (2009) Constrained (l)-*S*-adenosyl-L-homocysteine (SAH) analogues as DNA methyltransferase inhibitors, *Bioorg Med Chem Lett 19*, 2742-2746.
132. Broom, A.D. (1989) Rational design of enzyme inhibitors: Multisubstrate analog inhibitors, *J Med Chem 32*, 2-7.
133. Le Calvez, P.B., Scott, C.J., and Migaud, M.E. (2009) Multisubstrate adduct inhibitors: Drug design and biological tools, *J Enz Inhib Med Ch 24*, 1291-1318.
134. Mori, S., Iwase, K., Iwanami, N., Tanaka, Y., Kagechika, H., and Hirano, T. (2010) Development of novel bisubstrate-type inhibitors of histone methyltransferase SET7/9, *Bioorg Med Chem 18*, 8158-8166.
135. Dowden, J., Hong, W., Parry, R.V., Pike, R.A., and Ward, S.G. (2010) Toward the development of potent and selective bisubstrate inhibitors of protein arginine methyltransferases, *Bioorg Med Chem Lett 20*, 2103-2105.
136. Lerner, C., Masjost, B., Ruf, A., Gramlich, V., Jakob-Roetne, R., Zürcher, G., Borroni, E., and Diederich, F. (2003) Bisubstrate inhibitors for the enzyme catechol-*O*-methyltransferase (COMT): Influence of inhibitor preorganisation and linker length between the two substrate moieties on binding affinity, *Org Biomol Chem 1*, 42-49.
137. Ellermann, M., Jakob-Roetne, R., Lerner, C., Borroni, E., Schlatter, D., Roth, D., Ehler, A., Rudolph, M.G., and Diederich, F. (2009) Molecular recognition at the active site of catechol-*O*-methyltransferase: Energetically favorable replacement of a water molecule imported by a bisubstrate inhibitor, *Angew Chem Int Edit 48*, 9092-9096.
138. Anderson, G.L., Bussolotti, D.L., and Coward, J.K. (1981) Synthesis and evaluation of some stable multisubstrate adducts as inhibitors of catechol-*O*-methyltransferase, *J Med Chem 24*, 1271-1277.
139. Masjost, B., Ballmer, P., Borroni, E., Zürcher, G., Winkler, F.K., Jakob Roetne, R., and Diederich, F. (2000) Structure based design, synthesis, and *in vitro* evaluation of bisubstrate inhibitors for catechol-*O*-methyltransferase (COMT), *Chem-Eur J 6*, 971-982.
140. Paulini, R., Lerner, C., Diederich, F., Jakob Roetne, R., Zürcher, G., and Borroni, E. (2006) Synthesis and biological evaluation of potent bisubstrate inhibitors of the enzyme catechol-*O*-methyltransferase (COMT) lacking a nitro group, *Helv Chim Acta 89*, 1856-1887.
141. Vaubourgeix, J., Bardou, F., Boissier, F., Julien, S., Constant, P., Ploux, O., Daffe, M., Quemard, A., and Mourey, L. (2009) *S*-adenosyl-*N*-decyl-aminoethyl, a potent bisubstrate inhibitor of *Mycobacterium tuberculosis* mycolic acid methyltransferases, *J Biol Chem 284*, 19321-19330.
142. Wahnon, D.C., Shier, V.K., and Benkovic, S.J. (2001) Mechanism-based inhibition of an essential bacterial adenine DNA methyltransferase: Rationally designed antibiotics, *J Am Chem Soc 123*, 976-977.
143. Gowher, H., and Jeltsch, A. (2004) Mechanism of inhibition of DNA methyltransferases by cytidine analogs in cancer therapy, *Cancer Biol Ther 3*, 1062.
144. Goffin, J., and Eisenhauer, E. (2002) DNA methyltransferase inhibitors-State of the art, *Ann Oncol 13*, 1699-1716.
145. Yan, L., Nass, S.J., Smith, D., Nelson, W.G., Herman, J.G., and Davidson, N.E. (2003) Specific inhibition of DNMT1 by antisense oligonucleotides induces re-expression of estrogen receptor-alpha (ER) in ER-negative human breast cancer cell lines, *Cancer Biol Ther 2*, 552.

146. Ruiz-Herrera, J., Ruiz-Medrano, R., and Domínguez, A. (1995) Selective inhibition of cytosine-DNA methylases by polyamines, *FEBS Lett 357*, 192-196.
147. Benkovic, S.J., Baker, S.J., Alley, M.R., Woo, Y.H., Zhang, Y.K., Akama, T., Mao, W., Baboval, J., Rajagopalan, P.T., Wall, M., Kahng, L.S., Tavassoli, A., and Shapiro, L. (2005) Identification of borinic esters as inhibitors of bacterial cell growth and bacterial methyltransferases, CcrM and MenH, *J Med Chem 48*, 7468-7476.
148. Lee, V., Benkovic, S.J., Baker, S.J., Maples, K.R., Akama, T., Zhang, Y.K., Singh, R., Sauro, V.A., Pandit, C., and Su, Z. (2011) Antibiotics containing borinic acid complexes and methods of use, Anacor Pharmaceuticals Inc.
149. Mashhoon, N., Pruss, C., Carroll, M., Johnson, P.H., and Reich, N.O. (2006) Selective inhibitors of bacterial DNA adenine methyltransferases, *J Biomol Screen 11*, 497-510.
150. Naumann, T.A., Tavassoli, A., and Benkovic, S.J. (2008) Genetic selection of cyclic peptide Dam methyltransferase inhibitors, *Chembiochem 9*, 194-197.
151. Cheng, B., Horton, J.R., Yang, Z., Kalman, D., Zhang, X., Hattman, S., and Jeltsch, A. (2006) Small molecule inhibitors of bacterial Dam DNA methyltransferases, (Organisation, W.I.P., Ed.).
152. Rubin, R.A., and Modrich, P. (1977) EcoRI methylase. Physical and catalytic properties of the homogeneous enzyme, *J Biol Chem 252*, 7265.
153. Schurter, B.T., Koh, S.S., Chen, D., Bunick, G.J., Harp, J.M., Hanson, B.L., Henschen-Edman, A., Mackay, D.R., Stallcup, M.R., and Aswad, D.W. (2001) Methylation of histone H3 by coactivator-associated arginine methyltransferase 1, *Biochemistry 40*, 5747-5756.
154. Jeltsch, A., Friedrich, T., and Roth, M. (1998) Kinetics of methylation and binding of DNA by the EcoRV adenine-N-6 methyltransferase, *J Mol Biol 275*, 747-758.
155. Zhang, X., Tamaru, H., Khan, S.I., Horton, J.R., Keefe, L.J., Selker, E.U., and Cheng, X. (2002) Structure of the Neurospora SET domain protein DIM-5, a histone H3 lysine methyltransferase, *Cell 111*, 117-127.
156. Roth, M., and Jeltsch, A. (2000) Biotin-avidin microplate assay for the quantitative analysis of enzymatic methylation of DNA by DNA methyltransferases, *Biol Chem 381*, 269-272.
157. Gowher, H., Zhang, X., Cheng, X., and Jeltsch, A. (2005) Avidin plate assay system for enzymatic characterization of a histone lysine methyltransferase, *Anal Biochem 342*, 287-291.
158. Jeltsch, A., Christ, F., Fatemi, M., and Roth, M. (1999) On the substrate specificity of DNA methyltransferases. Adenine-*N*6 DNA methyltransferases also modify cytosine residues at position *N*4, *J Biol Chem 274*, 19538-19544.
159. Hübscher, U., Pedrali-Noy, G., Knust-Kron, B., Doerfler, W., and Spadari, S. (1985) DNA methyltransferases: Activity minigel analysis and determination with DNA covalently bound to a solid matrix, *Anal Biochem 150*, 442-448.
160. Dorgan, K.M., Wooderchak, W.L., Wynn, D.P., Karschner, E.L., Alfaro, J.F., Cui, Y., Zhou, Z.S., and Hevel, J.M. (2006) An enzyme-coupled continuous spectrophotometric assay for *S*-adenosylmethionine-dependent methyltransferases, *Anal Biochem 350*, 249-255.
161. Hendricks, C.L., Ross, J.R., Pichersky, E., Noel, J.P., and Zhou, Z.S. (2004) An enzyme-coupled colorimetric assay for *S*-adenosylmethionine-dependent methyltransferases, *Anal Biochem 326*, 100-105.
162. Wang, C., Leffler, S., Thompson, D.H., and Hrycyna, C.A. (2005) A general fluorescence-based coupled assay for *S*-adenosylmethionine-dependent methyltransferases, *Biochem Biophys Res Commun 331*, 351-356.
163. Collazo, E., Couture, J.F., Bulfer, S., and Trievel, R.C. (2005) A coupled fluorescent assay for histone methyltransferases, *Anal Biochem 342*, 86-92.
164. Salyan, M.E.K., Pedicord, D.L., Bergeron, L., Mintier, G.A., Hunihan, L., Kuit, K., Balanda, L.A., Robertson, B.J., Feder, J.N., Westphal, R., Shipkova, P.A., and Blat, Y. (2006) A general liquid chromatography/mass spectroscopy-based assay for detection and quantitation of methyltransferase activity, *Anal Biochem 349*, 112-117.

165. Graves, T.L., Zhang, Y., and Scott, J.E. (2008) A universal competitive fluorescence polarization activity assay for S-adenosylmethionine utilizing methyltransferases, *Anal Biochem 373*, 296-306.
166. Liu, T., Zhao, J., Zhang, D.M., and Li, G.X. (2010) Novel method to detect DNA methylation using gold nanoparticles coupled with enzyme-linkage reactions, *Anal Chem 82*, 229-233.
167. Li, W., Liu, Z.L., Lin, H., Nie, Z., and Chen, J.H. (2010) Label-free colorimetric assay for methyltransferase activity based on a novel methylation-responsive DNAzyme strategy, *Anal Chem 82*, 1935-1941.
168. Woo, Y.H., Rajagopalan, P.T.R., and Benkovic, S.J. (2005) A nonradioactive DNA methyltransferase assay adaptable to high-throughput screening, *Anal Biochem 340*, 336-340.
169. Biggins, J.B., Prudent, J.R., Marshall, D.J., Ruppen, M., and Thorson, J.S. (2000) A continuous assay for DNA cleavage: The application of "break lights" to enediynes, iron-dependent agents, and nucleases, *Proc Natl Acad Sci USA 97*, 13537-13542.
170. Li, J., Yan, H.F., Wang, K.M., Tan, W.H., and Zhou, X.W. (2007) Hairpin fluorescence DNA probe for real-time monitoring of DNA methylation, *Anal Chem 79*, 1050-1056.
171. Wood, R.J., Maynard-Smith, M.D., Robinson, V.L., Oyston, P.C., Titball, R.W., and Roach, P.L. (2007) Kinetic analysis of *Yersinia pestis* DNA adenine methyltransferase activity using a hemimethylated molecular break light oligonucleotide, *PLoS ONE 2*, e801.
172. Wood, R.J., McKelvie, J.C., Maynard-Smith, M.D., and Roach, P.L. (2010) A real-time assay for CpG-specific cytosine-C5 methyltransferase activity, *Nucleic Acids Res 38*, e107.
173. DiMasi, J.A., Hansen, R.W., and Grabowski, H.G. (2003) The price of innovation: New estimates of drug development costs, *J Health Econ 22*, 151-185.
174. Dimasi, J.A. (2001) Risks in new drug development: Approval success rates for investigational drugs, *Clin Pharmacol Ther 69*, 297-307.
175. Cayen, M.N. (2010) Drug Discovery and Early Drug Development, In *Early Drug Development: Strategies and Routes to First-in-Human Trials*, pp 3-24, John Wiley & Sons, Inc.
176. Ashburn, T.T., and Thor, K.B. (2004) Drug repositioning: Identifying and developing new uses for existing drugs, *Nat Rev Drug Discov 3*, 673-683.
177. Overington, J.P., Al-Lazikani, B., and Hopkins, A.L. (2006) How many drug targets are there?, *Nat Rev Drug Discov 5*, 993-996.
178. Mayr, L.M., and Bojanic, D. (2009) Novel trends in high-throughput screening, *Curr Opin Pharmacol 9*, 580-588.
179. Wang, S., Sim, T.B., Kim, Y.S., and Chang, Y.T. (2004) Tools for target identification and validation, *Curr Opin Chem Biol 8*, 371-377.
180. Chan, J.N., Nislow, C., and Emili, A. (2010) Recent advances and method development for drug target identification, *Trends Pharmacol Sci 31*, 82-88.
181. Goddard, J.P., and Reymond, J.L. (2004) Enzyme assays for high-throughput screening, *Curr Opin Biotech 15*, 314-322.
182. Blundell, T.L., and Patel, S. (2004) High-throughput X-ray crystallography for drug discovery, *Curr Opin Pharmacol 4*, 490-496.
183. Pellecchia, M., Bertini, I., Cowburn, D., Dalvit, C., Giralt, E., Jahnke, W., James, T.L., Homans, S.W., Kessler, H., and Luchinat, C. (2008) Perspectives on NMR in drug discovery: a technique comes of age, *Nat Rev Drug Discov 7*, 738.
184. Sinz, A. (2007) Investigation of protein-ligand interactions by mass spectrometry, *Chemmedchem 2*, 425-431.
185. Chaires, J.B. (2008) Calorimetry and thermodynamics in drug design, *Annu Rev Biophys 37*, 135-151.
186. Yu, D., Blankert, B., Viré, J.C., and Kauffmann, J.M. (2005) Biosensors in drug discovery and drug analysis, *Anal Lett 38*, 1687-1701.
187. Renaud, J.P., and Delsuc, M.A. (2009) Biophysical techniques for ligand screening and drug design, *Curr Opin Pharmacol 9*, 622-628.

188. Sundberg, S.A. (2000) High-throughput and ultra-high-throughput screening: Solution- and cell-based approaches, *Curr Opin Biotech 11*, 47-53.
189. Lundblad, R.L. (2001) Approach to assay validation for the development of biopharmaceuticals, *Biotechnol Appl Bioc 34*, 195-197.
190. Bleicher, K.H., Bohm, H.J., Muller, K., and Alanine, A.I. (2003) Hit and lead generation: Beyond high-throughput screening, *Nat Rev Drug Discov 2*, 369-378.
191. Lengauer, T., Lemmen, C., Rarey, M., and Zimmermann, M. (2004) Novel technologies for virtual screening, *Drug Discov Today 9*, 27-34.
192. Schneider, G., and Bohm, H.J. (2002) Virtual screening and fast automated docking methods, *Drug Discov Today 7*, 64-70.
193. Pereira, D.A., and Williams, J.A. (2007) Origin and evolution of high throughput screening, *Brit J Pharmacol 152*, 53-61.
194. Carr, R.A., Congreve, M., Murray, C.W., and Rees, D.C. (2005) Fragment-based lead discovery: Leads by design, *Drug Discov Today 10*, 987-992.
195. Zartler, E.R., and Shapiro, M.J. (2005) Fragonomics: Fragment-based drug discovery, *Curr Opin Chem Biol 9*, 366-370.
196. Böhm, H.-J., Flohr, A., and Stahl, M. (2004) Scaffold hopping, *Drug Discovery Today: Technologies 1*, 217-224.
197. Gillet, V.J. (2008) New directions in library design and analysis, *Curr Opin Chem Biol 12*, 372-378.
198. Welsch, M.E., Snyder, S.A., and Stockwell, B.R. (2010) Privileged scaffolds for library design and drug discovery, *Curr Opin Chem Biol 14*, 347-361.
199. Shoichet, B.K. (2006) Screening in a spirit haunted world, *Drug Discov Today 11*, 607-615.
200. Keseru, G.M., and Makara, G.M. (2006) Hit discovery and hit-to-lead approaches, *Drug Discov Today 11*, 741-748.
201. Low, D.A., Weyand, N.J., and Mahan, M.J. (2001) Roles of DNA adenine methylation in regulating bacterial gene expression and virulence, *Infect Immun 69*, 7197-7204.
202. Zhang, J.H., Chung, T.D.Y., and Oldenburg, K.R. (1999) A simple statistical parameter for use in evaluation and validation of high throughput screening assays, *J Biomol Screen 4*, 67-73.
203. Tipton, K.F. (2002) Principles of enzyme assay and kinetic studies, In *Enzyme Assays: A Practical Approach* (Eisenthal, R., and Danson, M.J., Eds.), pp 1-47, Oxford University Press, Oxford.
204. Copeland, R.A. (2005) *Evaluation of enzyme inhibitors in drug discovery: A guide for medicinal chemists and pharmacologists*, Wiley-Interscience.
205. (2008) *Assay guidance manual version 5.0*. Eli Lilly and Company and National Institutes of Health Chemical Genomics Center. Available online at: http://www.ncgc.nih.gov/guidance/manual_toc.html. [Accessed 04 July 2011].
206. Rogers, A., and Gibon, Y. (2009) Enzyme kinetics: Theory and practice, In *Plant Metabolic Networks* (Schwender, J., Ed.), pp 71-103, Springer.
207. Kruger, N.J. (1995) Errors and artifacts in coupled spectrophotometric assays of enzyme activity, *Phytochemistry 38*, 1065-1071.
208. Herman, G.E., and Modrich, P. (1982) *Escherichia coli* dam methylase. Physical and catalytic properties of the homogeneous enzyme, *J Biol Chem 257*, 2605-2612.
209. de la Campa, A.G., Springhorn, S.S., Kale, P., and Lacks, S.A. (1988) Proteins encoded by the *Dpn*I restriction gene cassette. Hyperproduction and characterization of the *Dpn*I endonuclease, *J Biol Chem 263*, 14696-14702.
210. Maynard-Smith, M.D. (2011) Novel Antibiotics from DNA Adenine Methyltransferase Inhibitors, In *School of Chemistry*, University of Southampton, Southampton.
211. Bradford, M.M. (1976) A rapid and sensitive method for the quantitation of microgram quantities of protein utilizing the principle of protein-dye binding, *Anal Biochem 72*, 248-254.

212. Turini, P., Kurooka, S., Steer, M., Corbascio, A.N., and Singer, T.P. (1969) The action of phenylmethylsulfonyl fluoride on human acetylcholinesterase, chymotyrpsin and trypsin, *J Pharmacol Exp Ther 167*, 98-104.
213. Sanchez, J.A., Marek, D., and Wangh, L.J. (1992) The efficiency and timing of plasmid DNA replication in Xenopus eggs: Correlations to the extent of prior chromatin assembly, *J Cell Sci 103 (Pt 4)*, 907-918.
214. Perona, J.J. (2002) Type II restriction endonucleases, *Methods 28*, 353-364.
215. Cleland, W.W. (1964) Dithiothreitol, a new protective reagent for SH groups, *Biochemistry 3*, 480-482.
216. Bradbury, S.L., and Jakoby, W.B. (1972) Glycerol as an enzyme-stabilizing agent: Effects on aldehyde dehydrogenase, *Proc Natl Acad Sci USA 69*, 2373.
217. Gekko, K., and Timasheff, S.N. (1981) Mechanism of protein stabilization by glycerol: preferential hydration in glycerol-water mixtures, *Biochemistry 20*, 4667-4676.
218. Izsvak, Z., and Duda, E. (1989) 'Star' activity and complete loss of specificity of *Ceq*I endonuclease, *Biochem J 258*, 301.
219. Segel, I.H. (1975) *Enzyme kinetics: Behavior and analysis of rapid equilibrium and steady-state enzyme Systems* Wiley, New York.
220. Todar, K. (2008) *Textbook of Bacteriology*. Available online at: www.textbookofbacteriology.net. [Accessed 10 July 2011].
221. Cheng, Y., and Prusoff, W.H. (1973) Relationship between the inhibition constant (K_i) and the concentration of inhibitor which causes 50 per cent inhibition (IC_{50}) of an enzymatic reaction, *Biochem Pharmacol 22*, 3099-3108.
222. Ferguson, L.R., and Denny, W.A. (2007) Genotoxicity of non-covalent interactions: DNA intercalators, *Mutat Res 623*, 14-23.
223. Tse, W.C., and Boger, D.L. (2004) A fluorescent intercalator displacement assay for establishing DNA binding selectivity and affinity, *Accounts Chem Res 37*, 61-69.
224. Boger, D.L., and Tse, W.C. (2001) Thiazole orange as the fluorescent intercalator in a high resolution FID assay for determining DNA binding affinity and sequence selectivity of small molecules, *Bioorg Med Chem 9*, 2511-2518.
225. Nygren, J., Svanvik, N., and Kubista, M. (1998) The interactions between the fluorescent dye thiazole orange and DNA, *Biopolymers 46*, 39-51.
226. Leonardi, R. (2004) Biosynthesis of 4-methyl-5-(β-hydroxyethyl)thiazole phosphate in *Escherichia coli*.
227. Abràmoff, M.D., Magalhaes, P.J., and Ram, S.J. (2004) Image processing with ImageJ, *Biophotonics International 11*, 36-43.
228. Allen, J., Jeffrey, P., Williams, R., and Ratcliffe, A.J. (2010) Approaches to assessing drug safety in the discovery phase, *Drug Future 35*, 67-75.
229. Sanborn, M.E., Connolly, B.K., Gurunathan, K., and Levitus, M. (2007) Fluorescence properties and photophysics of the sulfoindocyanine Cy3 linked covalently to DNA, *J Phys Chem B 111*, 11064-11074.
230. Magde, D., Wong, R., and Seybold, P.G. (2002) Fluorescence quantum yields and their relation to lifetimes of rhodamine 6G and fluorescein in nine solvents: Improved absolute standards for quantum yields, *Photochem Photobiol 75*, 327-334.
231. Bonfils, C., Beaulieu, N., Chan, E., Cotton-Montpetit, J., and MacLeod, A.R. (2000) Characterization of the human DNA methyltransferase splice variant Dnmt1b, *J Biol Chem 275*, 10754-10760.
232. Lee, W.J., and Zhu, B.T. (2006) Inhibition of DNA methylation by caffeic acid and chlorogenic acid, two common catechol-containing coffee polyphenols, *Carcinogenesis 27*, 269.
233. Roehrl, M.H., Wang, J.Y., and Wagner, G. (2004) A general framework for development and data analysis of competitive high-throughput screens for small-molecule inhibitors of protein-protein interactions by fluorescence polarization, *Biochemistry 43*, 16056-16066.
234. Moerke, N.J. (2009) Fluorescence polarization (FP) assays for monitoring peptide protein or nucleic acid protein binding, *Curr Protoc Chem Biol 1*, 1-15.

235. Findlay, J.W., and Dillard, R.F. (2007) Appropriate calibration curve fitting in ligand binding assays, *AAPS J 9*, E260-267.
236. Steinitz, M. (2000) Quantitation of the blocking effect of Tween-20 and Bovine Serum Albumin in ELISA microwells, *Anal Biochem 282*, 232-238.
237. Ryan, A.J., Gray, N.M., Lowe, P.N., and Chung, C. (2003) Effect of detergent on "promiscuous" inhibitors, *J Med Chem 46*, 3448-3451.
238. Pingoud, A., and Jeltsch, A. (2001) Structure and function of type II restriction endonucleases, *Nucleic Acids Res 29*, 3705-3727.
239. Ruiz Garcia, A., Bermejo, M., Moss, A., and Casabo, V.G. (2008) Pharmacokinetics in drug discovery, *J Pharm Sci 97*, 654-690.
240. Cordell, R.L., Hill, S.J., Ortori, C.A., and Barrett, D.A. (2008) Quantitative profiling of nucleotides and related phosphate-containing metabolites in cultured mammalian cells by liquid chromatography tandem electrospray mass spectrometry, *J Chromatogr B 871*, 115-124.
241. Calmann, M.A., and Marinus, M.G. (2003) Regulated expression of the *Escherichia coli dam* gene, *J Bacteriol 185*, 5012.
242. Shoemaker, R.H. (2006) The NCI60 human tumour cell line anticancer drug screen, *Nat Rev Cancer 6*, 813-823.
243. Shannon, R.D. (1976) Revised effective ionic-radii and systematic studies of interatomic distances in halides and chalcogenides, *Acta Crystallogr A 32*, 751-767.
244. Lacks, S., and Greenberg, B. (1975) A deoxyribonuclease of *Diplococcus pneumoniae* specific for methylated DNA, *J Biol Chem 250*, 4060-4066.
245. Stefanidou, M., Maravelias, C., Dona, A., and Spiliopoulou, C. (2006) Zinc: A multipurpose trace element, *Arch Toxicol 80*, 1-9.
246. Daves Jr, G.D., Robins, R.K., and Cheng, C.C. (1961) The total synthesis of toxoflavin, *J Am Chem Soc 83*, 3904-3905.
247. Levenberg, B., and Linton, S.N. (1966) On the biosynthesis of toxoflavin, an azapteridine antibiotic produced by *Pseudomonas cocovenenans*, *J Biol Chem 241*, 846.
248. Phatak, S.S., Stephan, C.C., and Cavasotto, C.N. (2009) High-throughput and *in silico* screenings in drug discovery, *Expert Opin Drug Dis 4*, 947-959.
249. Rishton, G.M. (2003) Nonleadlikeness and leadlikeness in biochemical screening, *Drug Discov Today 8*, 86-96.
250. Sundar, S., and Chakravarty, J. (2010) Antimony toxicity, *Int J Environ Res Public Health 7*, 4267-4277.
251. Minodier, P., and Parola, P. (2007) Cutaneous leishmaniasis treatment, *Travel Med Infect Dis 5*, 150-158.
252. Guerin, P.J., Olliaro, P., Sundar, S., Boelaert, M., Croft, S.L., Desjeux, P., Wasunna, M.K., and Bryceson, A.D.M. (2002) Visceral leishmaniasis: current status of control, diagnosis, and treatment, and a proposed research and development agenda, *Lancet Infect Dis 2*, 494-501.
253. Haldar, A.K., Sen, P., and Roy, S. (2011) Use of antimony in the treatment of leishmaniasis: Current status and future directions, *Mol Biol Inter 2011*.
254. Das, B.B., Ganguly, A., and Majumder, H.K. (2008) DNA Topoisomerases of *Leishmania*: The potential targets for anti-Leishmanial therapy, In *Drug targets in kinetoplastid parasites* (Majumder, H.K., Ed.), p 103, Landes Bioscience.
255. Bond, A., Reichert, Z., and Stivers, J.T. (2006) Novel and specific inhibitors of a poxvirus type I topoisomerase, *Mol Pharmacol 69*, 547-557.
256. Kim, H., Cardellina, J.H., Akee, R., Champoux, J.J., and Stivers, J.T. (2008) Arylstibonic acids: Novel inhibitors and activators of human topoisomerase IB, *Bioorg Chem 36*, 190-197.
257. Seiple, L.A., Cardellina, J.H., Akee, R., and Stivers, J.T. (2008) Potent inhibition of human apurinic/apyrimidinic endonuclease 1 by arylstibonic acids, *Mol Pharmacol 73*, 669-677.
258. Rishi, V., Oh, W.J., Heyerdahl, S.L., Zhao, J.F., Scudiero, D., Shoemaker, R.H., and Vinson, C. (2010) 12 Arylstibonic acids that inhibit the DNA binding of five B-ZIP dimers, *J Struct Biol 170*, 216-225.

259. Yang, Q.E., Stephen, A.G., Adelsberger, J.W., Roberts, P.E., Zhu, W., Currens, M.J., Feng, Y., Crise, B.J., Gorelick, R.J., Rein, A.R., Fisher, R.J., Shoemaker, R.H., and Sei, S. (2005) Discovery of small-molecule human immunodeficiency virus type 1 entry inhibitors that target the gp120-binding domain of CD4, *J Virol 79*, 6122-6133.
260. Demicheli, C., Frezard, F., Lecouvey, M., and Garnier-Suillerot, A. (2002) Antimony(V) complex formation with adenine nuelcosides in aqueous solution, *Bba-Gen Subjects 1570*, 192-198.
261. Feng, B.Y., and Shoichet, B.K. (2006) A detergent-based assay for the detection of promiscuous inhibitors, *Nat Protoc 1*, 550-553.
262. Cornelis, G.R. (2002) *Yersinia* type III secretion, *J Cell Biol 158*, 401.
263. Perry, R.D., and Fetherston, J.D. (2011) Yersiniabactin iron uptake: mechanisms and role in *Yersinia pestis* pathogenesis, *Microbes Infect 13*, 808-817.
264. Englert, R.D., and Sweeting, O.J. (1948) The preparation of aromatic stibonic acids of certain benzenesulfonamides, *J Am Chem Soc 70*, 2977-2979.
265. Roje, S. (2006) *S*-adenosyl-l-methionine: Beyond the universal methyl group donor, *Phytochemistry 67*, 1686-1698.
266. Wahhab, A., Besterman, J., Isakovic, L., Llewellyn, D., Rahil, J., Saavedra, O., and Deziel, R. (2008) Inhibitors of DNA methyltransferase.
267. Hobley, G., McKelvie, J.C., Harmer, J.E., Howe, J., Oyston, P.C., and Roach, P.L. (2012) Development of rationally designed DNA N6 adenine methyltransferase inhibitors, *Bioorg Med Chem Lett 22*, 3079-3082.
268. Sills, M.A., Weiss, D., Pham, Q., Schweitzer, R., Wu, X., and Wu, J.J. (2002) Comparison of assay technologies for a tyrosine kinase assay generates different results in high-throughput screening, *J Biomol Screen 7*, 191-214.
269. Posner, B.A., Xi, H., and Mills, J.E.J. (2009) Enhanced HTS hit selection via a local hit rate analysis, *J Chem Inf Model 49*, 2202-2210.
270. Shu, C.-W., Madiraju, C., Zhai, D., Welsh, K., Diaz, P., Sergienko, E., Sano, R., and Reed, J.C. (2011) High-throughput fluorescence assay for small-molecule inhibitors of Autophagins/Atg4, *J Biomol Screen 16*, 174-182.
271. Frézard, F., Demicheli, C., and Ribeiro, R.R. (2009) Pentavalent antimonials: New perspectives for old drugs, *Molecules 14*, 2317-2336.
272. Brawer, R., Batista, F.D., Burrone, O.R., Sordelli, D.O., and Cerquetti, M.C. (1998) A temperature-sensitive DNA adenine methyltransferase mutant of *Salmonella typhimurium*, *Arch Microbiol 169*, 530-533.
273. Parkhill, J., Wren, B.W., Thomson, N.R., Titball, R.W., Holden, M.T.G., Prentice, M.B., Sebaihia, M., James, K.D., Churcher, C., and Mungall, K.L. (2001) Genome sequence of *Yersinia pestis*, the causative agent of plague, *Nature 413*, 523-527.